THE UNIVERSITY OF NEWCASTLE UPON TYNE

DEPARTMENT OF CIVIL ENGINEERING

EXPERIMENTAL INVESTIGATIONS ON THE MECHANICAL PROPERTIES OF ROCKS CONTAINING A SINGLE DISCONTINUITY

A thesis submitted for the degree of

Doctor of Philosophy

by

AHMAD FAHIMIFAR, BSc., MSc.

May 1990

ORIGINAL COPY TIGHTLY BOUND

In the name of ***ALLAH***, the Compassionate, the Merciful

To the memory of :

IMAM KHOMEINI , the great leader of the Islamic Revolution who was the great spirit of the time

ACKNOWLEDGEMENTS

The author wishes to express his sincer gratitude to the following:

- The Iranian Ministry of Culture and Higher Education and the Amir Kabir University of Technology for their financial support.

- My supervisor Dr. E. K. S. Passaris for his guidance, supervision, encouragement and discussion.

- Mr. F. Fayazi postgraduate student in the Department of Geology for his work on the petrological description of the rocks.

- Mr. M. Gharouni Nik postgraduate student in the Department of Civil Engineering for his help in formating the thesis.

Last but not least sincre thanks to:

Mr. J. Moore chief laboratory technician,
Mr. L. Moore rock mechanics laboratory technician,
Mr. F. Beadle rock cutting technician,
Mr. S. Patterson for his photographs.

ABSTRACT

An extensive experimental programme was undertaken to investigate the strength and deformational characteristics of six rock types containing a single joint under various loading and straining conditions.

A monitoring system was set up using a microcomputer controlled logger and the required computer programs for data logging and processing were also developed.

For the purpose of achieving reliable findings the effects of system constraints on the experimental results in triaxial testing of jointed specimens were investigated.

On the basis of a satisfactory end-specimen condition the results of triaxial compressive tests performed on the specimens of three rock types, containing artificial joints at different orientations, are presented, and the effects of joint inclination, confining pressure (0-70 MPa) and joint surface roughness on the mechanical behaviour of jointed specimens were investigated.

A method to calculated volumetric strain in the rock specimens has been developed and the volumetric strain, lateral strain and instantaneous Poisson's ratio for both intact and jointed specimens are calculated.

Time-dependency of jointed rocks for the three cases of different constant strain rates, changing strain rates and stress relaxation at various points on the complete stress-strain curve has examined.

The failure criteria applicable to jointed media are reviwed and the necessary parameters for an appropriate failure criterion have been defined.

The stick-slip characteristics of jointed rocks are investigated and two types of stick-slip phenomena are introduced in conjunction with the type of rock and type of testing system.

CONTENTS

CHAPTER 1

INTRODUCTION

The problem of discontinuities in the theoretical and practical rock mechanics is so important that it seems impossible to neglect it even when a structure is planned in or on an apparently competent rock mass. Although, the use of the term "discontinuous rock" implies that there are rocks which are truly continuous, this is not strictly correct for even the mightiest wall of granite has exfoliation surfaces (Goodman, 1976). For this reason from the early stages of developments in rock mechanics, investigators have considered the problem fundamentally, and it has been stated that "Rock mechanics is to be a mechanics of a discontinuum, that is, a jointed medium" (Muller, 1964). Similar comments have also been put forward by Jaeger (1972). Having emphasized the importance of discontinuities, one has to note that there are certain types of rocks, such as evaporites, where because of their visco-plastic nature no discontinuities may be identified as part of the rock structure.

During the last few decades, considerable research work has been conducted in conjunction with the problem of weakness planes in rocks in order to achieve comprehensive solutions for design purposes.

Use of triaxial compression testing to study the mechanical properties of jointed rock is a convenient method because of its several advantages. A distinct advantage of this test is that, with the exception of unconfined state, strength appears to be unaffected by specimen size and shape (Mogi, 1966).

For the work described in this thesis, since a stiff or servo-controlled testing system, that allows investigation of the post-failure behaviour of rock, was available for testing

discontinuous rock, a 5 MN servo-controlled testing system was used to study the sliding characteristics and post failure behaviour of rock specimens containing a single artificial joint at various orientations. Work has mainly concentrated in the laboratory testing of cylindrical jointed specimens of comparatively large diameter, not often used by previous workers. The specimens have been subjected to stress conditions such as those normally encountered in underground structures.

The first task of the investigations has been to assess the significance of the changes of geometry of the cell-specimen system during sliding through joint surface, and the effects of end-specimen conditions. Thereafter, on the basis of a satisfactory end-specimen condition, the work was extended to study the mechanical characteristics of jointed rocks by introducing single joints through cylindrical rock specimens.

Six rock types were selected for the experimental investigations: Limestone, slate, granite and three types of sandstone. The majority of the tests concerning strength and deformability of the jointed specimens were carried out using the three types of sandstone. In investigating the stick-slip characteristics of jointed rocks, the other types of rock were also used.

The research programme also included the measurement and assessment of volumetric changes in jointed specimens with different joint orientations. Furthermore, a series of tests were dedicated to investigate the effects of strain rate or displacement rate on the stress-strain characteristics of jointed specimens under both constant and variable strain rate.

CHAPTER 2

GENERAL CONSIDERATIONS

2.1 STATEMENT OF THE PROBLEM

Rock masses are rarely homogeneous, isotropic and intact, as commonly assumed for other engineering materials (Serafim et al, 1966). Failure of rock masses, particularly near the surface, usually results from sliding along a single discontinuity or a combination of discontinuities (Farmer, 1983). The influence of these discontinuities on the mechanical behaviour of rock is therefore significant.

According to Jaeger et al (1969) the most convenient method for the study of the frictional and mechanical properties of joints is the triaxial test technique. However, because of certain shortcomings of typical test techniques and particularly where it is used to study the sliding characteristics of joint surfaces, such a test is not a simple task. The major problems encountered in typical tests, whether uniaxial or triaxial, are (Hawkes and Meller, 1970):

1. Contact problems, which cause axial stress and displacement to vary across the end plane. These arise when platen face or sample end are not perfectly plane and normal to the longitudinal axis of the rock specimen.

2. Radial constraints, which restrict or exaggerate axial and circumferential strains at the end planes. These arise from friction between platens and rock, or from extrusion of interfacial layers.

3. Lateral translations, which displace the two end planes relative to each other, inducing "racking" distortion. These may be caused by imperfect head travel, ball seat rotation, or lack of flexural rigidity in long loading columns of the testing machine.

4. End-plane rotations, which cause the axial displacements to vary across the end-plane when platens tilt, and introduce shear strains when platens twist.

These difficulties indicate that provision of the appropriate test conditions in experimental work is very important, and that lack of comprehensive treatment will result in unrealistic and perhaps unreliable findings. The problems faced, when using a triaxial testing system to determine the sliding characteristics of joints (due to the progressive change in the geometry of cell-specimen system) are significant as will be discussed in chapter 4 and any carelessness in this respect may produce unacceptable results.

The change in geometry of the cell-specimen system when testing jointed specimen triaxially, was first pointed out by Jaeger (1959). Problems may develop when using one spherical seat in the system, as is often the case, or two spherical seats, or two pairs of flat platens with no lubrication. As sliding commences along the joint plane axial and lateral displacements may alter the configuration of the cell-specimen and lead to the development of frictional and lateral forces at the seats or platens which affect the sliding behaviour of the joint significantly.

An effort was made by Rosengren (1968) to examine end-effects on the cylindrical specimens containing a single joint. He concentrated his study to show the importance of the frictional restraints at the specimen ends when two spherical seats are used in the system and he introduced appropriate measures to reduce this effect to an acceptable level. These measures consisted of using two pairs of steel discs which were inserted

between the specimen and platens at each end. Each pair of discs contained molybdenum grease which acted as lubricant and allowed the two discs to move freely in the lateral direction. However, the effects of geometry associated with misalignment on the specimen, no thorough investigation has been undertaken concerning:

(i) peak strength,

(ii) deformational characteristics, and

(iii) other mechanical aspects of jointed surfaces, such as mechanism of failure and mode of sliding, particularly when one spherical seat is used in the system. In addition to the aforementioned topics a more fundamental research was undertaken to investigate thoroughly the mechanical response of rock specimens containing a single joint. During these investigations sophisticated testing facilities and appropriate logging equipment were utilized to allow acceptable conditions both for controlling the tests and for monitoring the specimens response.

2.2 OBJECTIVES

During the course of the present study the systematic testing which was undertaken employed cylindrical specimens containing a single joint, subjected to triaxial compressive load. The following aspects were explored in the process of this fundamental investigation:

(i) The effects of testing system constraints with respect to the sliding along joint surface.

(ii) The overall effects of the variation of the orientation of the smooth and rough surface joint planes on the strength and deformational behaviour of specimens of different rock types under variable stress systems (different confining pressures).

(iii) The determination of the post failure behaviour, residual strength, and deformational characteristics of jointed specimens for different rock types.

(iv) The influence of surface roughness and interlocking on the resistance to deformation and sliding of joint surfaces.

(v) The determination of the volumetric strain characteristics of jointed rock containing a single joint, and development of an indirect approach to determine the volumetric strain accurately.

(vi) The evaluation of the theoretical and experimental failure criteria for jointed rock and the determination of the important factors that must be taken into account when establishing an appropriate failure criterion.

(vii) The assessment of the time dependent characteristics of the strength and deformational behaviour of jointed rock.

(viii) The determination of the effects of testing system constraints with respect to the stick-slip phenomenon, and the investigation on the factors influencing the stick-slip characteristics.

CHAPTER 3

TESTING SYSTEM, DATA MONITORING SYSTEM AND TESTING PROCEDURES

3.1 THE 5 MN SERVO-CONTROLLED STIFF TESTING SYSTEM

A detailed description of the servo-controlled stiff testing system may be found in the work by Price (1979).

Basically, the testing apparatus consists of three parts:

a. Loading system

b. Electronic monitoring and control facilities

c. Data monitoring equipment

3.1.1 LOADING SYSTEM

The loading system consists of two stiff frames capable of 1 MN and 5 MN axial load. The 5 MN stiff frame was selected because of its suitability to the type of test (triaxial) and the range of axial load required in these investigations, i.e. a maximum of 2.5 MN. A hydraulic actuator is mounted in the centre of, and perpendicular to, the lower platen of the loading frame. The hydraulic manifold and electro-hydraulic servo-valve are mounted directly onto the side of actuator.

The axial loading system can be controlled by load or strain via closed loop servo-controlled system. In the present experimental studies a constant axial strain rate (0.25% per minute satisfying the ISRM suggested methods, Brown, 1986) was chosen as

the controlling parameter. The system allows the use of either a departmentally built 5 MN load cell or an NCB-MRE 1 MN load cell type 440.

A hydraulic power pack which has been supplied by RDP-Howden Ltd provides a supply of hydraulic oil at maximum confining pressure of 25 MPa and a maximum flow rate of 38 l/min.

3.1.2 ELECTRONIC CONTROL SYSTEM

The program signal is created by the electronics control. It also monitors the progress of the machine and by comparing the two, generates an error signal to correct the difference. In the present system which has been manufactured by using modulus from RDP and DARTEC Ltd (plate 3.2) the program signal is generated by a digital ramp generator. This unit was programmed to give a constant strain rate as the program signal, which is defined by a top ramp voltage and total ramp time. The total ramp times were 10^2, 10^3, and 10^4 seconds for fast, medium and slow strain rates respectively in this study.

During the test, signal from the Linear Variable Differential Transformer (LVDT) which is mounted parallel to the specimen, is transmitted to the servo-controller. The servo-amplifier constantly compares the feedback and program signals, producing an error signal in proportion to the magnitude and polarity of their difference. This signal is the drive for the servo-valve. If there is no difference the valve is closed, otherwise the valve opens allowing oil to flow into or out of the actuator in accordance with the error.

3.1.3 DATA MONITORING SYSTEM

The existing data recording system was a multipurpose Philips X-Y Recorder, type PM8141, connected to the servo-controller. The input is in mV which following the original calibration procedure, is then expressed into units of force and displacement .

Recording of data in this way, however, was not satisfactory and accurate enough for the subsequent analysis. For this reason, a multichannel analogue data acquisition unit capable of interfacing with a microcomputer and also with the servo-controlled system was used. The Analogue 1208 data acquisition system, manufactured by EDC Photonic Ltd.(plate 3.2) enables the use of a microcomputer to acquire data from a number of analogue signal sources and transmit it to digital form. The unit contains an analogue signal multiplexer enabling the required signal source to be monitored by means of a computer program. The signal is then processed by a high precision instrumentation amplifier and sample-and-hold circuit, so that noise and indeterminacy in the measurement is minimized. Finally a 12-bit analogue to digital converter is used to convert the voltage (obtained from the servo-controlled machine) into equivalent digits that can be stored and processed by the computer.

At first, a computer program that allowed a Sirius-1 microcomputer to interrogate the Analogue 1208 was written in MS-BASIC. The data obtained through this program were so scattered that they could not be used in the subsequent analysis. It was found that the BASIC program did not possess the required speed to monitor at an acceptable rate the signals generated during the test. For this reason the program was re-written in Pascal which was faster and allowed scanning of more than 900 readings per/min for two channels (load and displacement) and was also to record the data on a floppy disk.

One serious problem encountered in using this program is the very large amount of data recorded in each test, so that an entire floppy disc is needed for recording data during a test, and also the corresponding load-displacement plot is not smooth enough. For this reason another program was written to reduce the acquired data to an acceptable number with a sufficiently smooth load-displacement curve.

The calibration for each instrument (load cell and LVDT) was done independently using the logger and obtaining equivalent digits information for each instrument. Then, by using a third program the digital readings were converted to the appropriate engineering units, MPa for stress and percentage for strain.

The program can be easily changed to record data through more than two channels (up to 8 channels) for monitoring of the other test parameters such as volumetric strain, lateral strain and so on. This program and the two others corresponding to correction of data and calculation of stress and strain are given in appendix A.

3.2 TRIAXIAL TEST DESCRIPTION

The triaxial cell used in this experiment was developed by Buzdar (1968). The cell has sufficient internal space to allow large lateral displacement when sliding takes place along the joint surface. It has been designed for maximum confining pressure of 70 MPa. The base and piston units are capable of withstanding axial stress of more than 560 MPa (plate 3.1 and figure 3.1). Lateral confining pressure is applied hydraulically by a continuously operating electric pumping unit.

Uniaxial tests were also conducted in this cell by removing the relief valve from the system and swapping the air bleed for an overflow pipe. This procedure was necessary

in order to keep exactly the same conditions throughout the experiment whether confining pressure is zero (uniaxial) or non-zero (triaxial).

3.3 SELECTION OF ROCK MATERIAL

Six different rock types were selected for investigation and their thin section petrological description is given in appendix B. Rock material was selected from various locations in an attempt to allow the testing of more than one type of rock, so that conclusions of general applications could be reached. Therefore, three types of sandstone(i.e. Stainton, Dumfrith and Penrith sandstone), slate from Dinorwic, limestone from Matlock and granite from Dalbeatie were used in this experimental series.

3.4 VOLUMETRIC CHANGE MEASURING APPARATUS

The apparatus used was that of Price (1979) which was capable of coping with the large anticipated volume changes and fast rates of volume change.

The apparatus incorporates a pressure relief valve with a specified operating range of 7-70 MPa, but which in practice proved capable of operating even at zero pressure. This valve is mounted in series with the triaxial cell and a Bourdon type hydraulic pressure gauge. The pressure gauge was used both for the setting of the relief valve and for the monitoring of the confining pressure during the test (plate 3.1). An inlet valve is used for closing off the system from the confining pressure pump once the desired test pressure is reached.

3.5 SPECIMEN PREPARATION

The procedure used for the preparation of test specimens was in accordance with the ISRM suggested methods (Brown, 1986). The specimens were cored to a nominal diameter of 75 mm and length of 150 mm. They were smooth and free of any abrupt irregularities, with sides parallel to each other to within 0.01 mm and at right angles to the longitudinal axis. Prior to testing the diameter and length of each specimen were measured, and the average from at least three positions recorded for use in later calculations. Where possible, all specimens of a particular rock type were taken from the same host block. All specimen were kept at room temperature and were room dry when tested.

For testing the specimens after establishing the appropriate joints they were mounted between two platens, whose faces were flat, clean and dry. A flexible membrane was fitted over the first and folded back over and under two rubber O-rings at each end. The use of two flexible membranes was adopted when initial tests came to abrupt ends after about 4% axial strain due to rupture of the single membrane. This rupturing resulted from the flexible membrane becoming trapped in the joint or in the shear fracture plane along which differential sliding took place, tearing the membrane. Experimentation with two flexible membranes showed that whilst, the inner one became torn and punctured, the other one continued to act as an effective oil seal (plate 3.5).

3.6 STRAIN RATE

The rate at which the specimen is strained or loaded has an effect on the ultimate strength and other mechanical properties of rock (see chapter 7). A constant strain rate of 0.25% per minute (equivalent to 4.17 X 10^{-5}/s) was adopted, so that failure occurred

within 5-15 minutes of loading, which is in accordance with the ISRM suggested methods (Brown, 1986).

3.7 PREPARATION OF JOINTED SPECIMENS

Three groups or types of jointed specimens similar in size and shape were used in this investigation.

3.7.1 SPECIMENS CONTAINING SAW CUT PLANAR JOINTS

After preparation of cylindrical cores as in section 3.5 and ensuring that no visible fractures or cracks existed in the specimens, each of them was cut into two pieces with a diamond saw. The cuts were perfectly plane surfaces at angles of 0, 15, 30, 45, 60 and 90° with respect to σ_3 direction, taking into consideration that σ_1 is parallel to the axis of the specimen. If inclination exceeds 63° 30' where width/height = 0.5, the joint planes intersects the top and bottom platens of the specimens, and therefore, sliding along the joint is not possible. It is for this reason that no specimen tested with joint inclination in the range of 60-90°.

It is necessary to note that the nominal height of the jointed specimens have been taken the same as intact specimens (i.e. 150 mm), however, the height decreases slightly when the intact specimen is cut by diamond saw for establishing saw cut joint. This affects the results slightly quantitatively but not qualitatively.

In order to make the jointed specimens perfectly at right angle to the longitudinal axis and of squared ends, the following procedure was employed: Two halves of each core were placed on each other and fitted on that position by a piece of sticky tape, then, by fixing the whole specimen on a horizontal surface, the upper half of the specimen was

displaced up and down until adjusting horizontally with the size of 150 mm in length. In this position two halves of specimen were tightened to each other by insulation tape.

The surface texture of the joints was kept similar for all specimens, so that it can be reasonably assumed that all the joint surfaces are similar in frictional characteristics. Figure 3.2 shows a typical joint surface texture for both rough and smooth joints being taken by profilometer.

3.7.2 SHEAR-SURFACE JOINT

This type of joint simulating a natural joint, established by shear fracture of solid rock in confining pressures of zero (uniaxial) and 10 MPa. For the jointed specimens produced in this way, it was not possible to obtain predetermined joint orientations, since the angle of joint depended upon the magnitude of axial stress at failure for a given confining pressure. For this reason the solid specimens were fractured employing two variable confining pressures (0 and 10 MPa) representing two different joint orientations (70 to 85^{o} for 0 confinement and 65 to75^{o} for 10 MPa confining pressure). The surface texture in this type of joint was not smooth as the saw cut joints, instead it was felt that it simulated the appearance of a natural joint surface.

3.7.3 SPLIT BREAKAGE JOINT

The third joint type used in this experiment is an attempt to simulate natural joints. The cylindrical specimens with this type of joint were drilled from a block containing a split breakage at an inclination of 30, 45 and 60^{o}. Preparation of this type of specimen was very difficult and time consuming.

At the beginning attempts were made to form the specimens by making a groove over the solid core along the desired direction and then applying a small load through a steel bar to split the specimen. The few early specimens produced in this way were not acceptable because of high diversity from the appropriate inclinations. As a next step, a cubic block of rock with side dimension of 200 mm was cut and before coring the specimen, split breakage was formed in the appropriate direction. In coring the specimen through the block, because of the separation of the two halves of the core there was a possibility of damaging the core barrel and the surface texture of the joint. It was decided therefore to make a hole in the centre of each specimen (parallel to the longitudinal axis of the cores) before coring and the two halves of specimen were secured by using a locking stud. Plates 3.3 and 3.4 show the typical blocks before coring and the resulting specimens. The step by step details of producing split breakage cores is given in appendix C.

3.8 TRIAXIAL TESTING PROCEDURE

The initial procedure for applying the hydrostatic confinement is as follows: First, the inlet valve is open (system open) and the system purged of air by means of an air bleed located at the top of the pressure chamber. The air bleed is then closed off and a small axial load is applied to the specimen. The system is then subjected to the required confining pressure, whilst a hydrostatic stress field is maintained manually throughout by pacing the confining pressure acting on the specimen, against the axial stress which is controlled by the servo unit. Once the required confining pressure is reached, the relief valve is finely adjusted if needed, and the inlet valve closed (system closed). It should be noted that the operating level of the relief valve is initially set before the experiment whilst disconnected from the triaxial cell. Once the system is closed, any further axial loading of the specimen will cause an increase in the confining pressure and thus operate the relief valve. The oil displaced in this manner is collected and its

volume recorded manually with an accuracy of 0.5 cc against the axial strain. The axial displacement (axial strain) and axial load (axial stress) are continuously monitored by means of an LVDT and a load cell respectively, and recorded on both the X-Y plotter and the microcomputer data logger facilities. Thus, at any given moment during the test the volumetric strain of the specimen can be calculated as a function of the displaced oil and the axial displacement.

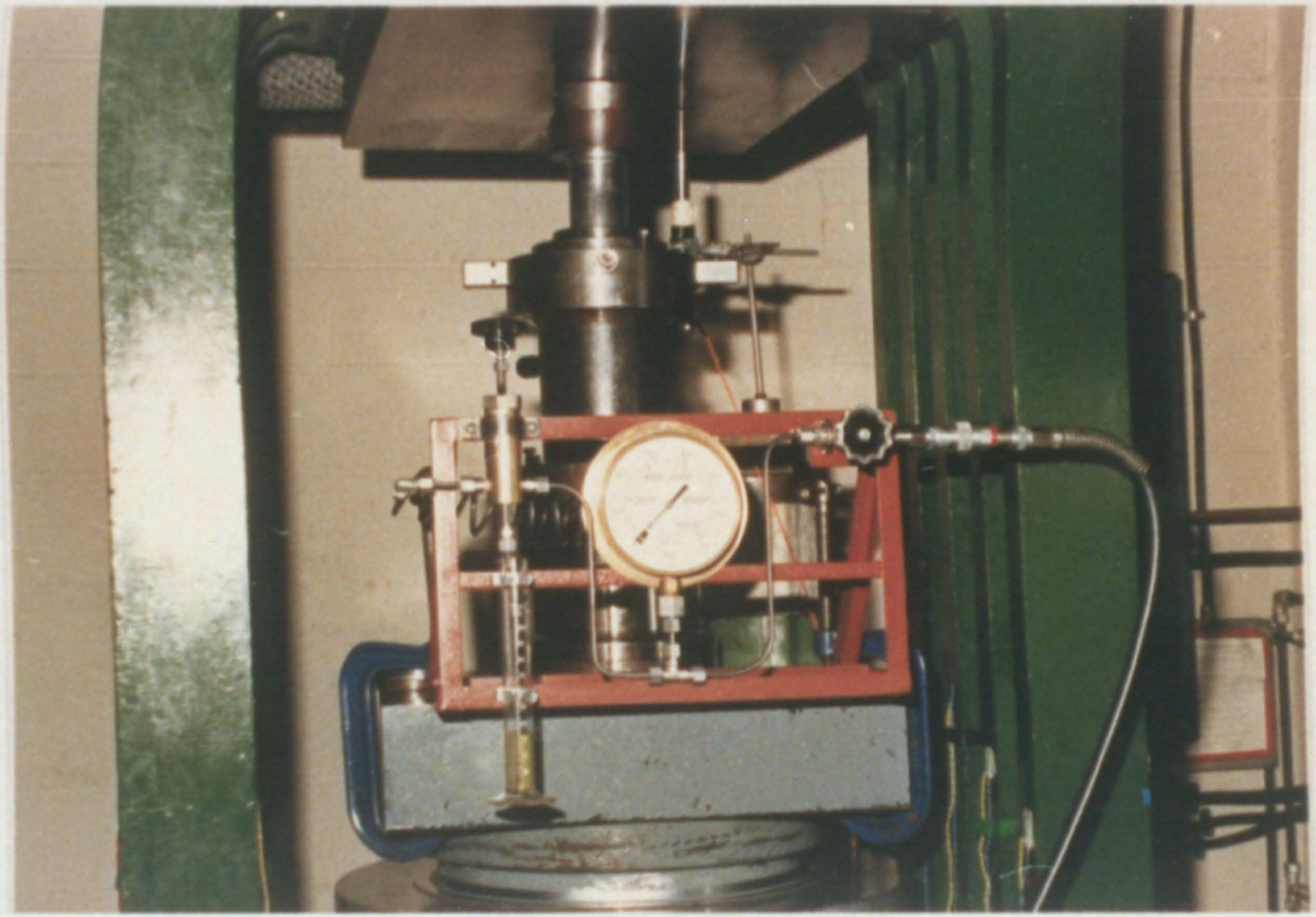

Plate 3.1 Triaxial Cell, Relief Valve and 5 MN stiff Frame

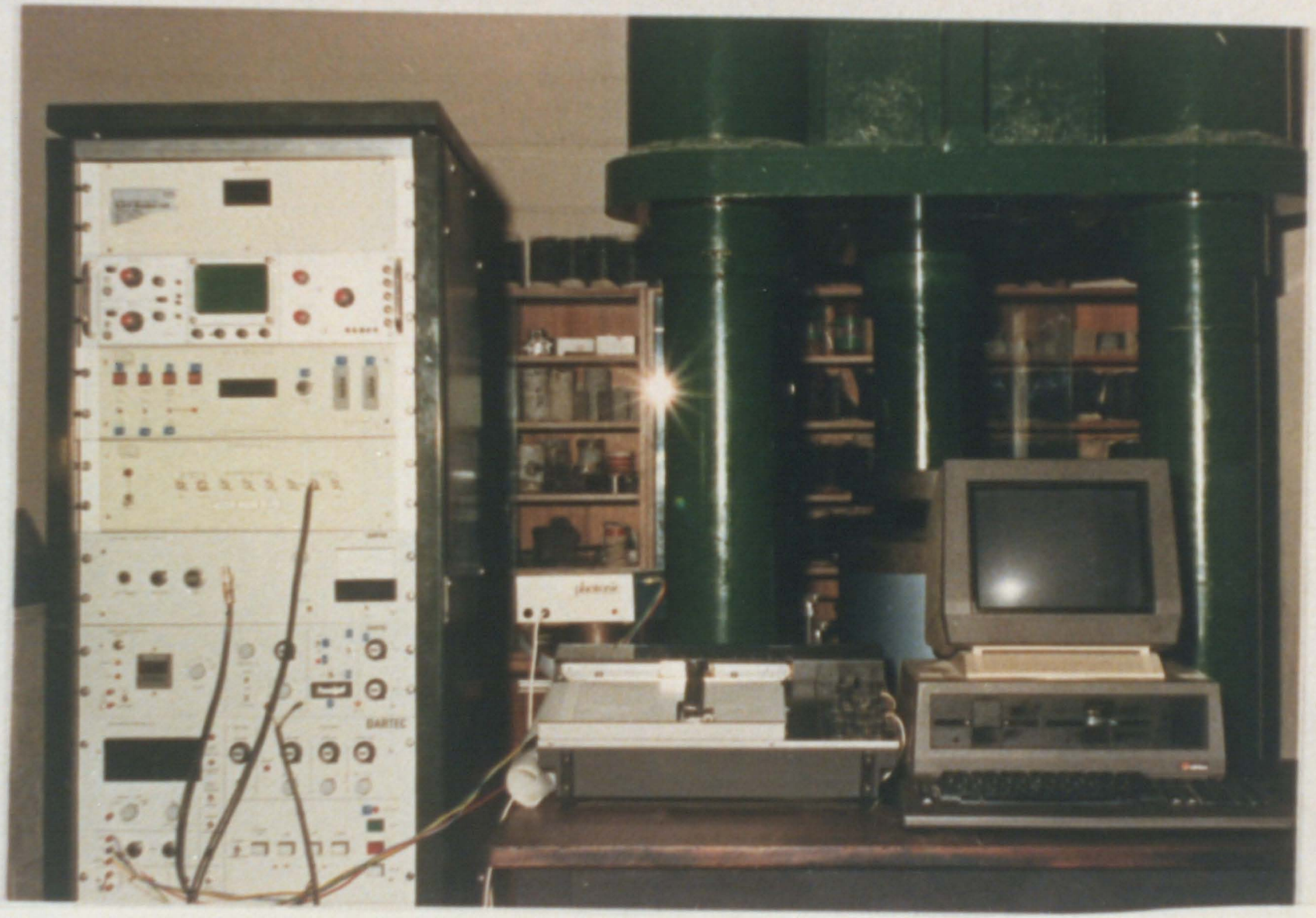

Plate 3.2 Servo-controlled and data acquisition systems

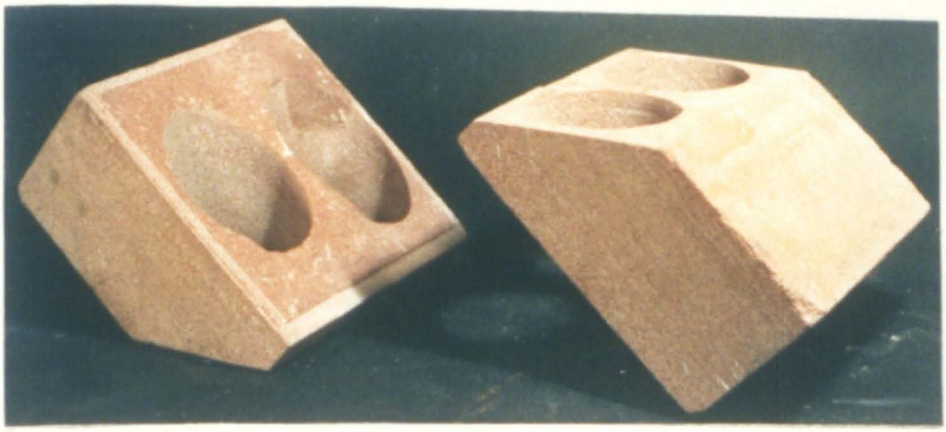

Plate 3.3 Blocks of rock after coring of natural joint.

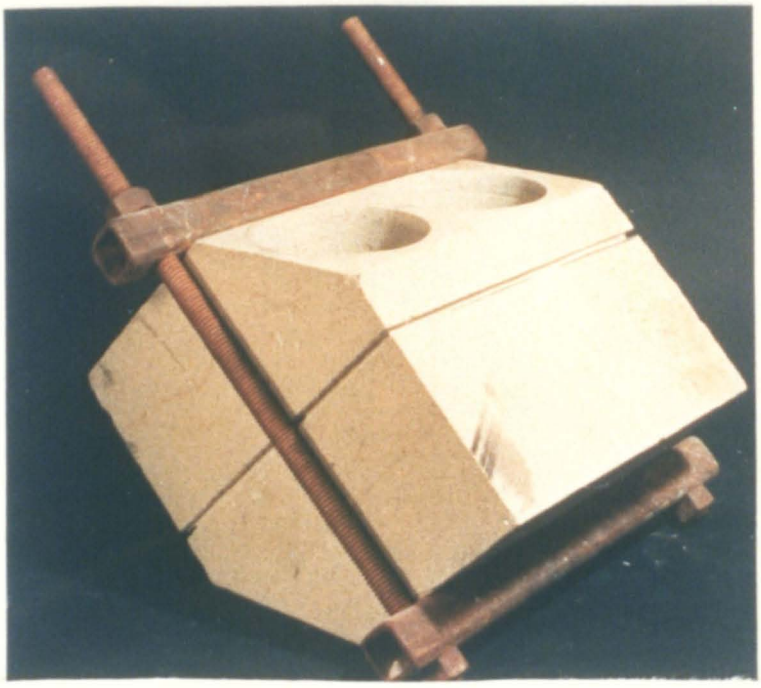

Plate 3.4 Prepared block of rock for establishing natural joint.

Plate 3.5 Rupture of single membrane during the deformation of specimen or sliding along joint plane.

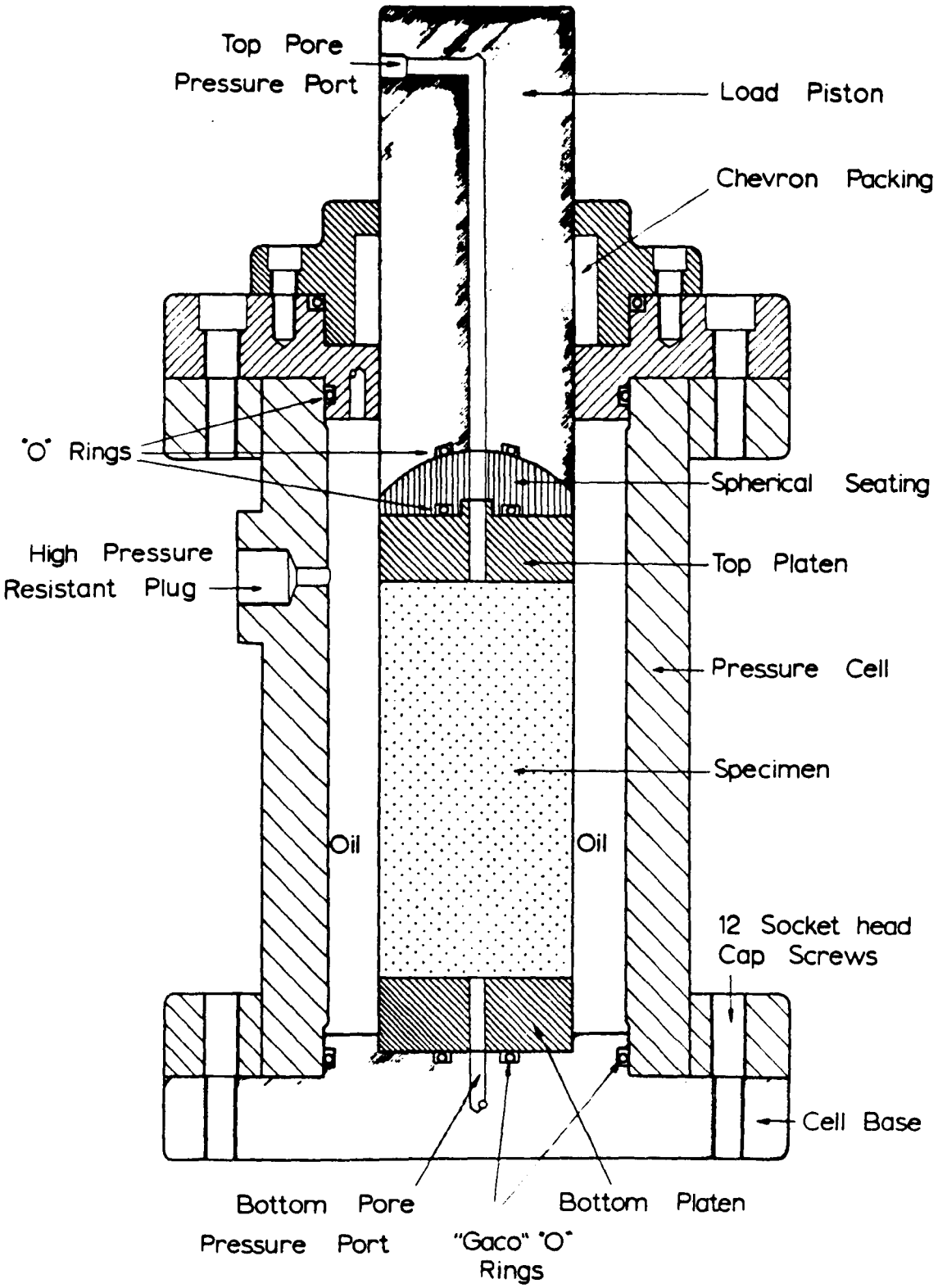

FIG 3.1: 70 MPa TRIAXIAL PRESSURE CELL

(after Buzdar, 1968)

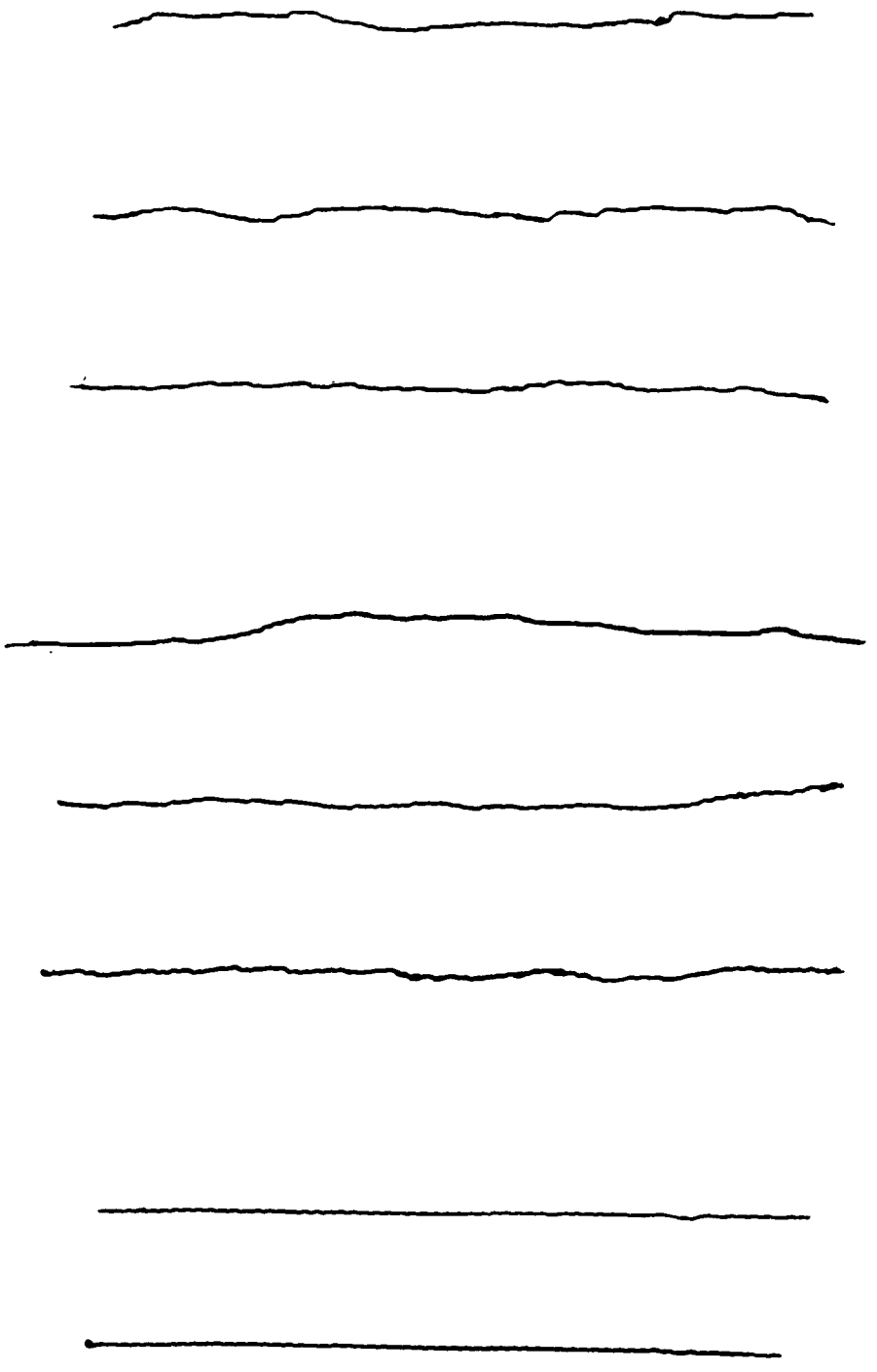

Figure 3.2: Typical surface profiles for natural and saw cut joints. Top set: natural Penrith sandstone, Middle set: natural Stainton sandstone and bottom set: saw cut Stainton sandstone. Scale 1: 1

CHAPTER 4

SIGNIFICANCE OF SYSTEM CONSTRAINTS IN TRIAXIAL TESTING OF JOINTED ROCK SPECIMENS

4.1 INTRODUCTION

After Von Carman (1911, quoted from Murrell, 1964) who pioneered the triaxial testing of rocks, it appears that the application of this test in the study of sliding behaviour of rock, was first used by the U S Bureau of Reclamation (1954) for testing the bond strength between concrete and rock. It was adopted for measurement of friction between the surfaces of a joint by Jaeger (1959), and has since been used extensively for investigating different aspects of discontinuous rock without giving enough attention to the end specimen condition, particularly to the problem of change of geometry of the specimen when sliding commences.

In an attempt to clarify the work conducted by previous researchers, a brief review is given with particular reference to the test condition characterizations of the triaxial test.

4.2 A REVIEW OF THE INVESTIGATIONS EMPLOYING THE TRIAXIAL TEST TO STUDY DISCONTINUOUS ROCKS

4.2.1 JOINTED ROCK CONTAINING SINGLE PLANE OF WEAKNESS

Jaeger (1959) used a triaxial apparatus to measure the angle or sliding friction of three rock types. Three types of joint were used: a 1 mm thickness plaster joint to act as a filler material, a bare surface of diamond saw cut, and a reasonably flat shear surface. Cylindrical specimens of length 125 mm and 50.8 mm diameter were subjected to axial

stresses and confining pressures up to 100 MPa. A spherical seat was used in the lower end of the specimens in the triaxial cell. He found that the initial coefficient of friction (prior to relative movement) was greater than the sliding coefficient of friction (the coefficient of friction when sliding is in progress along joint plane or the dynamic coefficient of friction; Jaeger and Cook, 1979). He concluded that, in general, the coefficient of friction does not vary widely among the three types of joints for a given material, and for a given angle. Jaeger mentioned the problem of change of geometry during sliding in this work, however, he did not apply any remedial solution.

He concluded that the Mohr-Coulomb theory of failure was applicable to the results, and identified the existence of a cohesive strength. It was attributed to the shear strength of the filler or the shearing off of protuberances.

Lane and Heck (1964) conducted a series of multi-stage triaxial tests (obtaining two or three stress points of the failure envelope with one specimen; Kovari and Tisa, 1975) using specimens of granite with a pre-established failure plane as the joint. The diameter of the specimens was 54 mm and the length 2 to 2.5 times the diameter. The specimens were tested after being saturated with water for three days, then the surface dried prior to testing. A spherical seat was used in the upper end of the specimen in the triaxial cell. They pointed out the difficulty of misalignment of the steel platens with specimen, due to the introduction of new stress from eccentric loading, as soon as sliding commences. For this reason in performing multi-stage triaxial test, care was taken, not to strain the specimens too far, in order to avoid sliding movement occurring along the joint surface.

They also used the Mohr-Coulomb theory to analyse their results, and the inclination of the Mohr envelope was considered as the joint friction angle. They showed that the highest envelope represents tests on intact cores, the lowest is from test on open joints.

One may accept these two envelopes as limits for the strength of the jointed rock mass, never as high as the strength of the intact joint, seldom as low as the strength of the open joint, but rather between these limits and often nearer to the lower one.

As noted Lane and Heck (1964) took care to avoid occurrence of sliding movement along the joint plane. Therefore, the friction angle measured is not a representative of sliding friction but, it is the initial coefficient of friction (prior to relative movement).

Handin and Stearns (1964) conducted triaxial tests to measure the sliding friction of dolomite. Specimens with diameter of 19 mm and length of 38 mm were cut with a diamond saw at different angles from 30 to 70° to the direction of major principal stress. The average coefficient of sliding friction calculated from the ratios of shear to normal stresses on the saw cuts at initiation of slipping was about 0.4, far different from internal friction which was equal to 1. There is no reference to the problem of end specimen condition in this work.

Jaeger and Cook (1969) conducted experiments on a number of different rocks and types of surface to study friction between rock surfaces. They used both the triaxial and a double shear apparatus with values of normal stress up to 48 MPa. The double shear apparatus consisted of three blocks in which one block was clamped between two others by a normal force applied through the side blocks. The shear load was applied through the middle block and caused to slide between the two others.

Experiments performed with shear apparatus showed in many cases that displacement took place linearly until the major stress or force reached a value above three-quarters of that necessary to maintain steady sliding. Displacement in excess of that due to compression then began and the frictional force increased asymptotically with

continued displacement. The same behaviour was observed in triaxial apparatus, but accompanied with occasional stick-slips during sliding.

The problem of change of geometry of cell-specimen system was pointed out in this study with no measures taken in this respect.

Jaeger (1970) in an experiment to study the behaviour of closely jointed rock, made a number of tests on cylindrical specimens containing a single joint in order to compare the results with those of cores having a considerable number of joints tested triaxially. He concluded that the multiple jointed material is substantially stronger than the material containing one joint, and that movement on one particular plane tends to dominate as strain increased.

Jaeger noted the problem of change of geometry of cell-specimen system during sliding and he adopted the procedure proposed by Rosengren (1968).

Horino and Ellickson (1970) conducted triaxial test experiments on three artificially and naturally jointed rock types in different confining pressures up to 28 MPa and different joint orientation angles. The specimens were of 54 mm diameter and 133.3 mm length. They applied the Mohr-Coulomb theory to analyze their data, by dividing the specimens into two groups: those that failed through the intact material and those that failed by sliding along the plane of weakness.

They concluded that the best method of determining the Mohr envelope for the solid material is by use of the mean normal stress and the maximum shear strength technique suggested by Jaeger (1960), and for the material having single plane of weakness, using the normal and shear stresses acting over the sliding surface is the most appropriate method. There is no reference to the problem of end condition in this study.

Byerlee (1975) carried out triaxial compression tests to study the frictional strength of Weber sandstone. The specimens used in this experiment were 25.4 mm diameter and 63.5 mm length. The specimens were cut at an angle of 30° to the axis of cylinder. The triaxial cell was that of Brace (1964) in which the axial load was applied on the specimen by a piston, and neither platen nor lubricant material were used between piston and specimen.

He concluded that, even though, the fracture strength of rock varies between wide limits, the frictional strength for both shear fracture surfaces and saw cuts is independent of rock type. Furthermore, he concluded from the results of this work and of his previous work (Byerlee, 1968) that the sliding strength of rocks can be fitted to two straight lines or to a curved line passing through the origin, and may be the same for all rock types.

4.2.2 TRIAXIAL TEST TO STUDY ANISOTROPIC ROCKS

A considerable amount of work has been carried out to study the effects of anisotropy in rocks, using triaxial testing techniques. In nearly all of them the effect of confinement on ultimate strength of anisotropic rock in different orientations has been investigated.

Donath (1961, 1962, 1966) made extensive experiments on different anisotropic rock using triaxial tests in a wide range of confining pressure. Cylindrical specimens of 25.4 mm diameter and length of 63.5 mm were selected containing anisotropy plane in different orientations from 0-90° with respect to the major principal stress. Results obtained for Martinsburg slate showed that two modes of deformation dominated, shear fracture and faulting with and without loss of cohesion. Furthermore the effect of anisotropy was pronounced on the peak strength. Specimens compressed perpendicular

to cleavage sustained the greatest stress, those compressed at an angle of 30° to cleavage showed the lowest strength. At confining pressures of 50 MPa and lower, faulting occurred with complete loss of cohesion. He showed that the curves of differential stress versus anisotropy orientation shifted upward with increased confining pressure, the shifting was proportional to the increase in confining pressure but not necessarily linear.

Donath made no reference to the effects of end conditions in these studies, he recognized, however, in another study (Donath, 1972), that boundary conditions can have a pronounced effect on the experimental results. He showed that the strength variability related to apparatus differences, ranging from 4 to 32% for different orientations of anisotropy plane.

Deklotz et al (1966) studied the effects of anisotropy on a schistose gneiss in confining pressure up to 70 MPa. The specimen diameter was 54 mm and the length 108 mm. The triaxial cell was that of Lane and Heck (1964) in which a spherical seat was used on the upper end of the specimen. They showed that stress and axial strain at failure are directionally dependent, so that the differences observed in stress and strain for different orientations were as much as 50% in shear stress and as high as 2 times in strain.

Youash (1966) used triaxial compression tests on four types of layered rocks for confining pressures of 0.1 to 31 MPa. Cores of 54 mm by 108 mm were prepared with the layer dipping from zero to 90° with respect to the major principal stress. He showed that the orientation of failure plane and rupture strength are highly affected by layering for all rocks tested, and that the plots of stress difference versus inclination of layering were concave upward with the maximum stress difference for zero and 90°, and minimum for 45 and 60° orientations. He concluded that in the deformation of layered rocks, slip along layers is the controlling mechanism of deformation for orientation

layering of 45 to 90° to major principal stress. Neither Deklotz et al (1966) nor Youash recognized the problems associated with the boundary conditions in their experiments.

Pomeroy et al (1971) studied the influence of a wide range of weakness plane orientations on the fracture of cylinders of coal subjected to triaxial compression. Specimens were 25.4 mm in diameter and 50 mm in length and a spherical seat was used at the top end of the specimen. They showed that for all orientations there is an increase in fracture strength with increase in confining pressure, the rate of increase being much the same for all orientations. They also fitted a power law equation to their results for each orientation. The general form of the equation was given as: $\sigma_1 = A\,\sigma_3^b + \sigma_c$, where A and b are constants, σ_c the uniaxial fracture strength and σ_1 the fracture strength at confining pressure σ_3.

4.2.3 TRIAXIAL TEST IN MODEL JOINT EXPERIMENTS

Triaxial tests on idealized jointed media have been carried out by a number of investigators. It seems that providing appropriate test conditions in triaxial testing of jointed models is of great significance. This is because of the fact that the mechanism of fracture, mode of failure and sliding through joint surfaces are more complicated in these types of experiments, in particular where a spherical seat or a steel ball has been used in the system they may lead to the development of high secondary stresses, and inhibit sliding along favourable directions. Reviews of the performed jointed model experiments reveal that no attempt has been made to modify testing systems.

Rosengren and Jaeger (1968) conducted triaxial tests on a random joint pattern instead of the more usual regular block pattern , by heating a course grain marble to 600° C, so that it became a compacted mass of crystals simulating a randomly jointed rock mass. The unconfined compressive strength of specimens increased rapidly with confining

pressure to nearly that of the original rock, and Young's modulus also increased with confining pressure, but was always considerably less than that of the original rock.

They showed that the mechanical properties of the heated marble were very different from those of soils and therefore, the soil mechanics theories were not applicable to such rock; and the attempts that have been made in the past to apply soil mechanics theories to poor and closely jointed rock were not justified.

Einstein et al (1969) performed triaxial tests on jointed models to investigate the influence of multiple joints on the strength of specimens using gypsum plaster as a model material. The specimens were of size 101.6 mm X 101.6 mm X 203.2 mm prepared with different sets of parallel, perpendicular and orthogonal joints. Confining pressure up to 14 MPa was applied, and a steel ball was used on the top platen of the specimen. They found that systematic variations occur in stress-strain behaviour for both different joint inclinations and joint spacings. Increased confining pressure resulted in transition from sliding behaviour to material fracture.

Brown and Trollope (1970) conducted triaxial experiments on a jointed model prepared with 25.4 mm cubes of gypsum plaster. Confining pressures up to 14 MPa were applied, and the triaxial cell was fitted with platens and a spherical seat at the top end of the specimen. They found that at low confining pressures the strength is minimum where the joints are inclined at 30/60^{o} to the specimen axes. At confining pressures of 7 and 14 MPa the behaviour was more ductile in character and the effects of joint pattern of the specimen strength became less noticeable. Most of specimens failed by sliding on one or more of the induced joint planes, or by one or more shear fracture planes across the intact and 0/90^{o} orientations.

Brown (1970) performed triaxial tests on jointed models using parallelepipedal and hexagonal blocks. The test conditions used were the same as those used by Brown and Trollope (1970). He showed that the Mohr-Coulomb concept with certain modification may be used to describe the strength of the specimens with discontinuous *joints. In none* of the reviewed jointed model experiments was there any attention paid to the boundary condition effects.

4.3 EFFECTS OF SYSTEM CONSTRAINTS ON THE EXPERIMENTAL RESULTS

In reviewing the previous investigations, it was pointed out that there was a lack of sufficient attention to the appropriate testing condition where a triaxial testing apparatus was used in experimental works on jointed rock. In order to show the significance of the end-specimen constraints on various aspects of the mechanical behaviour of jointed specimens, a series of triaxial tests were performed on jointed and intact specimens of three types of sandstone using different configurations of platen-specimen in the triaxial system.

In the conventional configuration of cell-specimen system in a triaxial apparatus a spherical seat is used at the top end of the specimen, which is referred to as the non-modified system in this study. In the other configuration a pair of steel discs were inserted on the top and bottom platens of the specimen and molybdenum grease was used to lubricate between the discs and platens of both ends. This configuration is referred to as the modified cell-specimen system. Other configurations such as the use of a platen and steel disc at two ends with no lubricant grease are also referred to as non-modified systems.

The most important mechanical characteristic aspects of intact and jointed rock types may be considered as the stress and strain at peak, sliding behaviour of jointed

specimens, and mode of deformation and sliding. It is for this reason that the following topics are discussed in detail:

(i) Effects on the stress and strain at peak;

(ii) Effects on the stress-strain and sliding characteristics;

(iii) Effects on the mode of sliding and failure.

Before discussing the effects of system constraints on the results care must be taken in the use of the terms such as Young's modulus and Poisson's ratio. By definition (Brown, 1986) Young's modulus can be calculated from the slope of the stress-strain curve of a specimen subjected to uniaxial loading. Similarly, Poisson's ratio may be calculated by employing the uniaxial compressive test results. Therefore, when triaxial loading conditions are used in testing rock specimens, one must differentiate between the axial stress-axial strain curves from the triaxial test and the equivalent one that would acquired from a uniaxial test. However, throughout this thesis for the sake of simplicity the expressions of modulus and ratio have been used, but efforts have been made to differentiate them by adding other terms. For this reason, the slope of the stress-strain curve (in triaxial and jointed specimens testing) is termed the "apparent modulus of deformation" or briefly "modulus of deformation" and the ratio of the lateral strain to the axial strain is termed the "instantaneous Poisson's ratio".

4.3.1 EFFECTS ON THE STRESS AND STRAIN AT PEAK

Ultimate strength and the corresponding strain of rocks whether jointed or intact are the most important factors for design purposes. These have been highly affected by the end-specimen conditions in this investigation.

Tables 4.1 to 4.3 illustrate the axial stress and axial strain at peak for Stainton sandstone specimens containing saw cut joints with 30, 45 and 60° orientations (with respect to the minor principal stress) tested in two systems under various confining pressures.The discrepancy in peak strength and displacement for each orientation as seen in the tables is significant, and differs for different confining pressures and orientations. The differences rise in order of magnitude from 30 to 60°. In specific, as the joint inclination angle becomes nearer to the sliding angle, the discrepancies increase. The differences between two systems in 5 MPa confining pressure, for instance, on the strength and deformation at peak, are 4.7% and 8.2% for 30°, 13.3% and 45.7% for 45°, and 80.4% and 64.7% for 60° respectively. For the 10 and 15 MPa confining pressures as one can see from tables 4.1 to 4.3 the trends are similar to those observed for 5 MPa confining pressure.

4.3.2 EFFECTS ON THE STRESS-STRAIN AND SLIDING CHARACTERISTICS

Figures 4.1 to 4.3 and 4.4 to 4.6 illustrate the stress-strain plots of Stainton sandstone specimens with saw cut joint tested in the non-modified and modified systems with orientation angles of 30, 45, and 60°, and confining pressures up to 30 MPa. Comparison of the plots reveals the pronounced effects of the two systems on the strength, deformability and sliding behaviour of jointed surfaces. In figure 4.6 which shows the stress-strain curve for 60° orientation in the modified system, with the beginning of loading, stress increases mostly linearly up to about three-quarters of the stress needed to maintain steady sliding over joint plane, then with the beginning of sliding along the joint, stress increases along a lower slope up to the peak, and eventually sliding continues through the joint plane at a near constant value. This implies that after peak in this case, shear and normal stresses are nearly independent of further displacement, indication a constant coefficient of sliding friction over the joint surfaces.

In figure 4.3 which illustrates stress-strain curves of the specimens with the same orientation and confining pressure as of figure 4.6 tested in the non-modified system, sliding characteristics are completely different from that of figure 4.6. In this case, after sliding initiated stress rises non-linearly up to a peak , it then drops to a certain point and rises again. These series of events are continued and accompanied by violent stick-slips (see chapter 9 for full investigation on stick-slip). The normal and shear stresses across the joint are thus variable, and therefore, the coefficient of sliding friction in this condition is not constant. The coefficient of sliding friction for 10 MPa confining pressure as determined using the modified system is 0.66, while with the non-modified system, it was found, ranging from 0.66 to 0.96. Comparing figures 4.2 and 4.5 the same discrepancies as 60^{o} orientation are observed for the specimens tested with orientation of 45^{o}.

Comparison of figures 4.1 and 4.4 for 30^{o} orientation shows that the discrepancy between the peak stresses is not as much as for 45 and 60^{o} orientations. However, the strain at peak and the apparent modulus of deformability have been highly affected. As is observed from figure 4.1 the non-modified system has affected the strain at peak in an unexpected manner. In figure 4.4 (modified system) both stress and strain at peak have increased with confining pressure. In figure 4.1 (non-modified system), however, there is no such trend and the differences of the strain at peak for the various confining pressures are insignificant.

In the post-failure region (figures 4.1 and 4.4), again as sliding commenced along shear failure plane,some difference is clearly observed. Sliding smoothly continued with no high fluctuation in the residual stress value for the modified system (figure 4.4); however, in the non-modified system (figure 4.1) sliding was accompanied by stick-slips with high fluctuations in the residual stress value.

In fact, in the case of 30° joint inclination and also in other cases in which failure mechanism is not dominated by sliding along the joint plane, but by a new shear failure through the intact rock transcending the joint plane, effects of the cell-specimen system on the magnitude of stress at peak are not very significant. However, effects of non-modified system on the strain at peak and modulus of deformability and also on the characteristics of post-failure, particularly on the residual stress region cannot be neglected.

In order to show the effects of cell-specimen system on stress-strain characteristics of intact specimens, triaxial tests were carried out on Penrith sandstone specimens under 15 and 30 MPa confining pressures using different conventional configurations of seat and platens in triaxial cell. The resulting curves can be seen in figures 4.7 4.8. Comparison of the plots with those of the modified system (figure 4.11 plots 15 and 30) reveals that in spite of near equality in peak stress value, the residual region in the non-modified systems is completely different from that of the modified system, in the sense that the residual stress region in the modified system with a negative slope continues asymptotically, in non-modified systems, however, this region does not have a steady slope, but different fluctuations in the stress level with occasional stick-slips. Therefore, the use of the modified cell-specimen system in triaxial testing of intact specimens also improves the studying of the deformability of the rock specimens.

Figures 4.13 and 4.14 illustrate the stress-strain curves of Stainton sandstone specimens with saw cut joints at inclination of 15 and 90° respectively, and under confining pressures up to 15 MPa tested in the non-modified system. Comparison of these with the plots in figure 4.1 (for 30° joint orientation tested in the same system) shows a higher peak stress for 30° orientation particularly in lower confinements (5 and 10 MPa).

This may be attributed to the inappropriate testing system, in the sense that at 30° orientation, mechanism of deformation is not purely by shear failure, but is a combination of sliding and shear fracture, i.e., before stress reaches the peak a little sliding occurs along joint surfaces while at lower confinement the sliding becomes greater. Such an event causes changes the geometry of cell-specimen, and it introduces a new condition at the ends of the specimen which is far different from the conditions in orientations for 15 and 90°; leading therefore to unexpected results.

4.3.3 EFFECTS ON THE MODE OF SLIDING AND FAILURE

The cell-specimen systems had pronounced effects on both mode of sliding and failure for the orientations in which the mechanism of failure dominates either by sliding along the joint plane or by a new shear failure through intact rock. Figures 4.15 to 4.18 illustrate the load-displacement curves of Penrith sandstone specimens containing a saw cut joint taken by X-Y recorder, tested in two systems for the joint orientations of 45 and 60° and confining pressures of 10 and 30 MPa. In the modified system, for both 45 and 60° orientations, sliding continues at a nearly constant stress value throughout with no significant fluctuation in stress during sliding. In the non-modified system, however, high amplitude fluctuations in load (stress) are observed continuously during sliding with occasional sudden stress drop in the form of stick-slip events. The continuous fluctuations in load in 60° orientation in this case is as high as 239 KN (equivalent to 52 MPa as in figure 4.18 upper plot).

Continuation of sliding in the non-modified system for 45° orientation under both 10 and 30 MPa confining pressures as in figures 4.15 and 4.16, eventually resulted in the fracture of specimen by a new shear plane through intact rock, whereas in modified system sliding continued asymptotically with no fracture through intact material.

The discrepancy in mode of sliding and failure, and also in other behavioural aspects of intact and jointed specimens discussed in the above sections is due to the fact that in a non-modified system as sliding along joint is initiated, because of change of the geometry of cell-specimen system, a full contact between two halves of a specimen cannot be maintained, and with further sliding it becomes worse. Consequently, the stress is concentrated on a portion of the joint sliding surface leading to the crushing of intact rock material in the strained portions which is appeared as fluctuations in stress and occasional stick-slips, and finally failure occurs by a shear fracture plane transcending the joint.

Plates 4.5 and 4.6 show the mode of failure for 45 and 60° orientations tested in both modified and non-modified systems. As can be seen, subsidiary fractures through the specimens tested in non-modified system are observed whether in the wedges of the sliding surfaces in 60° orientation or through the intact rock material in 45° orientation. It is interesting to note that, although 60° joint inclination is a very convenient angle for sliding, in some cases, in addition to the subsidiary fractures through the wedges of specimen, shear fracture also occurred through the intact rock (plate 4.6). On the other hand, subsidiary fractures in the specimens tested in modified system were not observed at all in 45 and 60° orientations.

Furthermore, examination of plates 4.2-4.4 reveals that the testing system affects the mode of failure in other orientations such as 0, 15 and 30°. In these orientations tested in non-modified system, the number of secondary fractures are considerably more than those of the modified system. Even in an intact specimen the discrepancy in mode of failure is clearly observed as in plate (4.1). However, for the intact specimens tested in the modified system a major shear failure plane is seen with very occasional secondary fractures.

Table 4.1 Stress and strain variations in Stainton sandstone specimens with 60° joint orientation tested in the modified and non-modified cell-specimen systems.

	non-modified		modified		difference	
σ_3 (MPa)	$\sigma_1-\sigma_3$ (MPa)	ε_1 at peak %	$\sigma_1-\sigma_3$ (MPa)	ε_1 at peak %	$\sigma_1-\sigma_3$ %	ε_1 %
5	37	2.80	20.5	1.7	80.4	64.7
10	65	3.2	35.3	1.8	84.1	77.7
15	63	4.3	40	1.8	57.5	13 7.7

Table 4.2 Stress and strain variations in Stainton sandstone specimens with 45° joint orientation tested in the modified and non-modified cell-specimen systems.

	non-modified		modified		difference	
σ_3 (MPa)	$\sigma_1-\sigma_3$ (MPa)	ε_1 at peak %	$\sigma_1-\sigma_3$ (MPa)	ε_1 at peak %	$\sigma_1-\sigma_3$ %	ε_1 %
5	88	2.55	75	1.75	13.3	45.7
10	117	3.1	102	2.25	14.7	37.8
15	135	3.25	123	2.3	9.7	41.3

Table 4.3 Stress and strain variations in Stainton sandstone specimens with 30° joint orientation tested in the modified and non-modified cell-specimen systems.

	non-modified		modified		difference	
σ_3 (MPa)	$\sigma_1-\sigma_3$ (MPa)	ε_1 at peak %	$\sigma_1-\sigma_3$ (MPa)	ε_1 at peak %	$\sigma_1-\sigma_3$ %	ε_1 %
0	64	1.25	60	1.15	6.6	8.6
5	101	1.31	106	1.21	4.7	8.2
10	116	1.35	125	1.26	7.2	7.1
15	144	1.38	140	1.4	2.8	1.43

Similar behaviour for other rock types tested in two systems also occurred. Among them figures 4.19 and 4.20, for instance, show the sliding characteristics of Dumfrith sandstone specimens containing saw cut joints with 60° orientation, tested in two systems. As is observed cell-specimen systems have influenced the various aspects of mechanical characteristics of jointed specimens in this rock the same as other rocks discussed before. Mode of sliding and magnitudes of stress and strain at peak have been highly affected through two systems under both 10 and 15 MPa confining pressures. The discrepancy in maximum stress for 10 MPa confinement, for instance, is seen to be about 42%.

Table 4.1 Stress and strain variations in Stainton sandstone specimens with 60° joint orientation (saw cut) tested in the modified and non-modified cell-specimen systems.

	non-modified		modified		difference	
conf. pres. (MPa)	axial str. at peak MPa	st. at peak % (axial)	axial str. at peak MPa	st. at peak % (axial)	stre. %	strain %
5	37	2.80	20.5	1.7	80.4	64.7
10	65	3.2	35.3	1.8	84.1	77.7
15	63	4.3	40	1.8	57.5	137.7

uniaxial
M NM

10 MPa
M NM

15 MPa
M NM

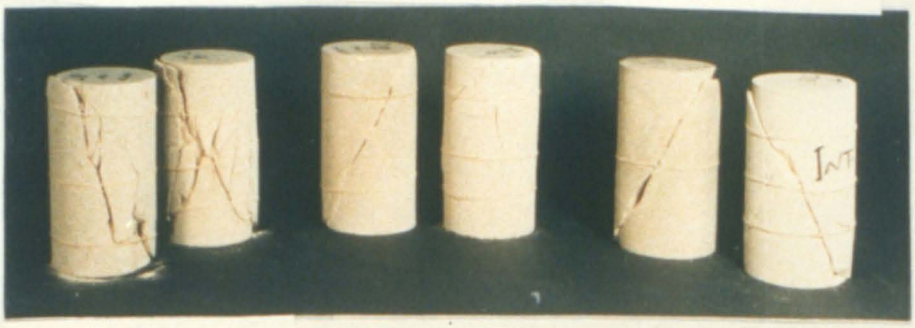

Plate 4.1

10 MPa
NM M

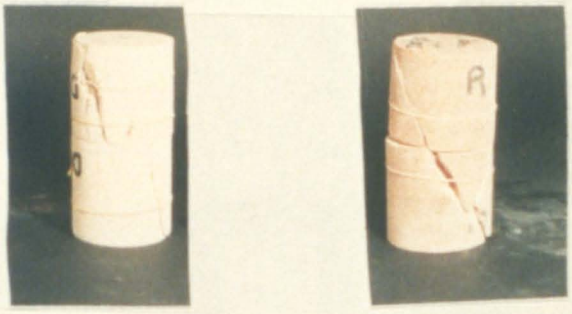

Plate 4.2

10 MPa
M NM

15 MPa
NM M

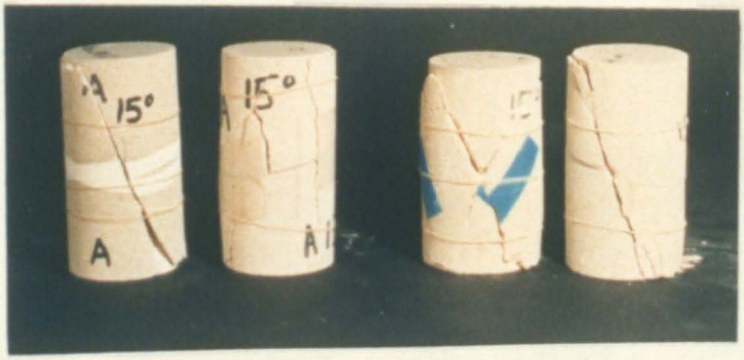

Plate 4.3

Plates 4.1 to 4.3 Fractured and deformed specimens affected by the end-specimen conditions using Modified (M) and Non-Modified (NM) cell-specimen systems, joint angle: unjointed (plate 4.1), zero degree (plate 4.2) and 15° (plate 4.3).

5 MPa 10 MPa 15 MPa
M NM M NM M NM

Plate 4.4

5 MPa 10 MPa 15 MPa
M NM NM M NM M

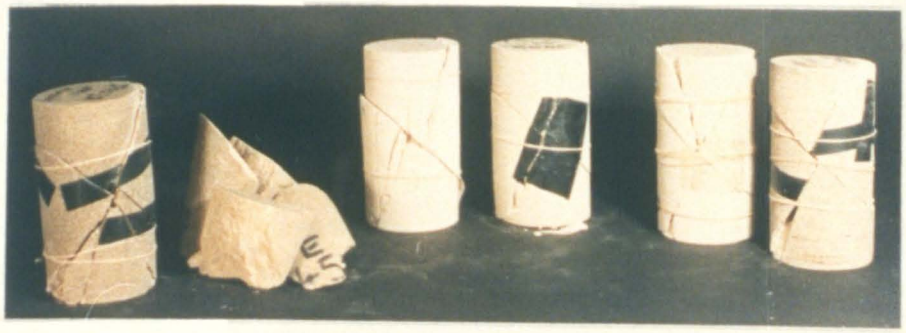

Plate 4.5

5 Mpa 10 MPa 15MPa
M NM M NM M NM

Plate 4.6

Plates 4.4 to 4.6 Fractured and deformed specimens affected by the end-specimen conditions using Modified (M) and Non-Modified (NM) cell-specimen systems, joint angle: 30° (plate 4.4), 45° (plate 4.5) and 60° (plate 4.6).

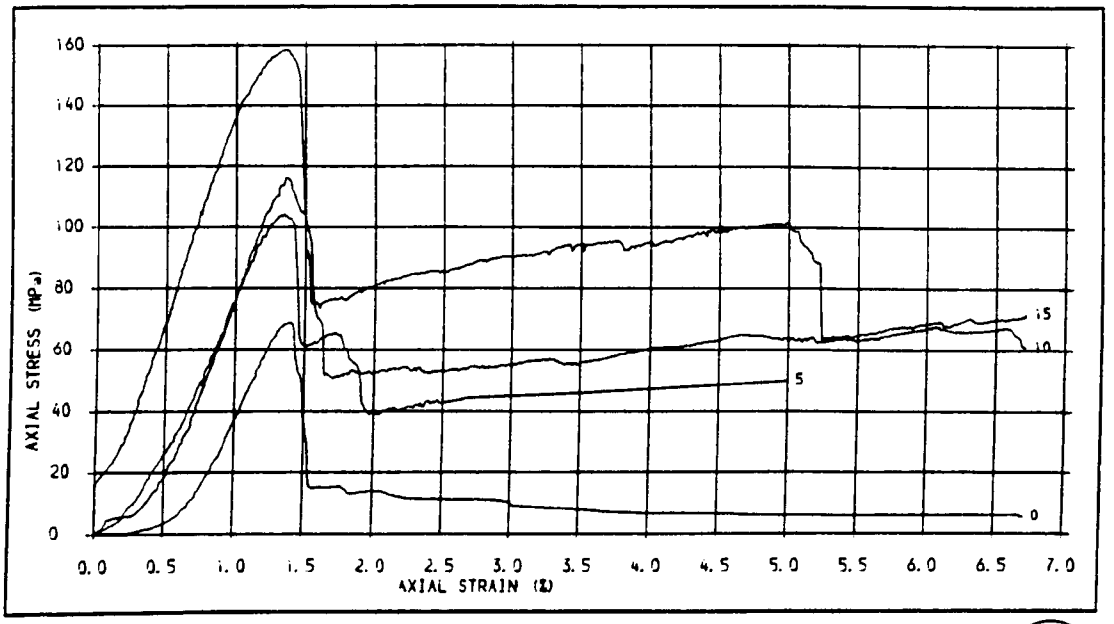

Fig. 41 . STRESS-STRAIN CURVES FOR SS SPECIMENS WITH SAW CUT JOINTS TESTED IN NON-MODIFIED CELL-SPECIMEN SYSTEM, JOINT ANGLE = 30 DEG. CONF. PRES. = 0, 5, 10 AND 15 MPa.

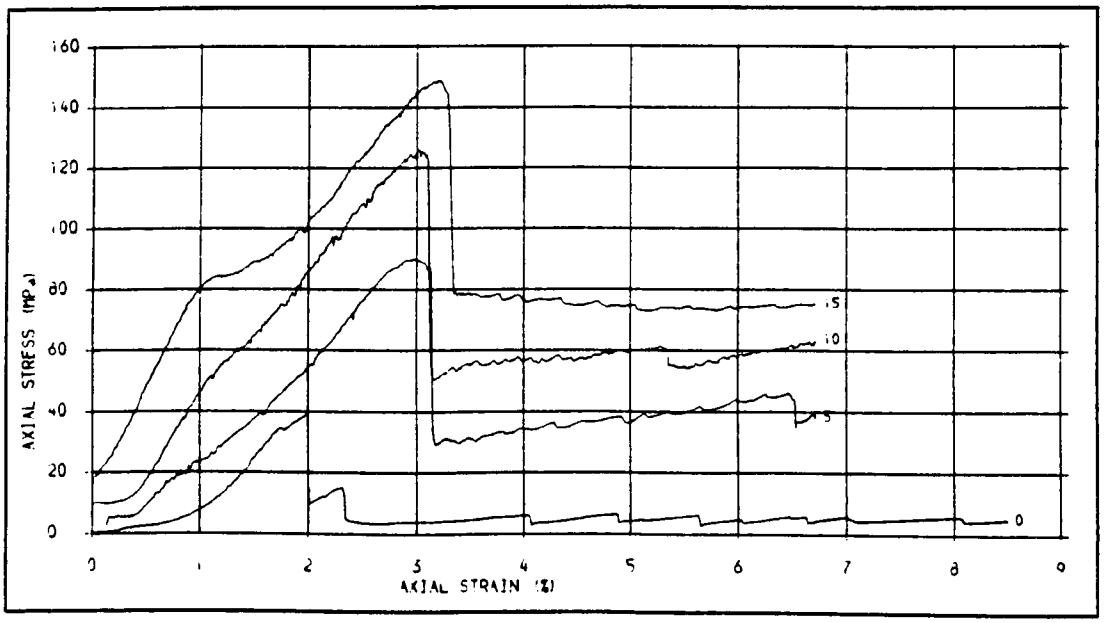

Fig. 42 . STRESS-STRAIN CURVES FOR SS SPECIMENS WITH SAW CUT JOINTS TESTED IN THE NON-MODIFIED SYSTEM, JOINT ANGLE = 45 DEG. CONFINING PRESSURES= 0, 5, 10 & 15 MPa

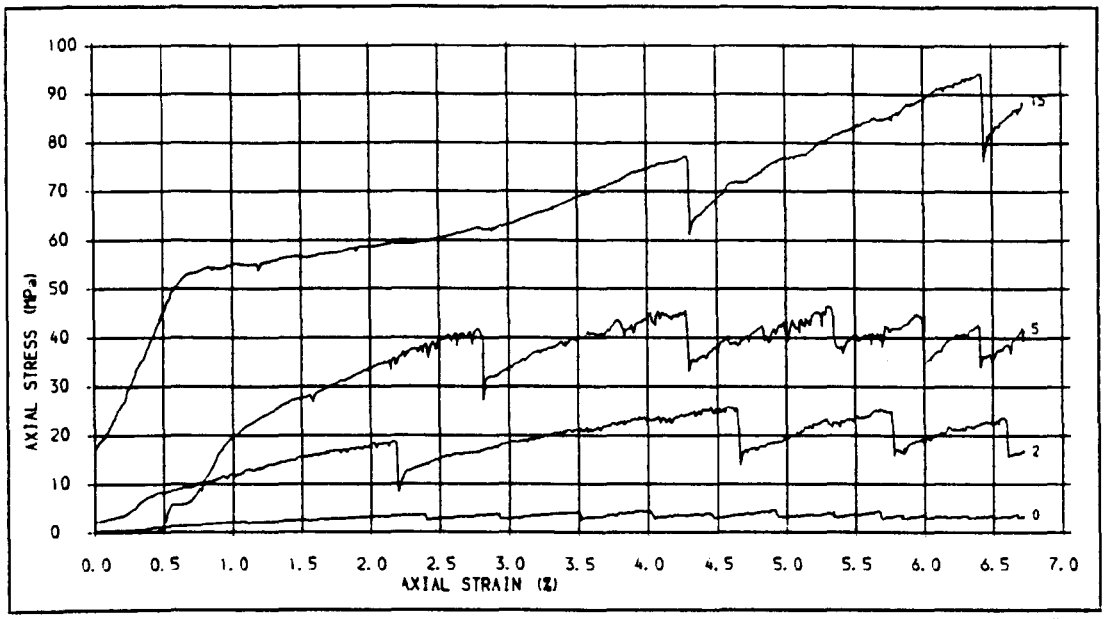

Fig. 43 . STRESS-STRAIN CURVES FOR SS SPECIMENS WITH SAW CUT JOINTS TESTED IN THE NON-MODIFIED SYSTEM, JOINT ANGLE= 60 DEG. CONFINING PRESSURES= 0, 2, 5 & 15 MPa.

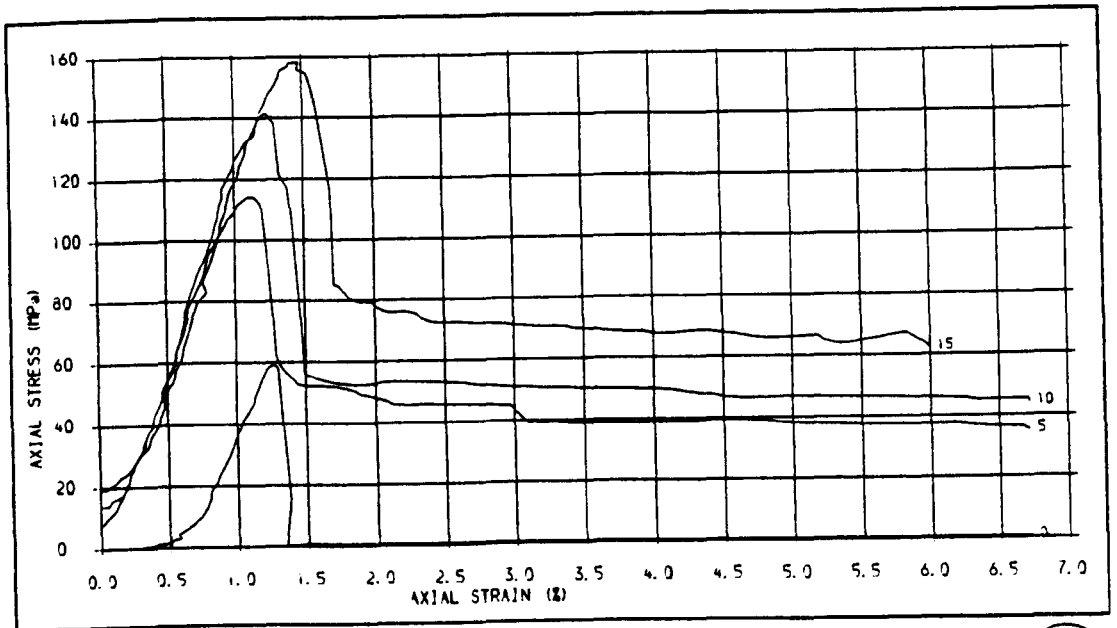

Fig. 44 . STRESS-STRAIN CURVES FOR SS SPECIMENS WITH SAW CUT JOINTS TESTED IN THE MODIFIED SYSTEM, JOINT ANGLE = 30 DEG., CONFINING PRESSURES = 0, 5, 10 AND 30 MPa.

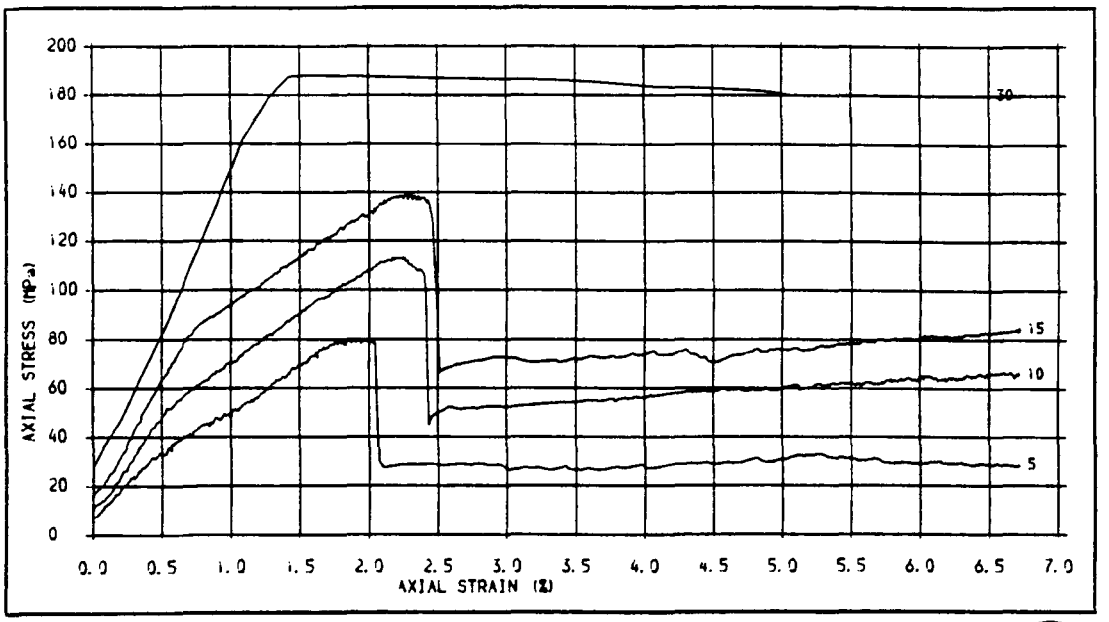

Fig. 45 . STRESS-STRAIN CURVES FOR SS SPECIMENS WITH SAW CUT JOINTS, JOINT ANGLE = 45 DEG. TESTED IN THE MODIFIED SYSTEM,, CONFINING PRESSURES = 5, 10, 15 AND 30 MPa.

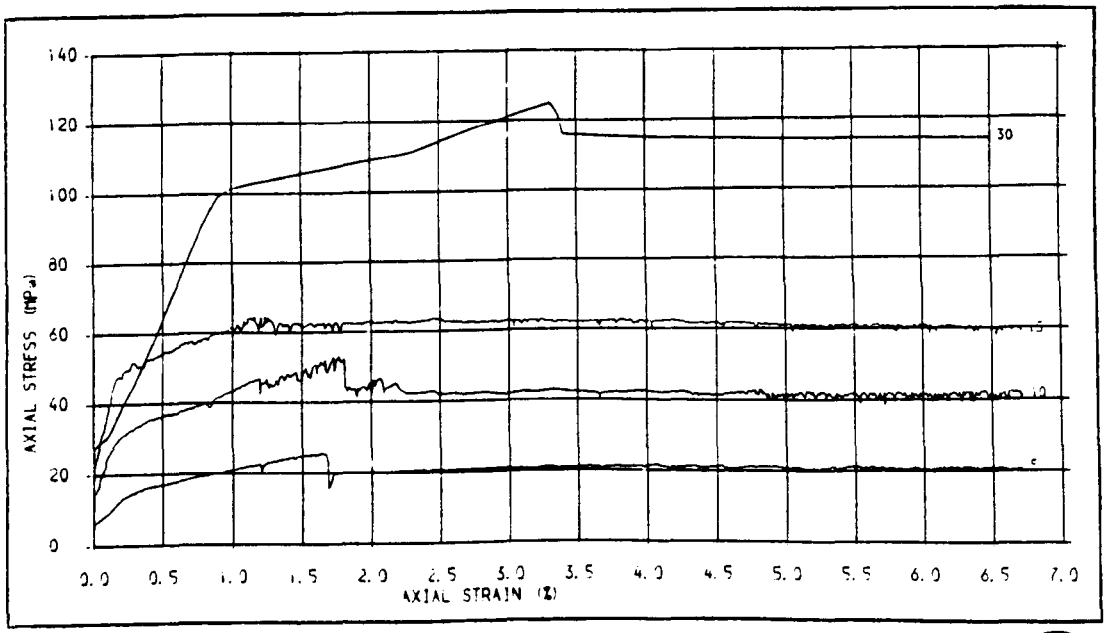

Fig. 46 . STRESS-STRAIN CURVES FOR SS SPECIMENS WITH SAW CUT JOINTS, JOINT ANGLE = 60 DEG. CONFINING PRESSURES = 5, 10, 15 AND 30 MPa, TESTED IN THE MODIFIED SYSTEM.

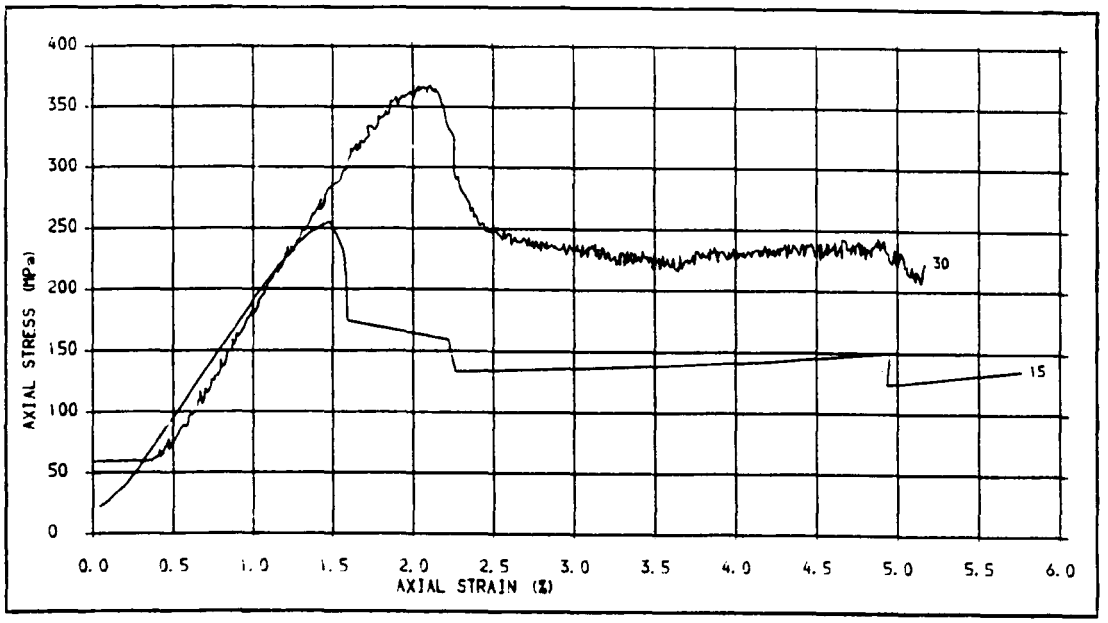

Fig. 47 . STRESS-STRAIN CURVES FOR PS SPECIMENS (INTACT) TESTED IN THE NON-MODIFIED SYSTEM CONF PRES= 15 AND 30 MPa, TYPE OF PLATENS. A PAIR OF DISCS WITH NO LUBRICANT GRE

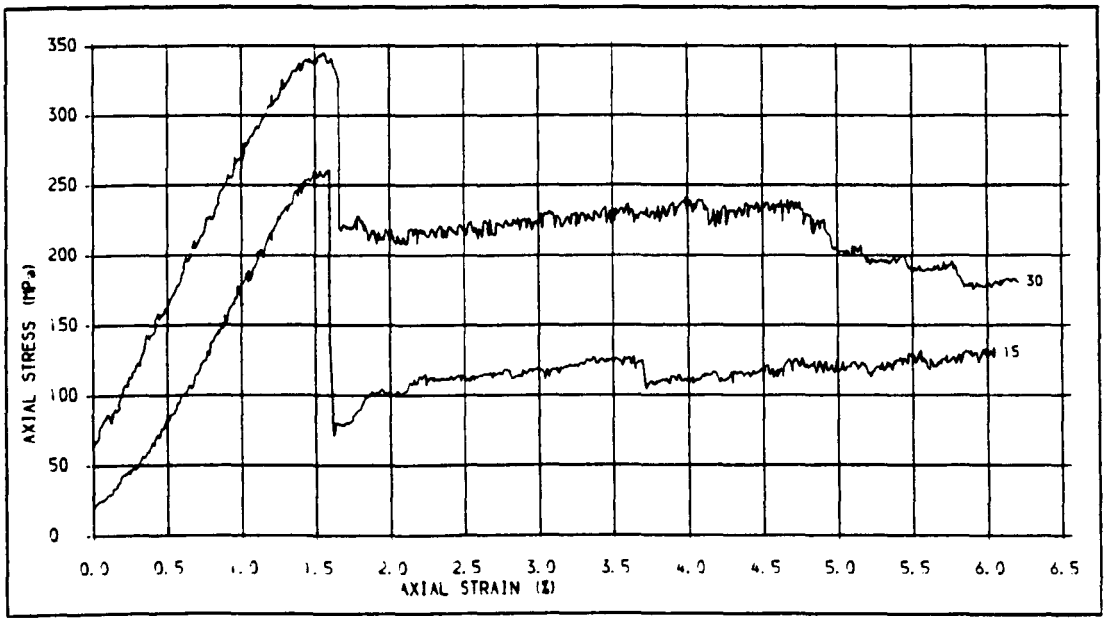

Fig. 48 . STRESS-STRAIN CURVES FOR PS INTACT SPECIMENS TESTED IN THE NON-MODIFIED SYSTEM (A SPHERICAL SEAT AT THE TOP), CONFINING PRESSURES= 15 AND 30 MPa.

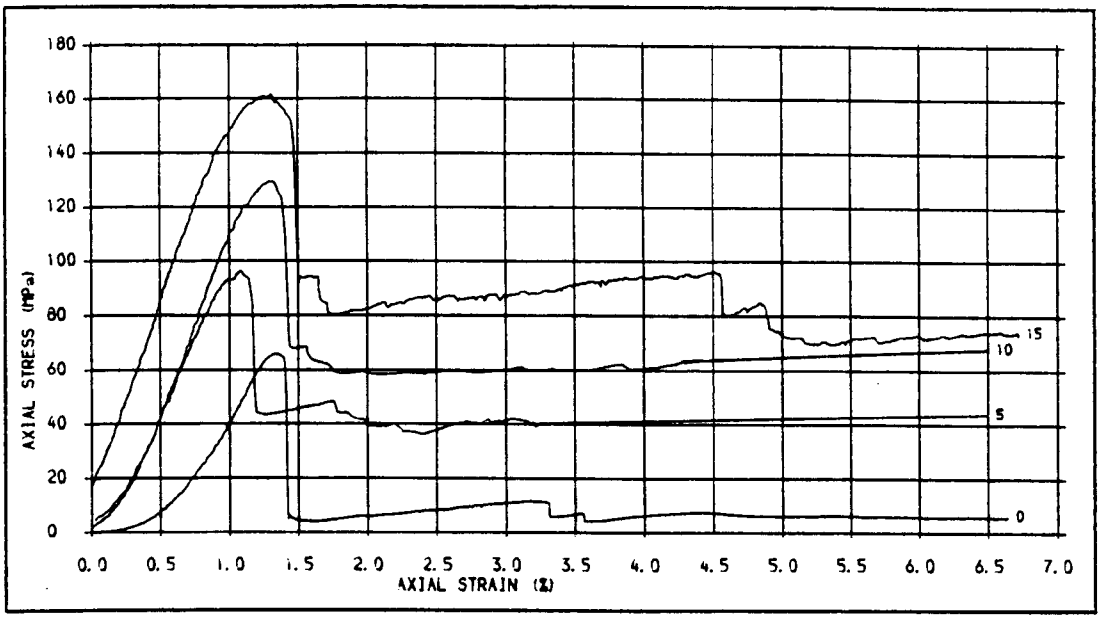

Fig. 49 . STRESS-STRAIN CURVES FOR SS SPECIMENS TESTED IN THE NON-MODIFIED SYSTEM, JOINT ANGLE = 0 DEG., CONFINING PRESSURES = 0, 5, 10, 15 MPa.

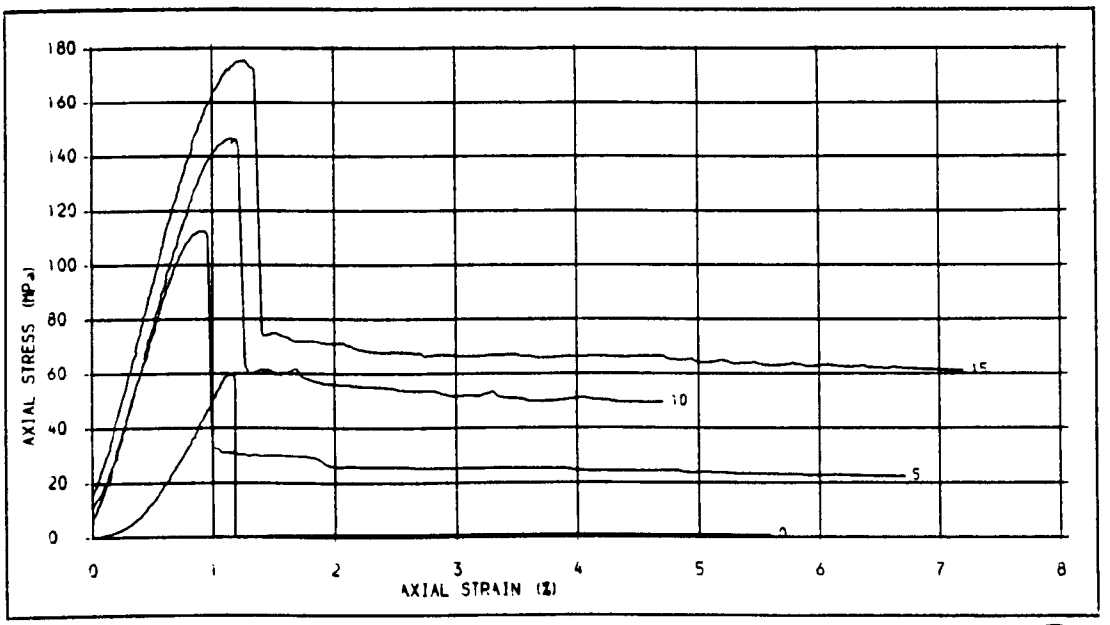

Fig. 410 . STRESS-STRAIN CURVES FOR INTACT SS SPECIMENS TESTED IN THE MODIFIED SYSTEM CONFINING PRESSURE = 0, 5, 10 AND 15 MPa.

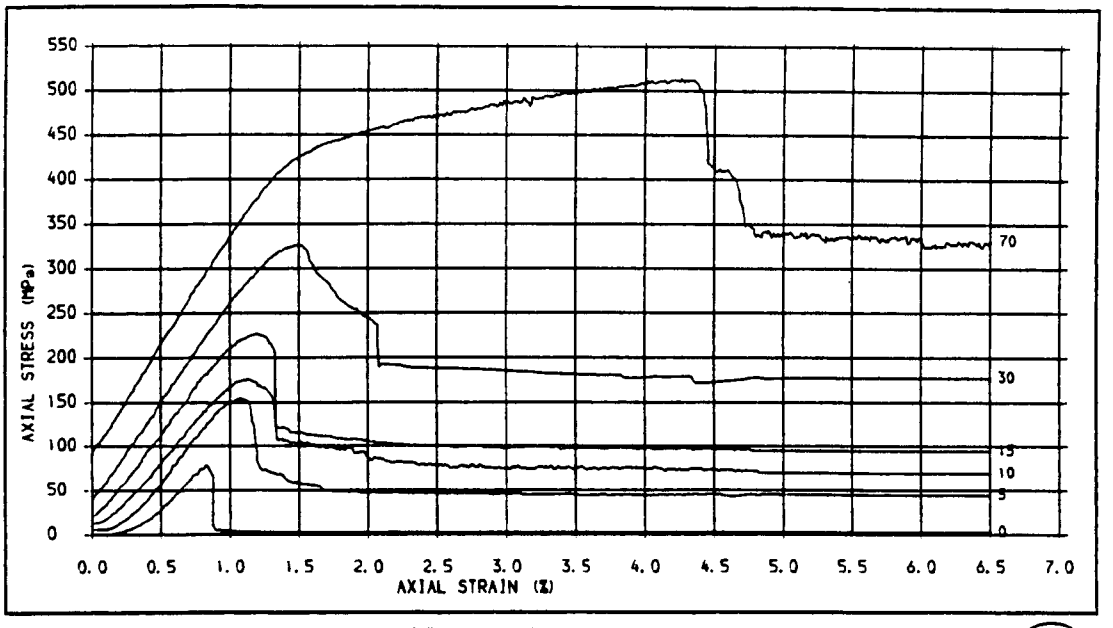

Fig. 4.11 . STRESS-STRAIN PLOTS FOR INTACT PENRITH SANDSTONE SPECIMENS, TESTED IN THE MODIFIED SYSTEM, CONFINING PRESSURES = 0, 5, 10, 15, 30 AND 70 MPa

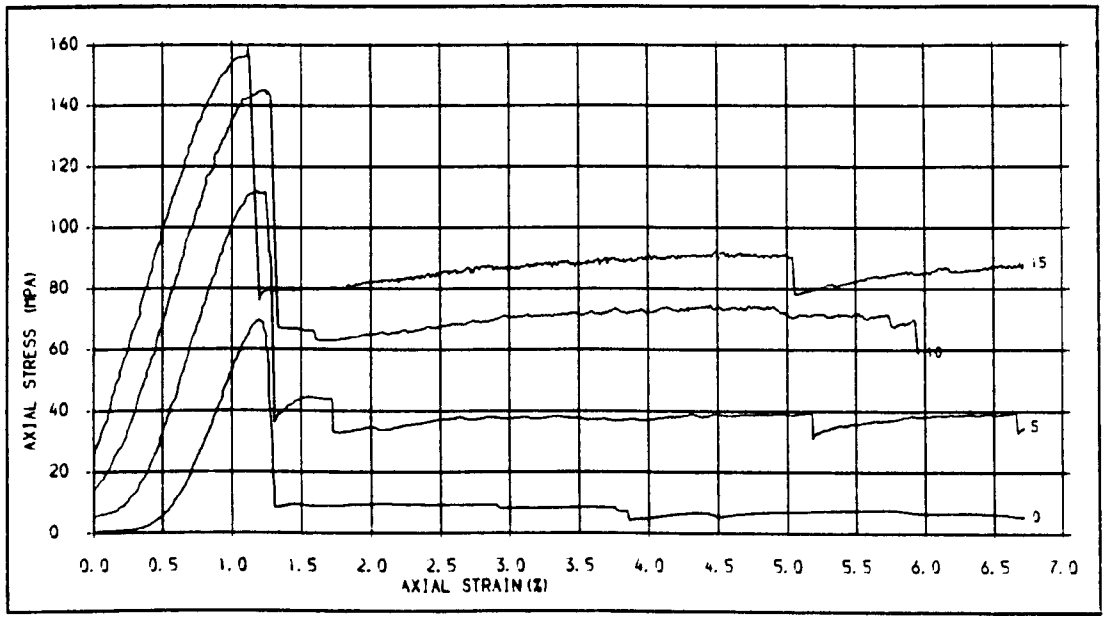

Fig. 4.12 . STRESS-STRAIN CURVES FOR INTACT SS SPECIMENS TESTED IN THE NON-MODIFIED SYSTEM CONFINING PRESSURES = 0, 5, 10 AND 15 MPa.

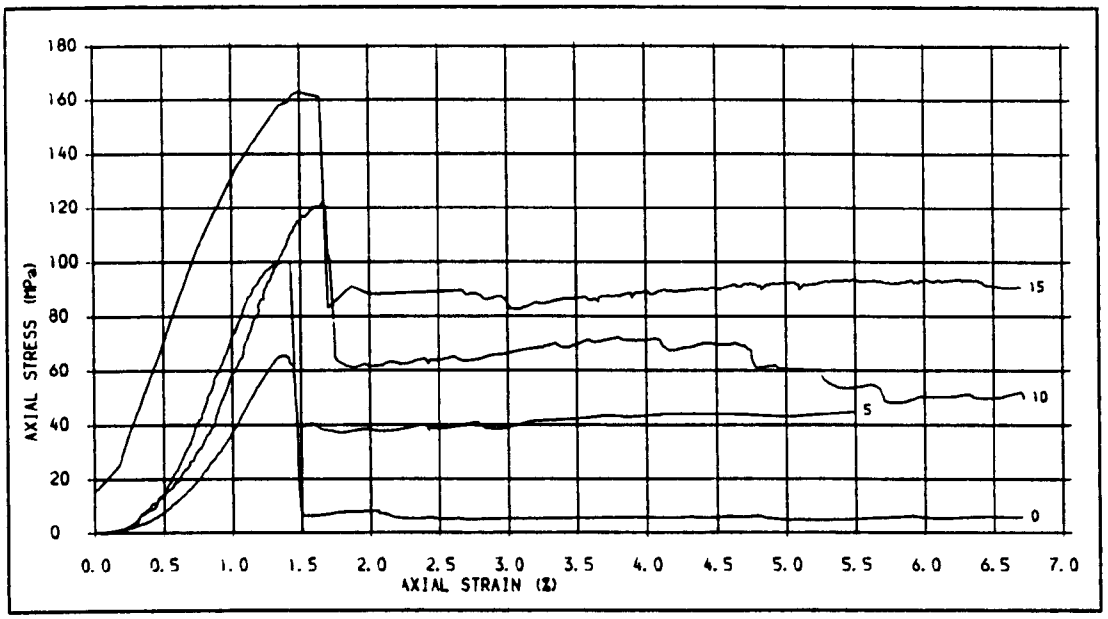

Fig. 4.13 . STRESS-STRAIN CURVES FOR SS SPECIMENS WITH SAW CUT JOINTS, JOINT ANGLE = 15 DEG. TESTED IN THE NON-MODIFIED SYSTEM, CONFINING PRESSURES = 0, 5, 10 AND 15 MPa.

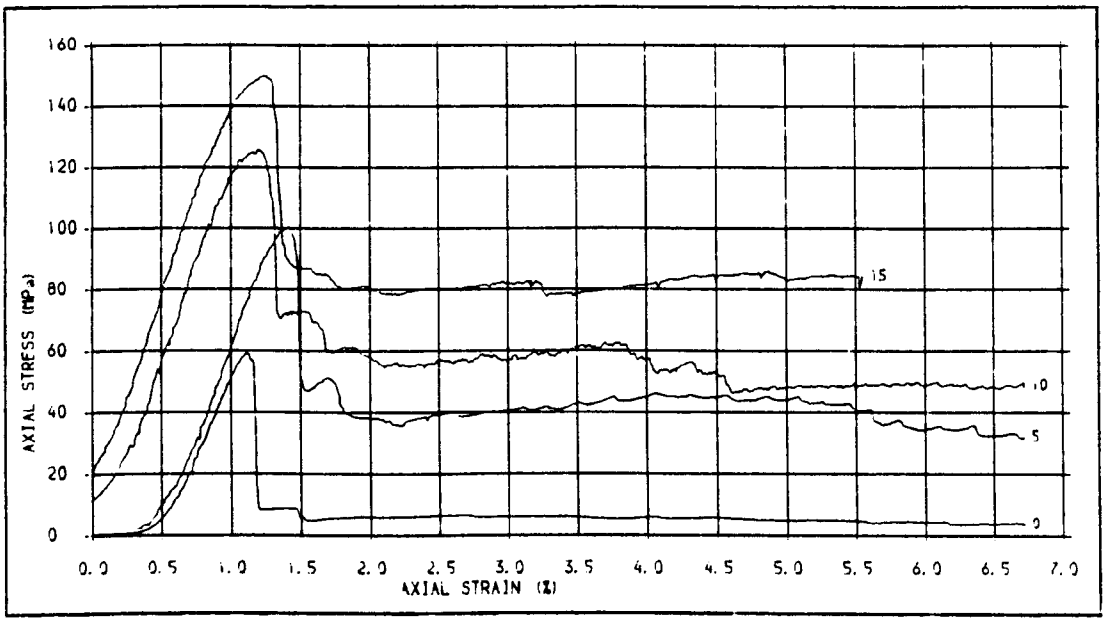

Fig. 4.14 . STRESS-STRAIN CURVES FOR SS SPECIMENS WITH SAW CUT JOINTS, JOINT ANGLE = 90 DEG. TESTED IN THE NON-MODIFIED SYSTEM, CONFINING PRESSURES = 0, 5, 10 AND 15 MPa.

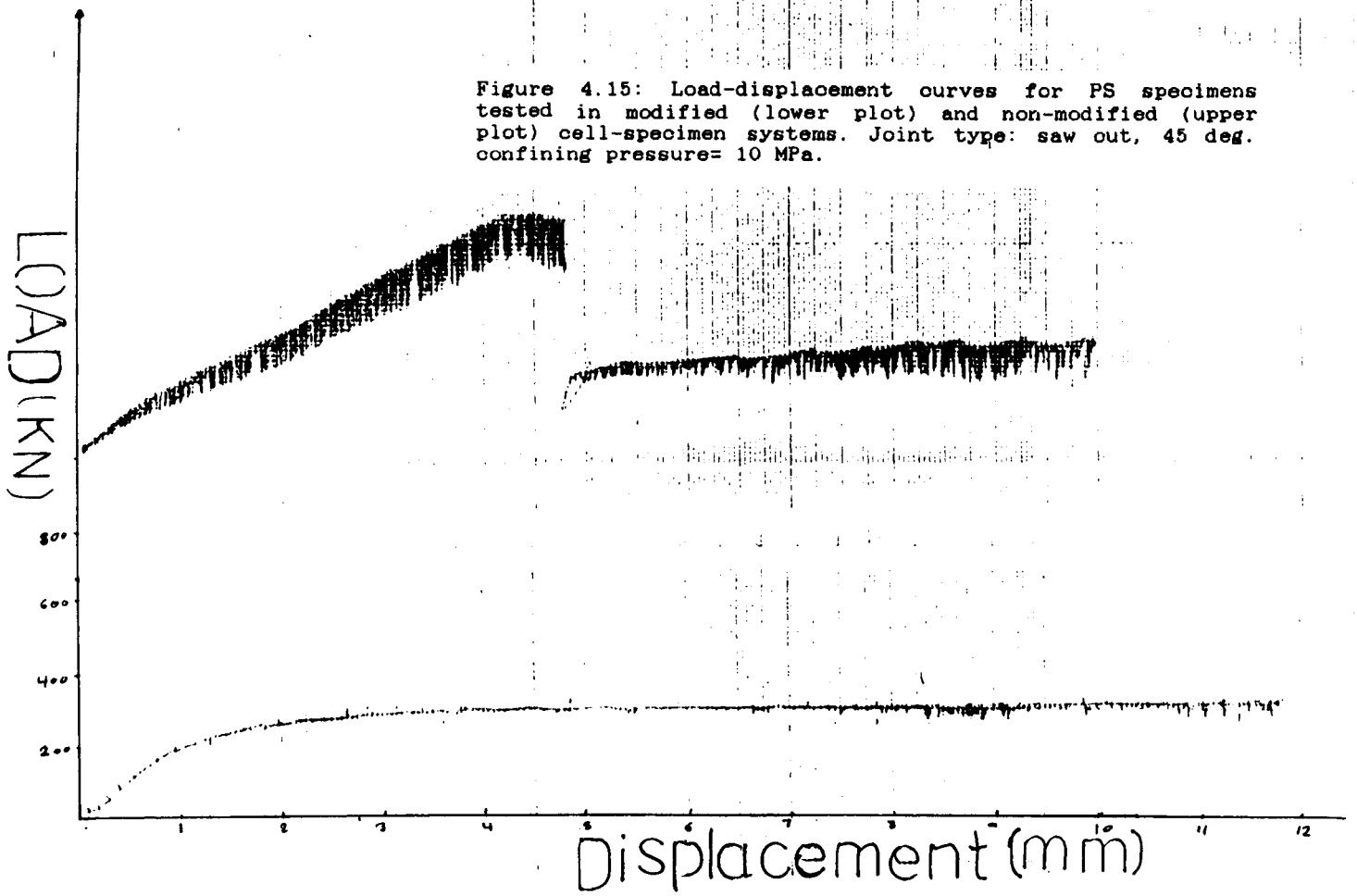

Figure 4.15: Load-displacement curves for PS specimens tested in modified (lower plot) and non-modified (upper plot) cell-specimen systems. Joint type: saw out, 45 deg. confining pressure= 10 MPa.

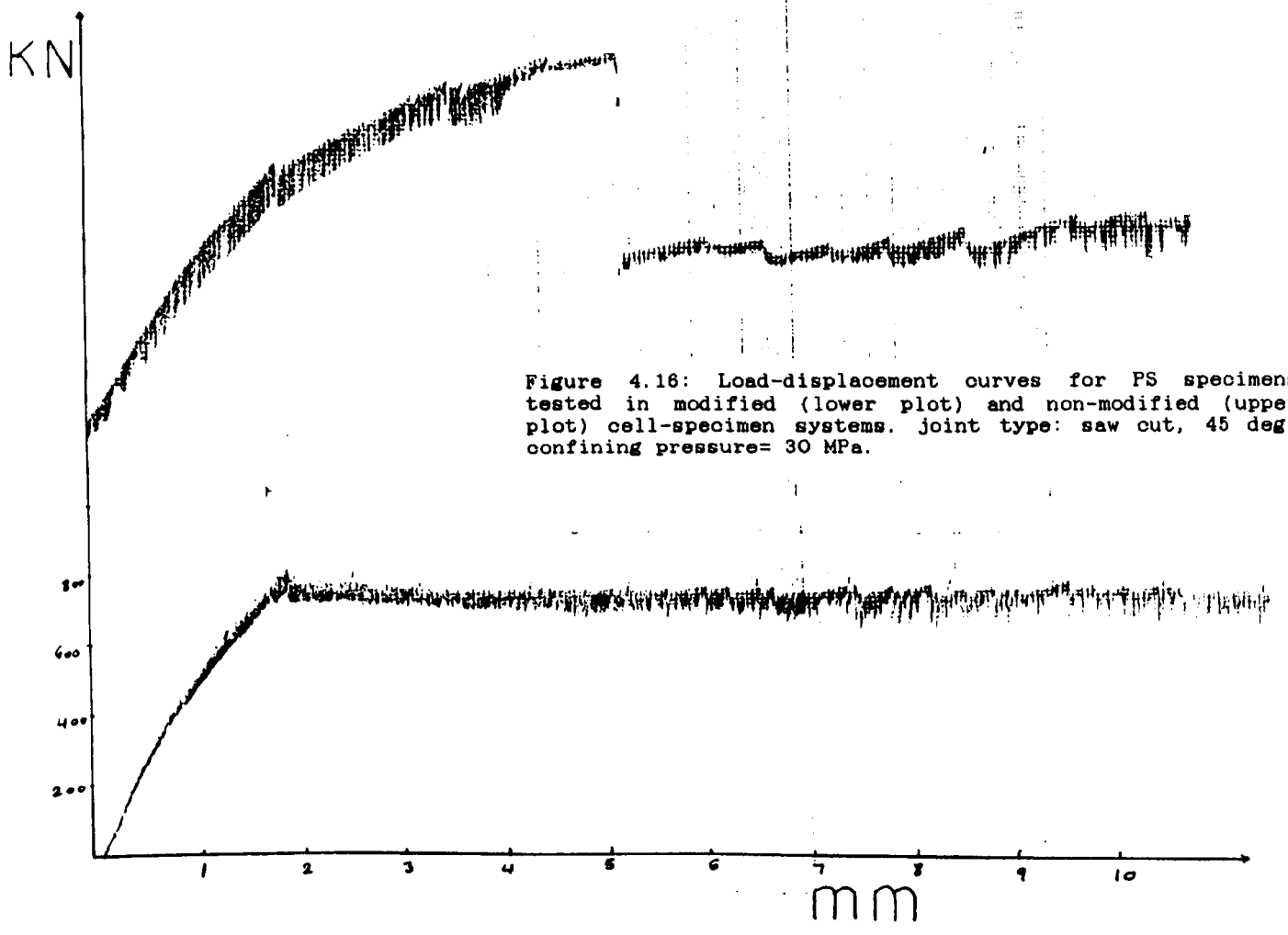

Figure 4.16: Load-displacement curves for PS specimens tested in modified (lower plot) and non-modified (upper plot) cell-specimen systems. joint type: saw cut, 45 deg. confining pressure= 30 MPa.

Figure 4.18: Load-displacement curves for PS specimens tested in modified (lower plot) and non-modified (upper plot) cell-specimen systems. joint type: saw out, 60 deg. confining pressure= 30 MPa.

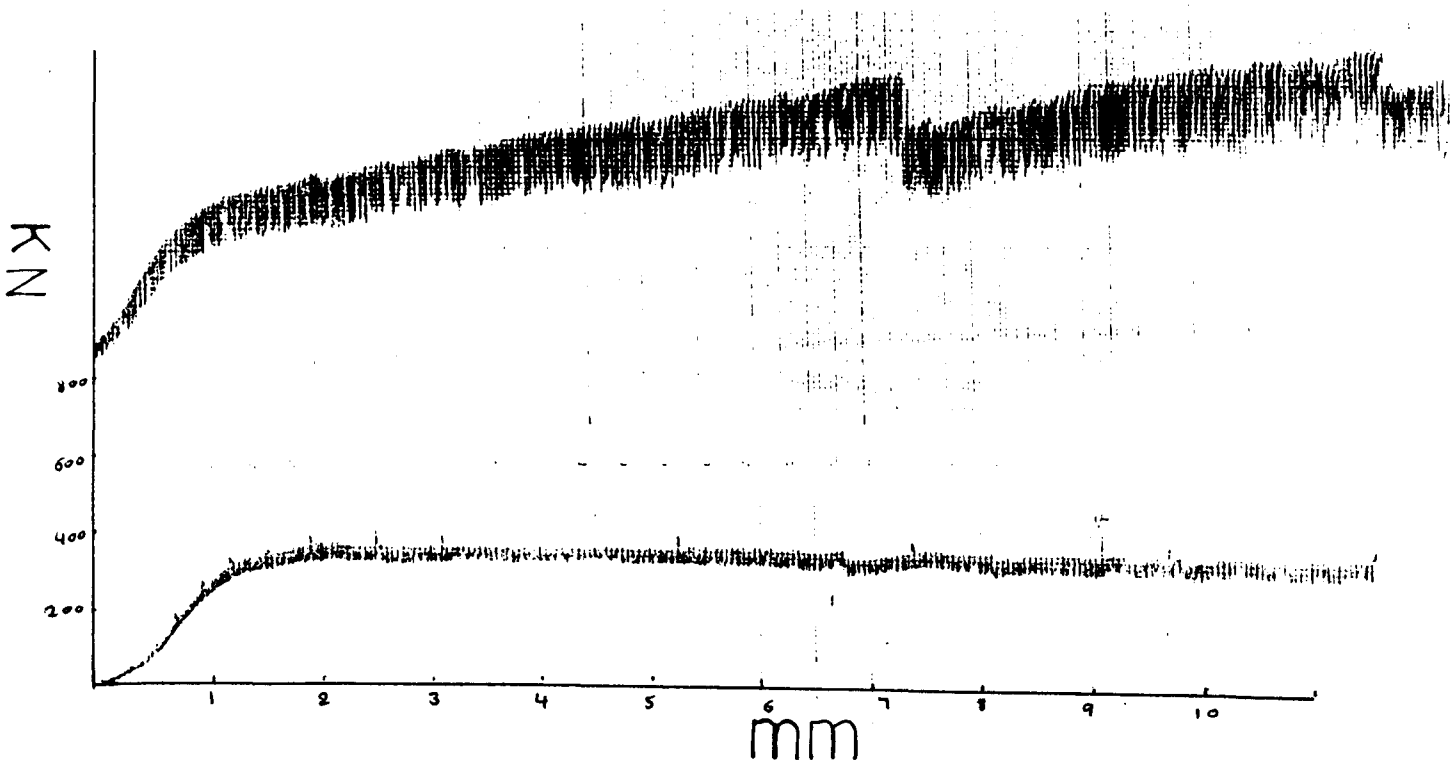

Figure 4.17: Load-displacement curves for PS specimens tested in modified (lower plot) and non-modified (upper plot) cell-specimen systems. joint type: saw out, 60 deg. confining pressure= 10 MPa.

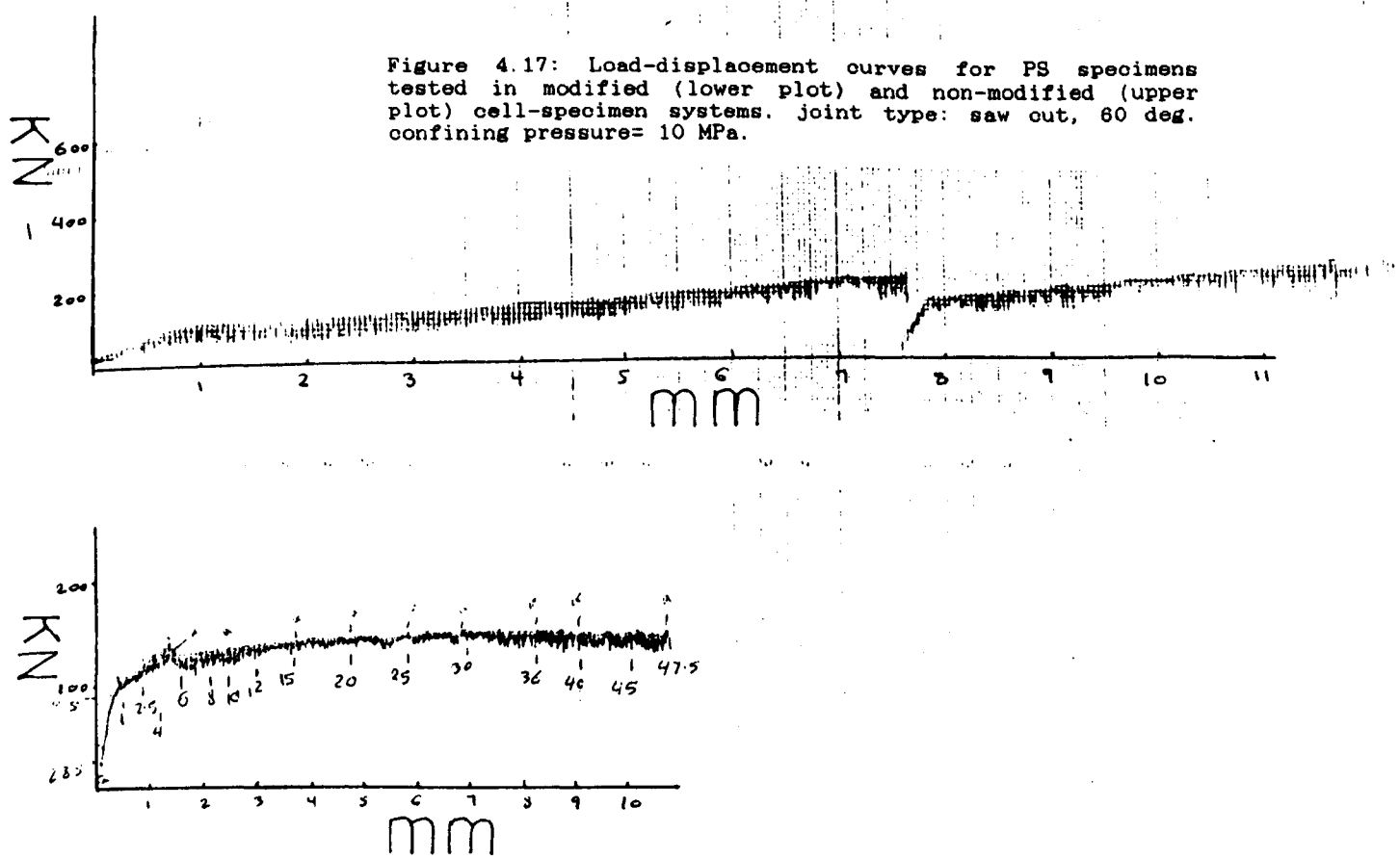

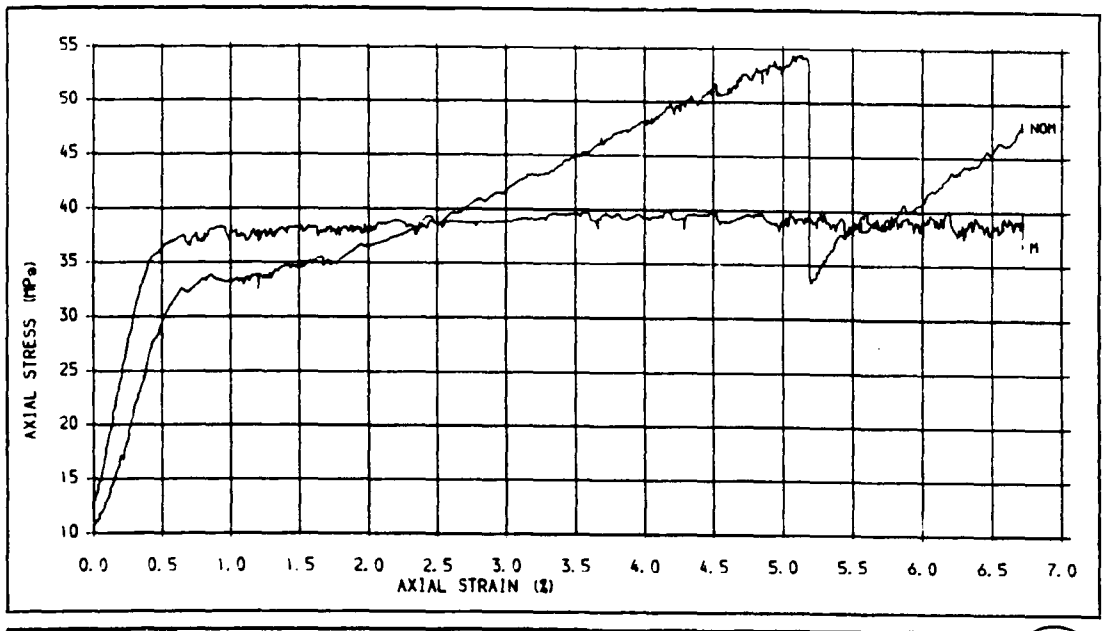

Fig. 4.19 : STRESS-STRAIN CURVES FOR DUMFRITH SANDSTONE SPECIMENS WITH SAW CUT JOINTS TESTED IN THE MODIFIED AND NON-MODIFIED SYSTEMS, JOINT ANGLE=60 DEG. CONF. PRES. = 10 MPa

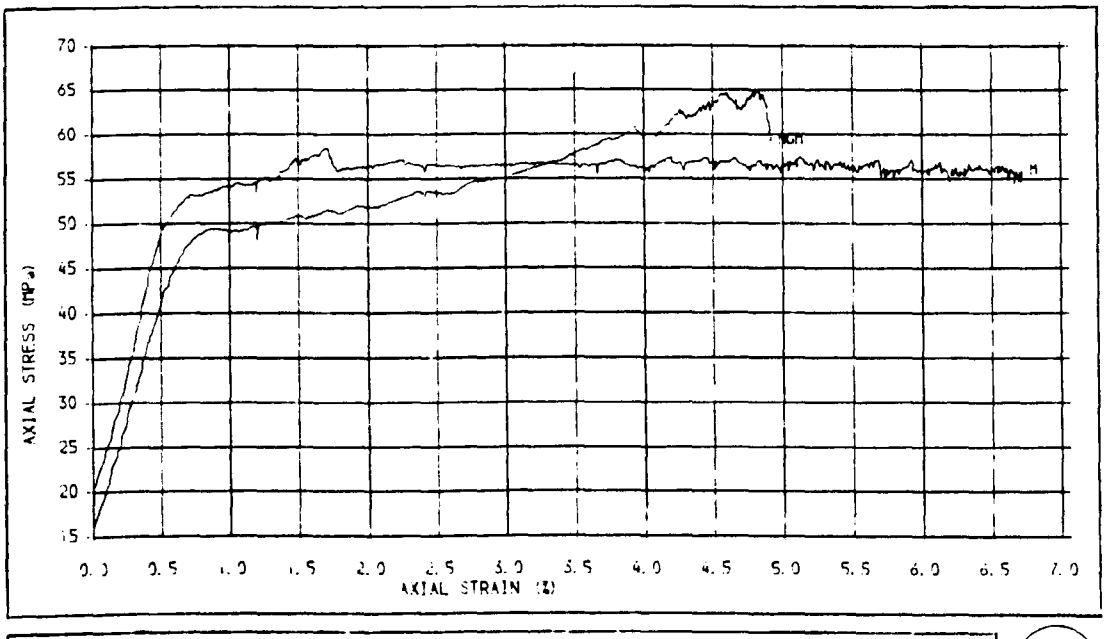

Fig. 4.20 : STRESS-STRAIN CURVES FOR DUMFRITH SANDSTONE SPECIMENS WITH SAW CUT JOINTS TESTED IN THE MODIFIED AND NON-MODIFIED SYSTEMS, JOINT ANGLE=60 DEG. CONF. PRES. = 15 MPa.

CHAPTER 5

TECHNIQUE FOR VOLUME CHANGE MEASUREMENTS

5.1. INTRODUCTION

Several techniques (directly and indirectly) are available to measure strains on rock specimens subjected to a constant confining pressure. The most commonly used direct method of measuring volumetric strains in the triaxial testing of rock relies on the use of resistance strain gauges which are mounted axially and circumferentially on the rock specimens. This is, however, the most convenient method for obtaining the small volumetric strains that occur prior to brittle failure (Paterson, 1978). It has been also indicated that all of the methods, direct and indirect, have the disadvantages of :

a) Only measuring over a limited portion of the specimen and
b) Most are impractical under triaxial conditions (Price, 1979).

In addition, all of the techniques are nearly impossible to use in the triaxial testing of jointed specimens successfully, where a large shear and normal displacements occurs through the joint. There is, however, a technique as described in the following, which is practical to use on jointed specimens tested triaxially for small and large sliding movements.

5.2. PRINCIPLE OF THE TECHNIQUE

The technique based on the principle that when a specimen immersed in a full fluid vessel is stressed and its volume changes; the volumetric change can be measured directly by collecting the displaced liquid in a graded capillary. In a triaxial test, with a

constant confining pressure, application of axial load to the specimen, results in axial and radial deformation. If the system is closed, and therefore the amount of confining fluid is held constant, as the stress is raised a change in confining pressure occurs. If the confining pressure is to be maintained constant, as indeed is expected from this type of tests, it is important to allow a certain amount of the confining fluid to be removed from the system. The quantity of the fluid is proportional to the changes in volumetric strain, and by monitoring continuously the amount of fluid during the test one can calculate the change in volumetric strain that the specimen suffered during the test.

Bridgman (1949) used this method for the first time by using a dilatometer in his testing system. Since 1949 this technique has been adopted by different workers (Crouch, 1970a, 1971; Wawersik, 1975; Price, 1979), and has successfully been used in triaxial test by designing and employing appropriate apparatus in order to control and measure the volume change.

5.3. MEASUREMENT PROCEDURE

In measuring the volume change the same apparatus was used as Price (1979). The displaced oil due to volume change of the specimen is collected in a graded cylinder by adjusting a relief valve manually (plate 3.1).

5.4. CALCULATION PROCEDURE

Applying axial load and confining pressure on the specimen deforms not only the specimen, but also the other parts of the system i.e.: loading ram, end platens, triaxial cell, rubber membranes and displaced oil. Therefore, a very accurate procedure to calculate true volumetric, axial, and lateral strains, is required to take into account all the components affected during a test. The following calibration procedure is an

improved method to the work of Price (1979) and is believed to give more accurate results.

Figures 5.2 to 5.4 illustrate three typical plots for an intact rock specimen (figure 5.2) and two artificially (saw cut) and naturally jointed specimens. The middle plot in each figure has been obtained directly by plotting the displaced oil from the triaxial cell versus the axial displacement (axial strain) for each test. The third plot in each figure shows the volumetric strain-axial strain curve which has been obtained by a series of calculations based on the proposed method and use of the displaced oil as row data in these calculations. The first plot shows the axial stress-axial strain curve for each test which is independent of the middle plot. Comparison of the three plots in each figure reveals that there is a close correlation between the axial stress-axial strain and volumetric strain-axial strain plots for three types of intact and jointed specimens which is in fact an indication of a very good accuracy of the method for both intact and jointed specimens.

As the oil released from the triaxial cell expands, due to the reduction in pressure, the true volume of oil displaced, V_t, is given by:

$$V_t = f\ V_o \qquad (5.1)$$

where

V_o = The measured volume of oil displaced, and

f = A factor of compressibility, taken from figure 5.1 which is plotted according to the technical notes supplied by Revol Ltd for the hydraulic oil (I.S.O.32) used in this experiment.

The true volume of oil (V_t) composed of three components:

-The oil displaced by the loading ram entering the cell (V_R);

-The oil displaced by the volumetric change of the specimen (ΔV), and

-The oil displaced by the volumetric change of the system (V_{sys}).

The volumetric change of the system (V_{sys}) includes: the end specimen platens, the O-rings, the rubber membranes, and the triaxial cell. Consequently, the specimen volumetric change is given by the following expression.

$$\Delta V = V_t - (V_{sys} + V_R) \qquad (5.2)$$

Taking into account the elastic deformation of the ram entering the cell, V_R, is given by:

$$V_R = \pi r^2 . l - \Delta V_R \qquad (5.3)$$

where

r = Ram radius

l = Measured displacement of the ram and

ΔV_R = Volumetric change of the ram.

ΔV_R is given by (Obert and Duval, 1967)

$$\Delta V_R = \frac{\pi r^2 . l}{E} (\sigma_1 + 2\sigma_3) (1 - 2\nu_s) \qquad (5.4)$$

Compression is taken as positive.

To obtain the displaced oil related to the volumetric change of system (cell, O-rings, rubber membranes and platens) a series of triaxially calibration tests must be carried out on a cylinder of a material of known elastic constants (such as steel, aluminium and so on) of the same dimensions and confining pressures as the rock specimens. In this case, the volumetric change corresponding to the system, V_{sys}, is given by:

$$V_{sys} = V_c . f - (\Delta V_s + \Delta V_{ro}) \qquad (5.5)$$

where

V_c = Displaced oil through the calibration test

f = Oil compressibility factor

ΔV_s = Volumetric change of steel cylinder

ΔV_{ro} = Volumetric change of the loading ram in calibration test.

ΔV_s and ΔV_{ro} are given as (Obert and Duval, 1967):

$$\Delta V_s = \frac{\pi r^2_s . H_s}{E} (\sigma_1 + 2\sigma_3)(1 - 2\nu_s) \qquad (5.6)$$

$$\Delta V_{Ro} = \frac{\pi r^2 . l_s}{E} [(\sigma_1 + 2\sigma_3)(1 - 2\nu_s) \qquad (5.7)$$

where

r_s = Radius of the steel cylinder

H_s = Specimen height

l_s = Measured axial displacement of the ram in

calibration test

E and ν_s are steel's modulus of elasticity and

Poisson's ratio.

Substituting equations 5.6 and 5.7 in 5.5, and 5.4 in 5.3, and then, the resultant equation in 5.2, the volumetric strain of the rock specimen (in %)is given by :

$$\Delta V / V = 100 / V \left[(V_o - V_c) \cdot f - \pi r^2 \cdot 1 + \pi/E (\sigma_1 + 2\sigma_3)(1-2\nu_s)(r^2_s \cdot h_s + r^2 . l_s + r^2 . l) \right] \quad \% \qquad (5.8)$$

In a simplified case, where confining pressure is not very high (below 70 MPa) the elastic deformation of system may be neglected, and therefore, volumetric strain is given by:

$$\Delta V / V = 100 / V \{ f . V_o - \pi r^2 . l [1 - (1 - 2\nu_s)(\sigma_1 + 2\sigma_3) / E] \} \quad \% \qquad (5.9)$$

where

V = the specimen original volume.

The average axial strain of the specimen, ε_1, is given by:

$$\varepsilon_1 = 1001 / L \left[1 - (\sigma_1 - 2\nu_s . \sigma_3)\right] \qquad (5.10)$$

where

L = the original specimen length.

Using the equation (Jaeger and Cook, 1983):

$$\Delta V / V = \varepsilon_1 + \varepsilon_2 + \varepsilon_3 \qquad (5.11)$$

that reduces here to:

$$\Delta V / V = \varepsilon_1 - 2\varepsilon_2 \qquad (5.12)$$

Radial strain, ε_2, is given by:

$$\varepsilon_2 = 1/2 \ (1 - \Delta V / V) \qquad \% \qquad (5.13)$$

and instantaneous Poisson's ratio, ν, is given by:

$$\nu = 1/2 \ [1 - (\Delta V / V) / \varepsilon_1] \qquad (5.14)$$

For the simplified case a program was written to calculate the volumetric strain, lateral strain and instantaneous Poisson's ratio as in appendix D.

FIGURE 5.1 OIL COMPRESSIBILITY FACTOR VS CONFINING PRESSUE

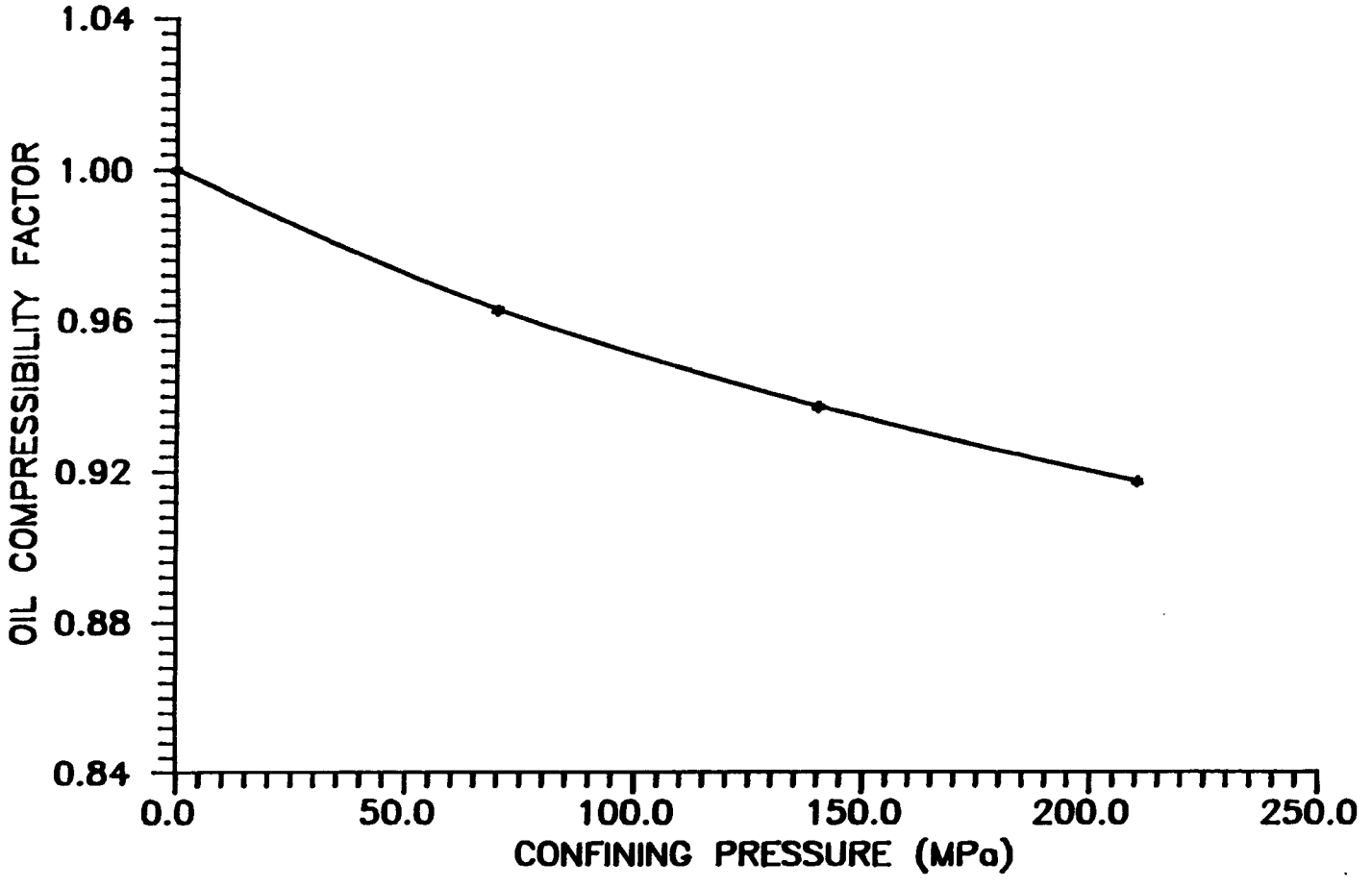

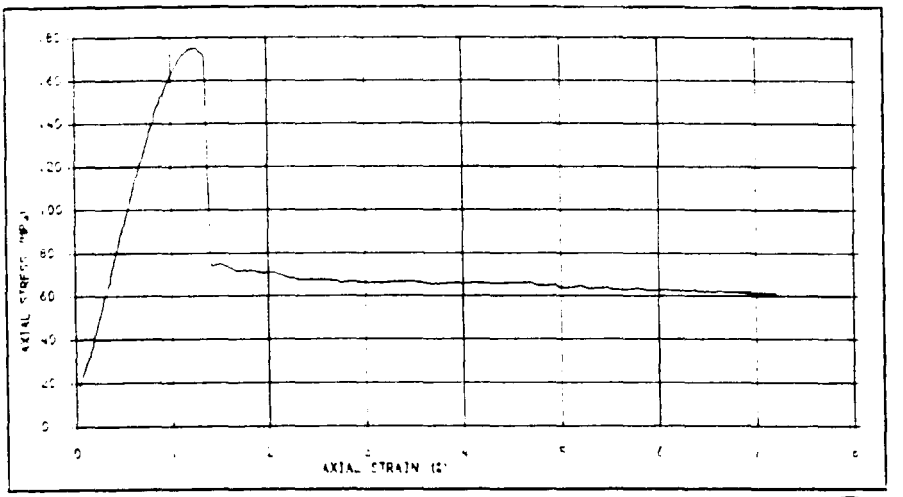

STRESS-STRAIN PLOT FOR AN INTACT SPECIMEN OF STAINTON SANDSTONE UNDER 15 MPa CONFINING PRESSURE

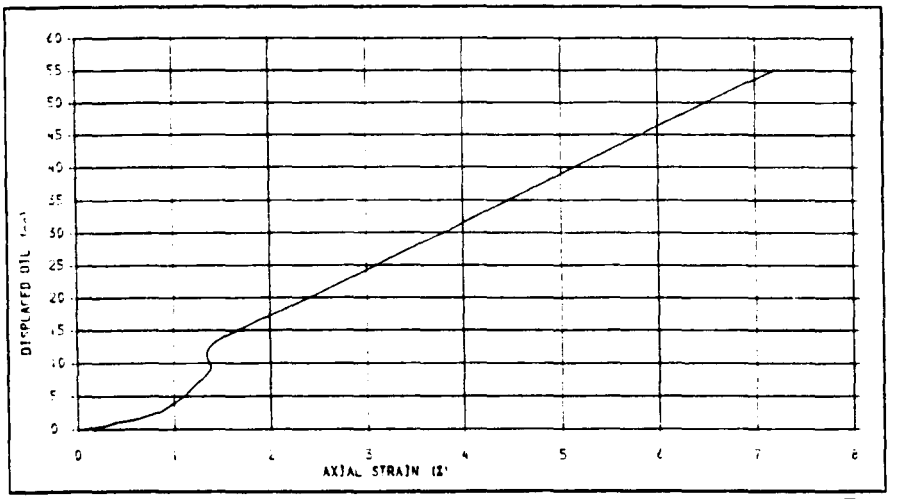

DISPLACED OIL-AXIAL STRAIN PLOT FOR AN INTACT SPECIMEN OF STAINTON SANDSTONE CONFINING PRESSURE= 15 MPa

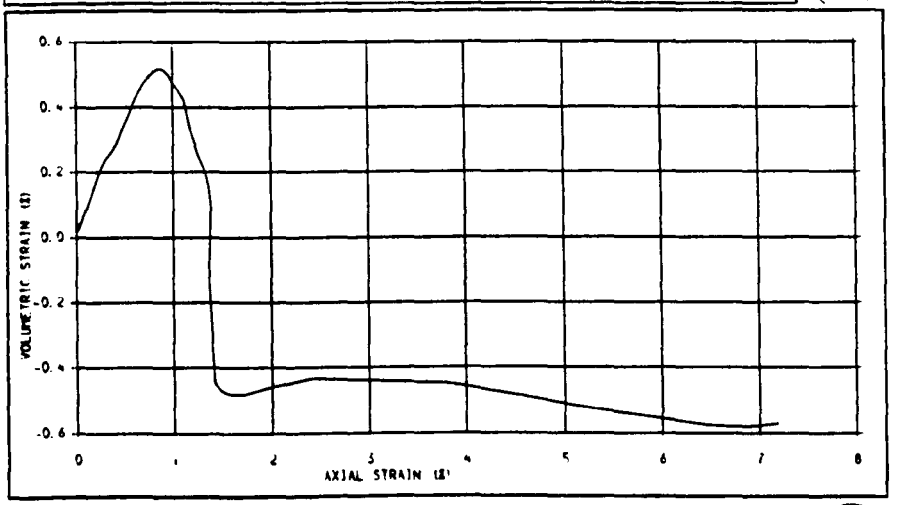

VOLUMETRIC STRAIN-AXIAL STRAIN PLOT FOR AN INTACT SPECIMEN OF STAINTON SANDSTONE, CONFINING PRESSURE = 15 MPa

Figure 5.2: Typical plots illustrate the correlation between the axial stress, axial strain (displacement) and volumetric changes for an intact specimen of Stainton sandstone.

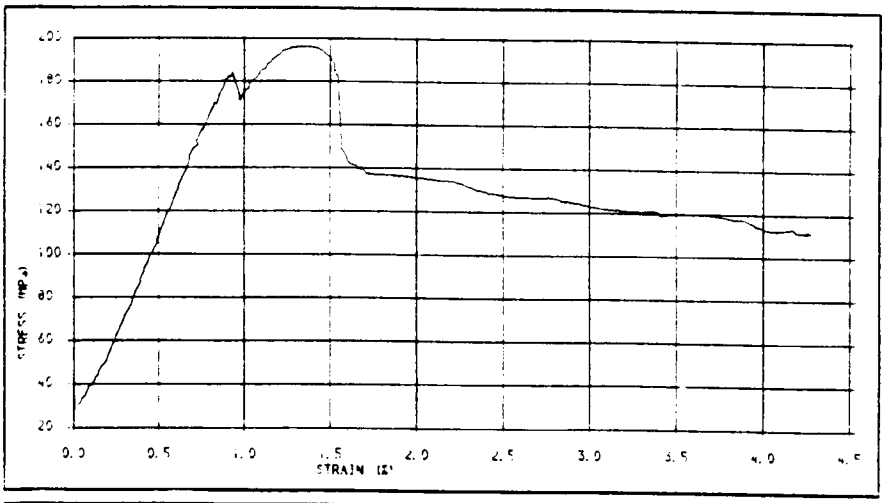

STRESS-STRAIN PLOT FOR A JOINTED SPECIMEN OF PENRITH SANDSTONE, TYPE OF JOINT NATURAL WITH 45 DEG. INCLINATION, CONFINING PRESSURE= 15 MPa

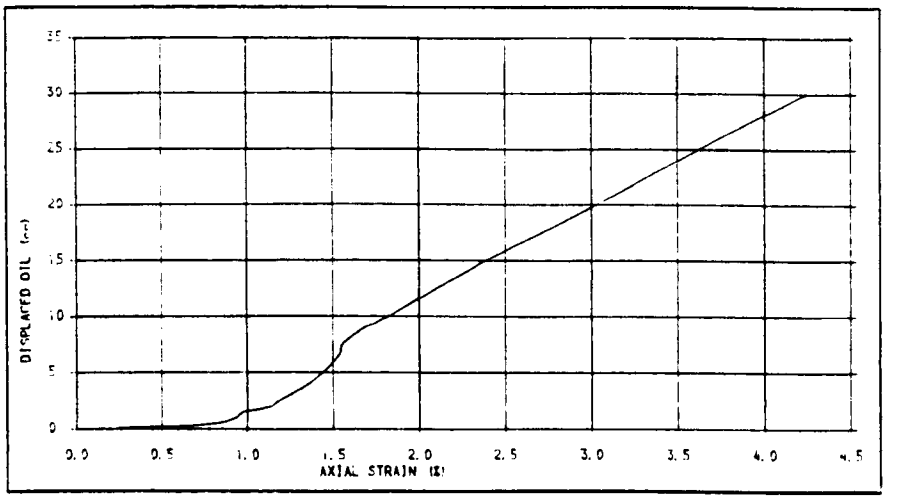

DISPLACED OIL-AXIAL STRAIN PLOT FOR A JOINTED SPECIMEN OF PENRITH SANDSTONE JOINT TYPE. NATURAL WITH 45 DEG. INCLINATION CONFINING PRESSURE = 15 MPa

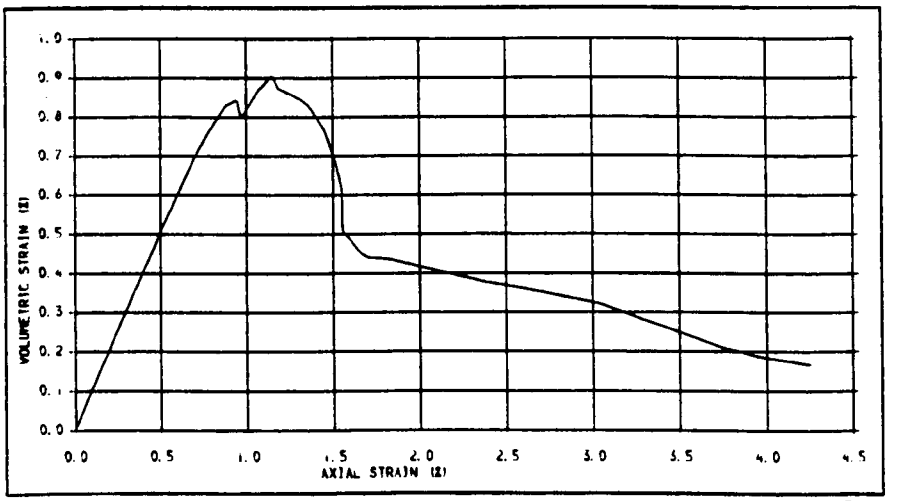

VOLUMETRIC STRAIN-AXIAL STRAIN PLOT FOR A JOINTED SPECIMEN OF PENRITH SANDSTONE TYPE OF JOINT. NATURAL, JOINT INCLINATION= 45 DEG. CONFINING PRESSURE= 15 MPa

Figure 5.3: Typical plots illustrate the correlation between axial stress, axial strain (displacement) and volumetric changes for a naturally jointed specimen of PS (45 deg.).

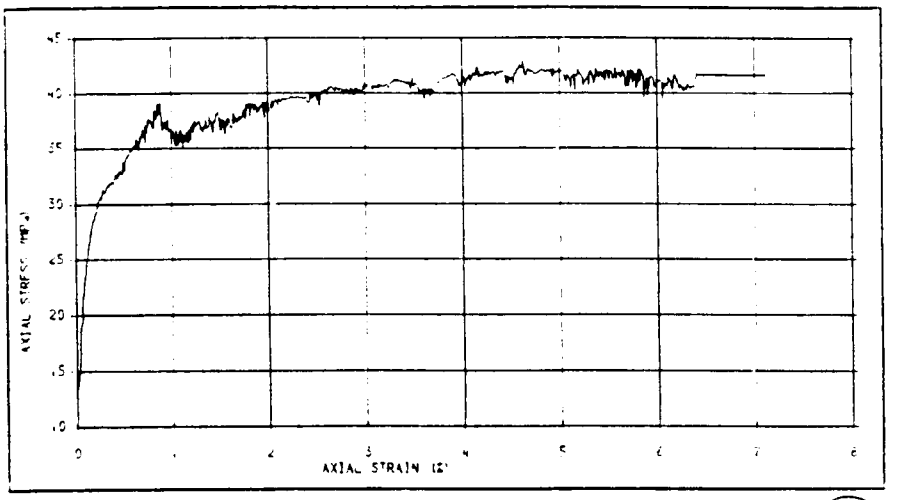

STRESS-STRAIN PLOT FOR A JOINTED SPECIMEN OF PENRITH SANDSTONE. SAW CUT JOINT WITH 60 DEGREES ORIENTATION, CONFINING PRESSURE=.0 MPa

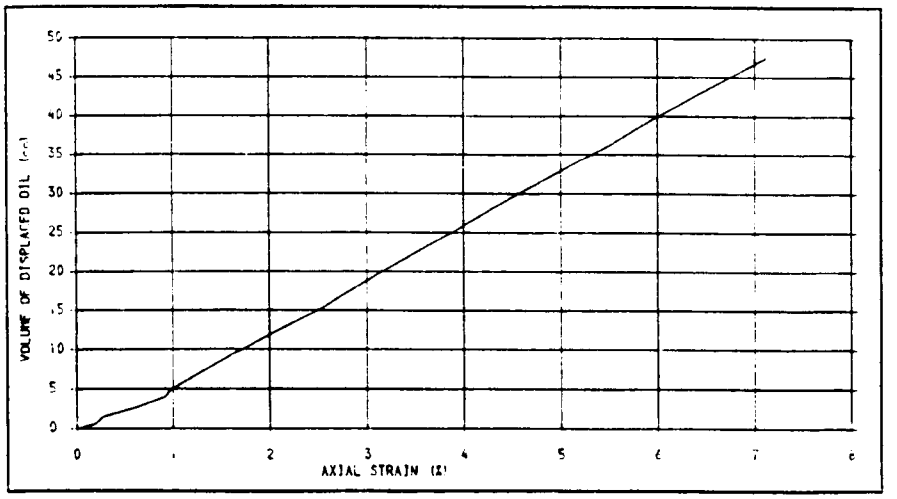

DISPLACED OIL-AXIAL STRAIN PLOT FOR A JOINTED SPECIMEN OF PENRITH SANDSTONE CONFINING PRESSURE= 10 MPa JOINT TYPE. SAW CUT WITH 60 DEC. INCLINATION

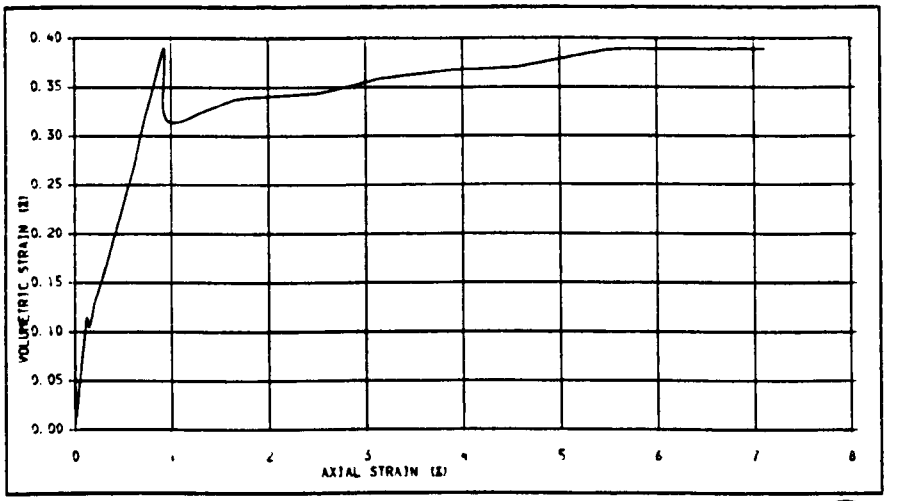

VOLUMETRIC STRAIN-AXIAL STRAIN PLOT FOR A JOINTED SPECIMEN OF PENRITH SANDSTONE, TYPE OF JOINT: SAW CUT, JOINT INCLINATION=60 DEGREES, CONFINING PRESSURE=10 MPa

Figure 5.4: Typical plots illustrate the correlation between axial stress, axial strain (displacement) and volumetric changes for a saw cut jointed specimen of PS (60 deg.).

CHAPTER 6

STRENGTH AND DEFORMABILITY OF ROCK CONTAINING A SINGLE PLANE OF WEAKNESS

6.1 INTRODUCTION

In chapter 4 it was shown that the modified cell-specimen system is the most satisfactory configuration providing favourable conditions for testing jointed specimens, where sliding along the joint plane is expected. On the basis of this modification a full experimental research was carried out to investigate the different mechanical aspects of six rock types containing a single plane of weakness. Three rock types were selected for study: Penrith sandstone (PS), Stainton Sandstone (SS) and Dumfrith Sandstone (DS). Triaxial tests were performed on jointed specimens with different orientation angles and in different confining pressures ranging from 0 to 70 MPa. The intact specimens of different rock types were also tested in the same range of confining pressure as the jointed specimens. Three types of joints were tested: saw cut, shear-surface and split breakage joints. Procedures for forming each joint type were given in chapter 3.

6.2 SAW CUT JOINT

Since it was easy to form the saw cut joints, a large number of tests were performed using this kind of joint in the three types of sandstone selected for study. This joint was introduced on Penrith sandstone specimens at orientation angles of 0, 15, 30, 45 and 60^o relative to the direction of σ_3, Stainton sandstone specimens at angles of 30, 45, and 60^o , and Dumfrith sandstone specimens at angles of 30 and 60^o Penrith sandstone specimens were tested at confining pressures of 0, 5, 10, 15, 30 and 70 MPa, Stainton sandstone specimens at confining pressures of 0, 5, 10, 15 and 30 MPa, and Dumfrith sandstone specimens for the confining pressures of 0, 5, 10 and 15 MPa.

The axial stress-axial strain plots for intact and jointed specimens for different confining pressures are given in figures 6.1 to 6.6 for Penrith sandstone, 6.7 to 6.10 for Stainton sandstone, and 6.11 to 6.13 for Dumfrith sandstone specimens. The typical results obtained for all the rock types demonstrate well the effects of the increased confining pressure and variation of the joint orientation on the strength and deformability of the rock studied (for both intact and saw cut jointed specimens). The results are also summarized in tables 6.1 to 6.7 for Penrith sandstone, 6.8 to 6.13 for Stainton sandstone and 6.14 to 6.17 for Dumfrith sandstone.

The jointed specimens with 0, 15 and 30^{o} orientations failed in a brittle manner through a shear fracture plane transcending the joint plane. Some specimens failed uncontrollably over a small interval of strain, as indicated by a steep solid line in the post peak portion of the stress-strain curve (figure 6.1 plots 0,10,15 and figure 6.3 plots 0, 5 and 10).

The specimens with orientations of 0, 15 and 30^{o} behaved in a strain softening manner, typically with stress dropping to a residual strength value of about half or two thirds of its peak stress which generally demonstrate similar behaviour to the intact specimens, but with lower peak strength, and further peak strain (figures 6.2, 6.3, 6.4, 6.8 and 6.12). The exception was the uniaxial tests where stress dropped to a token residual strength for all orientations; probably this is a measure of the artificial cohesion created by the rubber sleeves. Sliding movement along the joint for 30^{o} orientation is very high in uniaxial test (figure 6.14) which is an indication of the significance of weakness plane at low confinement, as in cases encountered the rock slope stability problems.

For 45 and 60^{o} orientations the behavioural characteristics are quite different from other orientations. Failure is predominantly by sliding rather than by shear fracture.

Exception occurred in Stainton sandstone specimens containing joints with 45° orientation. In Penrith sandstone specimens for all confining pressures failure took place by sliding along the joint, and then the sliding movement was continued nearly at a constant level of stress at different strains. However, in Stainton sandstone specimens failure started by sliding along the joint, but axial stress was also increased up to a peak, and eventually the specimens failed by a new shear fracture plane transcending the joint (figure 6.9 plots 5, 10 and 15). This mode of failure occurred for confining pressures of 5, 10 and 15 MPa, but did not take place for 30 MPa where behaviour was similar to the Penrith sandstone specimens (figure 6.9 upper plot). For 45 and 60° orientations in lower confining pressures up to 15 MPa, a trend of slight increase in the stress with further sliding movement over the joint plane may be observed (figures 6.5, 6.6, 6.9, 6.10 and 6.13). For higher confining pressures a peak strength is often observed which appears after a little sliding along the joint surfaces.

A series of multi-stage tests on Penrith sandstone specimens with joint orientations of 45 and 60° were also carried out for confining pressures up to 70 MPa in order to compare the typical results with single stage tests. The typical plots obtained are presented in figures 6.77 and 6.78.

6.3 SPLIT BREAKAGE JOINT

This type of joint was introduced on Penrith sandstone and Stainton sandstone specimens at an angle of 30, 45 and 60° and confining pressures up to 30 MPa were used. The axial stress-axial strain plots for this type of joint are given in figures 6.44 to 6.49 for two types of rock,and demonstrate the typical results obtained, i.e the increased confining pressure and the variation of joint inclinations on the strength, deformability and sliding characteristics. The results are also summarized in tables 6.18 to 6.20 for Penrith sandstone and 6.21 and 6.22 for Stainton sandstone specimens, including the

peak strength, maximum axial strain at peak, mode of failure and average residual strength for the different orientations tested.

In specimens containing a split breakage joint with a 30° orientation, the same as a saw cut joint, failure took place through a new shear failure plane transcending the joint, however, in 45 and 60° orientations failure occurred by sliding along the joint surfaces. All the specimens, Penrith sandstone and Stainton sandstone, with various orientations and confining pressures behaved in a strain softening manner, typically dropping to a residual stress value, which is often equal to or slightly greater than the sliding strength on the saw cut joints (in 45 and 60° orientations). The behaviour of specimens containing a split breakage joint in any orientation is similar to the intact specimens , in the sense that stress rises to a peak and then it drops to a residual stress value.

In split breakage Stainton sandstone specimens with 45° orientation for both 5 and 15 MPa confining pressures failure occurred by sliding along the joint surfaces (figure. 6.48) which is quite different from the Stainton sandstone specimens with saw cut joints (with the same confining pressures and orientations) in which failure took place at first by sliding along the joint, then fractured through a new shear plane transcending the joint (figure 6.9 plots 5, 10 and 15).

The volumetric strain, lateral strain and instantaneous Poisson's ratio versus axial strain plots for Penrith sandstone specimens containing split breakage joints with inclinations of 45 and 60° are given in figures 6.50 to 6.55.

6.4 SHEAR-SURFACE JOINT

This joint type was only introduced in Penrith sandstone specimens by fracturing of intact specimens at zero or 10 MPa confining pressures. Two series of tests were

performed on this joint under the confining pressures of 30 and 70 MPa, and also two multi-stage tests for confining pressures from zero to 70 MPa. Typical stress-strain plots are given in figures 6.56 and 6.57 and the summarized results are also given in tables 6.23 and 6.24.

Specimens containing this joint type, in the range of confining pressures applied, did not demonstrate the same behaviour during straining for the two series of tests performed, because of the difference in the confining pressures applied (0 and 10 MPa) on the intact specimens for forming this type of joint. For 30 MPa confining pressure as in figure 6.56, for instance, a peak stress is observe and then, it decreases gradually to a residual strength value. However, in figure 6.57 (plot 30)for the same confining pressure (30 MPa), a peak stress is not observed, but stress has increased asymptotically. Furthermore, for 70 MPa confining pressure the same behaviour is observed.

6.5 MECHANISM OF FAILURE AND SLIDING CHARACTERISTICS

Considering different types of rock containing various types of joints, several distinct regions and types of behaviour are recognized:

1. In all cases, the stress-strain curves begin with an initial non-linearity. This may be attributed to the closure and interlocking of asperities in the jointed specimens, and to the closing of pre-existing microcracks or pore spaces in intact specimens.

2. After the initial non-linearity, in many cases, displacement took place linearly proportional to load until the stress reached a value about three quarters of that necessary to maintain steady sliding. Sliding in excess of that due to further compressive loading then began, and the frictional force increased asymptotically with

continued displacement. In some cases after a certain magnitude of sliding the specimens failed by a shear fracture transcending the joint (figure 6.9). In most cases(for 60° orientation in the saw cut joints), however, sliding continued until stress reached a peak value, then it dropped to a near to constant stress value after which sliding continued asymptotically. This behaviour is demonstrated well by the plots in figure 6.10 for the confining pressures of 5, 10, 15 and 30 MPa.

3. In many cases, with moderately flat surfaces of sliding in which the roughness is low (in the saw cut joints) an ideal constant frictional stress is observed throughout sliding, particularly at rather low confining pressures. This behaviour is demonstrated well in figures 6.5 (plots 5, 10, 15 and 30) and 6.6 (plots 5, 10, 15 and 30) in which for the confining pressures from 5 to 30 MPa, stress is reasonably constant beyond 1.5% axial strain.

4. For higher confining pressures (in the saw cut joints) stress rises to a peak value, then it falls steadily to a residual value nearly independent of further displacement as in figures 6.5 (plot 70)and 6.6 (plot 70) for 70 MPa confining pressure.

5. In the cases of 0, 15 and 30° joint inclinations for the two types of joint (saw cut and split breakage), the stress rose to a peak value and then it fell steeply and violently to a residual value. The fracture took place through a new shear fracture plane transcending the joint plane. On examination of the failed specimens for orientations of 0, 15 and 30° it was observed that in zero degree orientation there was no movement along the joint at all; for 15° orientation very little movement was observed and the joint surfaces and asperities were still integrated. The tips of asperities, however, were broken slightly when confining pressure was increased and a very thin layer of rock powder covered the joint surfaces. The sliding movement for 30° inclination in comparison with zero and 15° orientations was considerable, however, relative to 45° and higher orientations

it was very little. Furthermore, the tips of asperities were broken (in rough surfaces), but the overall roughness pattern still remained unchanged. This implies that the presence of joint in the range of zero to 30° orientations is not very significant, particularly when the confining pressure is high enough.

Figures 6.2 to 6.4, 6.8, 6.44 and 6.47 demonstrate the effect of joint with zero, 15 and 30° inclinations on the strength and deformability of Penrith sandstone and Stainton sandstone specimens. At zero MPa confining pressures in figure 6.4 for 30° orientation, the presence of a joint has a great effect, the peak strength has decreased about 56% for zero confining pressure. Figure 6.14 also demonstrates well the effect of a joint with 30° orientation in comparison with zero and 15° orientations and also the intact specimens. The mechanism of failure for the joint with orientation from zero to 30° is reasonably similar to the intact specimens. Plates 6.1 to 6.5 and 6.7 to 6.12 show the fractured and deformed intact and jointed specimens containing smooth or rough joints with different orientations and various confining pressures.

6. The shape of the stress-strain curves in the specimens with very rough discontinuities (the split breakage joint) is similar to that of intact specimens, not only for the orientations of zero to 30°, but also for 45 and 60° the stress rises to a peak value more or less elastically, then it falls steeply to a residual value. This behaviour is observed on a surface with interlocked grains. In the saw cut joints, however, with an orientation of 60° in which the interlocking of asperities is very low, in some cases, a small peak value is observed. The magnitude of strain at the peak in the interlocked joints is generally less than that of the saw cut joints. As is observed in figure 6.10 (plot 30), for instance, the magnitude of strain at the peak stress for 30 MPa confining pressures in a saw cut joint is about 3.4%, whereas in figure 6.49 (plot 30) for the same rock, confining pressure and joint orientation, but with a split breakage joint, it is about 1%. Furthermore, in split joints with 45 and 60° orientations the stress-strain relationship

often retains its linear direction with no sliding up to the area near the peak. However, in the saw cut joints, it is often non-linear with considerable sliding along the joint.

In the specimens containing split breakage joints the residual stress value does not remain at a constant level, but it decreases with further movement along the joint; however, after a large amount of sliding it reaches a near to constant value similar to the saw cut joints. This is due to the fact that in the split breakage joints, because of the high degree of surface roughness, after the beginning of sliding, asperities start shearing off, and this continues when sliding progresses. It is for this reason that further sliding results in a further reduction in residual stress. In the saw cut joints, however, the overall trend in the residual stress region is to hold a constant stress level, or a slight increase in the stress value with progressive sliding. This behaviour may be attributed to the fact that in the beginning of sliding the tips of asperities are in contact, therefore, the contact area is limited to only a part of the sliding area; however, when sliding continues the asperities are broken and the contact area increases. This process results in an increase in the friction through the sliding surfaces and therefore, an increase in the stress as sliding progresses.

7. The mechanism of sliding and failure through the joints formed by shear-surface, seems to depend upon the confining pressure applied to break the intact specimen. For the two confining pressures used in this experiment to establish the shear-surface joints (0 and 10 MPa), the mechanism of deformation is different for the same confining pressure. For the joint established uniaxially, and then loaded, after applying confining pressure of 30 MPa (figure 6.56), stress rises to a peak value, and then it drops to a residual value with a gradual decrease as deformation continues. However, for the joint established at 10 MPa confining pressure (figure 6.57 plot 30) for the same confining pressure (30 MPa) a peak value is not observed and the residual stress remains in a near constant value which is different from the figure 6.56.

The discrepancy may be attributed to the difference in the mechanism of failure of the intact specimens at two different confining pressures. As is shown in Plate 6.10 (two specimens, first and second from the left have failed uniaxially and the third one at 10 MPa confining pressure) in the third specimen a shear failure plane is clearly observed and the number of the secondary fractures is lower than in the other two specimens. Moreover, the inclination angle of the main fracture plane in the third specimen is about 63^{o} which is a convenient orientation for easy sliding (similar to 60^{o} in the saw cut joints). In the first and second specimens , however, the fracture plane is nearly vertical which clearly is not a convenient sliding plane.

8. Sliding behaviour for all types of the joints tested under 70 MPa confining pressure, seems to have the same characteristics: stress rises to a peak value, and then it gradually decreases to a residual value after a considerable sliding occurs along the joint (6.5, 6.6, 6.10, 6.56 and 6.57 plot 70). This is probably due to the effect of high confining pressure which causes the rock to exhibit a ductile behaviour. A similar effect is observed for intact specimens in 70 MPa confining pressure (figure 6.1 top graph).

9. Failure and sliding mechanism in split breakage joints are characterized by different stages, in each stage the degree of roughness, slickensided areas and the number of fractured asperities change as the sliding movement continues. After the first fractures which are usually accompanied by a sudden drop at the peak stress, the tips of asperities fail by extension cracks propagating from the sharp corners either vertically or subparallel to the discontinuity direction, the narrow teeth start shearing off and the wider asperities resist against shear sliding. It is for this reason that a second peak value in the stress-strain curve is often observed at this stage which is in some cases higher than the first peak. Continuation of sliding eventually leads to crushing of the asperities and development of the ultimate failure plane through a completely pulverized zone

(plate 6.8). The condition of the failure surface depends on the magnitude of the shear movement along the joint, and after relatively small deformation (1 to 1.5% in this experiment) slickensiding develops only over the tips of asperities and in limited areas. In the case of large deformation (sliding movement), the entire failure surface is covered by a zone of pulverized grains exhibiting slickensiding throughout (plate 6.7). Depending upon the applied confining pressure, the degree of slickensiding and the pulverized material vary significantly.

Similar observations were reported by Lajtai (1975) in uniaxial testing of model experiments on interlocked discontinuities.

6.6 STRENGTH AND DEFORMATION VARIATIONS

The present experiment indicates that the failure strength and deformation are affected significantly by the joint inclination, confining pressure, and joint surface roughness. The stress-strain plots for evaluating these factors are given in figures 6.58 to 6.64 for Penrith sandstone, 6.65 to 6.72 for Stainton sandstone and 6.73 to 6.75 for Dumfrith sandstone. The variation of peak strength versus joint inclination for Penrith sandstone specimens is given in figure 6.76. It demonstrates a typical plot of the effect of joint inclination on the failure strength of a jointed specimen at different levels of confining pressures.

In order to evaluate the effect of joint inclination on the failure strength quantitatively, a ratio is defined as the "strength descending coefficient" which is the compressive strength of the specimen containing a joint to that of the intact specimen. The strength descending coefficients for the three rock types studied are given in tables 6.7, 6.13 and 6.17.

The effects of joint inclination on the deformation behaviour of the three rock types may be observed in the stress-strain plots in figures 6.58 to 6.75 for different confining pressures and the two types of saw cut and split breakage joints. The plots demonstrate well the remarkable effect of joint inclination on the deformational behaviour of the rocks. The stress-strain curve of each specimen containing joint is different to a great or lesser extent from that of the intact specimens. The most interesting aspects of the deformational effects may be summarized as follows:

a. Most of the stress-strain curves of the jointed specimens having orientations less than 45° are flat S-shaped up to the peak.

b. The initial deformation is often greater than the rest of the deformation leading up to the failure. This observation in saw cut joints is much clearer than in the split breakage joints. It decreases with increased confining pressure.

c. All the stress-strain plots of the artificial (saw cut) jointed specimens, and most of the split breakages specimens were found to be flatter than those of the intact specimens under the same conditions of compressive loading.

d. The higher the angle of inclination of the joint, the flatter is the stress-strain plot (figures 6.14 to 6.19 and 6.65 to 6.75).

e. Deformation of the specimens containing a saw cut joint is much greater than that of the split breakage joint.

f. Deformational behaviour of the jointed specimens with any inclination is affected by the increased lateral pressure.

6.7 MODES OF DEFORMATION

The modes of deformation leading to failure may be divided into three different types:

(i) CONTINUOUS SLIDING ALONG THE JOINT

This mode of deformation was observed for the specimens containing joint with orientations of 60° in the three rock types studied, for all the confining pressures applied up to 70 MPa in the two types of saw cut and split joints (figures 6.6, 6.10 and 6.13). The same mode of deformation was also observed in Penrith and Stainton sandstone specimens containing joints with inclination of 45° for all the confining pressures except in Stainton sandstone specimens for the confining pressures of 5, 10 and 15 MPa.

(ii) NEW SHEAR FAILURE WITHIN THE INTACT ROCK MATERIAL

For the specimens containing joint with inclination of 30° and less, the mode of deformation is predominantly by shear fracturing of the intact rock transcending the joint plane. For the orientation of 30° and zero confining pressure, however, in addition to shear fracture, considerable sliding movement was also observed (figure 6.4 the lowest curve). This is of particular significance for the joints having low surface roughness, such as saw cut joints, when a very low confining pressure dominates. Therefore, it is necessary to pay sufficient attention to the jointed media containing low inclinations (25-40°) when they are surrounded by very low confinement.

(iii) COMPOSITE MODE OF DEFORMATION INVOLVING THE ROCK MATERIAL AND JOINT

This mode of failure was observed in Stainton sandstone specimens containing saw cut joints with 45° inclination (figure 6.9 plots 5, 10 and 15). After a considerable sliding movement along the joint surfaces, the specimens failed by a sudden drop in the stress accompanied by a new shear failure through the intact rock. The same mode of deformation was observed for 30° inclination at zero confining pressure (figure 6.4). Even at high confinement and low inclination such as 15° an occasional sudden drop in stress was observed in the stress-strain plot before the peak stress which is an indication of a little sliding along the joint surfaces. A clear example of this behaviour can be seen in figure 6.3 (the top plot) in which a slight drop in stress at about 1% axial strain is observed.

The main aspects of the deformation mechanism of jointed specimens with a plane of weakness may be summarized in the following stages:

a. At first, further deformation takes place by closing of microfissures and gaps within the rock and the joint surface, and also by compressing and extruding the softer filling material through the joint.

b. In the next stage, shear stress develops both in the rock and through the joint, and also is loosened the bond between the grains or the locked asperities.

c. In the third stage, depending on the joint inclination, shear stress is concentrated along the joint plane, or in the specimen body along a shear plane transcending the joint. In fact, because of the increased stress, cracks grow along the joint plane, or in the body.

d. Finally as the stress approaches its peak value, failure is started by sliding along the joint accompanied by shear failure of the interlocked asperities for the joint orientations

from 40 to 65°, or by sliding slightly along the joint and the shear fracture of the intact rock for the orientations of 25 to 40°, or by shear fracture of the specimen through the intact rock in the case of zero to 25° orientations.

6.8 EXPLANATION OF THE PLOTS WAVINESS

It is necessary to explain that the 'waviness', typical of most of the axial stress-strain curves, particularly in the sliding, or in the residual regions of the curves, is not due totally to stick-slip along the failure plane or sliding surfaces as one would initially think, but may also attributed to the following:

The small waviness throughout the stress-strain curves is partially due to the testing system, particularly the less sensitivity of the servo valve in the servo-controlled system, which results in a jerky manner in the curves plotted, and is partially the property of the data acquisition system in which data is logged in terms of digits and then being averaged in order to decrease the number of data to a level giving a smooth curve.

The greater waviness which is often observed in the residual and sliding regions of the curve is totally due to the sudden movements or volume changes in the specimen ,causing the relief valve to 'over-release' and thus to allow the pressure to drop too far. Prime examples of this were the sudden releases of oil and pressure drops, accompanying uncontrolled failure of the intact and jointed specimens containing joints with orientations of less than 30°. Once the relief valve had closed, again the pressure would slowly build up to the test pressure, and this course of events might repeat itself. This mechanism seemed more frequent at the higher confining pressure and further sliding movement (figures 6.5 and 6.6 at 70 MPa , for instance).

6.9 SHEAR AND NORMAL STRESSES ANALYSIS

In order to compare the frictional characteristics of the jointed specimens with those of intact, two different procedures were adopted here to obtain the Mohr envelopes for the intact and jointed rock types specimens. In the first procedure, by plotting the Mohr circles for each pair of confining pressure and differential stress the corresponding Mohr envelope was plotted. This method was used for the intact and the jointed specimens in which failure did not occur by sliding along the joint, but by a new shear failure plane within the rock material. The second method was used for the joint orientations in which failure occurred by sliding along the joint, namely the orientations of 45 and 60° in this experiment. Shear and normal forces over the joint were obtained directly by consideration of the equilibrium of one half of the joint specimen as in figure 6.86.

As the contact area changes permanently, because of the shear displacement over the joint, a correction must be taken into account by obtaining the actual contact area during sliding. The actual contact area (Ac) is given (Rosengren, 1968):

$$A_c = \frac{D^2 \ (2\beta - \sin 2\beta)}{4 \cos \alpha} \qquad (6.1)$$

in which the angle β is given by:

$$\cos \beta = 1 \cot \alpha \ / \ D \qquad (6.2)$$

where:

D = The specimen diameter

l = axial shortening of the specimen

a = joint inclination angle with respect to the direction of σ_3

The normal and shear stresses can be derived as follows:

Consider the equilibrium of the bottom half of a jointed triaxial specimen (figure 6.86) under a confining pressure σ_3. As sliding is initiated, the normal and shear forces (N and T) across the joint vary and is given by:

$$N = R_1 \cos \alpha + P_1 \sin \alpha - P_2 \qquad (6.3)$$

$$T = R_1 \sin \alpha - P_1 \cos \alpha \qquad (6.4)$$

where:

R_1 = axial deviatoric force,

$$P_1 = \sigma_3 D^2 / \cot \alpha \qquad (6.5)$$

$$P_2 = \sigma_3 (A_s / \cos \alpha - A_c) \qquad (6.6)$$

A_s = Specimen cross sectional area.

Having N and T, the normal and shear stresses across the joint (σ_n and τ_n) are given as:

$$\sigma_n = N / A_c \qquad (6.7)$$

$$\tau_n = T / A_c \qquad (6.8)$$

Using the equations (6.7) and (6.8) for each pair of data, and then, applying the least square analysis, Mohr envelopes for the orientations of 45 and 60° based on Coulomb theory ($\tau = c + \sigma_n \tan \phi$) are obtained.

Mohr envelopes for the jointed and intact specimens for the three rock types and different orientations, thus are given in figures 6.83 to 6.85. The average coefficient of

friction, cohesive strength, angle of internal friction and coefficient of sliding friction are given in tables 6.31 to 6.33.

6.10 DISCUSSION

Examination and observation of the tables and plots reveal that several parameters affect the stress-strain and stress at failure-joint inclination, and the deformational characteristics of the rocks tested.

6.10.1 CONFINING PRESSURE EFFECTS

Confining pressure had a pronounced effect upon the stress-strain properties of the rocks tested with any orientation. The axial stress-strain curves as presented (6.1 to 6.13) all show that increased confining pressure both strengthens the intact and jointed rocks, and results in an eventual transition from strain softening to hardening behaviour for the intact specimens. There is also an increase in the axial strain to failure and often a shallower post-failure curve as confining pressure increases.

Effects of increased confining pressure on the jointed rock having orientations of 45 and 60°, namely the orientations in which failure occurs by sliding along the joint surfaces, is more remarkable. Comparison of the peak stresses for these orientations with those of the intact specimens in the same confining pressure, shows that the increased confining pressure decreases the joint effect significantly, even in the critical orientations. In other words, it may be concluded that increased confining pressure, eventually results in the diminishing of the weakness plane effect on the rock strength.

Table 6.7 illustrates the strength descending coefficients (the ratio of the strength of jointed specimen to that of the intact) for Penrith sandstone specimens with saw cut

joints. Comparison of the ratios for 45° orientation shows that increase of confining pressure from 15 to 30 and then to 70 MPa resulted in an increase in the ratios from 0.424 (15 MPa) to 0.604 (30 MPa) and to 0.761 (70 MPa). This implies that the strength of the jointed specimens becomes nearer to the strength of the intact specimens in proportion to the increase in the confining pressure. The same trend is observed for 60° orientation and the other joint types. For 60° orientation (table 6.7, for instance) the ratio in 15 MPa confining pressure is 0.171. It has increased to 0.292 for 30 MPa and to 0.450 for 70 MPa, or in a shear-surface joint (table 6.25 column 10) the ratio from 0.560 for 30 MPa confinement has increased to 0.800 for 70 MPa confining pressure.

The effect of confining pressure on the sliding characteristics of joints at low confining pressures seems to be different from that of the higher confining pressures. As figures 6.5 (plots 5 and 10) and 6.6 (plots 5 and 10) illustrate, up to 10 MPa confining pressure (5 and 10) sliding has continued asymptotically with a slightly ascending order of magnitude, or nearly at a constant stress level, however, with an increase in confining pressure from 15 to 30 and then to 70 MPa, sliding has continued in an descending order, so that the rate of reduction has increased with increased confining pressure. The same trend is observed in figures 6.10 (plots 30 and 70), 6.13 (plots 10 and 15) and 6.56 (plots 30 and 70) for Stainton sandstone and Dumfrith sandstone, and for shear-surface in Penrith sandstone respectively.

The behaviour of sliding in split breakage joints seems to be the same in both low and high confining pressures, after dropping the stress to a residual value sliding continues in a descending order at all levels of confining pressures (figures 6.45, 6.46 6.48 and 6.49).

The reason for the difference in sliding manner in low and high confining pressures, and also in saw cut and split joints may be explained as follows:

In the saw cut joints at low levels of confining pressures, the rate of damage due to sliding is very low in comparison with high confining pressure,therefore, the amount of debris material produced during sliding is much less than that of high pressures. Examination of the specimens after tests confirmed that a rather thick layer of pulverized material coated the surfaces of sliding in high confining pressures, it was very thin, however, in low pressures. Because of such a layer of wear over the sliding surfaces it may be postulated that a filled joint has been formed which is much weaker than the rock material. With continuation of sliding the wear becomes thicker, and therefore, a further reduction in the stress valve results.

In the split breakage joints because of the high degree of surface roughness, as sliding is initiated, at first the tips of asperities start fracturing, and with continuation of sliding further asperities fracture and bring about a thick layer of wear material. This process results in a permanent reduction in the residual stress value until a complete slickensided surface is produced which in this case the residual stress reaches a nearly constant value.

Increase of confining pressure increases the rate of axial deformation both in the jointed and intact specimens tested (figures 6.1 to 6.13). This becomes more remarkable at the higher angles of inclination (45 and 60^{o} as in figures 6.5, 6.6, 6.9, 6.10 and 6.13). This behaviour for the intact and jointed specimens in which the mechanism of failure is not dominated by sliding along the joint may be attributed to the tendency of the rocks to the transition from strain softening behaviour to hardening.

In jointed specimens with higher angles of orientations (45 and 60^{o}) in which the mechanism of deformation is dominated by frictional sliding, the behaviour seems to be different. For lower confining pressures a near to constant value, or a gradual increase

in the stress is observed as sliding progresses (figures 6.5 and 6.6 plots 5 and 10). With an increase in confining pressure (figures 6.5 and 6.6 for 30 MPa and higher pressures) when sliding continues the stress decreases gradually, and the rate of decreasing becomes higher with confining pressures. This dual behaviour is very important in engineering practice, where it is planned to construct a structure in a jointed rock mass. Whether the structure is confined by a low or high stress level, the deformational behaviour of the structure for the critical joint orientations (45 to 65°) will be different. It is therefore important to pay attention to the magnitude of the deformation before and after peak stress, and in fact, the maximum magnitude of allowable strain should be determined in addition to the maximum stress. For this reason selecting a failure criterion that employs only peak stress may be wrong.

Confining pressure has also important effects on the peak strength and deformational behaviour of the jointed specimens with even low inclinations (15 to 30°) where low confining pressure (around zero) is applied. This effect is demonstrated well in figure 6.14 for zero confinement and 30° joint orientation in which a large amount of deformation along the joint has taken place before fracturing through a new shear failure. Increase of confining pressure from zero to 5 MPa, however, has limited the deformation at peak significantly, so that the sliding over the joint has nearly stopped, and also the peak strength has reached near to the 15° orientation for the same confining pressure.

6.10.2 EFFECTS OF JOINT INCLINATION

Joint inclination has pronounced effects on both failure strength and strain. The failure strength tends to be reduced when joint inclination exceeds 15° and with further increase in inclination failure strength decreases more noticeably (figures 6.14 to 6.19). This being at its minimum at about the inclination of 60° (figure 6.76) when width /

height ratio = 0.5, the curve rises steadily near to the intact strength at the line of 90° inclination.

As the inclination exceeds the angle 63° 30' with width / height ratio = 0.5, the joint plane cuts the top and bottom surfaces of the specimen. As a result, sliding along the joint is resisted by the end platens, and if a compressive test is carried out the failure strength increases. The increase in strength in this case is due to the concentration of stresses on the wedges of the specimen, and thus depends upon the strength of the rock material. In fact, the stress is not distributed homogeneously through the specimen and therefore the corresponding failure strength and strain will not be the real representative of the jointed specimen. For this reason, in the range of 60 to 90° orientations no test was performed; instead, in order to obtain complete curves for different orientations in the range of zero to 90°, the failure strength for 75° orientation was selected the same as 15° inclination. The same failure strengths were also assumed for zero and 90° inclinations after examination and comparison of the results of a series of primary tests performed on the specimens having the two orientations of zero and 90°.

The curves of differential stresses versus inclination (figure 6.76) are concave and shift upwards with increased confining pressure. The curves are flatter in low confining pressures especially around zero; this is an indication of the greater influence of the joint inclination on the failure strength at lower confinements.

The effects of joint inclination on the failure strength are shown more clearly by the differential stress versus confining pressure envelopes in figures 6.79 to 6.82 for the different rock types containing split or saw cut joints in different orientations. The three rocks tested hold linear relationships between differential stress and confining pressure for the cases of 45 and 60° inclinations for both saw cut (figures 6.79 to 6.81) and split

joint (figure 6.82). It implies that, the linear Coulomb-Navier ($\sigma_1 = \mu\sigma_3 + c$) relationship holds well in the range of confining pressures from zero to 70 MPa.

The envelopes for intact Stainton sandstone and Dumfrith sandstone specimens exhibit linear relationships, in the range of zero to 30 MPa confining pressures but a non-linear relationship for intact Penrith sandstone up to 70 MPa confining pressure. For Penrith sandstone specimens in the range of zero to 30 MPa a linear relationship is also fitted the same as the two other rocks, therefore, it may be concluded that the linear Coulomb-Navier theory is an appropriate relationship to evaluate the ultimate strength of intact rock in the range of confining pressures from zero to 30 MPa. For both zero and 15° orientations a linear relationship is also held (up to 30 MPa as in figure 6.79). For 30° joint angle the relationship is non-linear, but with increase in confining pressure the envelope tends towards linearity. This implies that a unique behaviour for this particular orientation and of the orientations near to it may not be observed in low and higher confining pressures. The envelopes for the zero and 15° orientations are very close to each other and to the intact envelope (figure 6.79). It is an indication of less significance of joint inclination on the failure strength up to 15°.

Differential stress-confining pressure envelopes for the split breakage joints (figure 6.82) hold linear relationships for all the orientations of 30, 45, and 60°. A very interesting point in split joint plots is the higher slope of the 60° orientation envelope with respect to the 45 and 30°. Despite the fact that it has been placed entirely below the 45° envelope (figure 6.82), and also for the same confining pressure the shear and normal stresses belonging to each point on the 45° orientation envelope are higher than those of the 60°, however, as normal stress increases across the joint the 60° envelope comes closer to that of 45°. This behaviour demonstrates well the role of surface roughness for the critical joint orientations, and is of great importance for design purposes in jointed media, where a high sliding friction is vital.

Further significance of joint surface roughness may be evaluated by studying the Mohr envelopes for rough surfaces (split joint) as in figures 6.83 and 6.84. In these figures for both sandstones (Penrith and Stainton sandstone), Mohr envelopes for 60° orientation containing split breakage joint (rough surface joint) are above those of 45° in both saw cut and split joints that is to say, a higher coefficient of sliding friction and therefore a higher shear strength across the joint in this case. It is necessary to note that this trend does not imply that for the same confining pressure the shear strength on 60° orientation is higher than that of 45°. Tables 6.34 and 6.35 show the ratios of the shear to normal stresses, namely the coefficient of sliding friction for each pair of principal stresses for the two orientations of 45 and 60°. Although the magnitudes of the shear and normal stresses for 60° orientation with rough surface for the confining pressures of 5, 15 and 30 MPa are lower than those of 45°, however, the ratios of each pair of shear to normal stresses for 60° orientation are considerably higher than those of 45°. The mean of the ratios of t/s for 60° orientation is 0.994, whereas that of 45° is 0.741. This trend,however, for saw cut joints (smooth surface) is not observed, and the mean of the t/s for 45° orientation is 0.584 which is higher than 0.416 of the 60°. It implies that a rough sliding surface through a critical joint orientation (60°, for instance) provides a higher coefficient of friction with respect to a lower orientation such as 45°.

Examination of tables 6.7 and 6.36 which illustrate the strength descending coefficients for saw cut and split joints with different orientations for Penrith sandstone specimens show that the degree of joint surface roughness in a joint with 60° orientation has a greater importance than in a joint with 45° orientation. The strength coefficients for saw cut joints in 45 and 60° orientations for 5 MPa confining pressure as in table 6.7 are 0.194 and 0.074 ,and in the same confining pressure, for split joint (rough surface) as in table 6.36, are 0.414 and 0.213 respectively. The ratio of the strength coefficients for 45 and 60° for two cases of saw cut and split thus obtained is 0.414/0.194 = 2.13 and

0.213/0.074 = 2.87 respectively which demonstrates clearly that the ratio for 60° (2.87) is greater than the 45° (2.13). At 15 and 30 MPa the ratios for 45 and 60° orientations are 1.78 and 3.59 (in 15 MPa) and 1.22 and 2.2 (in 30 MPa) respectively which shows that the 60° ratios are greatly higher than those of the 45°. This implies that in the same condition (the same rock and under the same confining pressure) a rough joint surface plays a more important role in a critical joint orientation (60°) than the other orientations (45°, for instance). The same trend in Stainton sandstone specimens for rough and saw cut joints with orientations of 45 and 60° is also observed (compare the strength coefficients in table 6.13 and 6.37). This behaviour may be explained as follows:

The main reason may be attributed to the non-planarity of the sliding surface in the split breakage joints. When the sliding surface is smooth and completely planar (saw cut joint), distribution of shear stress throughout the joint surface will be homogeneous. In a split breakage joint with rough sliding surface, however, the joint can be non-planar and therefore, distribution of shear stress may not be homogeneous. Such a difference in behaviour in planar and non-planar joints may result in different behaviours in the shear resistance of a non-planar joint at various inclinations. That is to say, when joint inclination increases and reaches a critical (say 60°) orientation, the joint shear resistance in a non-planar joint against a shear stress increases in a greater proportion with respect to the joint shear resistance with a lower orientation (say 45°). In fact, in the case of 60° orientation because of the convenient direction of sliding a higher degree of interlocking asperities is provided through a rough surface. This leads to the failure of asperities from their bases rather than the tops or the middles, and therefore a greater shear resistance results. Increased confining pressure also causes further intrusion of asperities into the others and therefore,a stronger bond is produced through the bases of asperities leading to higher coefficient of friction in the case of critical orientations such as 60°.

A better understanding of the effects of joint inclination on the failure strength of the rocks tested may be obtained by the strength descending coefficients (the proportion of the compressive strength of the specimen containing joint to that of the intact specimen) as in tables 6.7,6.13 and 6.36 for both saw cut and split joints in different orientations for the three rocks tested. Examination of the tables show that the effect of joint inclination on the peak strength of the specimens having zero and 15° orientations are not significant, however as the joint inclination increases to 30° and more, reduction in peak strength accelerates so that at zero confining pressure for 30° orientation the strength has reduced to 18.9% of the intact rock. The strength coefficients for 45 and 60° orientations in zero confining pressure are very near to zero; however, with an increase in confining pressure the strength coefficient increases up to 45% for 60° orientation in 70 MPa confining pressure (table 6.7).

Comparison of the strength descending coefficients for saw cut joints, shear-surface, and split breakage joints reveals that the joint inclination has had the highest effect on the failure strength of the specimens containing saw cut joint with 60° orientation. However, the effects on the split breakage joints were minimum (tables 6.7, 6.13 and 6.17). Stress level during sliding on the saw cut joints with 60° inclination at all levels of confining pressures applied (0-70 MPa) is below the stress level in other types of joints with any orientation in the same confining pressure (figure 6.63 to 6.67, for instance). It is also under the residual stress level in the intact specimens at different confining pressure levels applied in this experiment (figure 6.63 and 6.65 to 6.67).

Effects of joint inclination on the deformational behaviour of the rocks tested were quite pronounced, even at low inclinations of 0 and 15°. Figures 6.14 to 6.19 and 6.65 to 6.75 illustrate the stress-strain plots of the three rocks tested in different confining pressures and joint orientations. The peak stresses for even zero and 15° inclinations

have shifted towards further axial deformation. For 30° orientation after a considerable amount of sliding over the joint the specimen failed through a new shear failure plane. For 45 and 60° orientations in low and high confining pressures the peak shifting is clearer (figures 6.65 and 6.66, for instance). For further consideration of the deformational behaviour of jointed specimens tested , the maximum axial strain at peak is given in the tables for different situations.

6.10.3 EFFECTS ON THE APPARENT MODULUS OF DEFORMATION

Examination of the stress-strain plots for jointed and intact specimens and comparing them with each other for various inclinations, confining pressures, type of joint, and type of rock as in figures 6.65 to 6.72 suggest that in assessment of the effects of a single joint in a rock specimen on its modulus of deformation some distinct considerations must be made. In the first step a close attention should be paid to differentiate between the modulus of deformation in an intact specimen and a jointed specimen particularly when the surface roughness is very low because the sliding movement from the initiation of loading is appreciable.

It seems that the conventional method of determining the modulus of deformation in which the slope of the stress-strain curve in the linear portion is taken as the modulus of deformation is not the most appropriate way in jointed specimens. Using this method in many cases with no consideration of other parameters may result in findings which are not at all realistic. For instance, in figure 6.65 determining the modulus of deformation in this way for both 45 and 60° inclinations the magnitude of it is nearly the same as that of the intact specimen, or in figure 6.68 for a split joint with 45 and 60° orientations the modulus of deformation for both jointed and intact specimens and also for both 45 and 60° orientations using the conventional method is exactly the same.

It seems the most reliable method of evaluating the modulus of deformation in a jointed rock is to consider the displacement through the rock as the first and major factor. In other words before any judgement is made on the amount of modulus of deformation the maximum allowable displacement must be identified. Thereafter, it is possible to assess and determine a correct and appropriate modulus of deformation with respect to the real conditions prevailing in the jointed rock. In figure 6.66, for instance, if a maximum displacement equal to the displacement at the peak in the intact specimen (about 1.2%) is considered, the modulus of deformation for the specimen with 60° inclination at this amount of strain is dramatically affected by the joint and reduced to a very low level. However, if a very low axial strain is chosen as the criterion, for instance 0.15%, as is seen in figure 6.66, the modulus of deformation for the specimen with 60° inclination is nearly the same as that of the intact specimen. The same observations may be made for the split breakage joint as in figure 6.68. Therefore, in assessment and determination of the modulus of deformation in a jointed specimen or in fact in a jointed rock mass the upper limit of the allowable displacement through the joint must be introduced; thereafter, the corresponding modulus of deformation will be determined. This implies that it is not possible to introduce an identifiable modulus of deformation for a jointed rock similar to that of an intact rock.

6.10.4 SHEAR STRENGTH AND THE COEFFICIENT OF FRICTION

Shear strength of the rocks tested was highly affected by the presence of the joint and of its inclination. Figures 6.83 to 6.85 show that the shear strength of the jointed specimens has greatly reduced in comparison with the intact specimens. Increase in shear strength for both intact and jointed specimens is stress-dependent. In some orientations and in the split joint types the relationship between shear stress and normal stress holds non-linear, whereas in the critical joint inclinations (45 to 65°) it holds linear.

Figure 6.83 demonstrates well that, although the shear strength of the jointed specimens with respect to the intact has begun to decrease at about 30° orientation, the average coefficient of frictions has not changed so much (table 6.31). For zero and 15° orientations the friction angles do not differ too far from the intact specimens (table 6.31).

Reduction in both shear strength and coefficient of friction or angle of friction for orientations of 45 and 60° containing saw cut joints is very considerable, so that the angle of friction for 60° orientation has decreased to about 22° which is less than half of the intact Penrith sandstone specimens. This comparison demonstrates very well the significance of bare joints (saw cut) having critical orientations when subjected to a stress field.

The Mohr envelope for saw cut joint in the orientations of 45 and 60° holds linear for the three rock types tested. In the split joints, however, with the same inclinations (45 and 60°) the envelopes are non-linear. This implies that Coulomb theory is an appropriate criterion to evaluate the shear strength across the joint with low surface roughness, but not for rough surfaces. The difference in envelopes for the split and saw cut joints may be attributed to the fact that the joint surfaces in the split breakage joints is non-planar which exhibits a higher shear resistance and therefore, a higher coefficient of friction. For this reason the coefficient of friction in the split breakage joints is very near to the intact specimens (table 6.31).

The shape of the split joint envelopes is typical of those reported for rock types tested in direct shear apparatus (Patton, 1966 and Barton and Chouby, 1977).

6.10.5 VOLUMETRIC STRAIN, LATERAL STRAIN AND INSTANTANEOUS POISSON'S RATIO

The volumetric strain versus axial strain curves show a systematic change with confining pressure both in intact and jointed specimens. All the curves for intact specimens show the same general form; a small volume decrease occurs at low strains, the slope of the curve then changes rapidly in the yielding region, and a final, near linear curve, after yielding (figures 6.20, 6.29 and 6.38). This behaviour is greatly affected by the increased confining pressure, so that a high volume decrease is observed in higher confining pressures (70 MPa for instance, as in figure 6.20).

The uniaxially-tested intact specimens give very large volumetric expansions with increasing lateral strain. The effect of confining pressure on the volumetric expansion is very marked, with a large reduction for an increase in confining pressure at low confining pressures, diminishing as confining pressure is increased. If the confining pressure increases to above a certain threshold value, dependent upon the rock type, no volumetric expansion will occur (in this experiment as in figures 6.20 and 6.38 the threshold values are 30 and 15 MPa for Penrith sandstone and Dumfrith sandstone respectively).

In jointed specimens the volumetric strain versus axial strain curves do not show a unique form, but depend upon the joint orientation, joint type, and the mechanism of deformation. It is necessary to differentiate between the concept of volumetric strain in intact specimens and jointed one particularly when the mechanism of deformation is dominated by sliding movement along the joint. In this case volumetric strain is directly a measure of joint closure (joint normal displacement or joint shortening; Barton, 1986) or joint dilation (normal displacement or joint thickening; Goodman, 1976) and joint shear displacement. There is not an absolute increase in specimen volume at all during

the deformation process, but relative increases in volume at some portions which are an indication of dilation at those positions. It is also necessary to note that occasional fluctuations in the sliding portion of the volumetric strain-axial strain curves particularly those related to saw cut joints, are mainly due to errors in reading the displaced oil by eye. As the magnitude of volume change in the jointed specimens was very little (less than 1%) it was very sensitive to a small error in reading the oil level from the graded cylinder. For instance, a change of 0.2 cc in the amount of oil dripping through the relief valve affects the calculations considerably.

For the specimens containing joint with orientations less than 30^{o}, there is a similarity in the volumetric strain behaviour with the intact specimens. For those in the range of 25 to 45^{o} orientations in which the mode of deformation is a combination of sliding along the joint and then occurrence of a new shear failure through the intact rock, decrease in volume occurs at a relatively high axial strain, and then, the slope of the curve changes rapidly accompanied by a high volume expansion similar to the intact specimens. As figure 6.32 shows in the first portion of the curve there is not a steady slope, but it changes at different times which is a measure of relative expansion and contraction (joint dilation and closure) in this region.

This behaviour is attributed to the sliding characteristics of the joint in which the asperities are damaged and sheared off regularly during sliding. This is in fact, a measure of dilation through the joint and not through the whole specimen.

For the orientations in which the mechanism of deformation is characterized by sliding along the joint surface, volumetric deformation is completely different from that of the intact specimens, no volumetric expansion occurs in this case, both at low and high confining pressures, but decrease in volume is observed at low axial strain, and with a further increase in the axial strain, volume change tends to a near constant value. The

remarkable aspects of the volumetric strain-axial strain curves, in this case, are as follows:

1. All the curves have steep slopes at low axial strains representing a volume decrease up to a peak, the slope then changes slowly and continues towards a reasonably constant volumetric strain at higher axial strains (figures 6.23, 6.26, 6.35, 6.41, 6.50 and 6.53).

2. The first portion of the curves depending on the amount of interlocking of asperities and in fact,on the degree of surface roughness, is near to linear. This part indicates the elastic behaviour of the joint in the beginning of the loading process and before sliding through the joint is initiated.

3. Increased confining pressure results in a further decrease in volumetric strain up to a certain axial strain, then a relative expansion (not real expansion) begins and it increases as axial strain increases, i.e. the slope of the curve after peak at higher confining pressure is steeper than that of a lower confining pressure (figures 6.23 and 6.26 for 70 MPa).

4. Occasional portions in the volumetric strain-axial strain plots are observed in which the slope direction changes inversely (in a fluctuating manner). These events are repeated several times in the split breakage joints in which the joint surface roughness is very high (figures 6.50 and 6.53). These indicate that at some points during sliding successive relative expansions and contractions have occurred. This behaviour demonstrates the dilation characteristics of a rough joint very well. In figure 6.50, for instance, after loading was initiated the volume rapidly decreased to a maximum (because of the joint closure), then the slope changed steeply in an inverse direction which is the beginning of some dilation (displacement perpendicular to the joint) accompanied by sliding along joint. The dilation appears in terms of a relative

volumetric expansion by dropping the curve to a lower volumetric strain. The beginning of dilation in a rough joint coincides with the beginning of sliding along the joint plane and also with a dropping of the peak stress in the axial stress-strain curve as in figure 6.45. After the first dilation occurs through the joint, decreasing in the volume again continues at a rate proportional to the applied confining pressure, and also to the degree of surface roughness. Again, similar changes in the slope direction may occur as sliding continues. These processes are repeated until all the asperities are almost sheared off, and a reasonably smooth surface is formed. This behaviour corresponds to the axial stress-strain behaviour of the jointed specimens with orientations in the range of 45 to 65o in which the mechanism of deformation is dominated by frictional sliding, and eventually reaches an approximately constant stress value with no further increase in the volumetric strain.

The shape of the curves for intact rocks is typical of those reported for soils and rocks (Atkinson and Bransby, 1978; Scholz, 1968a; Edmond and Paterson, 1972; Crouch, 1970 and 1972b and Price, 1979), and correspond to the axial stress-strain of the rock. At all pressures below the threshold point, axial deformation results in first to linear deformation of the specimens corresponding to the elastic region of the axial stress-strain curves. The specimen then expands at a rate depending upon the rate of fracturing, reflected in the rate of unloading in the axial stress-strain curve. Then, once fracturing has occurred, the mechanism of deformation is frictional sliding, similar to the jointed specimens in the last region of the stress-strain curve, giving approximately constant residual stress and linear volumetric strain curves.

A better understanding of the difference in deformational behaviour of the jointed and intact specimens may be drawn by comparison of the axial stress-volumetric strain curves. Figures 6.35 to 6.37 illustrate the typical axial stress-volumetric strain plots for the intact and jointed specimens containing saw cut and split joints. Each curve has its

own particular characteristic shape, for the intact specimens both expansion and contraction have occurred clearly in 10 and 30 MPa confining pressures, the specimens have contracted up to a point (at the point in which the instantaneous Poisson's ratio is 0.5) and then with increased axial stress, it has started expanding and in the post failure region expansion has accelerated. In jointed specimens (figures 6.35 and 6.36), however, a clear distinction can be made with the intact specimens, in which only a limited reduction in volume with no expansion relative to the initial volume is observed. The difference between the saw cut and split joints plots is also of particular interest, the saw cut joint curves are S-shaped, whereas in the split joint curves a closed loop is observed, which is an indication of dilation at the peak stress, and shows that the direction of the volumetric strain from reduction in volume has changed to expansion in a limited portion.

The values of instantaneous Poisson's ratio plotted here are the ratio of the lateral to the axial strains, calculated at different axial strains.

Poisson's ratio decreases rapidly as confining pressure is increased both in the intact and jointed specimens, and appears to reach a constant value which for both jointed and intact rock types seems to be 0.5, corresponding to no volume change in the specimen with deformation (figures 6.21, 6.24, 6.27, 6.30, 6.33, 6.39, 6.42, 6.51 and 6.54). Figures 6.21 and 6.24, for instance, illustrate the Poisson's ratio versus axial strain plots for intact and jointed (orientation of 45o) Penrith sandstone specimens, the change in the shape due to increase in confining pressure is readily observed, and also the reduction in uniaxial value of Poisson's ratio with strain is completely clear (figure 6.21), which is typical of all the intact specimens. The magnitude of Poisson's ratio approaches to a near constant value for each confining pressure in both the jointed and intact specimens once frictional sliding occurs along the shear-surface failure in intact specimens and along the joint surface in the jointed specimens.

Variation of Poisson's ratio in the jointed specimens has a direct relation with the sliding characteristics and the degree of surface roughness. For this reason some difference between the Poisson's ratio-axial strain curves in the saw cut (smooth) and rough joints mainly at low strains (up to about 1%) may be observed. In the rough joints because of the very low rate of lateral displacement (lateral strain) before sliding initiation, the axial strain-lateral strain curve at low strains is very flat (figure 6.51). In the saw cut joints, however, due to sliding movement from the beginning of loading the rate of lateral displacement is very high. for this reason the axial strain-lateral strain plot has a steep slope at low strains (figures 6.27, 6.33 and 6.42).

The shape of the plots for intact rocks is similar to those reported elsewhere (Scholz, 1968a; Walsh and Brace, 1966).

The experimental results indicate that the lateral strain-axial strain curves have a characteristic shape both in intact and jointed specimens: initially linear, then non-linear, and then linear again (figures 6.22, 6.25, 6.28, 6.31, 6.34, 6.40, 6.43, 6.52, and 6.55). Lateral strains decrease with increased confining pressure for both jointed and intact rocks. In the intact specimens the maximum rate of change of lateral straining occurs in the neighbourhood of the peak axial stress and then reduces to a near constant value giving a near linear curve. In the jointed specimens the rate of change of lateral straining depends upon the joint orientation angle and the degree of surface roughness. For the orientations up to 30o, the maximum rate occurring in the neighbourhood of the peak axial stress is similar to the intact specimens. In fact in this case, as the mechanism of failure is by shear fracture through the intact rock, a great similarity exists with the intact specimens. This similarity reduces when the mechanism of deformation is a combination of sliding along the joint and shear failure through the intact material (figure 6.34).

For the orientations in which the mechanism of deformation is by sliding along the joint, the surface roughness has a significant role in the rate of lateral strains at low axial strains. When the joint surface is rougher a higher rate of lateral strains particularly at low confining pressures is observed at the initiation of sliding over the joint (figure 6.52). This is in fact a measure of dilation of the joint at that point. Because of dilations in subsequent points during sliding (in the split breakage joint) the lateral strain versus axial strain curves in rough joints continues non-linear in a wider interval of straining (figures 6.52 and 6.55). Similar results have been reported for intact rock by other workers (Crouch ,1970 & 1972a & b and Price, 1979).

Table 6.1 Summary of the results of triaxial tests on intact and jointed (saw cut) Penrith sandstone specimens.

confining pressure = 0

joint angle deg.	stress at failure MPa	mode of failure	axial strain at failure %	residual strength MPa
intact	79	shear failure	0.83	3
0	73	//	0.875	3
15	71	//	0.96	2
30	15	sli+shea	3.35	1.8
45	3	sliding	-	3
60	0	//	-	0

Table 6.2 Summary of the results of triaxial tests on intact and jointed (saw cut) Penrith sandstone specimens.

confining pressure = 5 MPa

joint angle deg.	stress at failure MPa	mode of failure	axial strain at failure %	residual strength MPa
intact	154.5	shear failure	1.08	40
0	125	//	1.123	23
15	123	//	1.22	25
30	117	//	1.27	28
45	30	sliding	2.1	30
60	11.5	//	1.1	11

Table 6.3 Summary of the results of triaxial tests on intact and jointed (saw cut) Penrith sandstone specimens.

confining pressure = 10 MPa

joint angle deg.	stress at failure MPa	mode of failure	axial strain at failure %	residual strength MPa
intact	166	shear failure	1.125	68
0	157	//	1.128	38
15	153	//	1.31	47
30	139	//	1.35	36
45	65	sliding	1.5	65
60	30	//	0.9	30

Table 6.4 Summary of the results of triaxial tests on intact and jointed (saw cut) Penrith sandstone specimens.

confining pressure = 15 MPa

joint angle deg.	stress at failure MPa	mode of failure	axial strain at failure %	residual strength MPa
intact	205	shear failure	1.21	85
0	172	//	1.24	60
15	1170	//	1.28	68
30	158	//	1.31	38
45	87	sliding	0.82	85
60	35	//	1.5	35

Table 6.5 Summary of the results of triaxial tests on intact and jointed (saw cut) Penrith sandstone specimens.

confining pressure = 30 MPa

joint angle deg.	stress at failure MPa	mode of failure	axial strain at failure %	residual strength MPa
intact	298	shear failure	1.45	150
0	295	//	1.6	140
15	290	//	1.63	145
30	288	//	1.80	160
45	180	sliding	1.25	170
60	87	//	1.5	87

Table 6.6 Summary of the results of triaxial tests on intact and jointed (saw cut) Penrith sandstone specimens.

confining pressure = 70 MPa

joint angle deg.	stress at failure MPa	mode of failure	axial strain at failure %	residual strength MPa
intact	440	shear failure	4.35	265
45	335	sliding	2.5	280
60	198	//	2	190

Table 6.7 Strength descending coefficients for Penrith sandstone with saw cutjoints. (Strength descending coefficient is the ratio of the strength of jointed specimen to that of intact)

confining pressure MPa	joint orientation angle degrees					intact compressive strength MPa
	0	15	30	45	60	
0	0.924	0.898	0.189	0	0	79
5	0.809	0.796	0.757	0.194	0.074	154.5
10	0.945	0.921	0.837	0.391	0.181	166
15	0.839	0.829	0.771	0.424	0.171	205
30	0.990	0.973	0.966	0.604	0.292	298
70	-	-	-	0.761	0.450	440

Table 6.8 Summary of the results of triaxial tests on intact and jointed (saw cut) Stainton sandstone specimens.

confining pressure = 0

joint angle deg.	stress at failure MPa	mode of failure	axial strain at failure %	residual strength MPa
intact	60	shear failure	1.15	2
30	26	sli+shear	1.3	1.8
45	4	sliding	-	3
60	0	//	-	0

Table 6.9 Summary of the results of triaxial tests on the artificially jointed and intact Stainton andstone.

confining pressure = 5 MPa

joint angle deg.	stress at failure MPa	mode of failure	axial strain at failure %	residual strength MPa
intact	108	shear failure	1.2	27
30	85	//	1.3	30
45	74	sli+shear	1.82	23
60	20.5	sliding	1.7	15

Table 6.10 Summary of the results of triaxial tests on intact and jointed (saw cut) Stainton sandstone specimens.

confining pressure = 10 MP

joint angle deg.	stress at failure MPa	mode of failure	axial strain at failure %	residual strength MPa
intact	137	shear failure	1.22	50
30	130	//	1.33	58
45	102	sli+shear	2.25	37
60	43	sliding	1.8	33

Table 6.11 Summary of the results of triaxial tests on intact and jointed (saw cut) Stainton sandstone specimens.

confining pressure = 15

joint angle deg.	stress at failure MPa	mode of failure	axial strain at failure %	residual strength MPa
intact	160	shear failure	1.3	53
30	145	//	1.45	58
45	123	sli+shear	2.3	55
60	50	sliding	1.2	40

Table 6.12 Summary of the results of triaxial tests on intact and jointed (saw cut) Stainton sandstone specimens.

confining pressure = 30 MPa

joint angle deg.	stress at failure MPa	mode of failure	axial strain at failure %	residual strength MPa
intact	250	shear failure	1.8	140
45	160	sliding	1.5	150
60	100	//	3.3	90

Table 6.13 Strength descending coefficients for Stainton andstone specimens with saw cut joints.

confining pressure MPa	joint orientation angle degrees					intact compressive strength MPa
	0	15	30	45	60	
0	-	-	0.433	0.050	0	60
5	-	-	0.787	0.685	0.190	108.5
10	-	-	0.949	0.744	0.317	137
15	-	-	0.906	0.768	0.262	160
30	-	-	-	0.640	0.400	250

Table 6.14 Summary of the results of triaxial tests on the jointed (saw cut) and intact Dumfrith sandstone specimens.

confining pressure = 5 MPa

joint angle deg.	stress at failure MPa	mode of failure	axial strain at failure %	residual strength MPa
intact	55	shear failure	0.85	20
30	52	//	0.9	25
60	15.8	sliding	1.15	15

Table 6.15 Summary of the results of triaxial tests on the jointed (saw cut) and intact Dumfrith sandstone specimens.

confining pressure = 10 MPa

joint angle deg.	stress at failure MPa	mode of failure	axial strain at failure %	residual strength MPa
intact	82	shear failure	1	45
30	68	//	1.08	40
60	28	sliding	2	28

Table 6.16 Summary of the results of triaxial tests on the jointed (saw cut) and intact Dumfrith sandstone specimens.

confining pressure = 15 MPa

joint angle deg.	stress at failure MPa	mode of failure	axial strain at failure %	residual strength MPa
intact	95	shear failure	1.1	60
30	80	//	1.2	50
60	41.5	sliding	1.7	36

Table 6.17 Strength descending coefficients for Dumfrith sandstone specimens with saw cut joint.

confining pressure MPa	joint orientation angle degrees		intact compressive strength MPa
	30	60	
0			32
5	0.94	0.29	55
10	0.83	0.34	82
15	0.84	0.43	95

Table 6.18 Summary of the results of triaxial tests on the jointed (split breakage) and intact Penrith sandstone specimens.

confining pressure = 5 MPa

joint angle deg.	stress at failure MPa	mode of failure	axial strain at failure %	residual strength MPa
intact	154.5	shear failure	1.08	40
30	146	//	.92	35
45	64	sliding	.62	28
60	33	//	.55	21

Table 6.19 Summary of the results of triaxial tests on the jointed (split) and intact Penrith sandstone specimens.

confining pressure = 15 MPa

joint angle deg.	stress at failure MPa	mode of failure	axial strain at failure %	residual strength MPa
intact	205	shear failure	1.21	85
30	183	//	1.1	88
45	155	sliding	.85	90
60	126	//	.65	60

Table 6.20 Summary of the results of triaxial tests on the jointed (split) and intact Penrith sandstone specimens.

confining pressure = 30 MPa

joint angle deg.	stress at failure MPa	mode of failure	axial strain at failure %	residual strength MPa
intact	298	shear failure	1.45	150
30	263	//	1.42	133
45	202	sliding	1	130
60	192	//	.85	100

Table 6.21 Summary of the results of triaxial tests on the jointed (split) and intact Stainton sandstone specimens.

confining pressure = 5 MPa

joint angle deg.	stress at failure MPa	mode of failure	axial strain at failure %	residual strength MPa
intact	108	shear failure	1.2	27
30	108	//	1	32
45	74	sliding	.8	34

Table 6.22 Summary of the results of triaxial tests on the jointed (split)m and intact Stainton sandstone specimens.

confining pressure = 15 MPa

joint angle deg.	stress at failure MPa	mode of failure	axial strain at failure %	residual strength MPa
intact	160	shear failure	1.3	53
30	160	//	1.35	73
45	108	sliding	.85	70
60	76	//	.65	52

Table 6.23 Summary of the results of triaxial tests on the jointed (shear-surface) Penrith sandstone specimens.

confining pressure = 30

conf. pre. to form joint MPa	stress at failure MPa	mode of failure	axial strain at failure %	residual strength MPa
0	217.62	sliding	1.97	174.5
10	168.84	//	-	170
0 Mul. stage	175	//	-	174
10 Mul. stage	166	//	-	163

Table 6.24 Summary of the results of triaxial tests on the jointed (shear-surface) Penrith sandstone specimens.

confining pressure = 70

conf. pre. to form joint MPa	stress at failure MPa	mode of failure	axial strain at failure %	residual strength MPa
0	353.55	sliding	2.223	325
10	351.5	//	2.25	335.25
0 Mul. stage	332	//	-	329
10 Mul. stage	329.23	sliding	-	319.23

Table 6.25 Strength descending coefficients for penrith sandstone specimens with shear-surface joints.

confining pressure MPa	joint forming condition (MPa)				intact compressive strength MPa
	0	10	0 Mult.	10 Mult.	
30	0.73	0.56	0.59	0.55	298
70	0.80	0.80	0.75	0.73	440

Table 6.26 Differential stress vs confining pressure for jointed (saw cut) and intact Penrith sandstone specimens.

confining pressure MPa	differential stress MPa					intact compressive strength MPa
	0	15	30	45	60	
0	73	71	15	3	0	79
5	125	123	117	30	11.5	154.5
10	157	153	139	65	30	166
15	172	170	158	87	35	205
30	295	290	288	180	87	298
70	-	-	-	335	198	440

Table 6.27 Differential stress vs confimimg pressure for jointed (split breakage joint) Penrith sandstone specimens.

confining pressure MPa	differential stress MPa		
	30	45	60
5	146	64	33
15	183	155	126
30	263	202	192

Table 6.28 differential stress vs onfining pressure for jointed (saw cut) and intact Stainton sandstone specimens.

confining pressure MPa	differential stress MPa			intact compressive strength MPa
	30	45	60	
0	26	4	0	60
5	85	74	20.5	108
10	130	102	43	137
15	145	123	50	160
30	-	160	100	25

Table 6.29 Differential stress vs confining pressure for jointed (split) Stainton sandstone specimens.

confining pressure MPa	differential stress Mpa		
	30	45	60
5	108	74	-
10	-	-	56
15	160	108	76
30	-	-	129

Table 6.30 Differential stress vs confining pressure for intact and jointed (saw cut) Dumfrith sandstone specimens.

confining pressure MPa	differential stress MPa		intact compressive strength MPa
	30	60	
5	52	15.8	55
10	68	28	826
15	80	41.5	98

Table 6.31 Average shear stength, angle of internal friction and coefficient of sliding friction for jointed (saw cut and split) and intact Penrith sandstone specimens.

joint angle deg.	shear strength MPa	coefficient of friction	friction angle deg.	min.
intact	28.95	1.05	46	23
0	20.07	0.96	43	50
15	19.52	0.94	43	10
30	18	0.8	38	39
saw cut	3.59	0.584	30	17
45 split	4.11	0.741	36	32
saw cut	0	0.416	22	35
60 split	1.89	0.994	44	49

Table 6.32 Average shear strength, angle of friction and coefficient of sliding friction for Stainton sandstone specimens.

joint angle deg.	shear strength MPa	coefficient of friction	friction angle deg.	min.
intact	15	1.02	45	34
30	13	0.94	43	13
45 (saw cut)	0.46	0.622	31	53
saw cut	1.11	0.5	26	31
60 split	1.76	0.766	37	27

Table 6.34 Summary of the shear and normal stresses through the joints in Penrith sandstone specimens with saw cut and split joints in 45 and 60 degrees orientations.

confining pressure MPa	joint angle deg.	joint type	normal stress MPa	shear stress MPa	ratio of shear to normal stresses
5	45	split	35.66	29.27	0.82
15	45	//	85	70	0.823
30	45	//	126	96	0.761
5	60	//	12	12.12	1.01
15	60	//	42.75	48.06	1.12
30	60	//	70.5	70.14	0.995
5	45	saw cut	18.89	12.45	0.659
10	45	//	42.02	27.18	0.679
15	45	//	53.97	34.77	0.644
30	45	//	111.78	73.29	0.655
70	45	//	221.85	131.39	0.592
5	60	//	7.69	2.25	0.292
10	60	//	7.15	7.58	0.442
15	60	//	23.25	8.66	0.372
30	60	//	50.85	21.6	0.424
70	60	//	117.87	48.67	0.413

Table 6.35 Summary of the shear and normal stesses across the joints in Stainton sandstone specimens with saw cut and split breakage joints and inclinations of 45 and 60 degrees.

confining pressure MPa	joint angle deg.	joint type	normal stress MPa	shear stress MPa	ratio of shear to normal stresses
5	45	split	40.91	34.51	.843
15	45	//	61.5	46.5	.756
10	60	//	21.5	19.92	.926
15	60	//	30.25	26.41	.873
30	60	//	55.5	42.86	.77
5	45	saw cut	41.88	35.45	.822
10	45	//	60.24	41.74	.692
15	45	//	74.52	55.16	.74
30	45	//	101.83	63.3	.621
5	60	//	10.02	6.27	.625
10	60	//	21.18	14.23	.671
15	60	//	27.04	13.61	.503
30	60	//	54.85	28.11	.512

Table 6.33 Average shear strength, angle of friction and coefficient of sliding friction for Dumfrith sandstone specimens.

joint angle deg.	shear strength MPa	coefficient of friction	friction angle deg. min.
intact	8.75	0.9	42
30	7.05	0.766	37 28
60 (saw cut)	0.26	0.392	21 24

Table 6.36 Strength descending coefficients for penrith sandstone specimens with split joints.

confining pressure MPa	joint orientation angle degrees			intact compressive strength MPa
	30	45	60	
5	0.945	0.414	0.213	154.5
15	0.893	0.756	0.615	205
30	0.882	0.678	0.644	298

Table 6.37 Strength descending coefficients for Sainton sandstone with split joints.

confining pressure MPa	joint orientation angle degrees			intact compressive strength MPa
	30	45	60	
5	1	0.685	-	108
15	1	0.675	0.475	160

Plate 6.1 Fractured and deformed unjointed (intact) PS specimens, confining pressure, left to right, 0, 5, 10, 15, & 30 MPa.

Plate 6.2 Fractured and deformed PS specimens with saw cut joint, confining pressure, left to right, 0, 5, 10, 15, & 30 MPa, joint angle=0°.

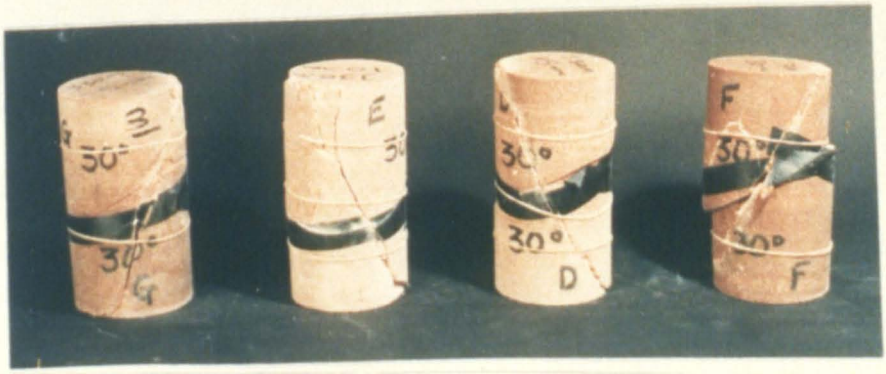

Plate 6.3 Fractured and deformed PS specimens with saw cut joint, confining pressure, left to right, 5, 10, 15, & 30 MPa, joint angle=30°.

PLate 6.4 Fractured and deformed SS specimens with saw cut joint, confining pressure, left to right, 5, 10, & 15 MPa, joint angle= 45°.

Plate 6.5 Fractured and deformed PS specimens with natural joint, confining pressure, left to right, 5, 15 & 30 MPa, joint angle= 30°.

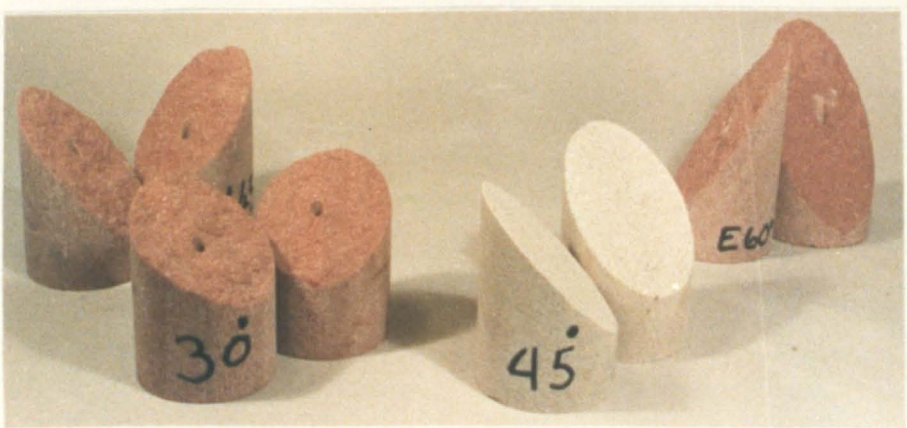

Plate 6.6 Natural and artificial joint sections befor test.

Plate 6.7 Natural and artificial joint sections after sliding and deforming along joint plane, joint angle =45° & 60°, confining pressure, left to right, 30, 15, 30 & 15 MPa.

Plate 6.8 Natural and artificial joint sections after sliding and deforming along joint plane, joint angle =60°, confining pressure, left to right, 15, 5, 15, & 30 MPa.

Plate 6.9 Natural shear surfaces established in intact PS specimens at zero (from left, 1 & 2) and 10 MPa (3 & 4) confining pressure, and then tested as jointed specimens, left to right, 70 MPa, multi-stage test, 70 MPa & multi-stage test.

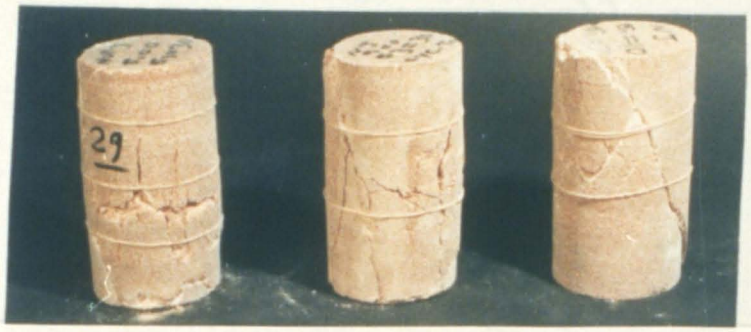

Plate 6.10 Natural shear surfaces established in intact PS specimens at zero (from left, 1&2) and 10 MPa (no. 3) confining pressure ,and then tested as jointed specimens; confining pressure 30 MPa; type of loading, left to right, constant loading and straining, cyclic loading and constant loading and straining.

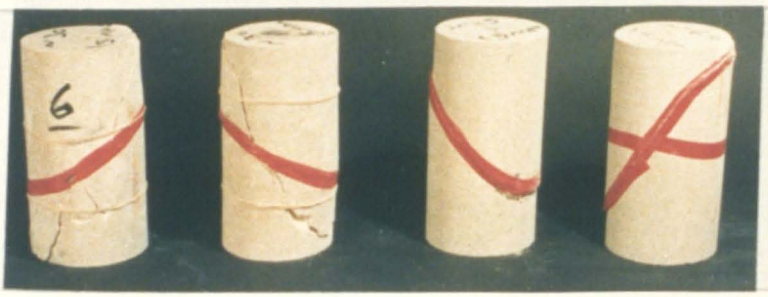

Plate 6.11 Fractured, deformed and slided (sliding along joint plane) SS specimens with natural joint, joint angle, left to right, 30, 30, 45 & 60°, confining pressure 5, 15, 15 & 15 MPa.

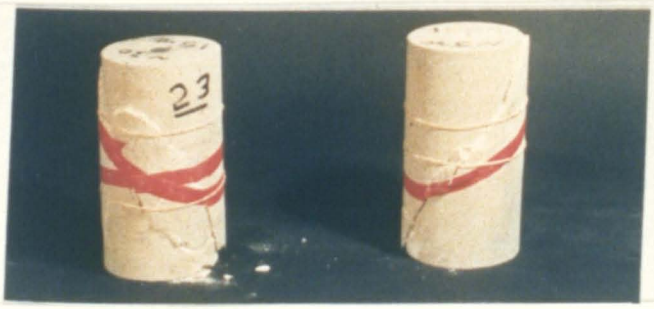

Plate 6.12 Fractured and deformed SS specimens with natural joint, different strain rates during the test: slow-fast-slow (left specimen) and fast-slow-fast (right specimen), confining pressure, left to right, 15 & 30 MPa, joint angle= 30°.

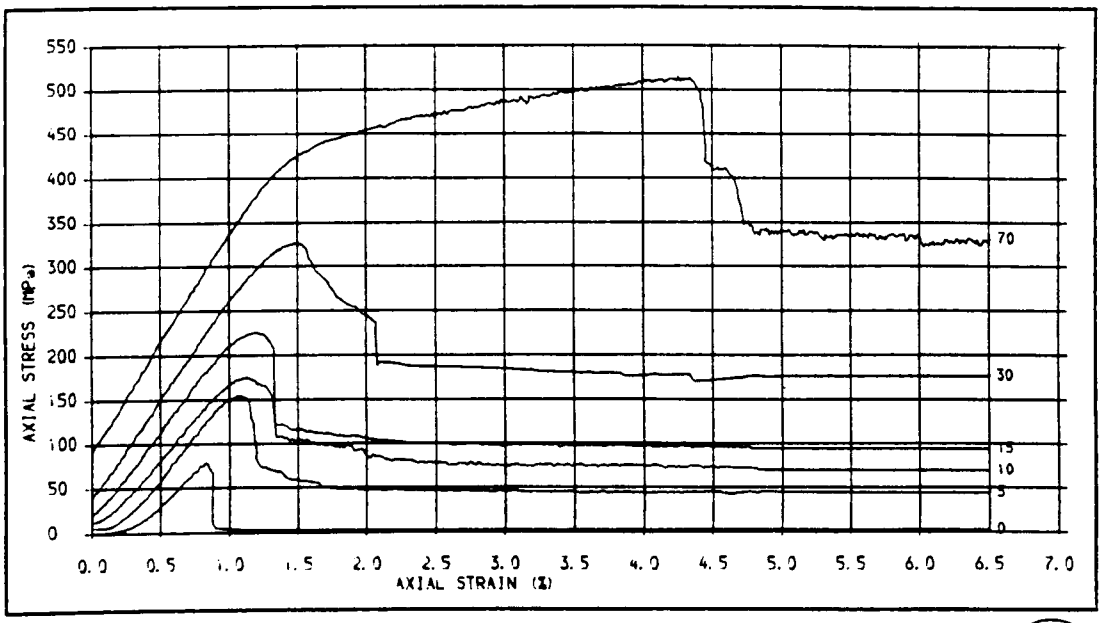

Fig. 61 . STRESS-STRAIN PLOTS FOR INTACT PENRITH SANDSTONE SPECIMENS
CONFINING PRESSURES = 0, 5, 10, 15, 30 AND 70 MPa

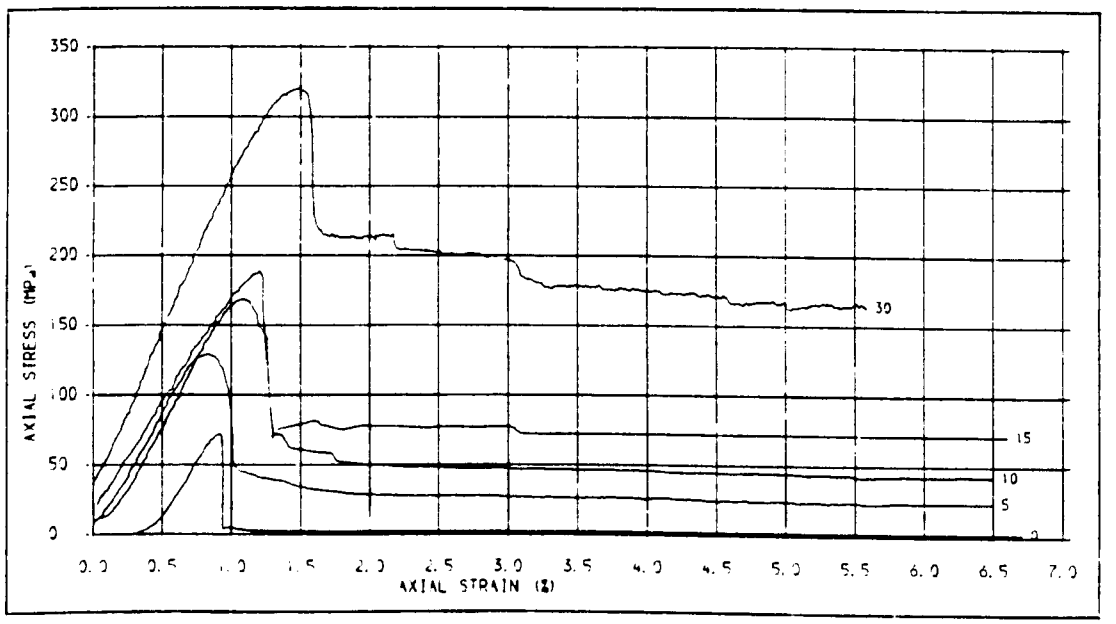

Fig. 62 . STRESS-STRAIN PLOTS FOR PS SPECIMENS WITH SAW CUT JOINTS, JOINT ANGLE = 0 DEC.
CONFINING PRESSURES. 0, 5, 10, 15 AND 30 MPa.

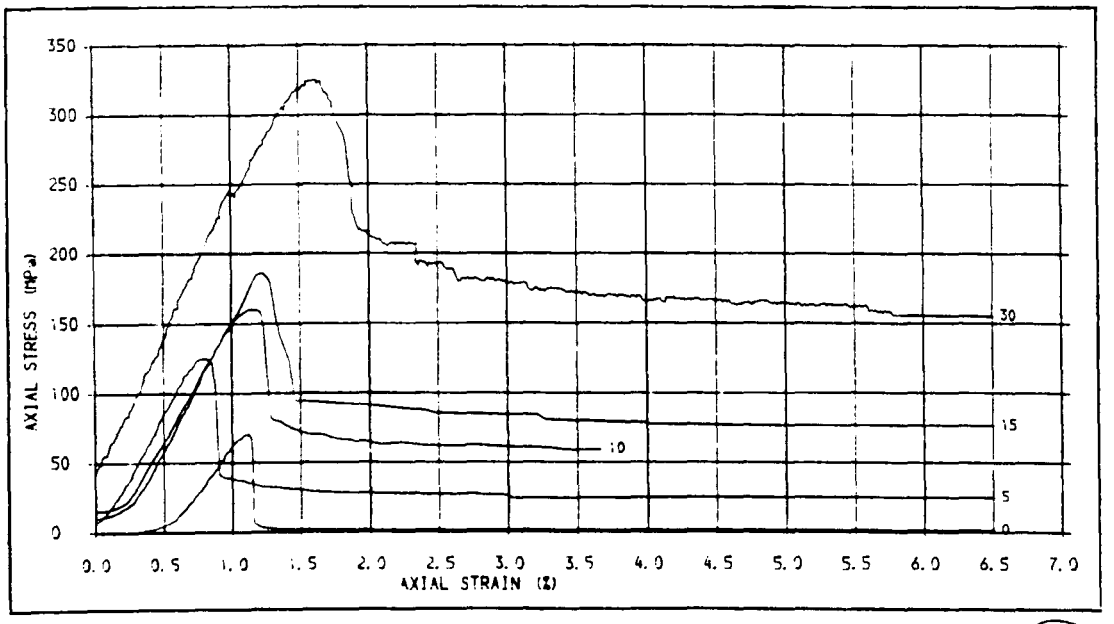

Fig. 53 . STRESS-STRAIN PLOTS FOR PS SPECIMENS WITH SAW CUT JOINTS, JOINT ANGLE = 15 DEG. CONFINING PRESSURES. 0, 5, 10, 15 AND 30 MPa.

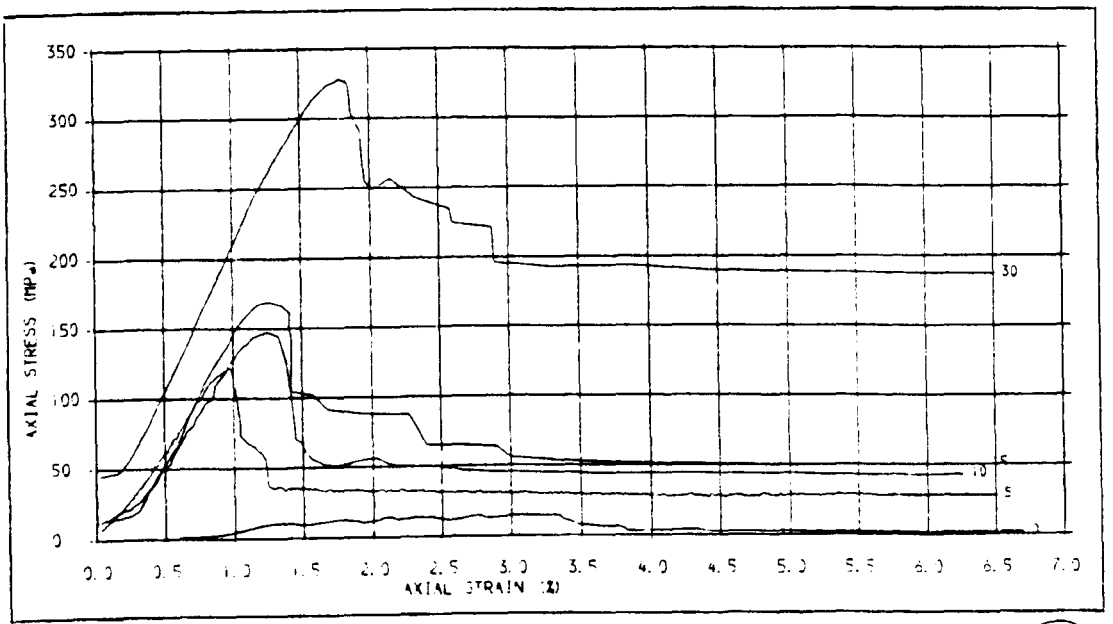

Fig. 54 . STRESS-STRAIN PLOTS FOR PS SPECIMENS WITH SAW CUT JOINTS, JOINT ANGLE = 30 DEG. CONFINING PRESSURES = 0, 5, 10, 15 AND 30 MPa.

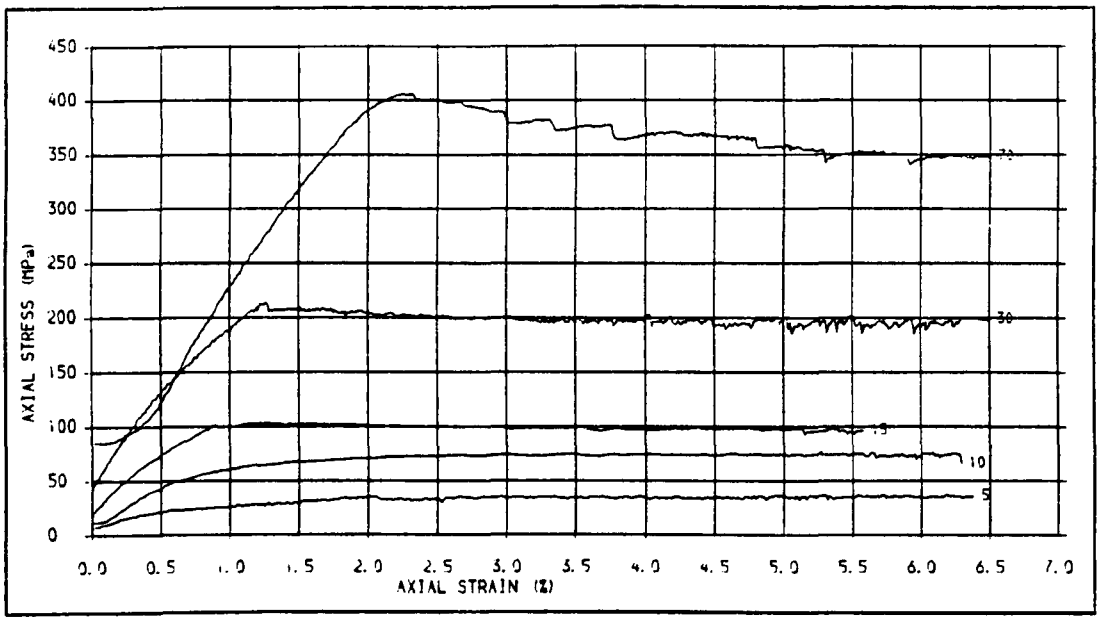

Fig. 65 . STRESS-STRAIN PLOTS FOR PS SPECIMENS WITH SAW CUT JOINTS, JOINT ANGLE = 45 DEC.
CONFINING PRESSURES = 5, 10, 15, 30 AND 70 MPa

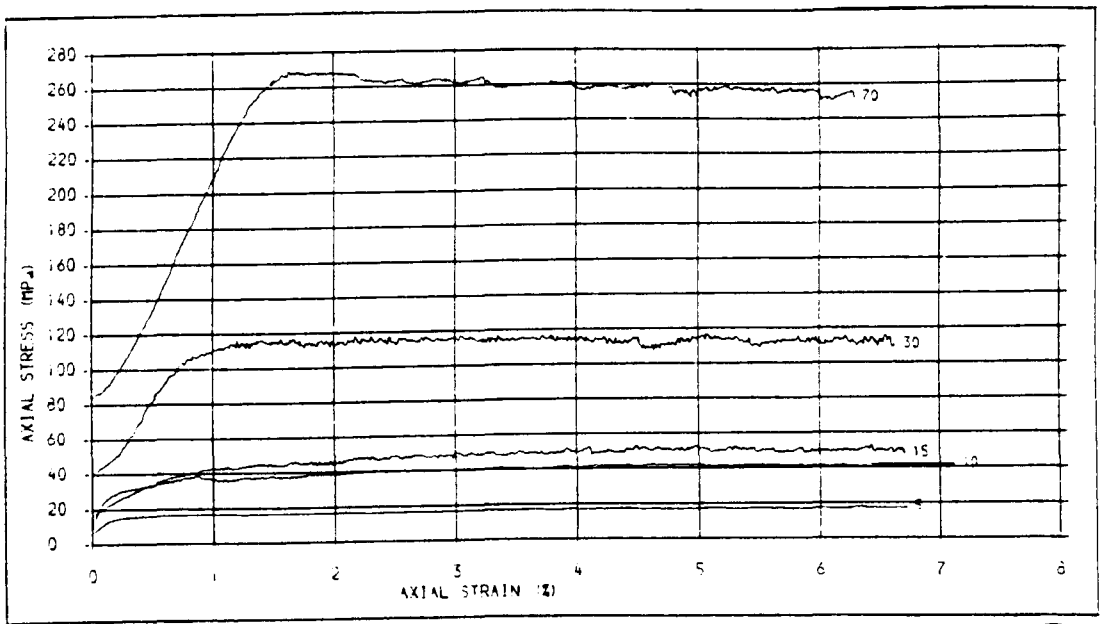

Fig. 66 . STRESS-STRAIN PLOTS FOR PS SPECIMENS WITH SAW CUT JOINTS, JOINT ANGLE = 60 DEC.
CONFINING PRESSURES = 5, 10, 15, 30 AND 70 MPa.

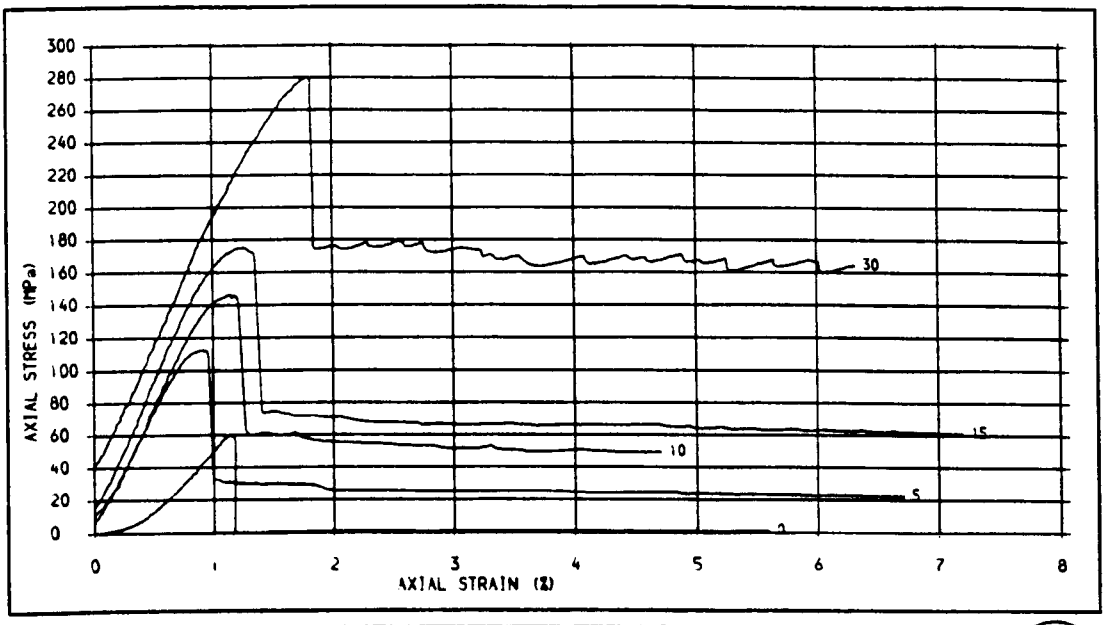

Fig. 67 . STRESS-STRAIN CURVES FOR INTACT STAINTON SANDSTONE SPECIMENS, CONFINING PRESSURES = 0, 5, 10 AND 15 AND 30 MPa.

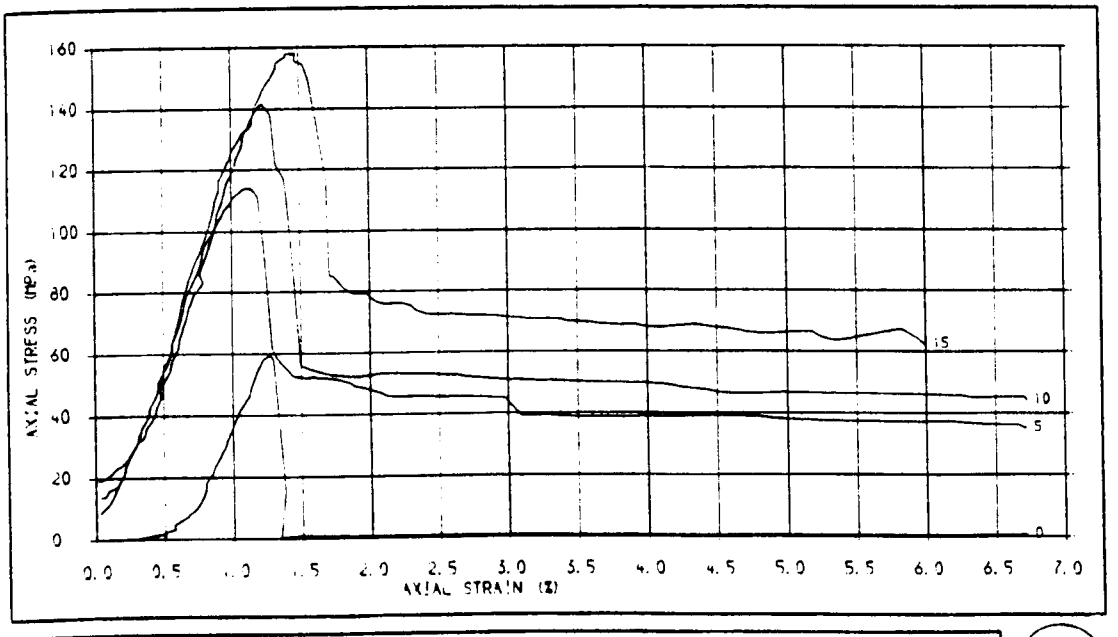

Fig. 68 STRESS-STRAIN PLOTS FOR SS SPECIMENS WITH SAW CUT JOINTS, JOINT ANGLE = 30 DEG. CONFINING PRESSURES = 0, 5, 10, AND 15 MPa.

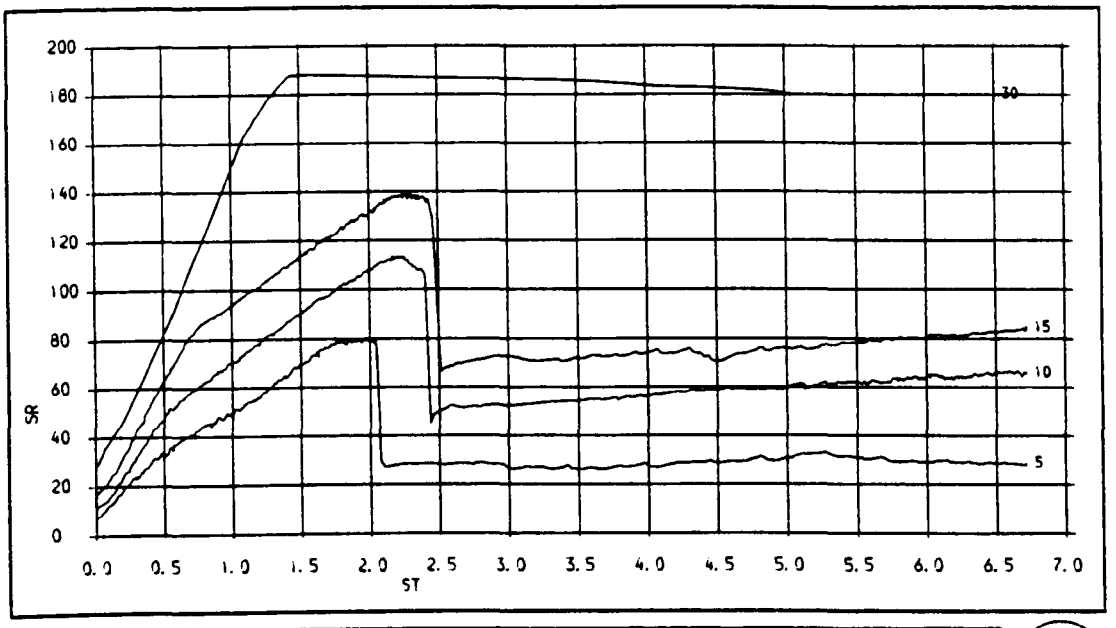

Fig. 69 . STRESS-STRAIN PLOTS FOR SS SPECIMENS WITH SAW CUT JOINTS, JOINT ANGLE = 45 DEG. CONFINING PRESSURES = 5, 10, 15 AND 30 MPa.

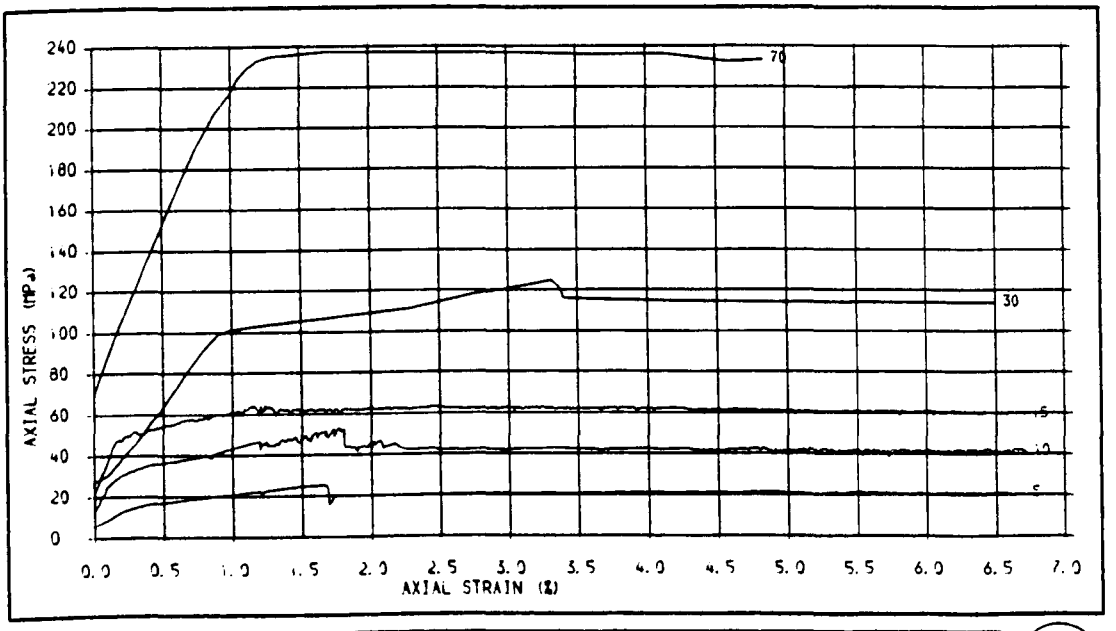

Fig. 610 . STRESS-STRAIN PLOTS FOR SS SPECIMENS WITH SAW CUT JOINTS, JOINT ANGLE = 60 DEG. CONFINING PRESSURES = 5, 10, 15, 30 AND 70

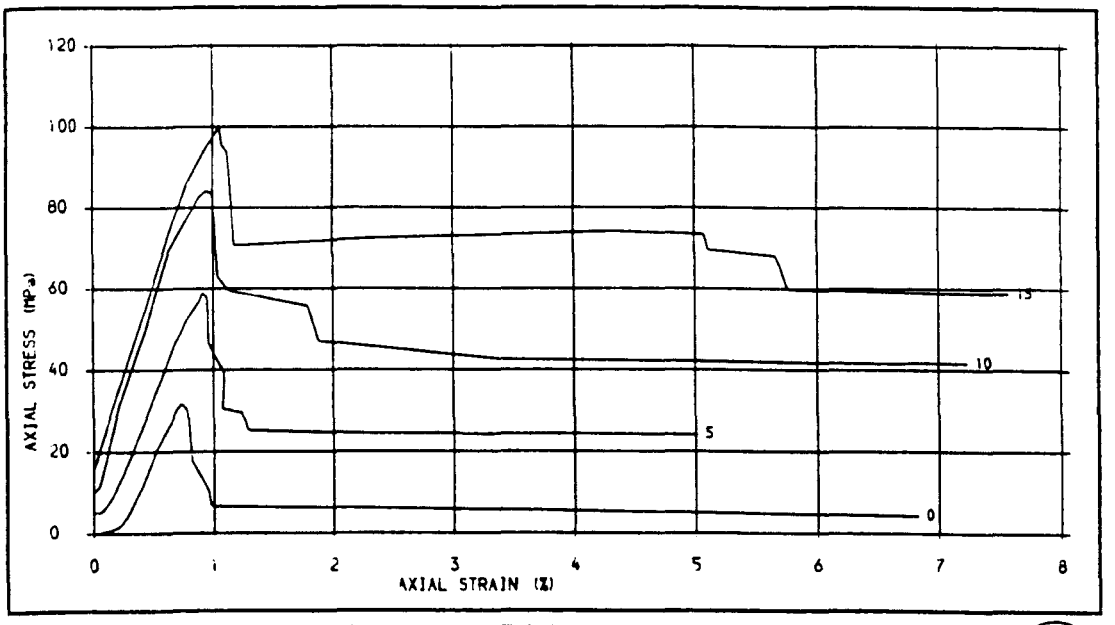

Fig. 6.11 .STRESS-STRAIN PLOTS FOR DUNFRITH SANDSTONE (INTACT), CONFINING PRESSURES. 0, 5, 10 AND 15 MPa.

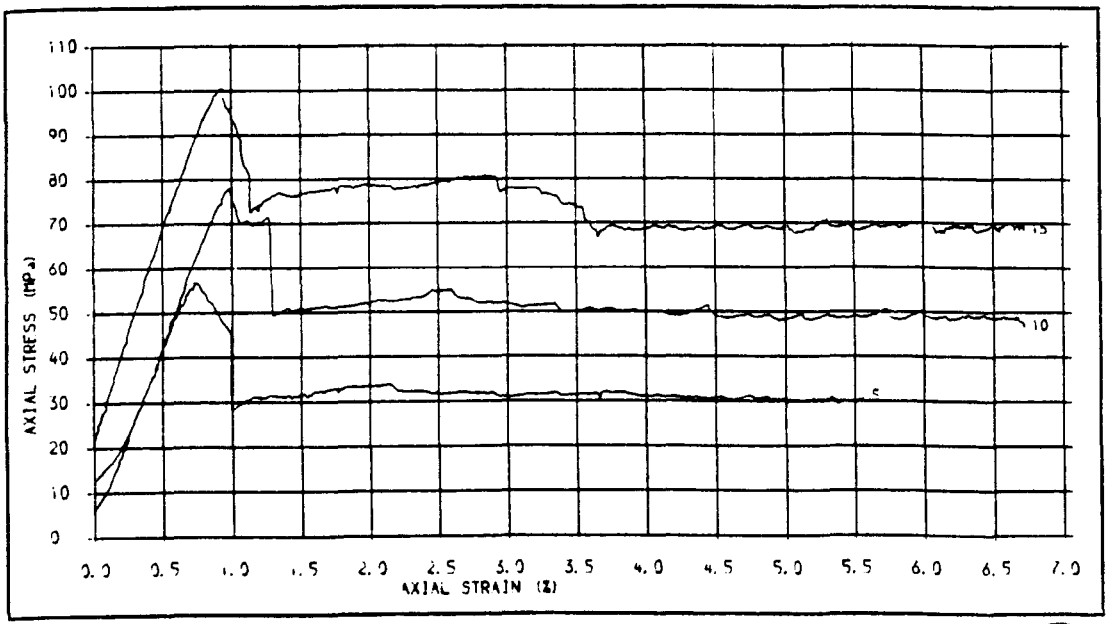

Fig. 6.12 .STRESS-STRAIN PLOTS FOR DS SPESIMENS WITh SAW CUT JOINTS , JOINT ANGLE = 30 DEG. CONFINING PRESSURES. 5, 10 AND 15 MPa.

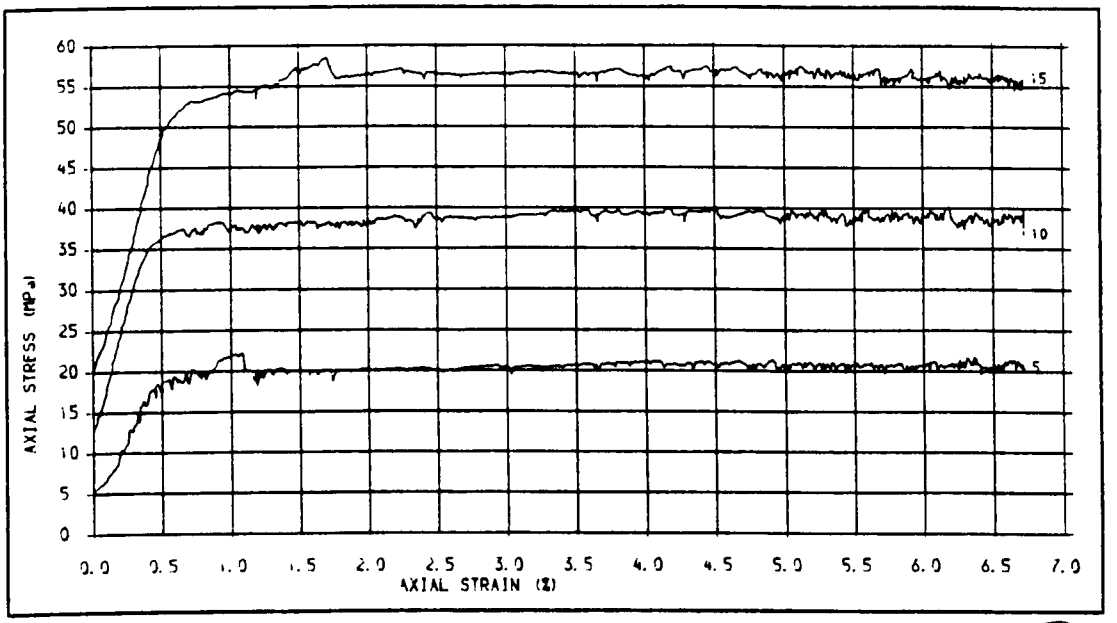

Fig. 6.13 . STRESS-STRAIN PLOTS FOR DS SPECIMENS WITH SAW CUT JOINTS, JOINT ANGLE. 60 DEG. CONFINING PRESSURES. 5, 10 AND 15 MPa.

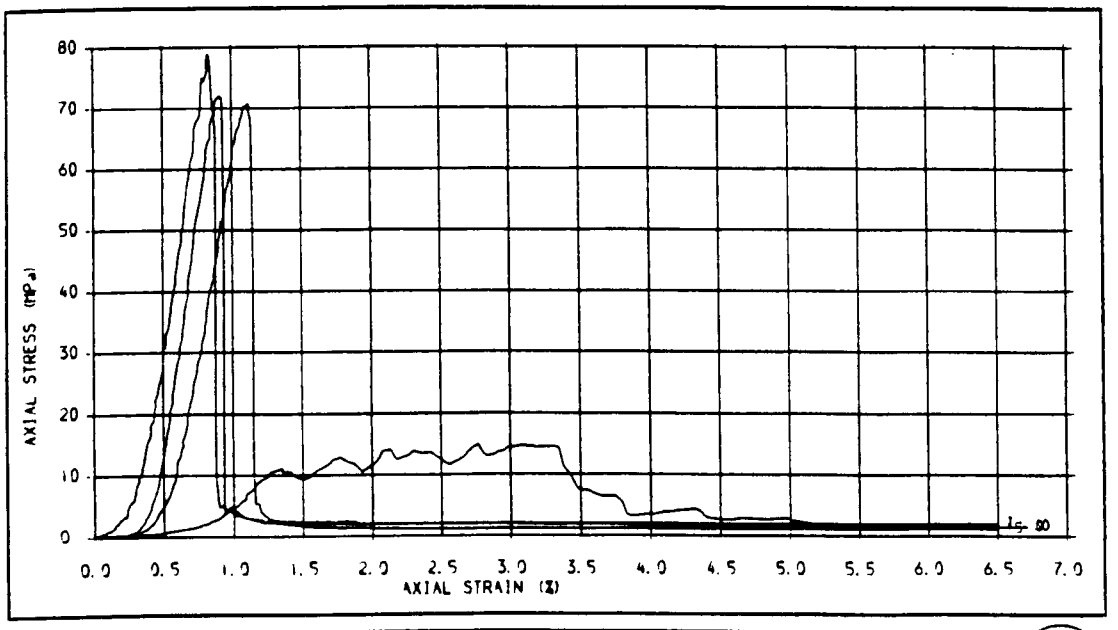

Fig. 6.14 . STRESS-STRAIN PLOTS FOR INTACT AND JOINTED (SAW CUT) PENRITH SANDSTONE SPECIMENS FOR 0 CONFINING PRESSURE (UNIAXIAL), JOINT ANGLE = 0, 15, 30

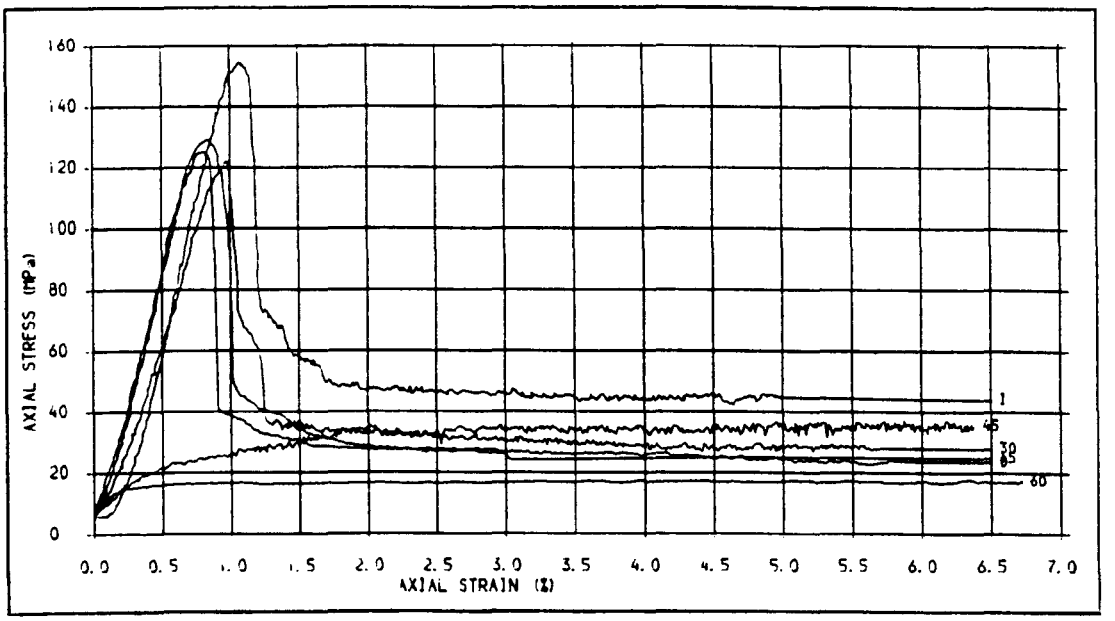

Fig. 6.15 : STRESS-STRAIN PLOTS FOR INTACT AND JOINTED (SAW CUT) PS SPECIMENS FOR 5 MPa CONFINING PRESSURE. JOINT ANGLES. 0, 15, 30, 45 AND 60 DEC.

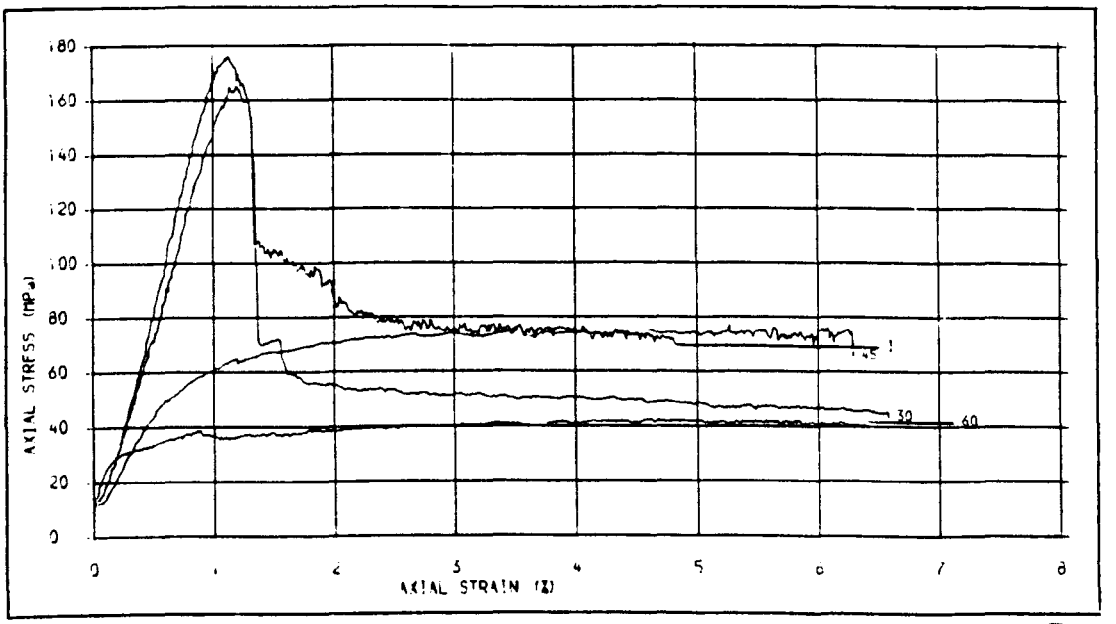

Fig. 6.16 : STRESS-STRAIN PLOTS FOR INTACT AND JOINTED (SAW CUT) PS SPECIMENS FOR 10 MPa CONFINING PRESSURE. JOINT ANGLES. 30, 45 AND 60 DEC.

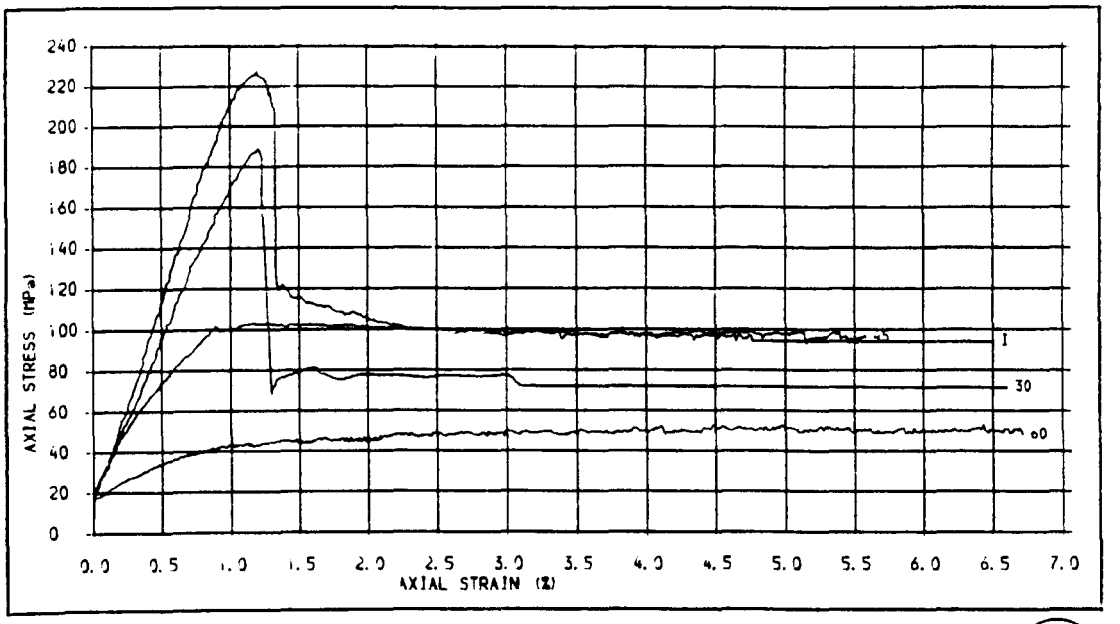

Fig. 6.17 .STRESS-STRAIN PLOTS FOR INTACT AND JOINTED (SAW CUT) PS SPECIMENS FOR 15 MPa CONFINING PRESSURE, JOINT ANGLES. 30, 45 AND 60 DEC.

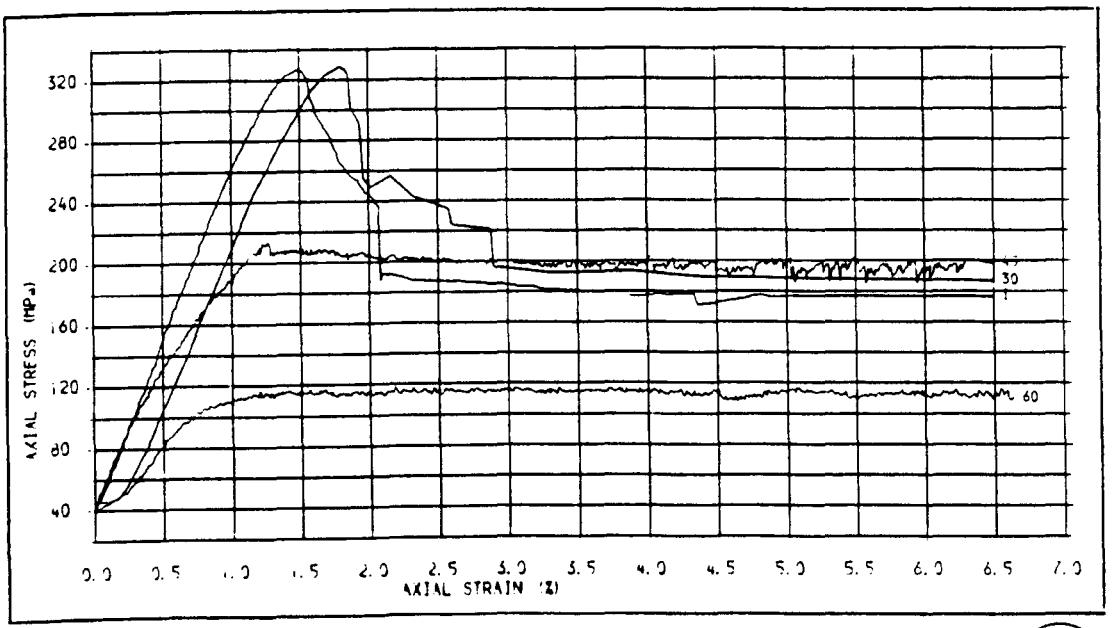

Fig. 6.18 .STRESS-STRAIN PLOTS FOR INTACT AND JOINTED PS SPECIMENS FOR 30 MPa CONFINING PRESSURE, JOINT ANGLE. 30, 45 AND 60 DEC.

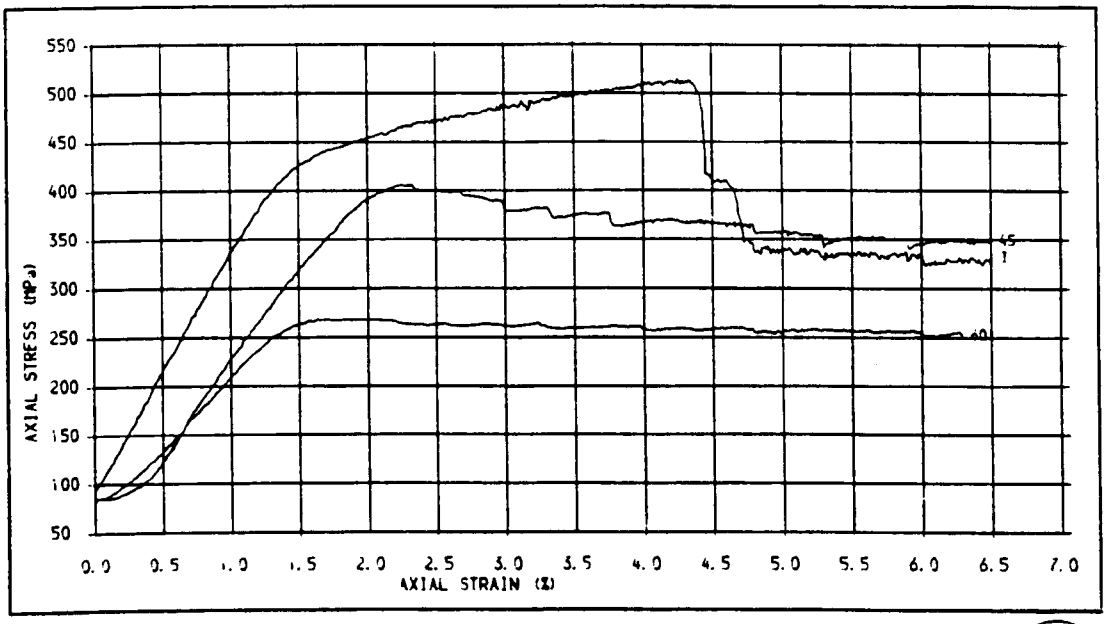

Fig. 6.9 . STRESS-STRAIN PLOTS FOR INTACT AND JOINTED PS SPECIMENS (SAW CUT) FOR 70 MPa CONFINING PRESSURE, JOINT ANGLES, 45 AND 60 DEC.

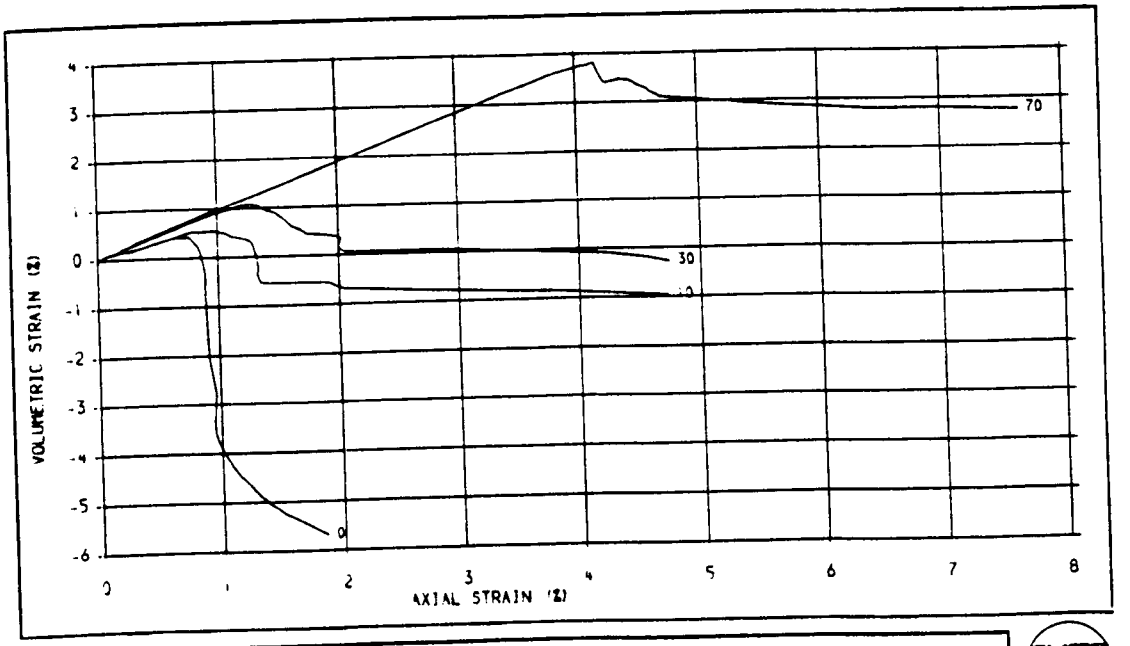

Fig. 6.20 . VOLUMETRIC STRAIN-AXIAL STRAIN PLOTS FOR INTACT PENRITH SANDSTONE. CONFINING PRESSURES, 0, 10, 30 AND 70 MPa.

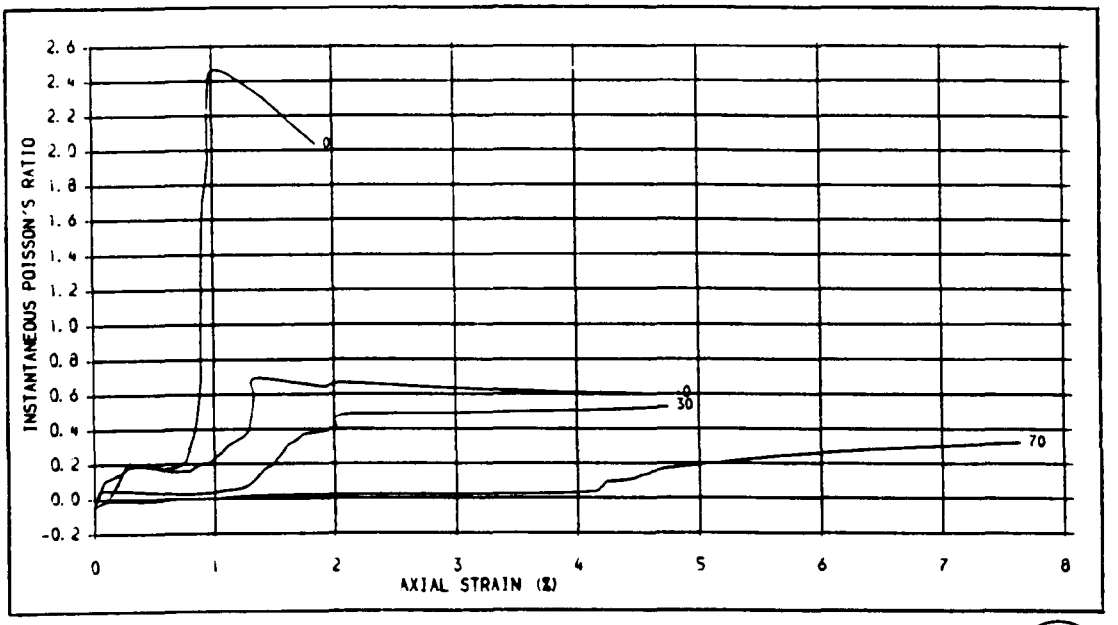

Fig. 621 . INSTANTANEOUS POISSON'S RATIO-AXIAL STRAIN PLOTS FOR PS SPECIMENS (INTACT), CONFINING PRESSURES. 0, 10, 30 AND 70 MPa.

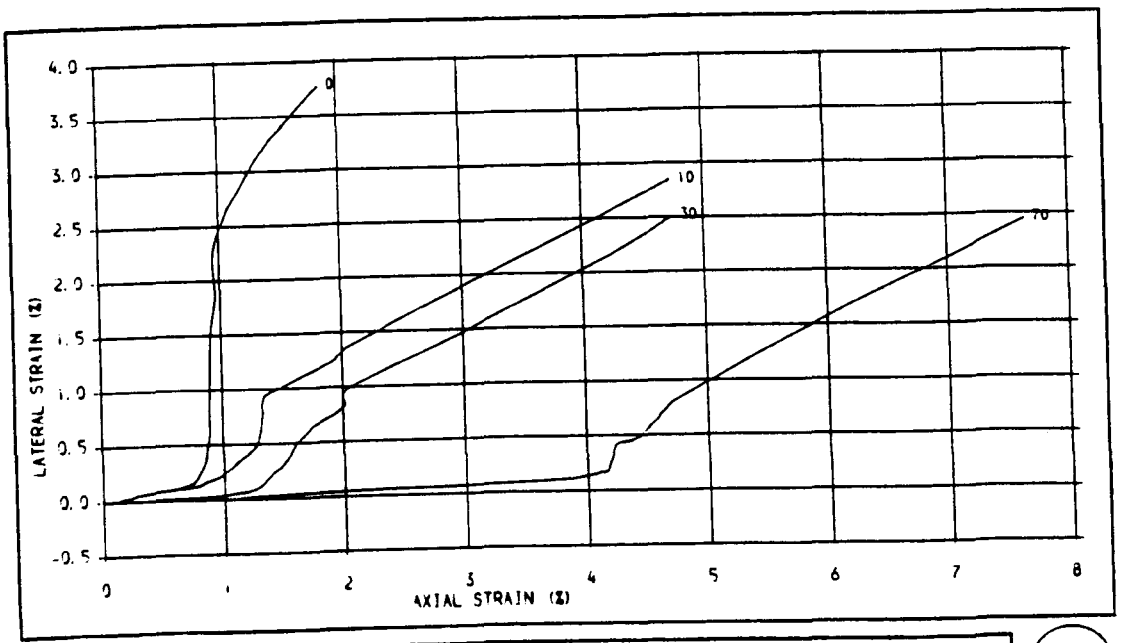

Fig. 622 . LATERAL STRAIN-AXIAL STRAIN PLOTS FOR PS SPECIMENS (INTACT), CONFINING PRESSURES. 0, 10, 30 AND 70 MPa.

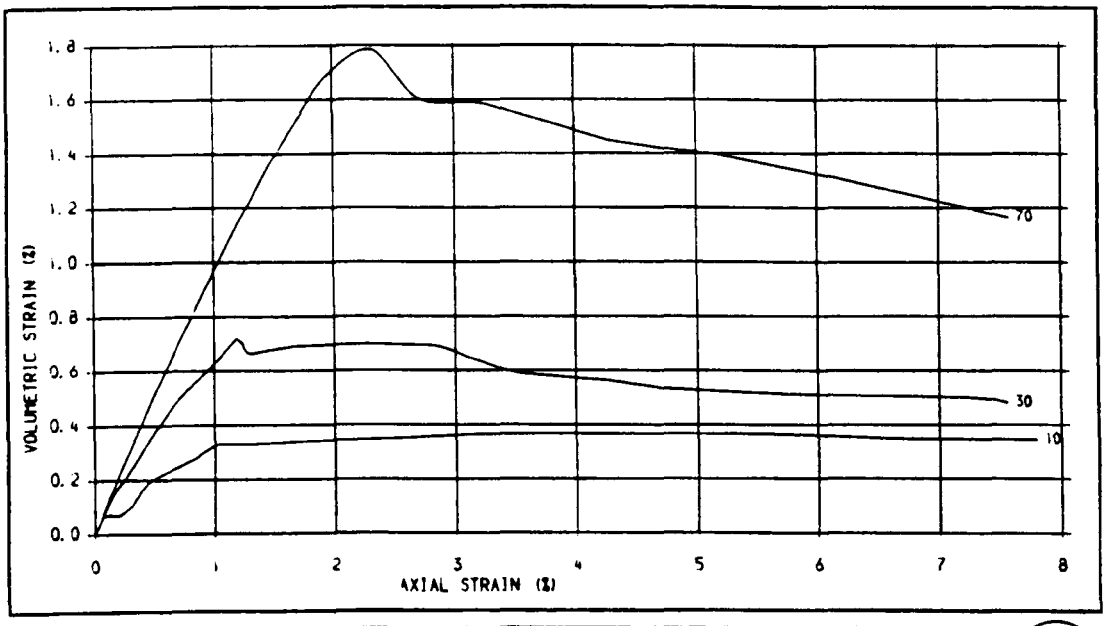

Fig. 623 . VOLUMETRIC STRAIN-AXIAL STRAIN PLOTS FOR PS SPECIMENS WITH SAW CUT JOINTS, JOINT ANGLE = 45 DEC., CONFINING PRESSURES. 10, 30 AND 70 MPa.

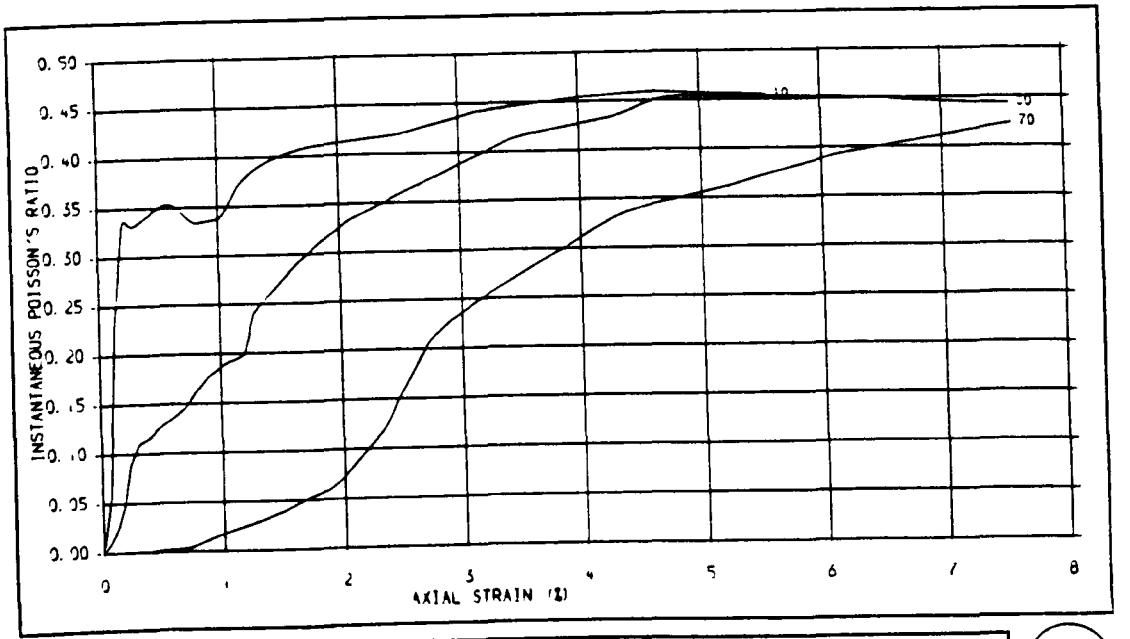

Fig. 624 . INSTANTANEOUS POISSON'S RATIO-AXIAL STRAIN PLOTS FOR PS SPECIMENS WITH SAW CUT JOINTS, JOINT ANGLE = 45 DEC., CONFINING PRESSURES. 10, 30 AND 70 MPa.

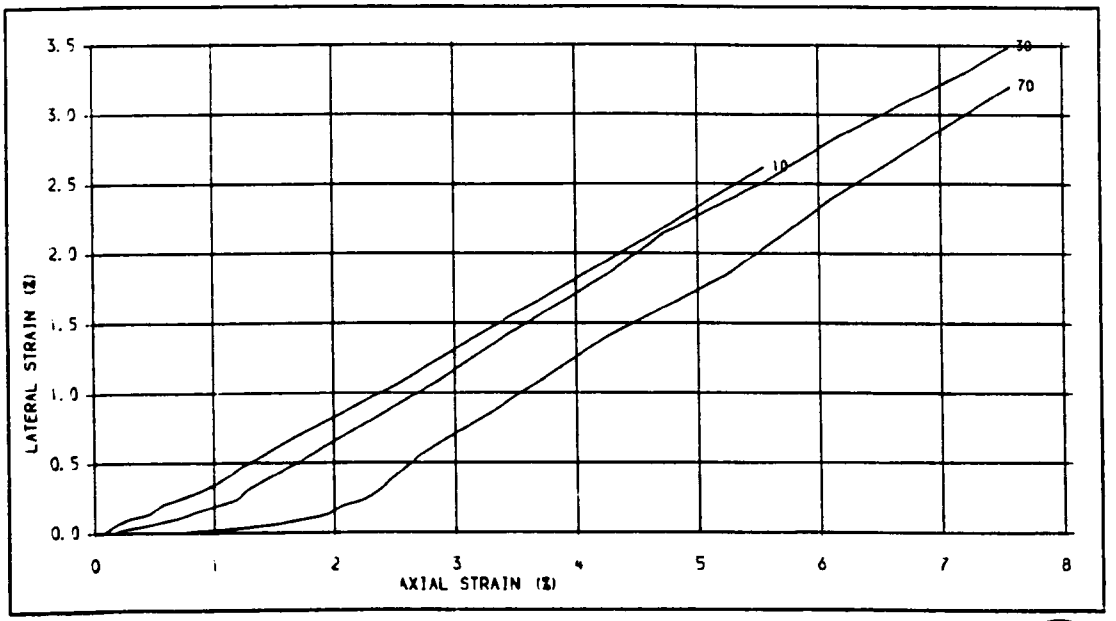

Fig. 625 LATERAL STRAIN-AXIAL STRAIN PLOTS FOR PS SPECIMENS WITH SAW CUT JOINTS, JOINT ANGLE = 45 DEC., CONFINING PRESSURES. 10, 30 AND 70 MPa.

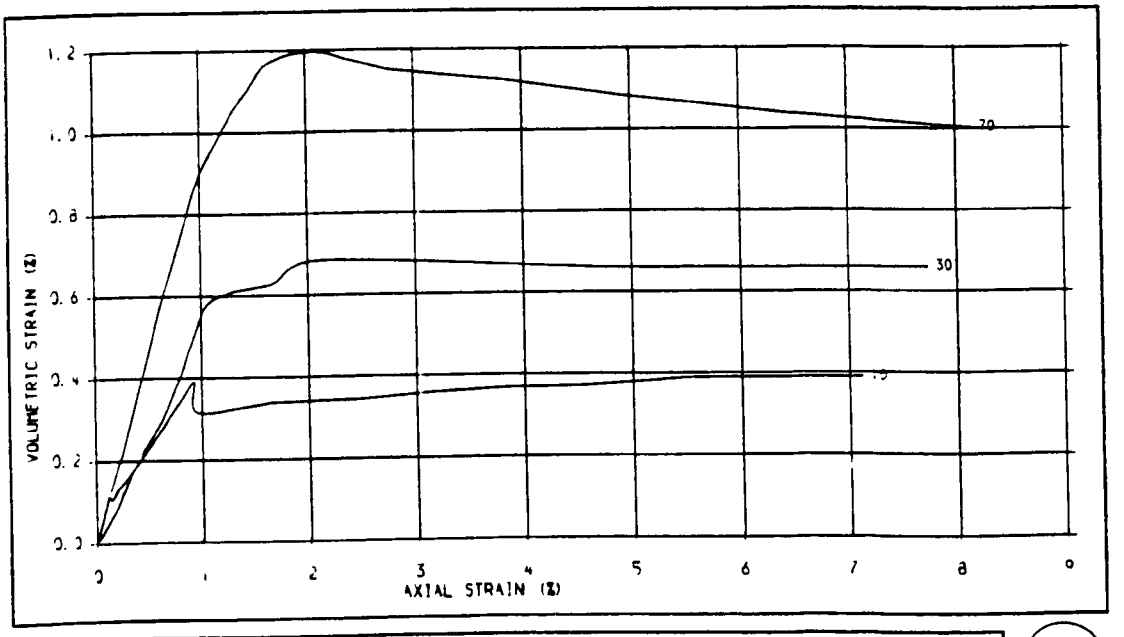

Fig. 626 VOLUMETRIC STRAIN-AXIAL STRAIN PLOTS FOR PS SPECIMENS WITH SAW CUT JOINTS, JOINT ANGLE = 60 DEC., CONFINING PRESSURES. 10, 30 AND 70 MPa.

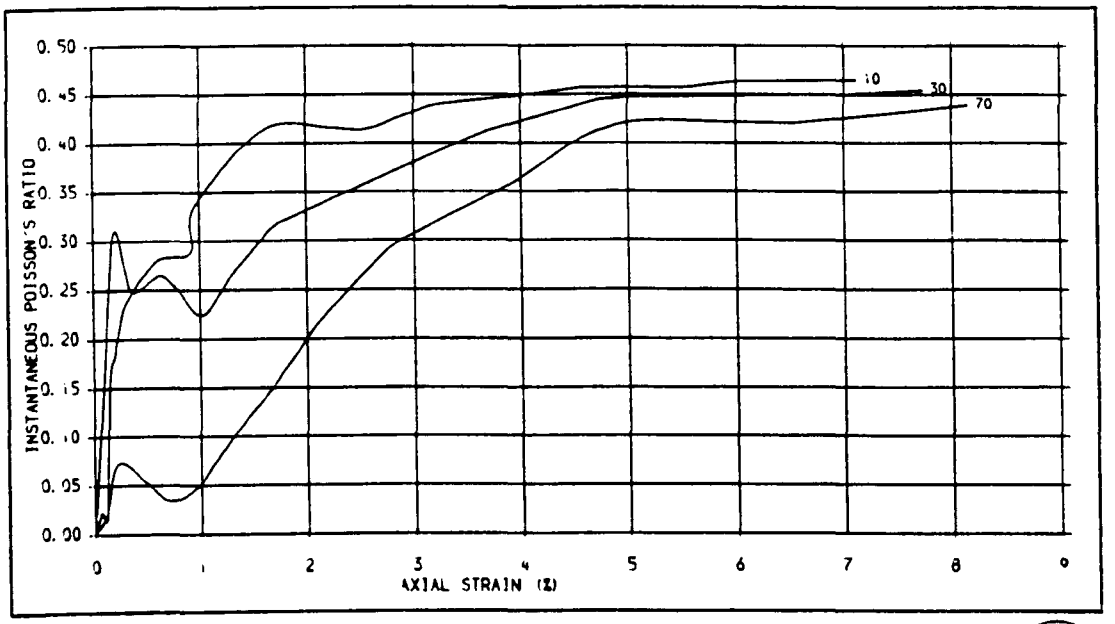

Fig. 627 . INSTANTANEOUS POISSON'S RATIO-AXIAL STRAIN PLOTS FOR PS SPECIMENS WITH SAW CUT JOINTS, JOINT ANGLE = 60 DEG., CONFINING PRESSURES. 10, 30 AND 70 MPa.

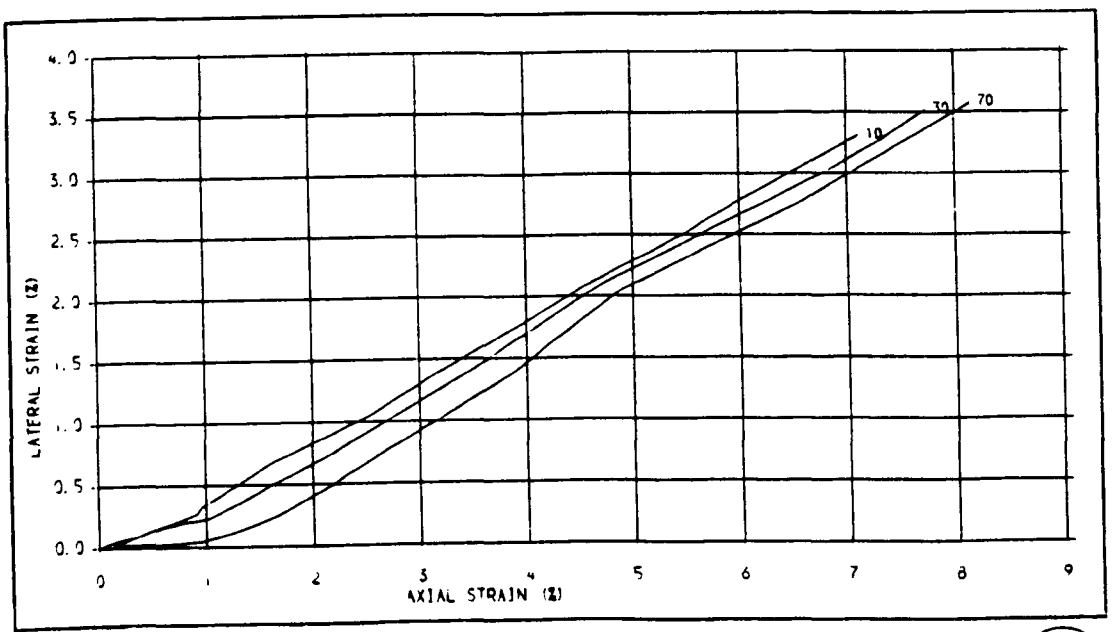

Fig. 628 . LATERAL STRAIN-AXIAL STRAIN PLOTS FOR PS SPECIMENS WITH SAW CUT JOINTS, JOINT ANGLE = 60 DEG., CONFINING PRESSURES. 10, 30 AND 70 MPa.

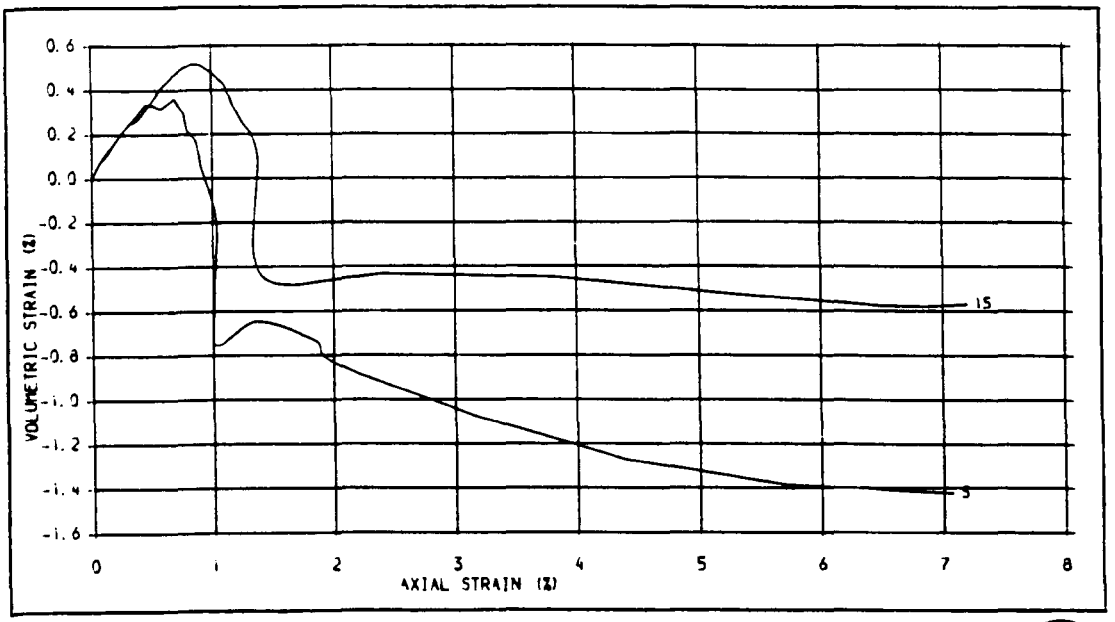

F.g. 629 . VOLUMETRIC STRAIN-AXIAL STRAIN PLOTS FOR SS SPESIMENS (INTACT), CONFINING PRESSURES. 5 AND 15 MPa.

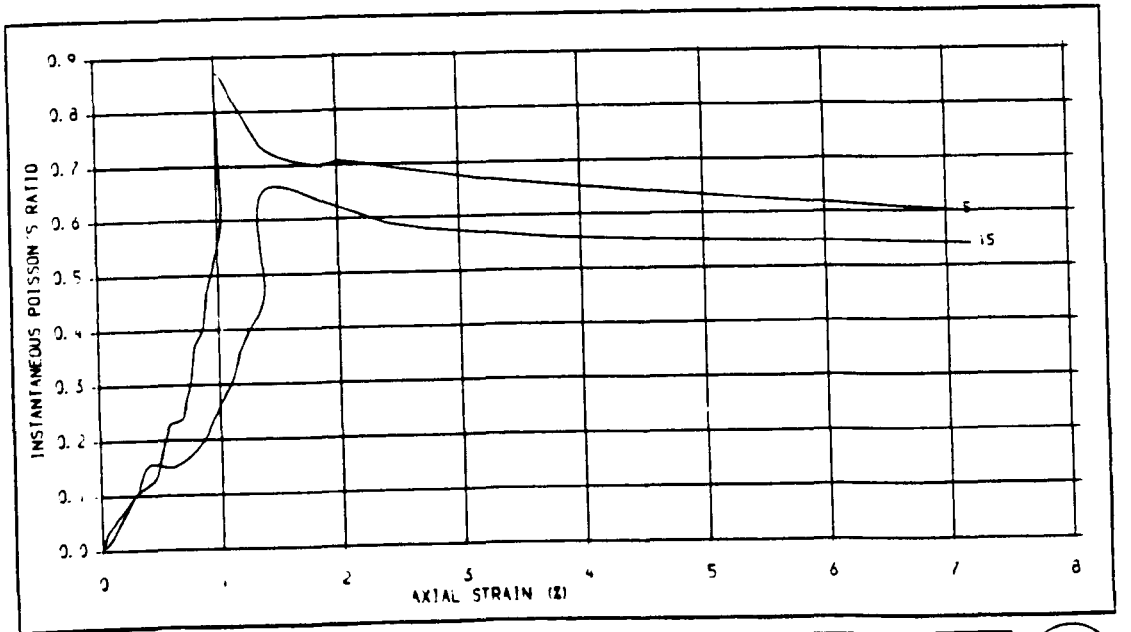

F.g. 630 . INSTANTANEOUS POISSON'RATIO-AXIAL STRAIN PLOTS FOR SS SPECIMENS (INTACT), CONFINING PRESSURES. 5 AND 15 MPa.

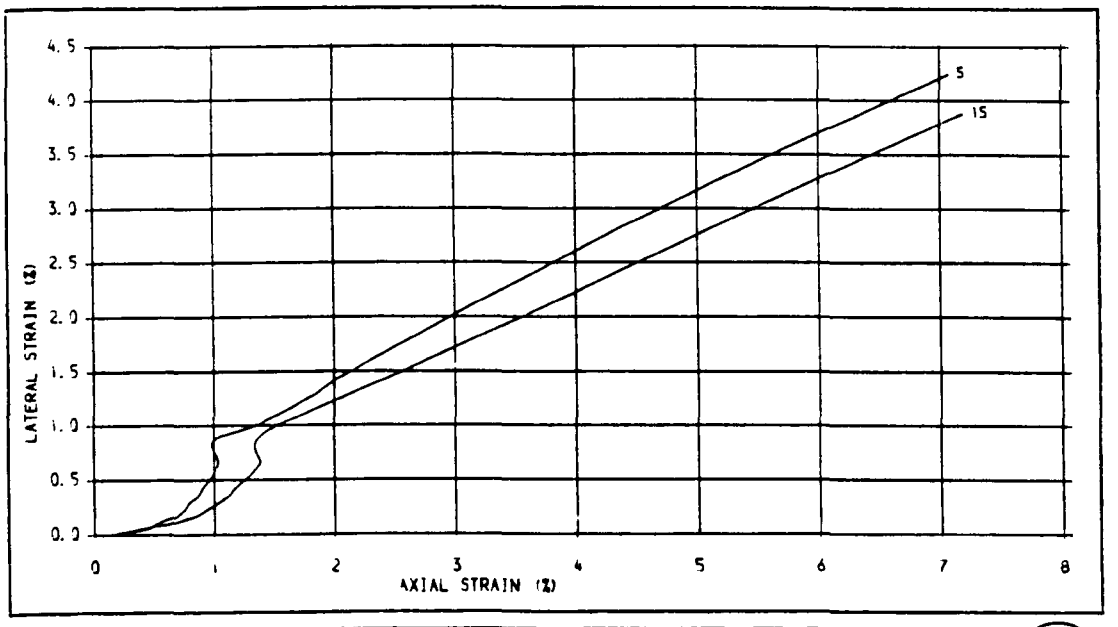

Fig. 631 : LATERAL STRAIN-AXIAL STRAIN PLOTS FOR SS SPECIMENS (INTACT), CONFINING PRESSURES. 5 AND 15 MPa.

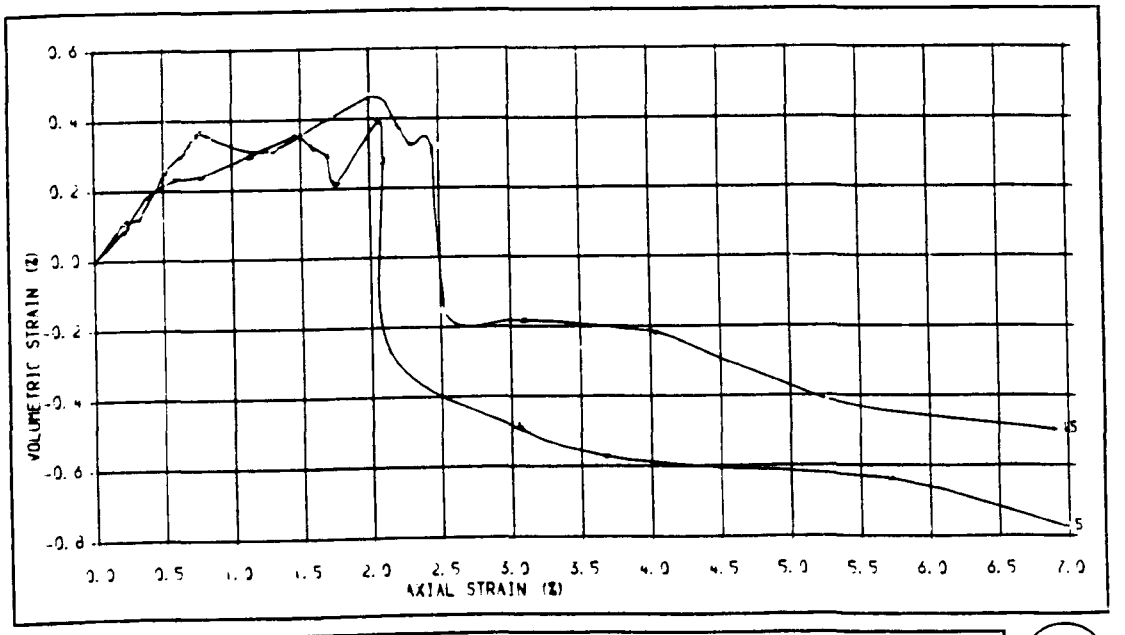

Fig. 632 : VOLUMETRIC STRAIN-AXIAL STRAIN PLOTS FOR SS SPESIMENS WITH SAW CUT JOINTS, JOINT ANGLE = 45 DEG., CONFINING PRESSURES. 5 AND 15 MPa.

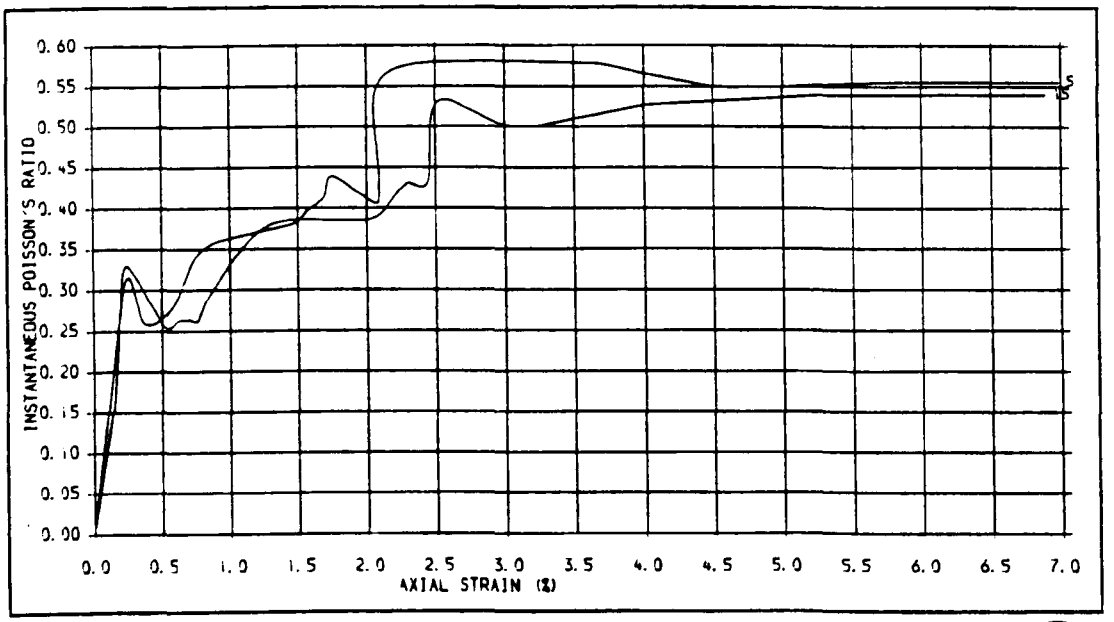

Fig. 6.33 : INSTANTANEOUS POISSON'S RATIO-AXIAL STRAIN PLOTS FOR SS SPECIMENS WITH SAW CUT JOINTS, JOINT ANGLE = 45 DEG., CONFINING PRESSURES, 5 AND 15 MPa.

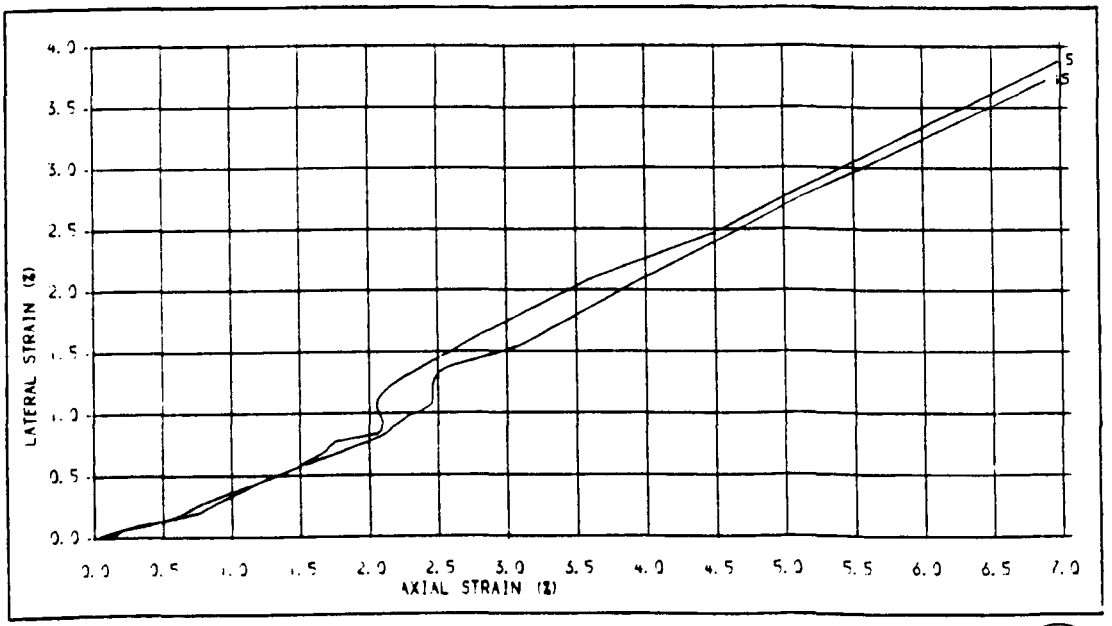

Fig. 6.34 : LATERAL STRAIN-AXIAL STRAIN PLOTS FOR SS SPECIMENS WITH SAW CUT JOINTS, JOINT ANGLE = 45 DEG., CONFINING PRESSURES, 5 AND 15 MPa.

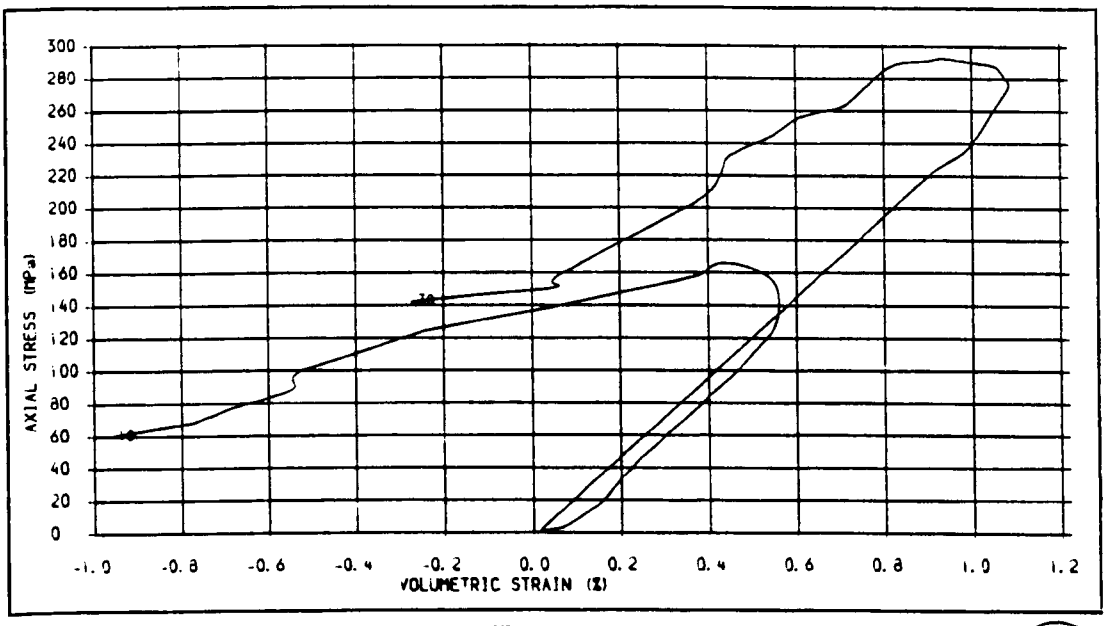

Fig. 6.35 : AXIAL STRESS-VOLUMETRIC STRAIN PLOTS FOR PS SPECIMENS (INTACT) CONFINING PRESSURES. 10 AND 30 MPa.

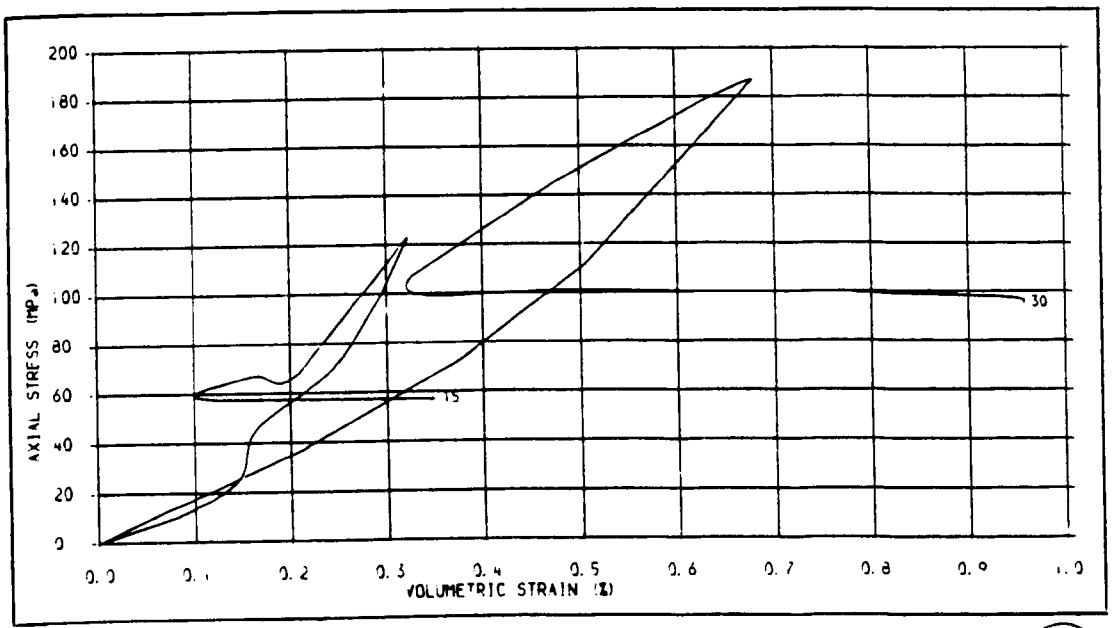

Fig. 6.36 : AXIAL STRESS-VOLUMETRIC STRAIN PLOTS FOR PS SPECIMENS WITH SPLIT JOINTS, JOINT ANGLE = 60 DEG., CONFINING PRESSURES. 15 AND 30 MPa.

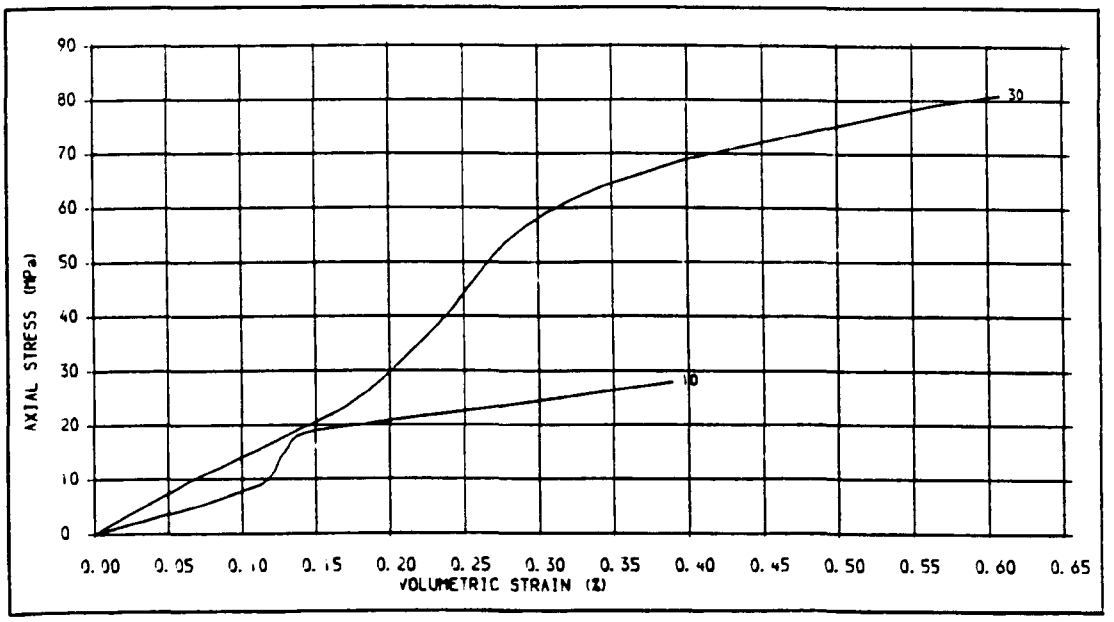

Fig. 637 . AXIAL STRESS-VOLUMETRIC STRAIN PLOTS FOR PS SPECIMENS WITH SAW CUT JOINTS, JOINT ANGLE = 60 DEC., CONFINING PRESSURES. 10 AND 30 MPa.

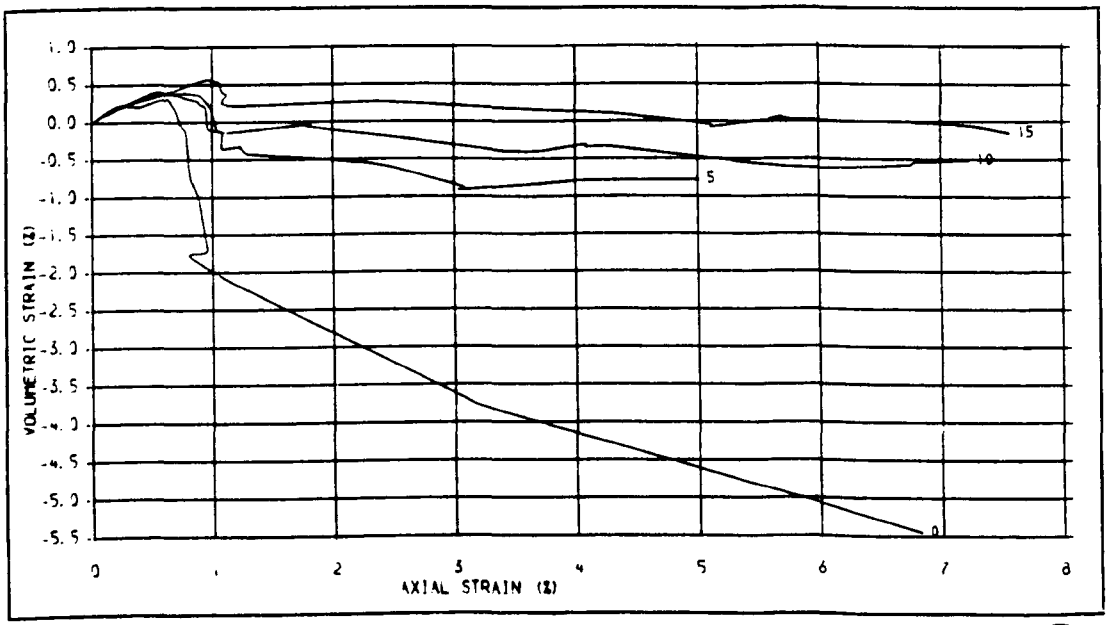

Fig. 638 . VOLUMETRIC STRAIN-AXIAL STRAIN PLOTS FOR DUMFRITH SANDSTONE SPECIMENS (INTACT) CONFINING PRESSURES. 0, 5, 10 AND 15 MPa.

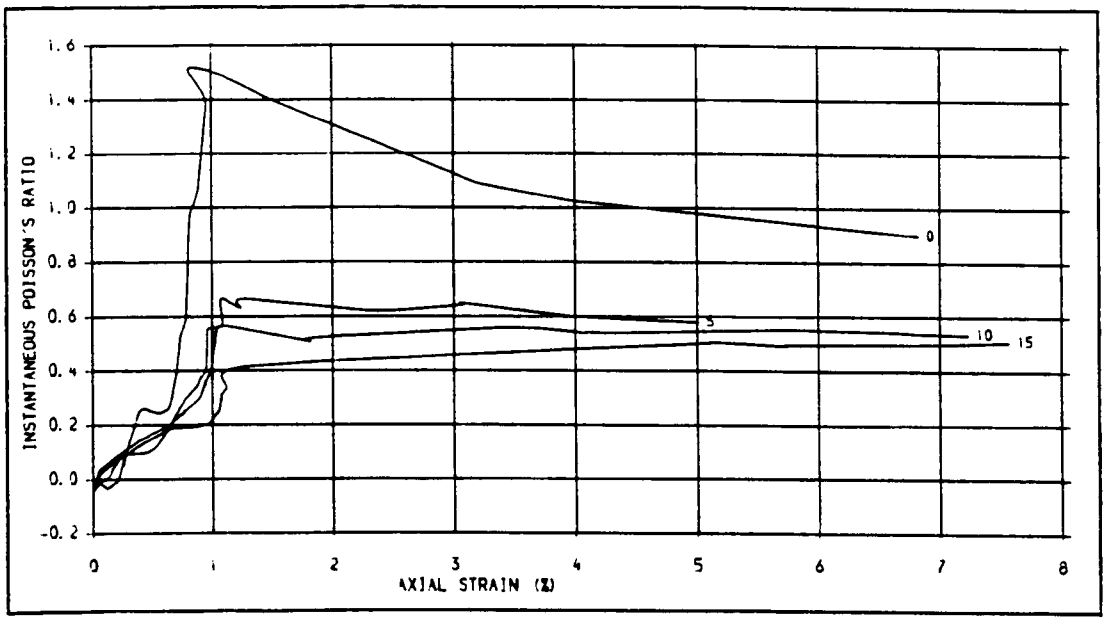

Fig. 639 . INSTANTANEOUS POISSON'S RATIO-AXIAL STRAIN PLOTS FOR DS SPECIMENS (INTACT) CONFINING PRESSURES. 0, 5, 10 AND 15 MPa.

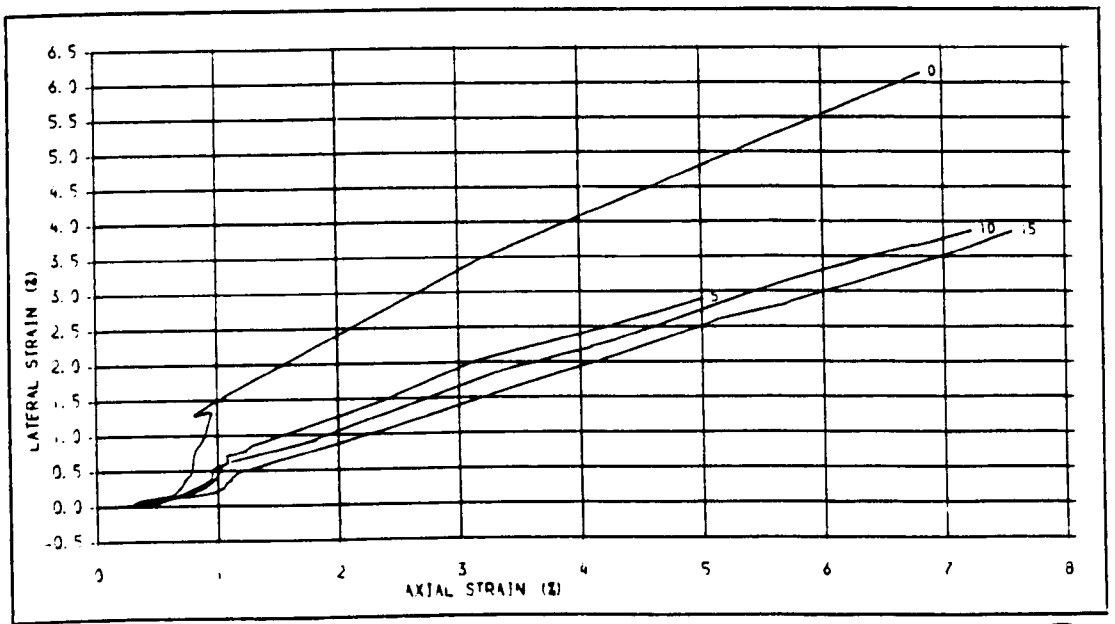

Fig. 640 . LATERAL STRAIN-AXIAL STRAIN PLOTS FOR DS SPECIMENS (INTACT), CONFINING PRESSURES. 0, 5, 10 AND 15 MPa.

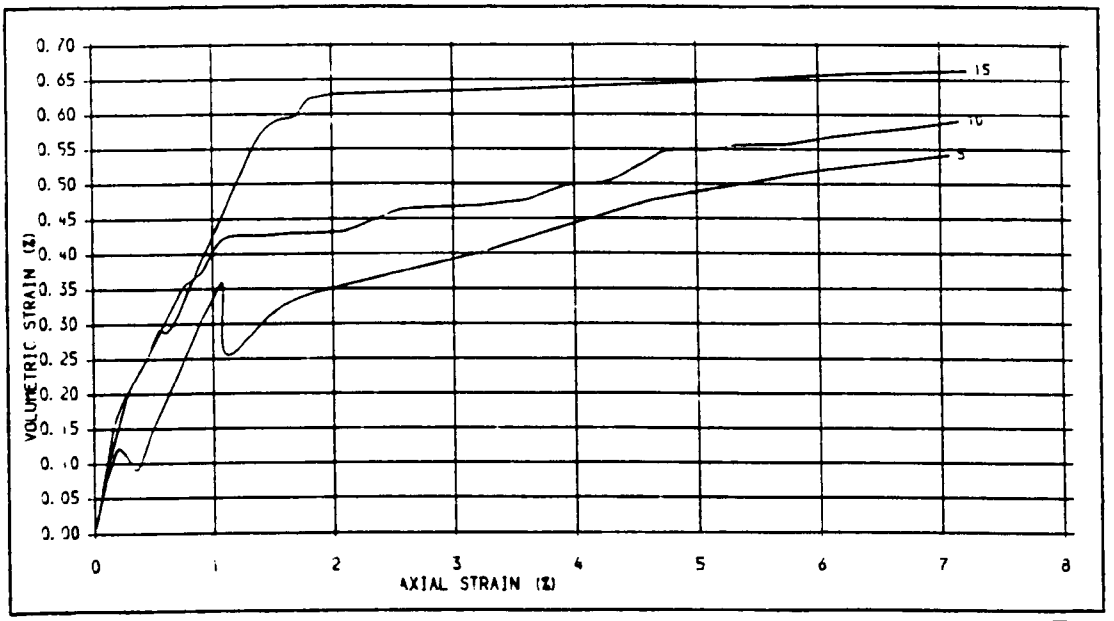

Fig. 6.41 . VOLUMETRIC STRAIN-AXIAL STRAIN PLOTS FOR DS SPECIMENS WITH SAW CUT JOINTS, JOINT ANGLE = 60 DEC., CONFINING PRESSURES. 5, 10 AND 15 MPa.

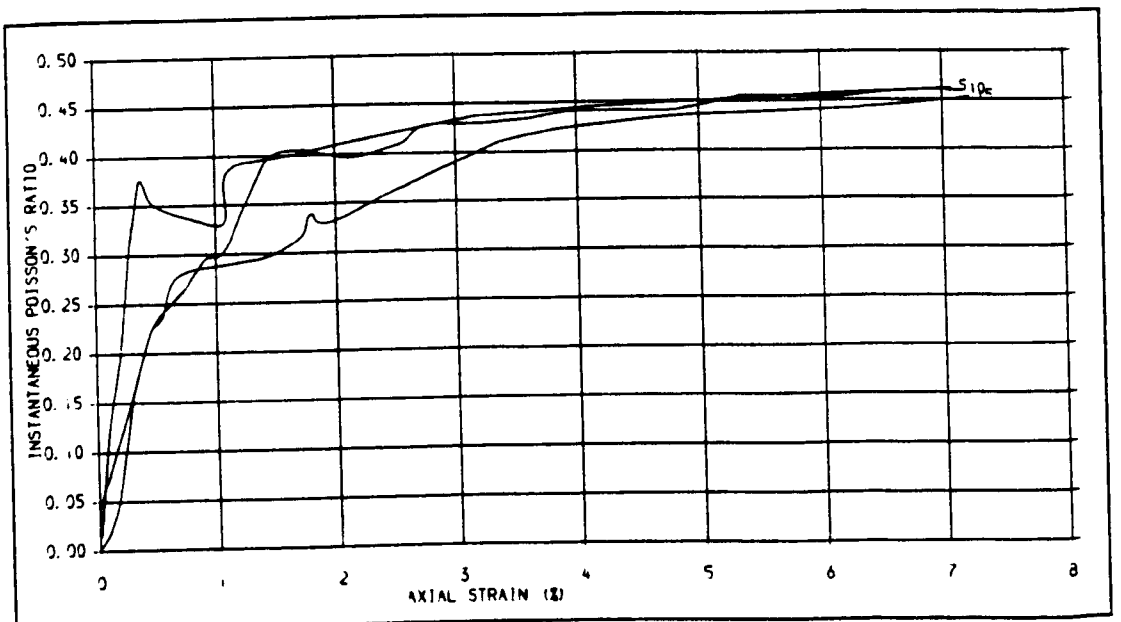

Fig. 6.42 . INSTANTANEOUS POISSON'S RATIO-AXIAL STRAIN PLOTS FOR DS SPECIMENS WITH SAW CUT JOINTS, JOINT ANGLE = 60 DEC., CONFINING PRESSURES. 5, 10 AND 15 MPa.

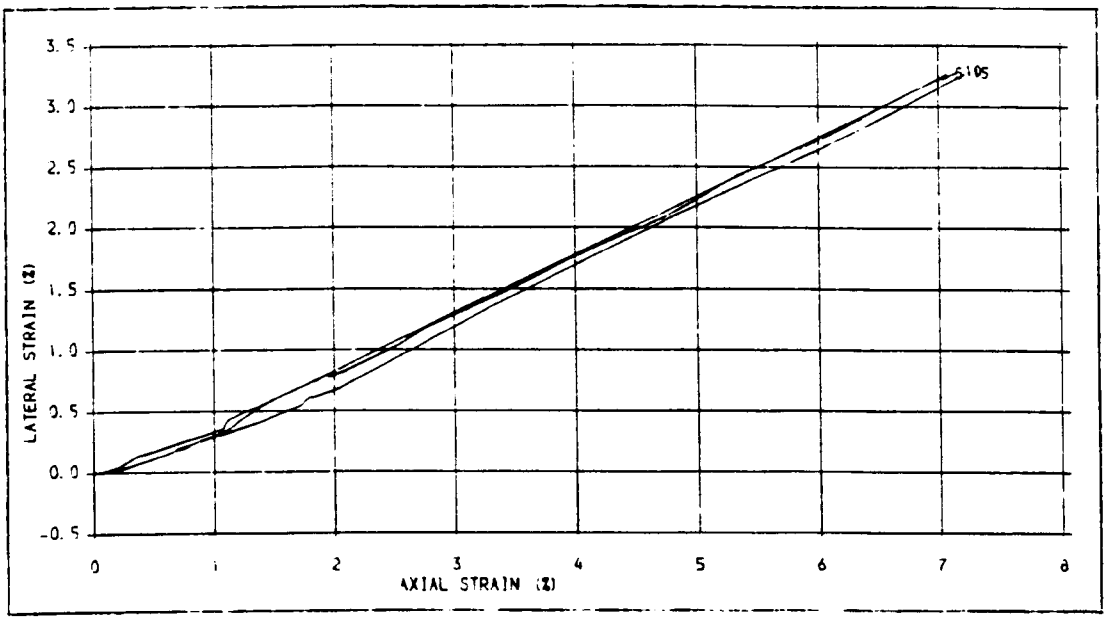

Fig. 643 : LATERAL STRAIN-AXIAL STRAIN PLOTS FOR DS SPECIMENS WITH SAW CUT JOINTS, JOINT ANGLE = 60 DEG., CONFINING PRESSURES. 5, 10 AND 15 MPa.

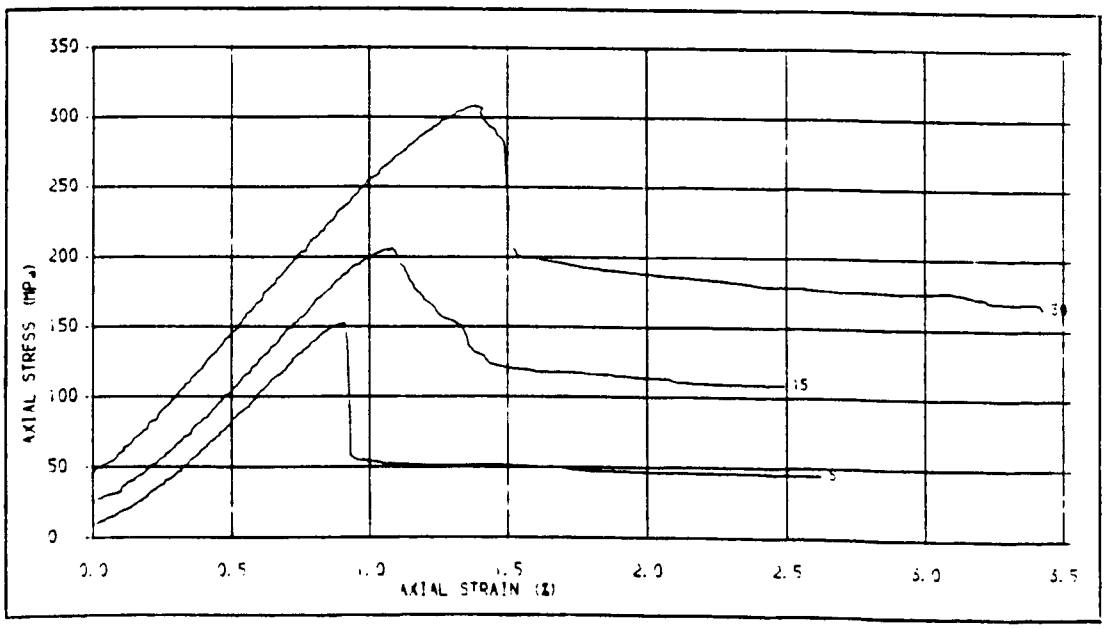

Fig. 644 : STRESS-STRAIN PLOTS FOR PS SPECIMENS WITH NATURAL JOINTS, JOINT ANGLE =30 DEG. CONFINING PRESSURES. 5, 15 AND 30 MPa

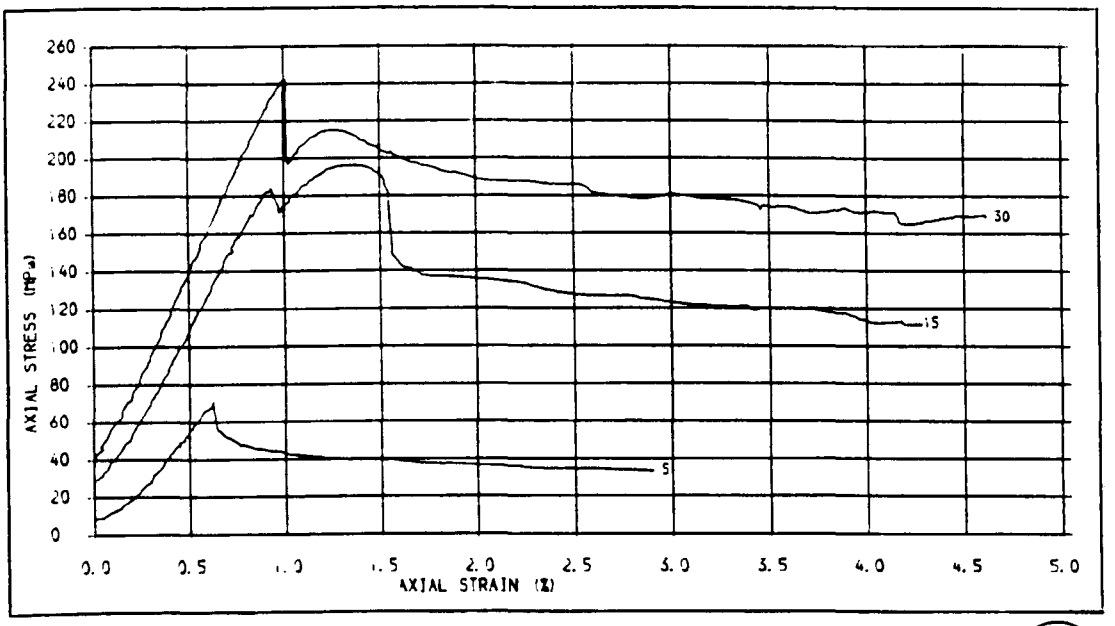

Fig. 6.45 : STRESS-STRAIN PLOTS FOR PS SPECIMENS WITH NATURAL JOINTS , JOINT ANGLE = 45 DEC. CONFINING PRESSURES, 5, 15 AND 30 MPa.

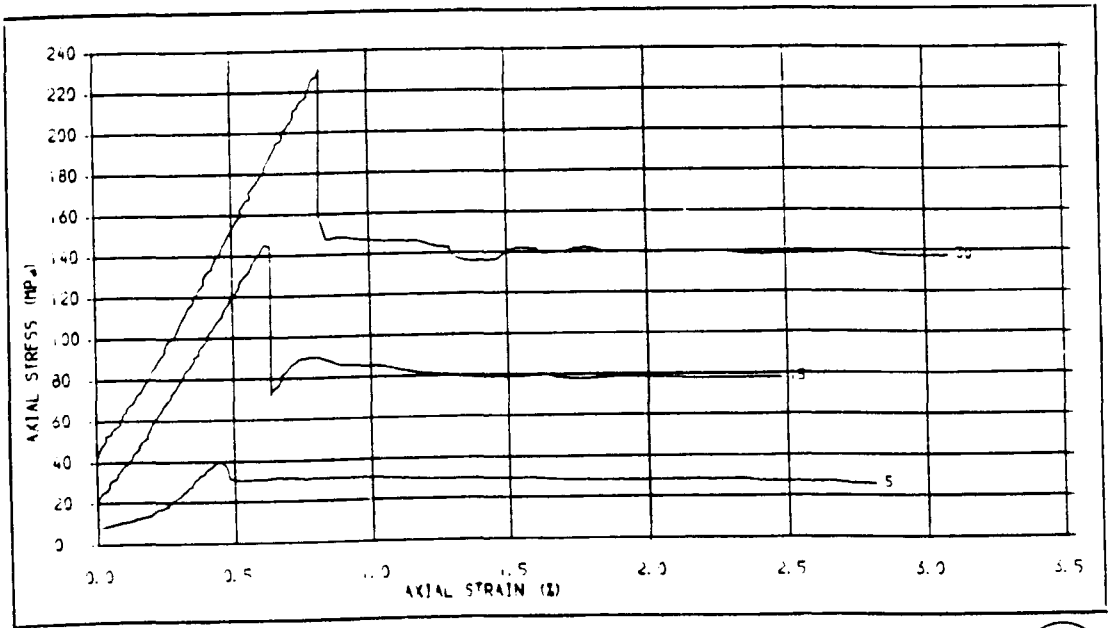

Fig. 6.46 : STRESS-STRAIN CURVES FOR PS SPECIMENS WITH NATURAL JOINTS, JOINT ANGLE = 60 DEC. CONFINING PRESSURES = 5, 15 AND 30 MPa.

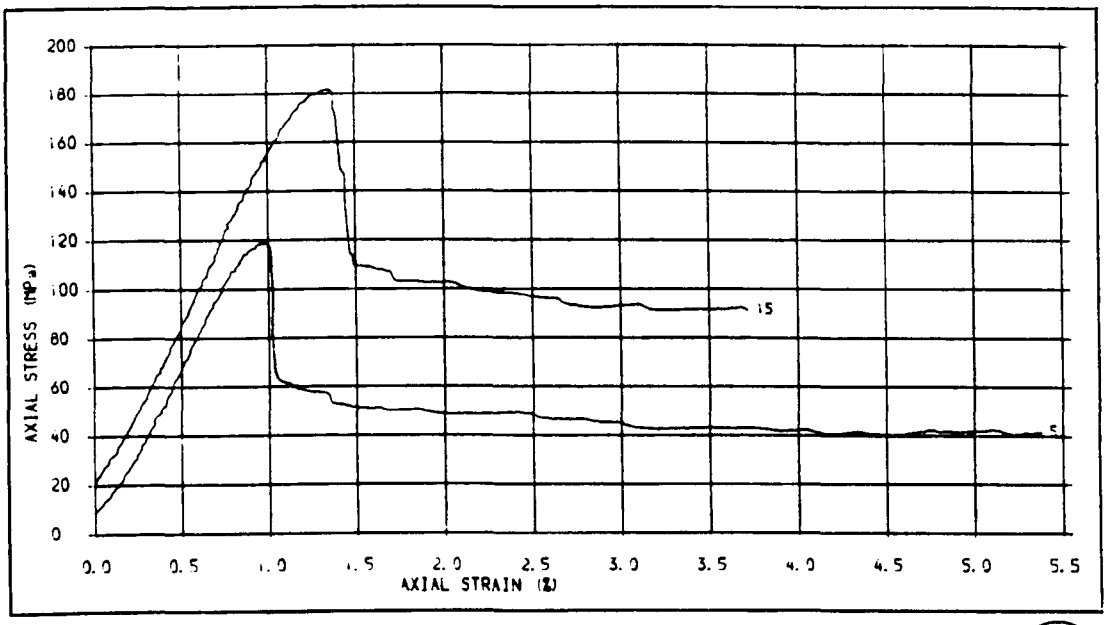

Fig. 6.7 : STRESS-STRAIN PLOTS FOR SS SPECIMENS WITH NATURAL JOINTS, JOINT ANGLE = 30 DEG. CONFINING PRESSURES. 5 AND 15 MPa

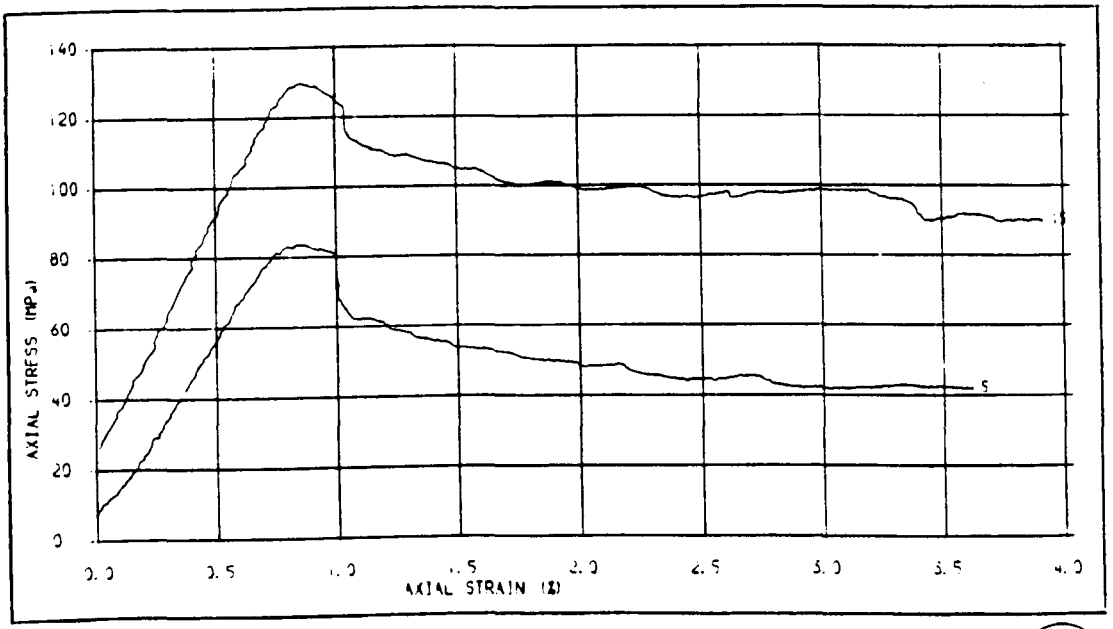

Fig. 6.8 : STRESS-STRAIN PLOTS FOR SS SPECIMENS WITH NATURAL JOINTS , JOINT ANGLE = 45 DEG. CONFINING PRESSURES. 5 AND 15 MPa.

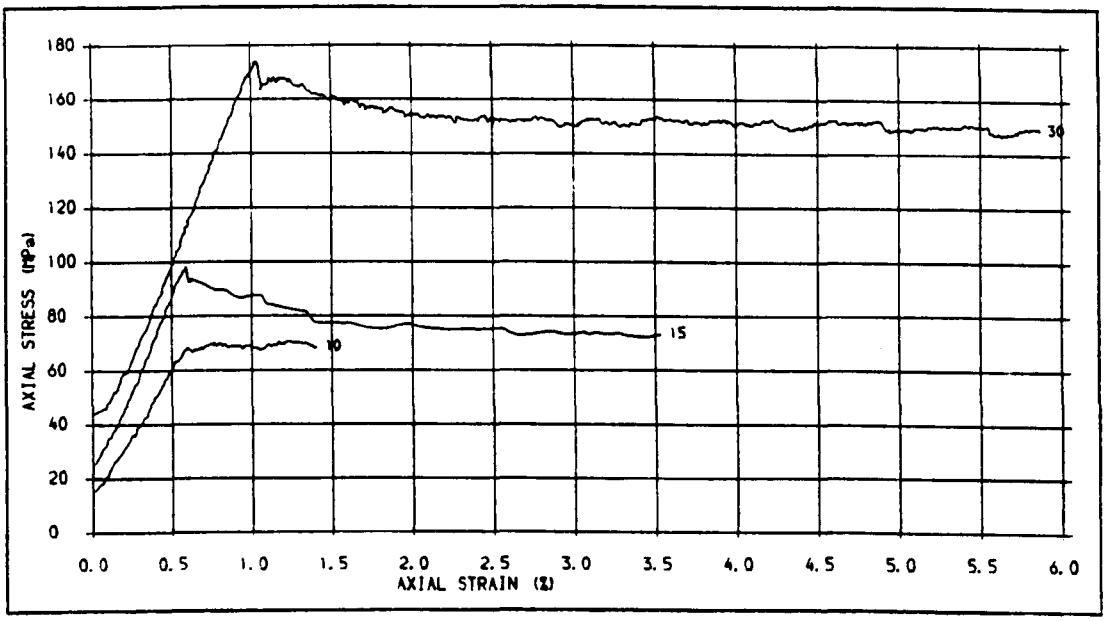

Fig. 6.49 : STRESS-STRAIN PLOTS FOR SS SPECIMENS WITH NATURAL JOINTS, JOINT ANGLE = 60 DEG. CONFINING PRESSURES. 10, 15 AND 30 MPa.

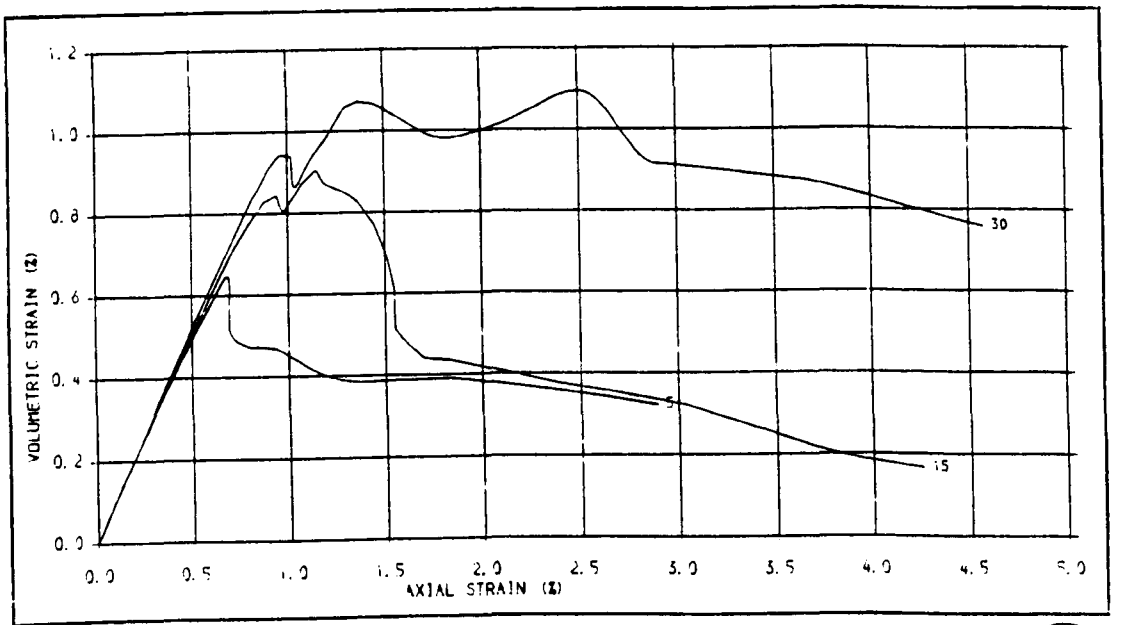

Fig. 6.50 : VOLUMETRIC STRAIN-AXIAL STRAIN PLOTS FOR PS SPECIMENS WITH SLIPT JOINTS, JOINT ANGLE = 45 DEC., CONFINING PRESSURES. 5, 15 AND 30 MPa.

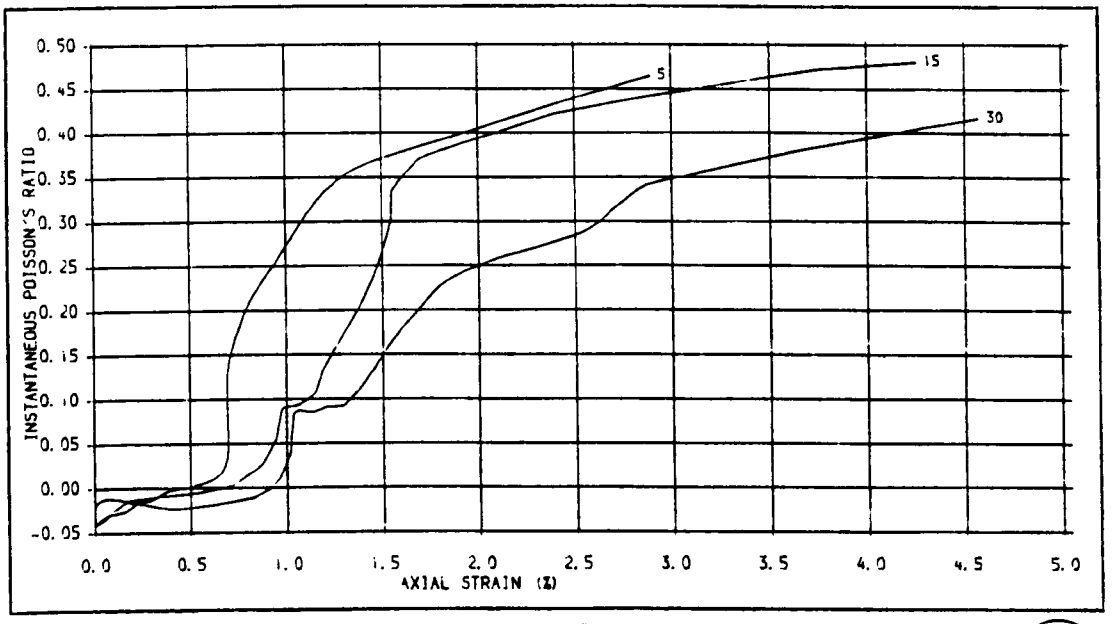

Fig. 651 . INSTANTANEOUS POISSON'S RATIO-AXIAL STRAIN PLOTS FOR PS SPECIMENS WITH SPLIT JOINTS, JOINT ANGLE = 45 DEG., CONFINING PRESSURES. 5, 15 AND 30 MPa.

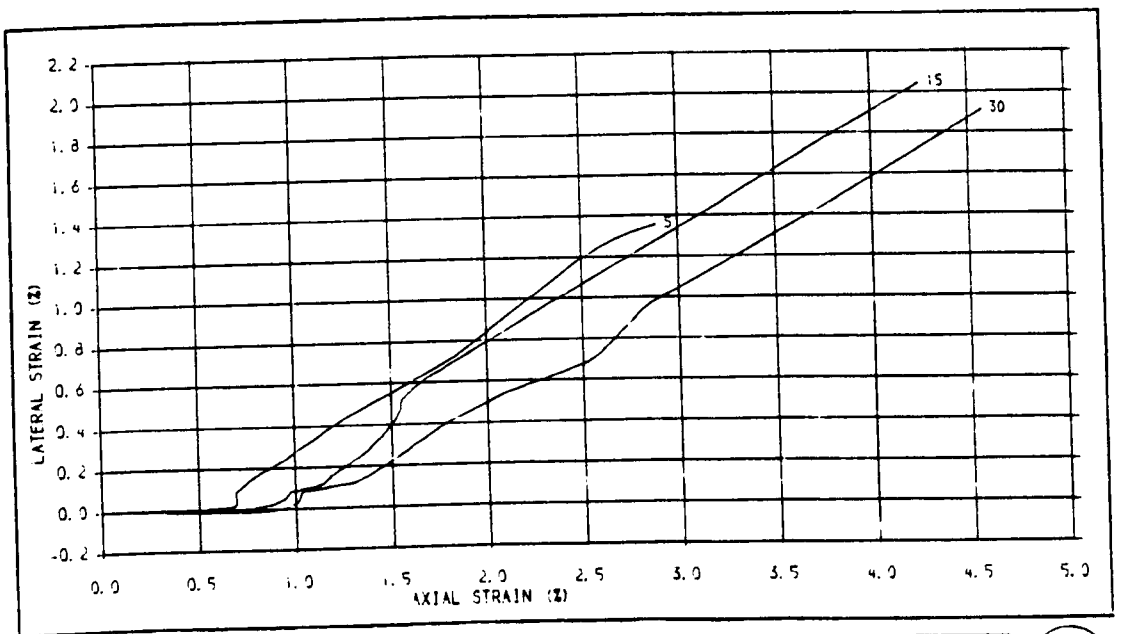

Fig. 652 . LATERAL STRAIN-AXIAL STRAIN PLOTS FOR PS SPECIMENS WITH SPLIT JOINTS, JOINT ANGLE = 45 DEG., CONFINING PRESSURES. 5, 15 AND 30 MPa.

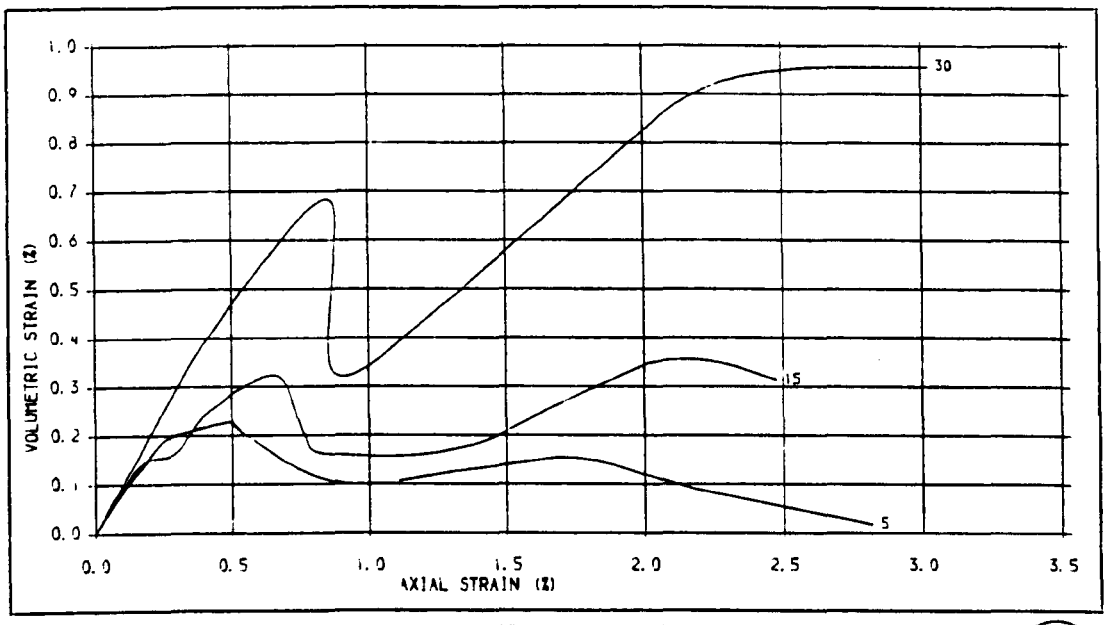

Fig. 653 . VOLUMETRIC STRAIN-AXIAL STRAIN PLOTS FOR PS SPECIMENS WITH SPLIT JOINTS
JOINT ANGLE = 60 DEG., CONFINING PRESSURES. 5, 15 AND 30 MPa.

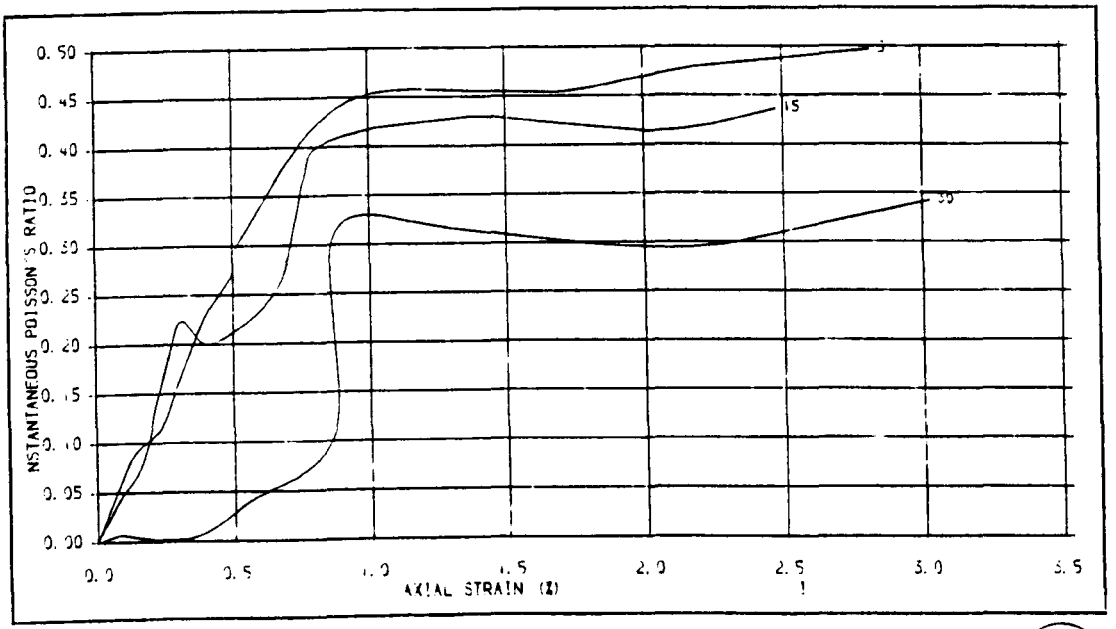

Fig. 654 . INSTANTANEOUS POISSON'S RATIO-AXIAL STRAIN PLOTS FOR PS SPECIMENS WITH
SPLIT JOINTS, JOINT ANGLE = 60 DEG., CONFINING PRESSURES. 5, 15 AND 30 MPa.

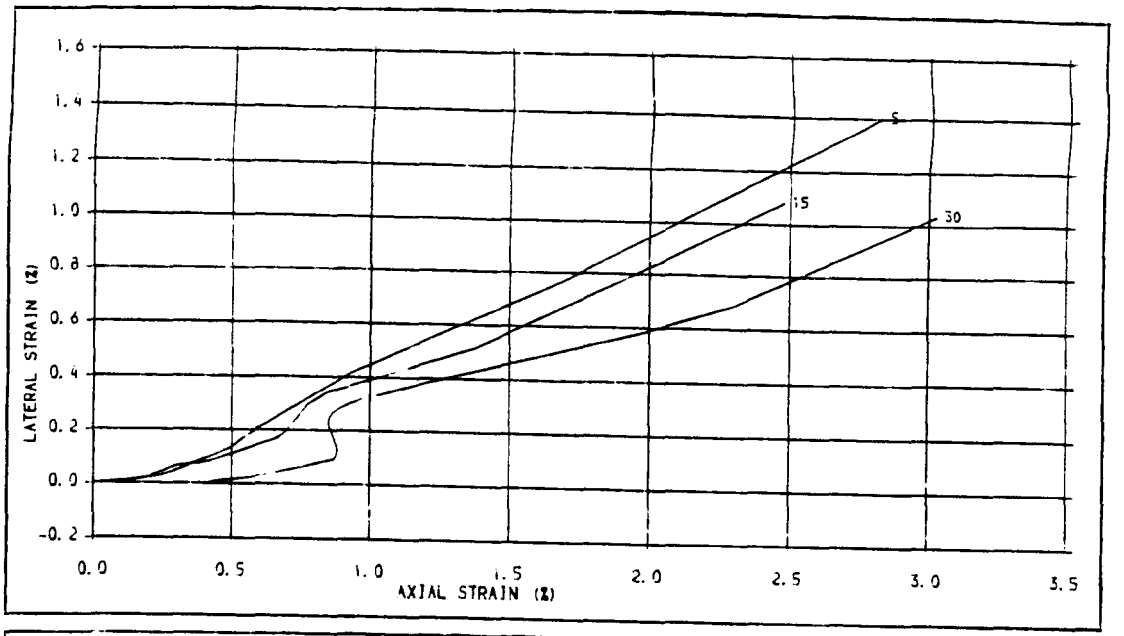

Fig. 655 .LATERAL STRAIN-AXIAL STRAIN PLOTS FOR PS SPECIMENS WITH SPLIT JOINTS, JOINT ANGLE = 60 DEG., CONFINING PRESSURES. 5, 15 AND 30 MPa.

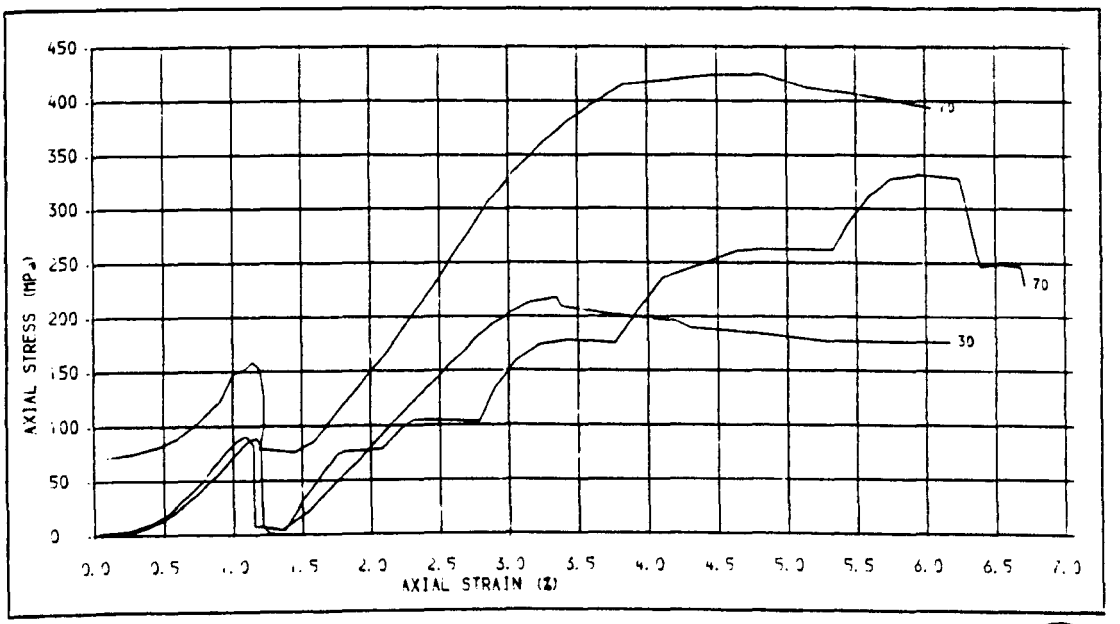

Fig. 656 .STRESS-STRAIN PLOTS FOR PS SPECIMENS WITH SHEAR-SURFACE JOINTS. CONF. PRES. FOR JOINT FORMATION= 0, ONE AND MULTI-STAGE TESTS, CONFINING PRESSURES. 30 & 70 MPa

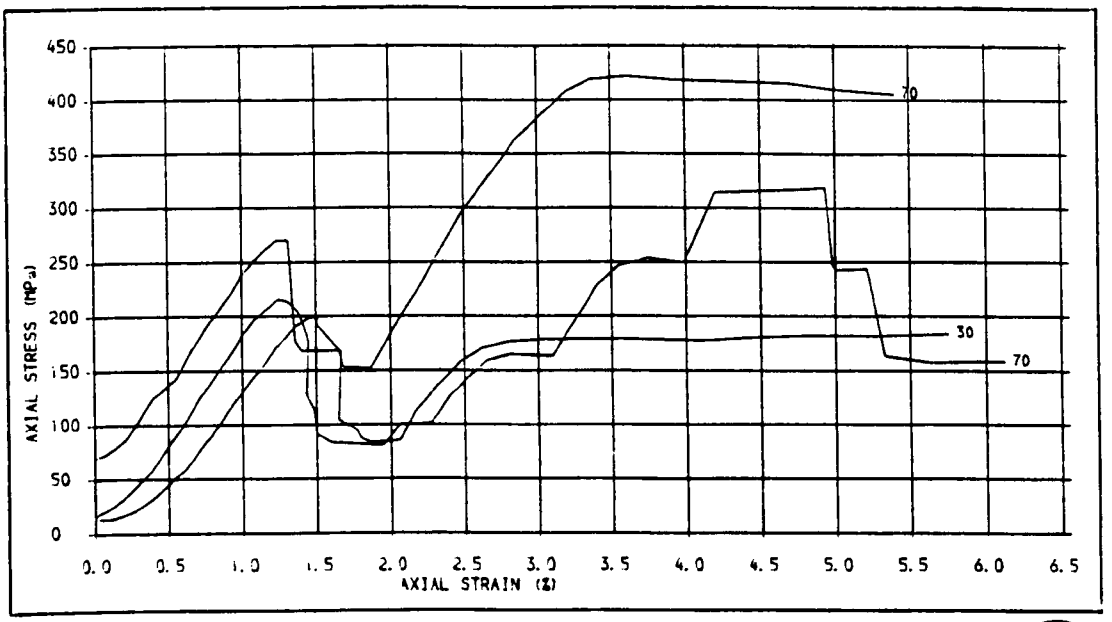

Fig. 657 .STRESS-STRAIN PLOTS FOR PS SPECIMENS WITH SHEAR-SURFACE JOINTS, CONF. PRES. FOR FORMING JOINT= 10 MPa, ONE & MULTI-STAGE TESTS, CONFINING PRESSURES. 30 & 70 MPa.

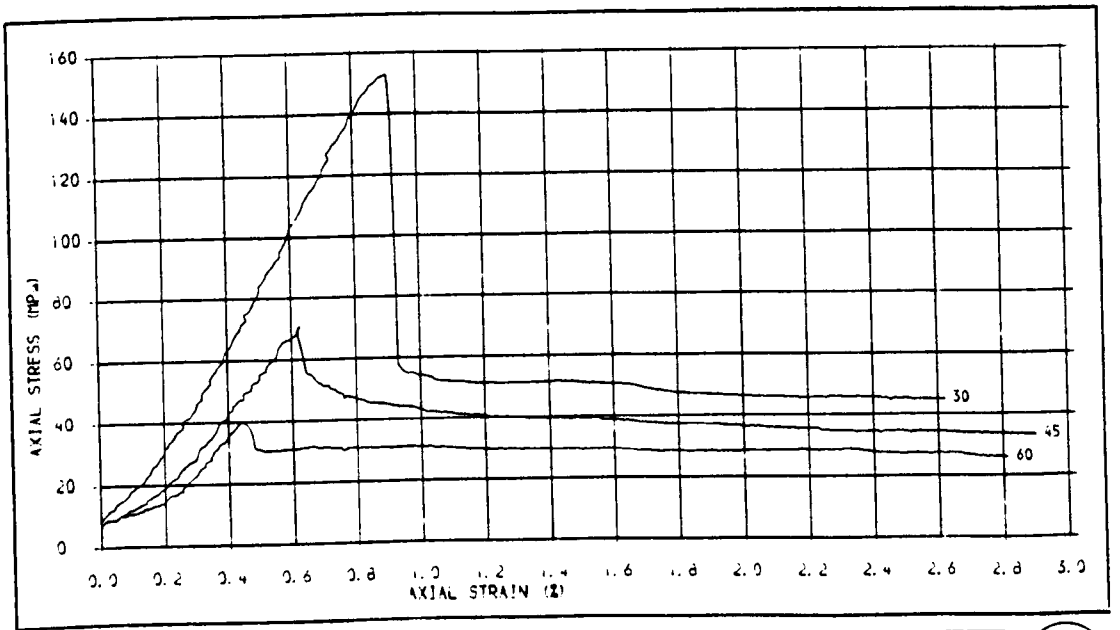

Fig. 658 .STRESS-STRAIN PLOTS FOR PS SPECIMENS WITH NATURAL JOINTS FOR 5 MPa CONFINING PRESSURE, JOINT ANGLES. 30, 45 AND 60 DEC.

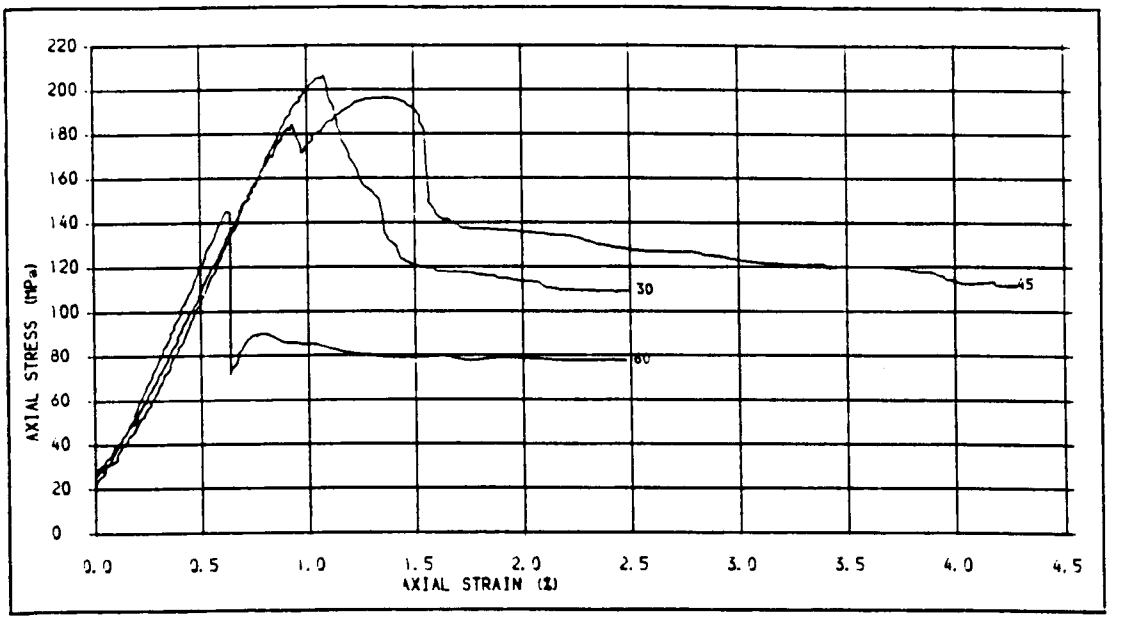

Fig. 659 .STRESS-STRAIN PLOTS FOR PS SPECIMENS WITH NATURAL JOINTS IN 15 MPa CONFINING PRESSURE, JOINT ANGLES. 30, 45 AND 60 DEG.

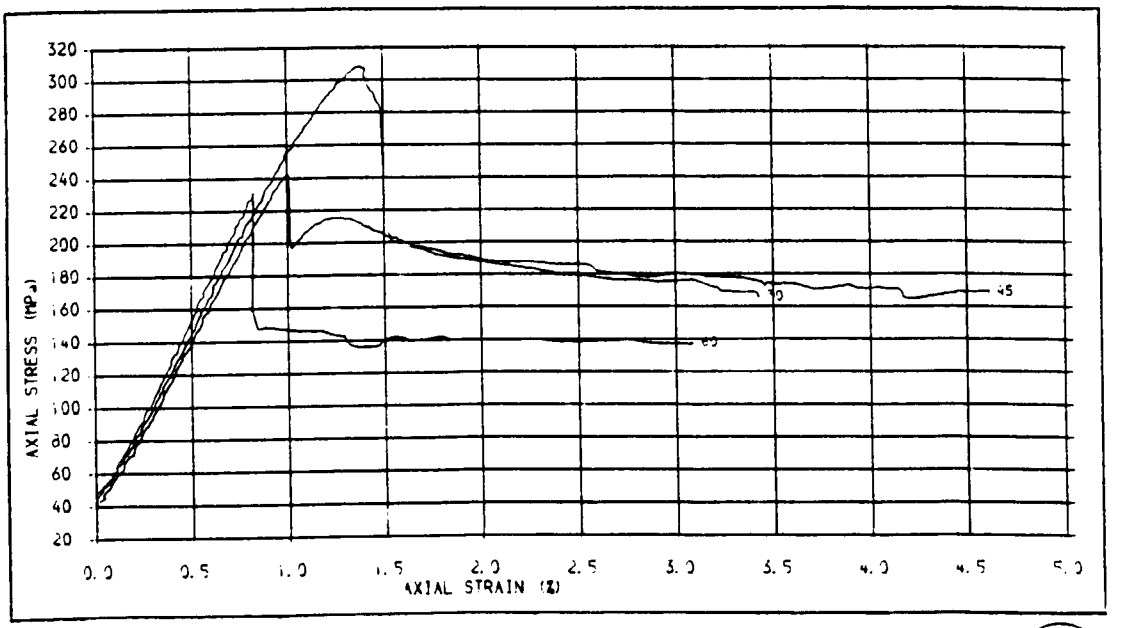

Fig. 660 .STRESS-STRAIN PLOTS FOR PS SPECIMENS WITH NATURAL JOINTS IN 30 MPa CONFINING PRESSURE, JOINT ANGLES. 30, 45 AND 60 DEC.

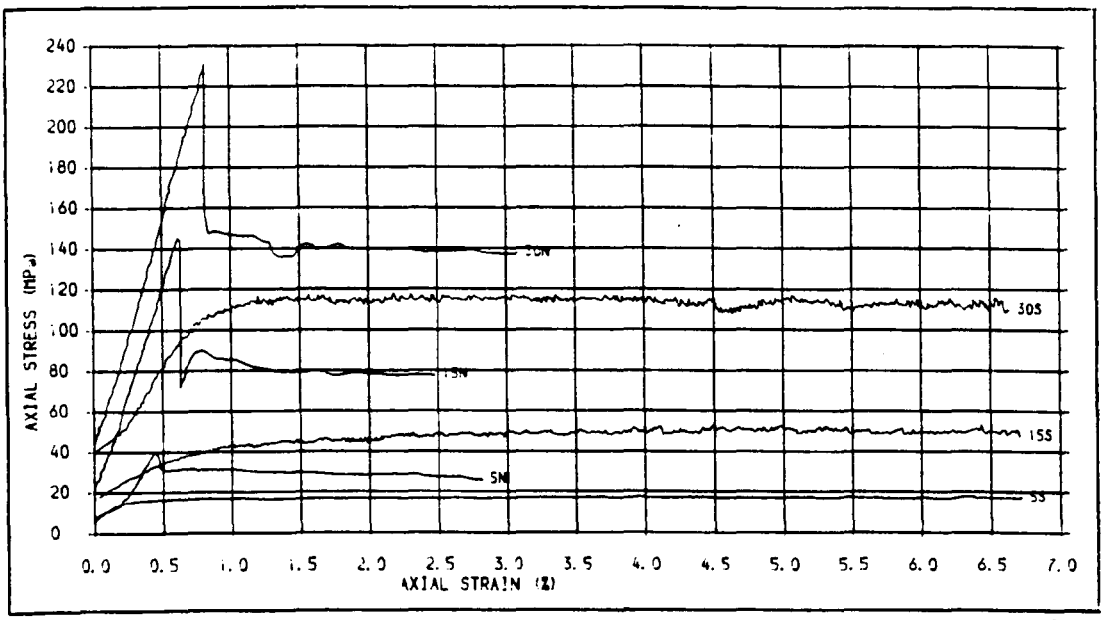

Fig. 661 .STRESS-STRAIN PLOTS FOR PS SPECIMENS WITH NATURAL AND SAW JOINTS
JOINT ANGLE = 60 DEG. CONFINING PRESSURES. 5, 15 AND 30 MPa.

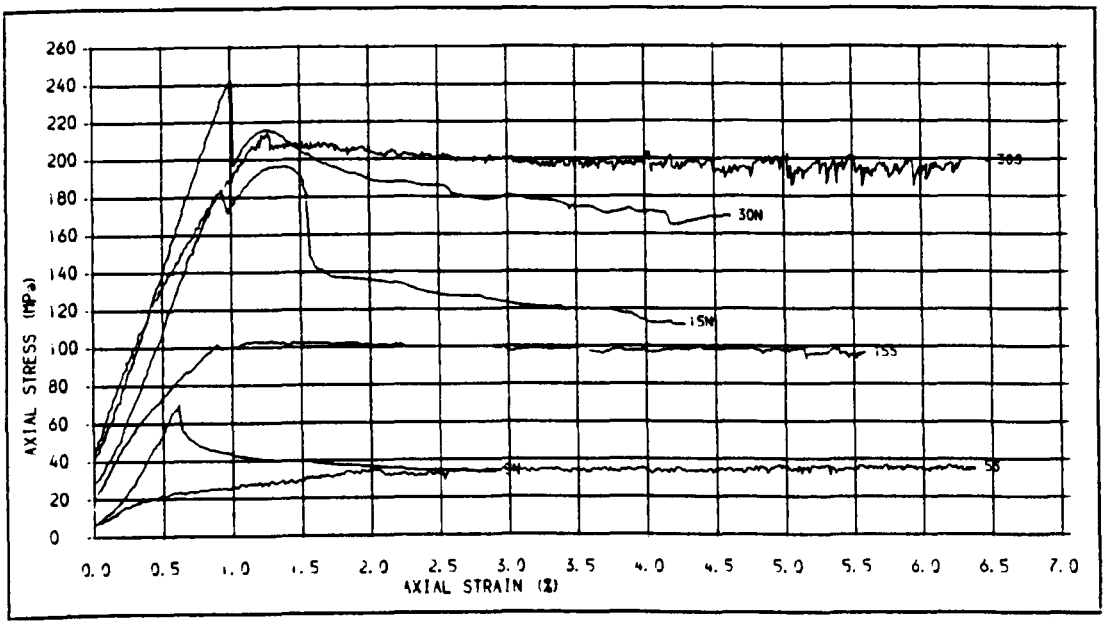

Fig. 662 .STRESS-STRAIN PLOTS FOR PS SPECIMENS WITH SAW CUT AND NATURAL JOINTS
CONFINING PRESSURES. 5, 15 AND 30 MPa, JOINT ANGLE = 45 DEG.

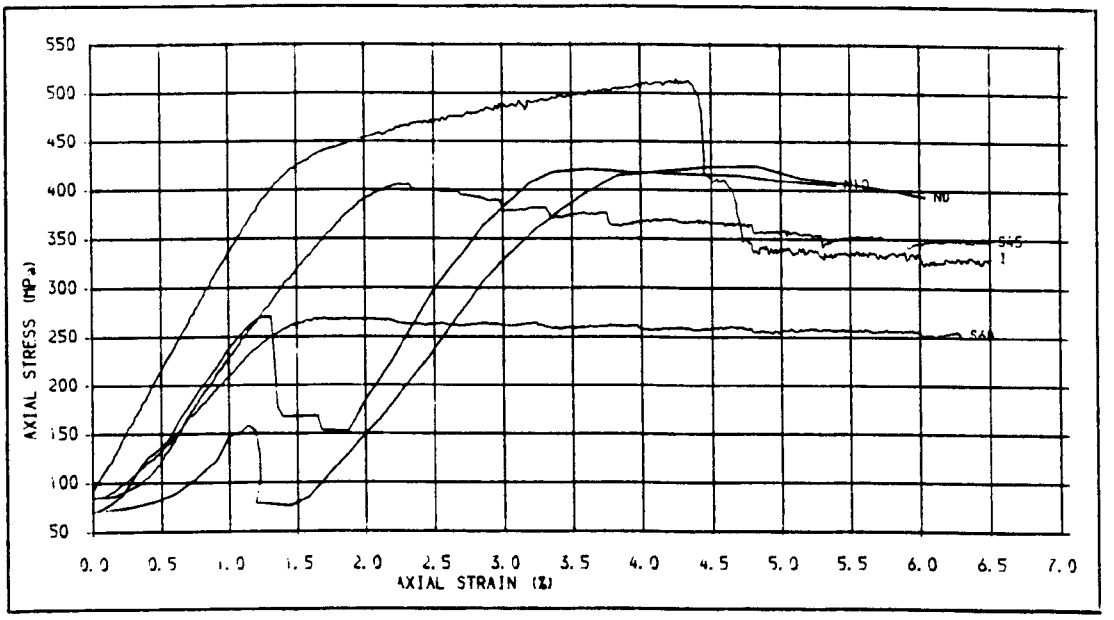

Fig. 663 .STRESS-STRAIN PLOTS FOR INTACT AND JOINTED PS SPECIMENS, SAW CUT WITH 45 AND 60 DEC., AND SHEAR-SURFACE JOINTS (AT 0 AND 10 MPa), CONFINING PRESSURE 70 MPa.

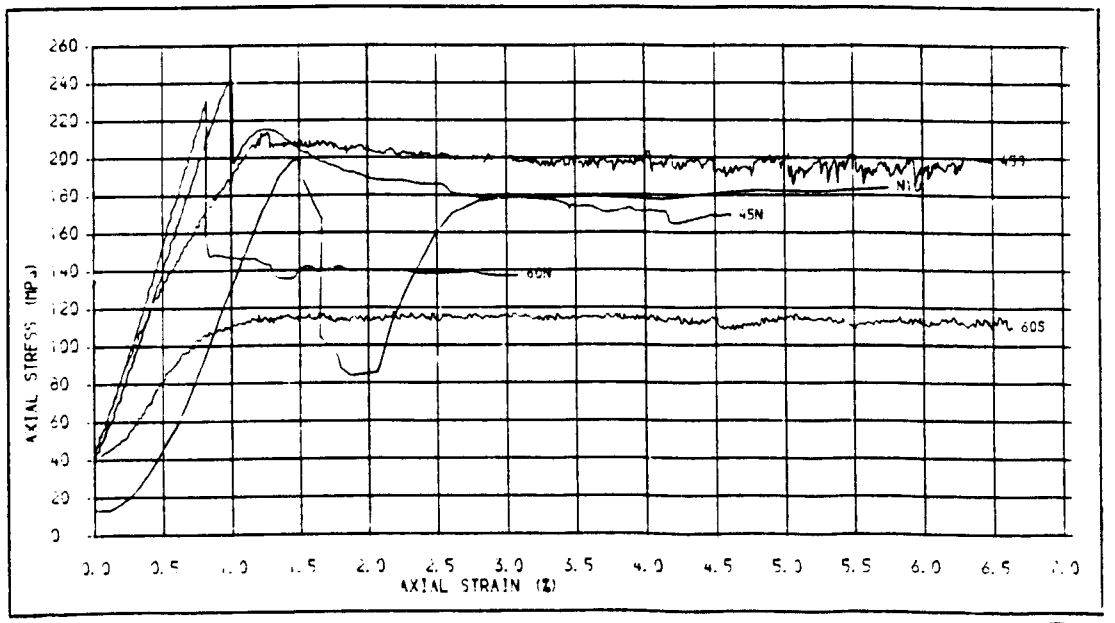

Fig. 664 .STRESS-STRAIN PLOTS FOR PS SPECIMENS WITH SAW CUT AND NATURAL (45 & 60 DEC.) AND SHEARC SURFACE (AT 10 MPa) JOINTS, CONFINING PRESSURE = 30 MPa.

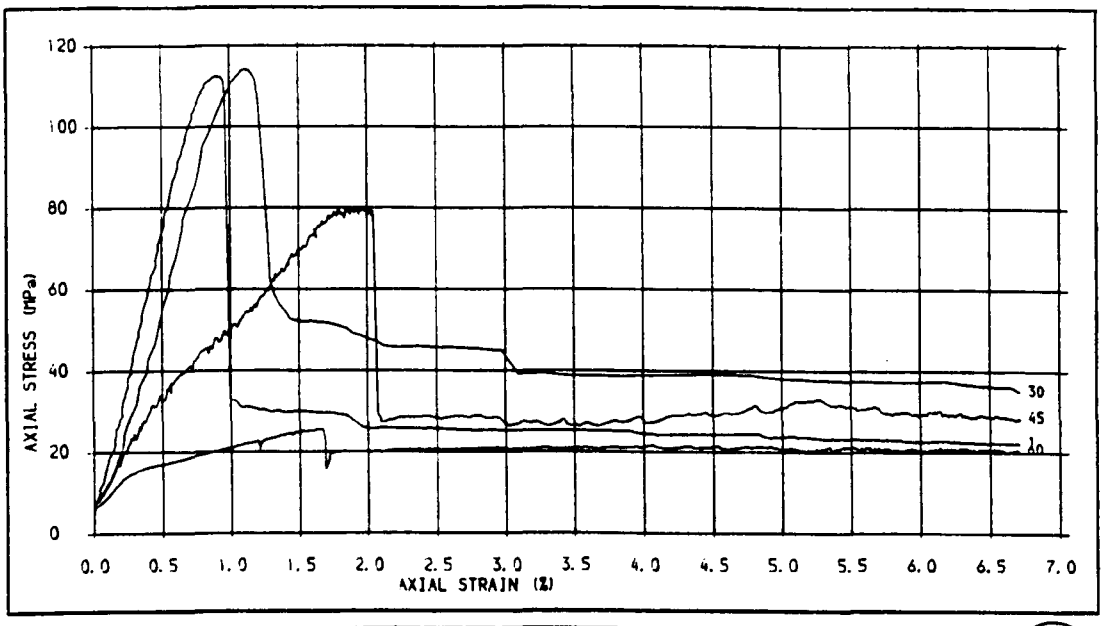

Fig. 665 .STRESS-STRAIN PLOTS FOR INTACT AND JOINTED (SAW CUT) SPECIMENS IN 5 MPa CONFINING PRESSURE, JOINT ANGLES. 45, 30, AND 60 DEG.

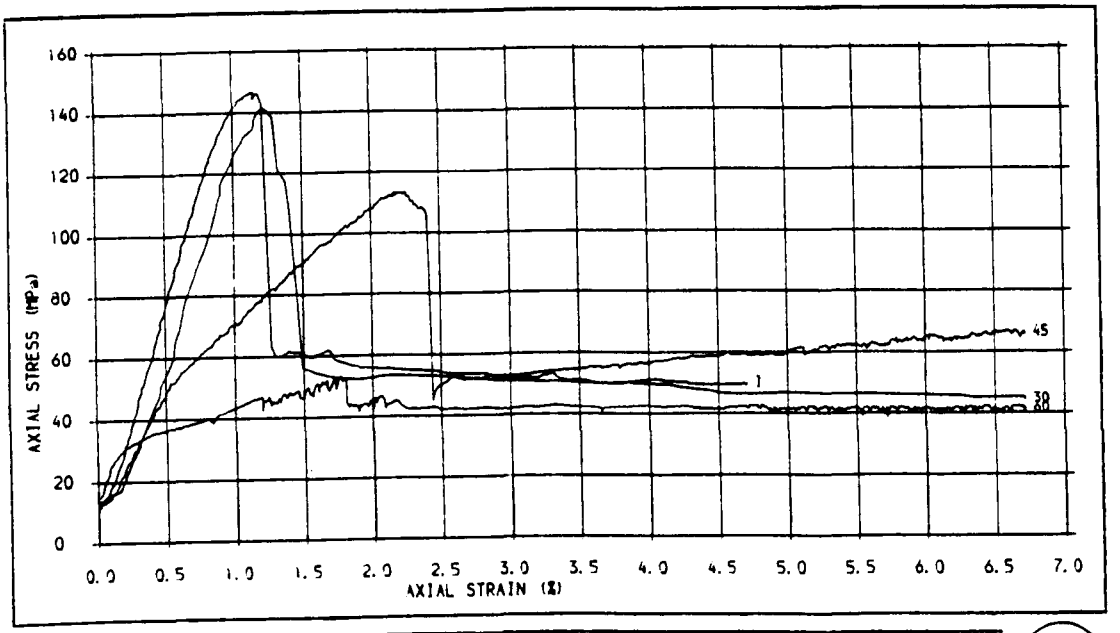

Fig. 666 .STRESS-STRAIN PLOTS FOR 55 INTACT AND JOINTED (SAW CUT) SPECIMENS JOINT ANGLES. 30, 45 AND 60 DEG., CONFINING PRESSURE = 10 MPa.

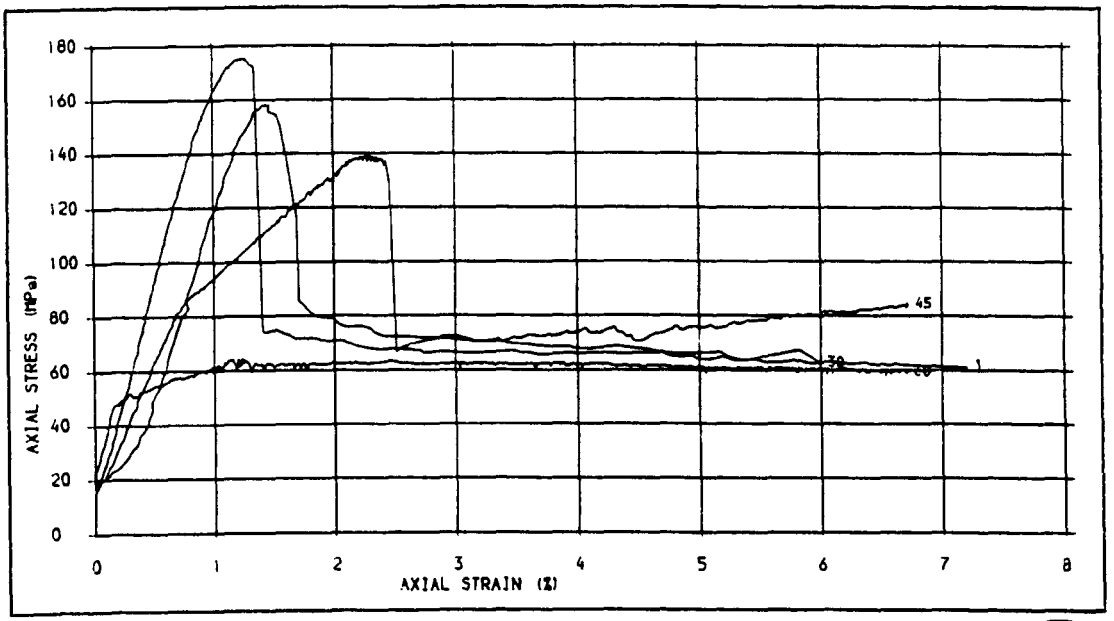

Fig. 667 . STRESS-STRAIN PLOTS FOR SS SPECIMENS (INTACT AND SAW CUT JOINTED)
JOINT ANGLES. 30, 45 AND 60 DEG., CONFINING PRESSURE = 15 MPa.

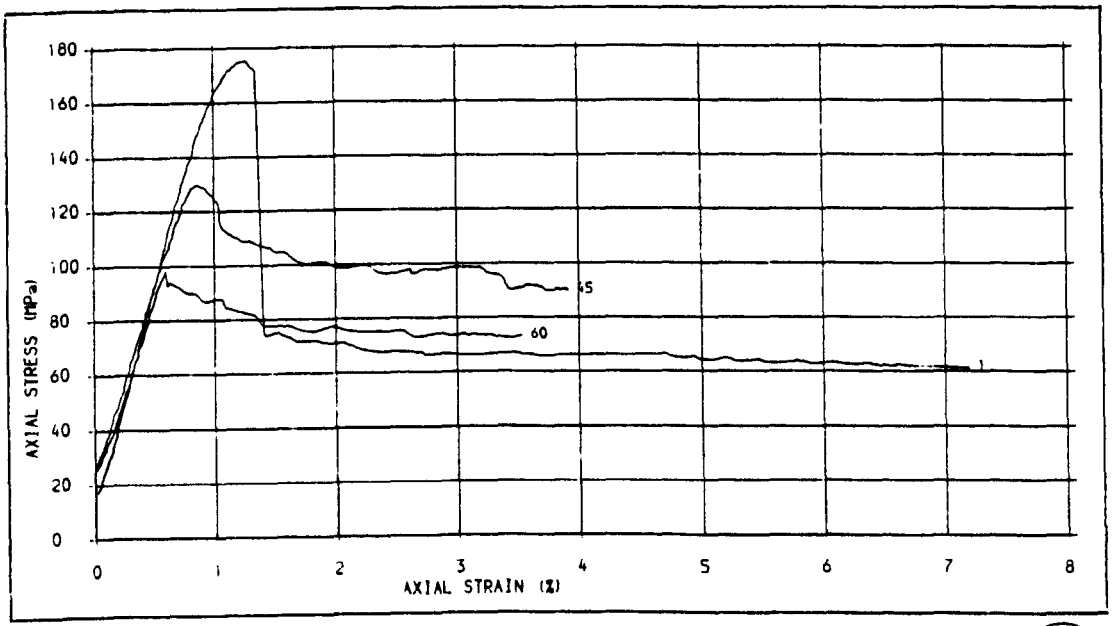

Fig. 668 . STRESS-STRAIN PLOTS FOR SS SPECIMENS (INTACT AND NATURAL JOINTED)
JOINT ANGLES. 45 AND 60 DEG., CONFINING PRESSURE = 15 MPa.

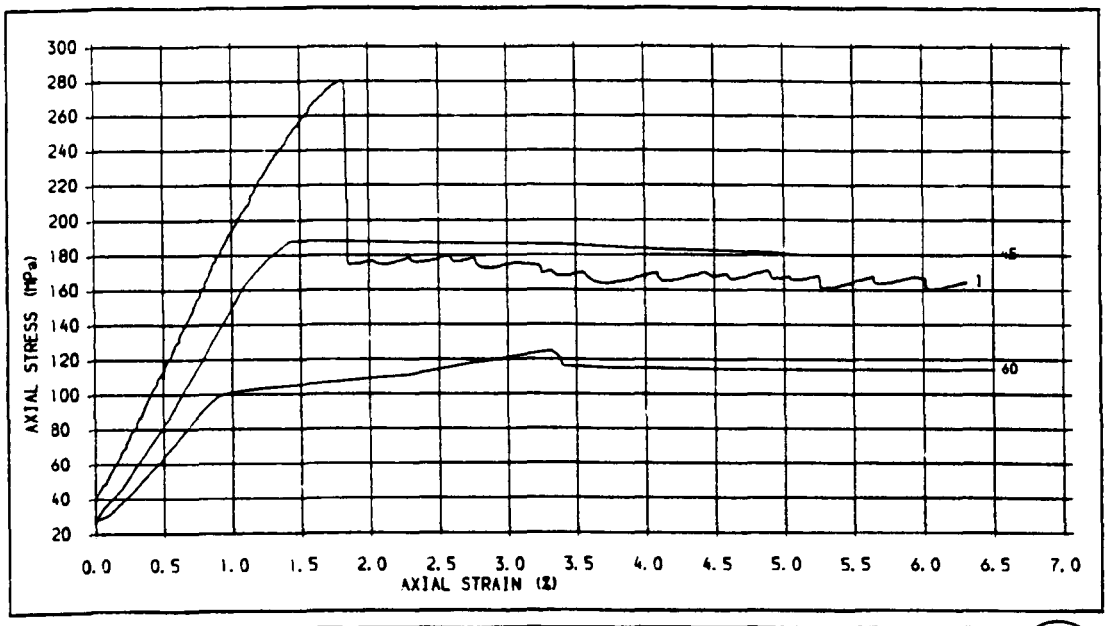

Fig. 669 .STRESS-STRAIN PLOTS FOR SS SPECIMENS (INTACT AND SAW CUT JOINTS)
JOINT ANGLES. 45 AND 60 DEG., CONFINING PRESSURE = 30 MPa.

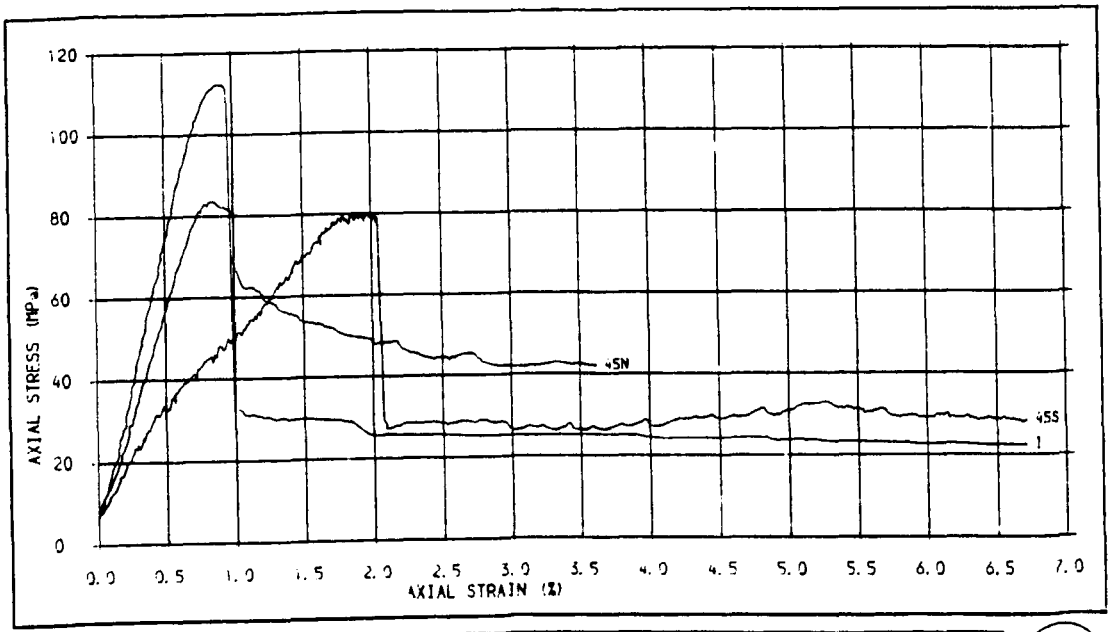

Fig. 670 .STRESS-STRAIN PLOTS FOR INTACT AND JOINTED (SAW CUT & NATURAL) SPECIMENS
CONFINING PRESSURE = 5 MPa, JOINT ANGLE. 45 DEG.

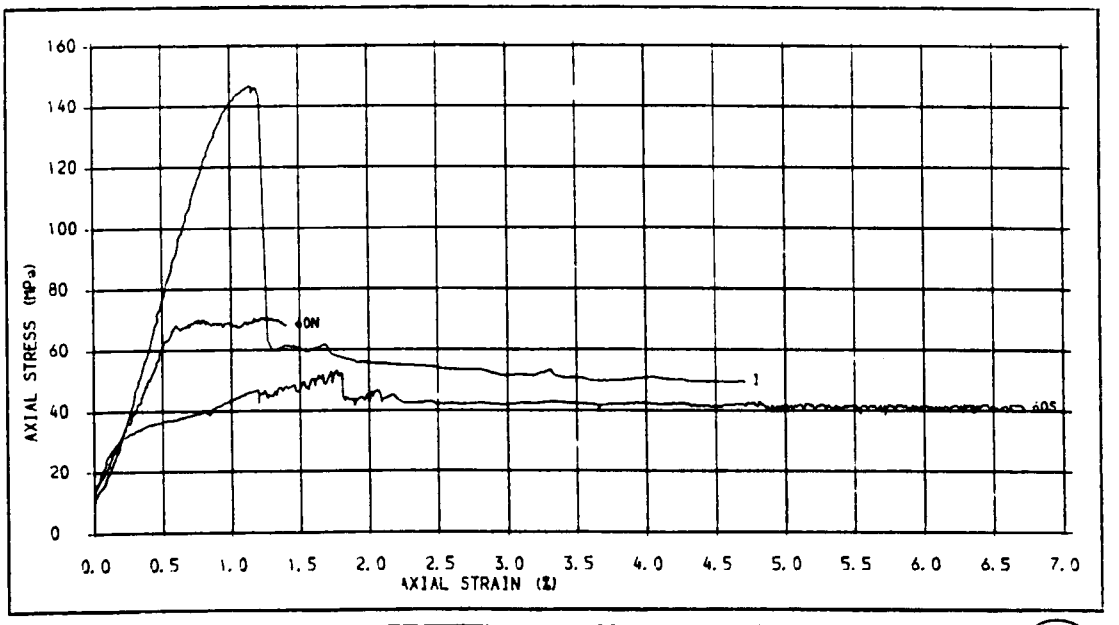

Fig. 6.71 .STRESS-STRAIN PLOTS FOR SS INTACT AND JOINTED (SAW CUT AND NATURAL) SPECIMENS
JOINT ANGLE. 60 DEG., CONFINING PRESSURE = 10 MPa.

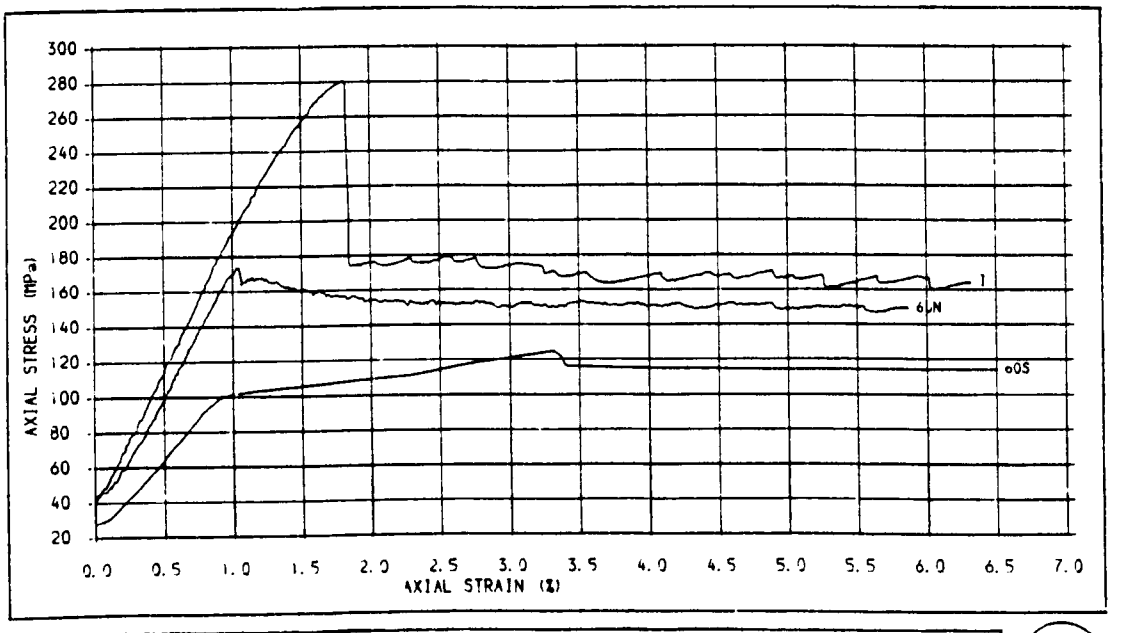

Fig. 6.72 .STRESS-STRAIN PLOTS FOR SS SPECIMENS (INTACT, NATURAL AND SAW CUT JOINTS)
JOINT ANGLE. 60 DEG., CONFINING PRESSURE = 30 MPa.

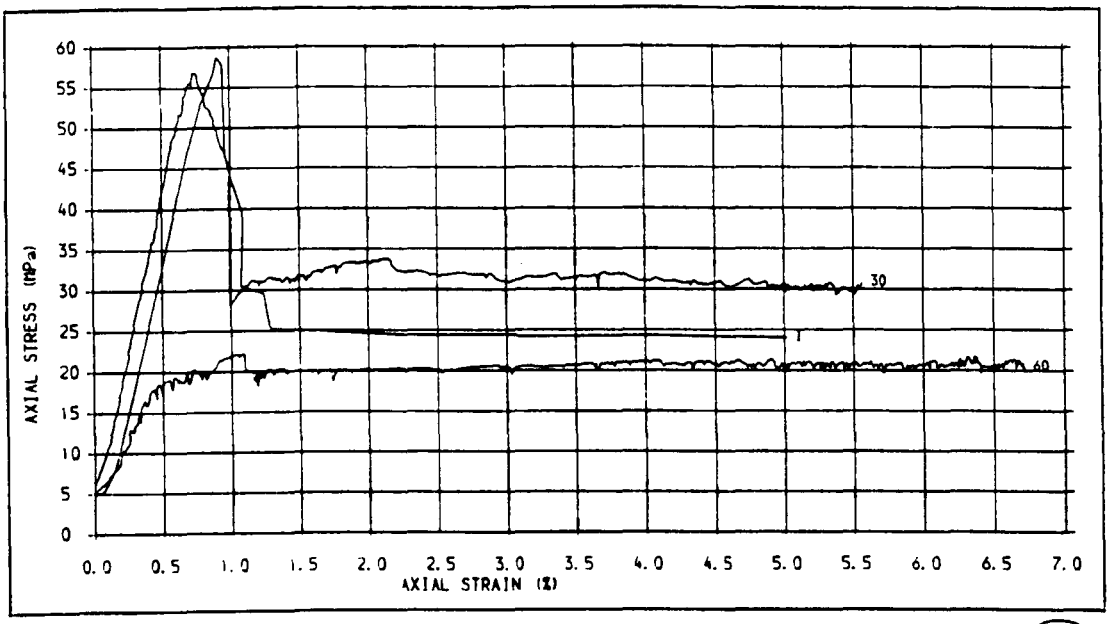

Fig. 673 . STRESS-STRAIN PLOTS FOR DUMFRITH SANDSTONE SPECIMENS (INTACT AND SAW CUT JOINTS)
JOINT ANGLES. 30 AND 60 DEG., CONFINING PRESSURE. 5 MPa.

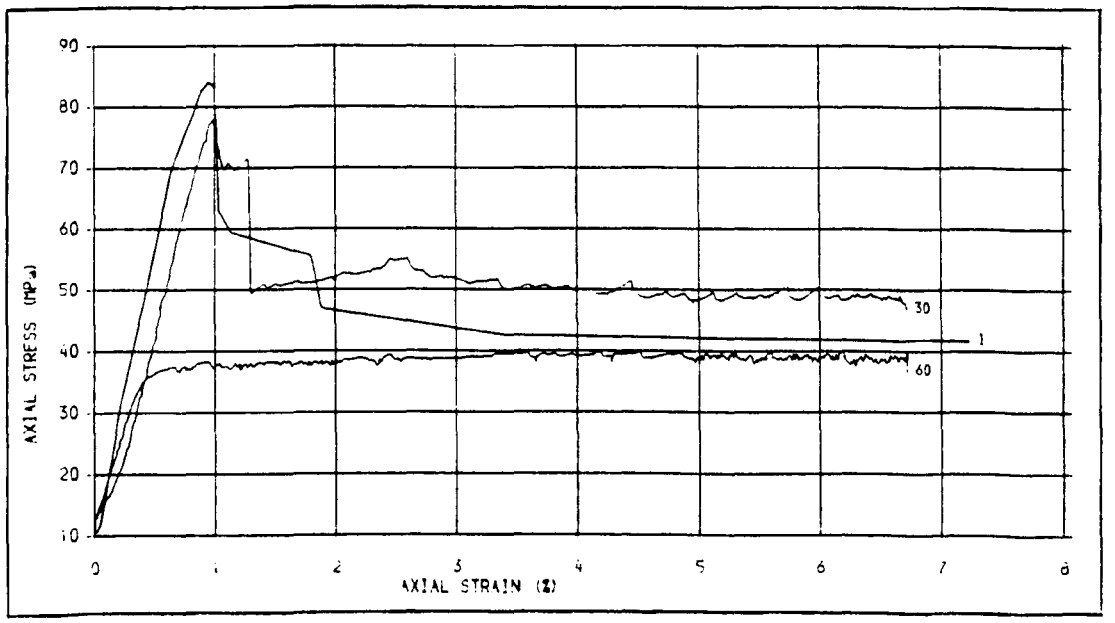

Fig. 674 . STRESS-STRAIN PLOTS FOR DS SPECIMENS (INTACT AND SAW CUT JOINTS)
JOINT ANGLES = 30 AND 60 DEG., CONFINING PRESSURE = 10 MPa.

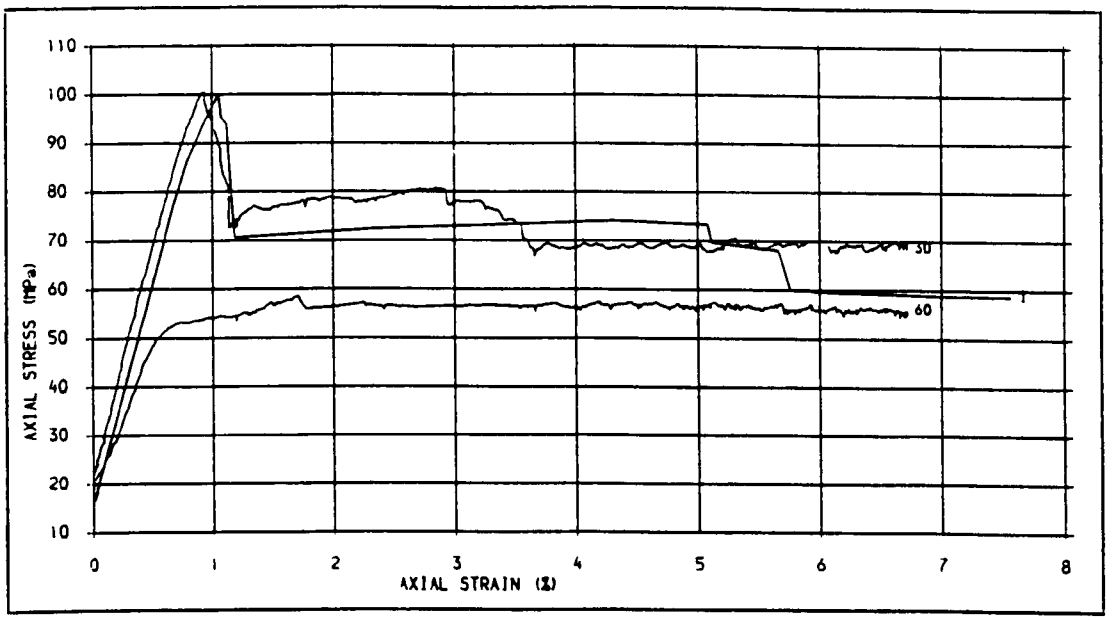

Fig. 675 .STRESS-STRAIN PLOTS FOR DS SPECIMENS (INTACT AND SAW CUT), JOINT ANGLES = 30 AND 60 DEG., CONFINING PRESSURE = 15 MPa.

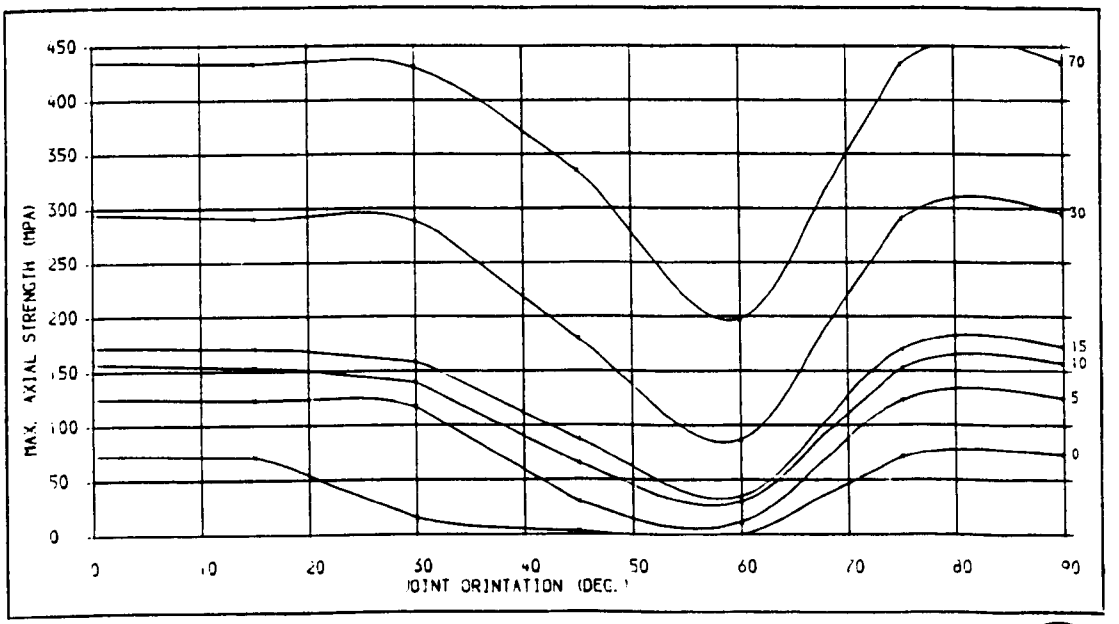

Fig. 676 .PEAK STRESS-JOINT ORIENTATION PLOTS FOR PENRITH SANDSTONE, JOINT ANGLES. 0, 15, 30, 45, 60, 75 AND 90 DEG., CONFINING PRESSURES. 0, 5, 10, 15, 30 AND 70 MPa.

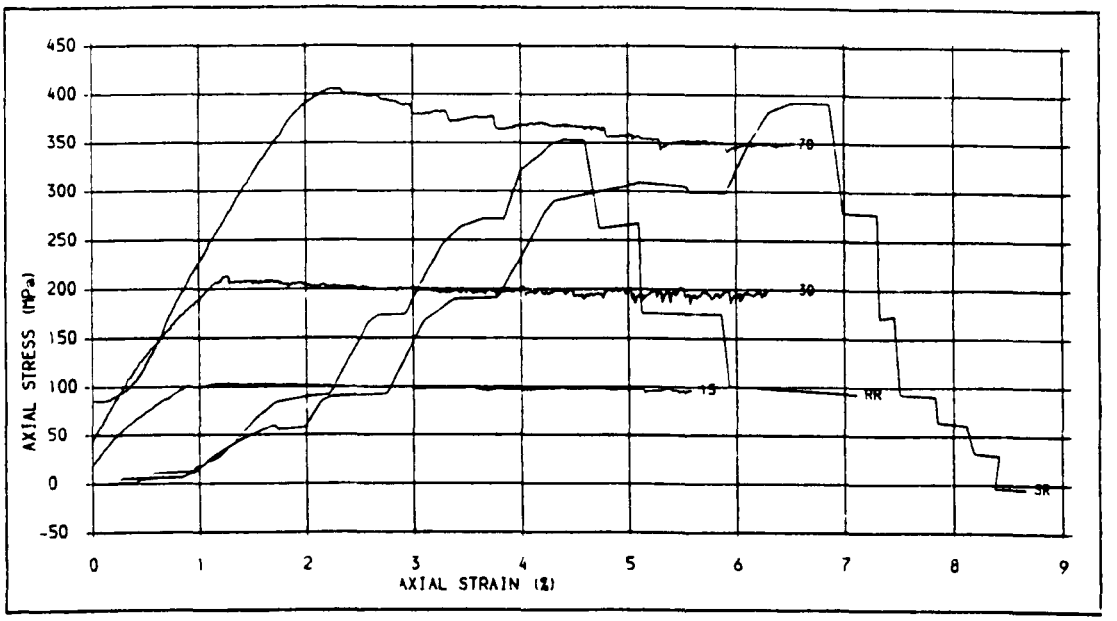

Fig. 6.77 : STRESS-STRAIN PLOTS FOR PS SPECIMENS WITH SAW CUT JOINTS, JOINT ANGLE = 45 DEG. ONE AND MULTI-STAGE TESTS, FRESH (SR) AND REUSED SLIDING SURFACES.

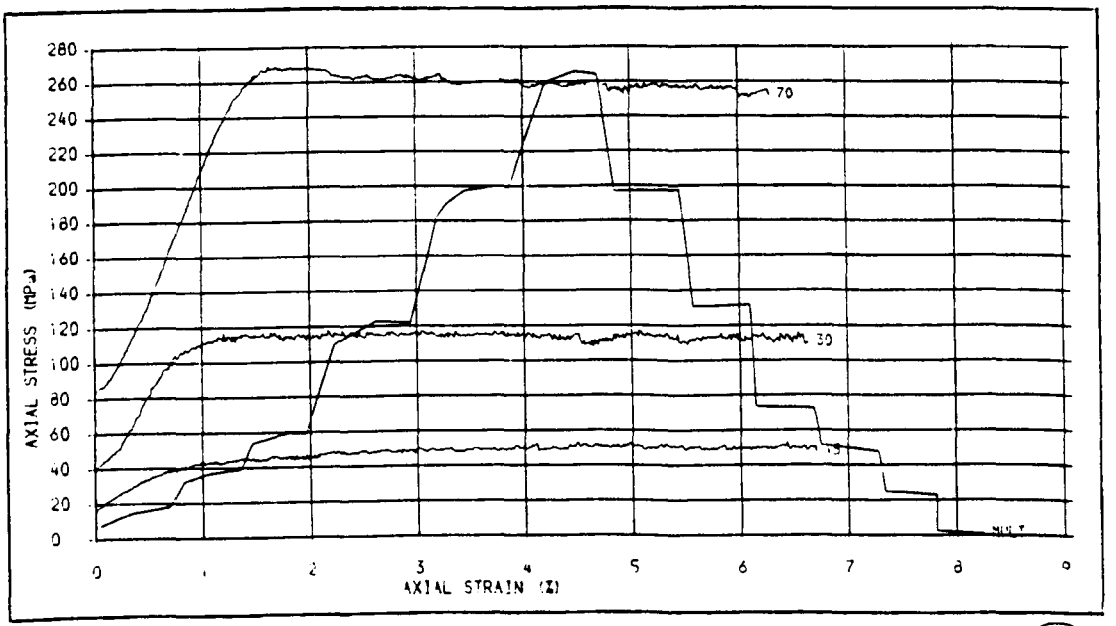

Fig. 6.78 : STRESS-STRAIN PLOTS FOR PS SPECIMENS WITH SAW CUT JOINTS, JOINT ANGLE= 60 DEG. ONE AND MULTI-STAGE TESTS, CONFINING PRESSURES: 5, 10, 15, 30, 50 AND 70 MPa.

FIG 6.79 DIFFERENTIAL STRESS–CONFINING PRESSURE ENVELOPES FOR JOINTED (SAW CUT) AND INTACT PS SPECIMENS

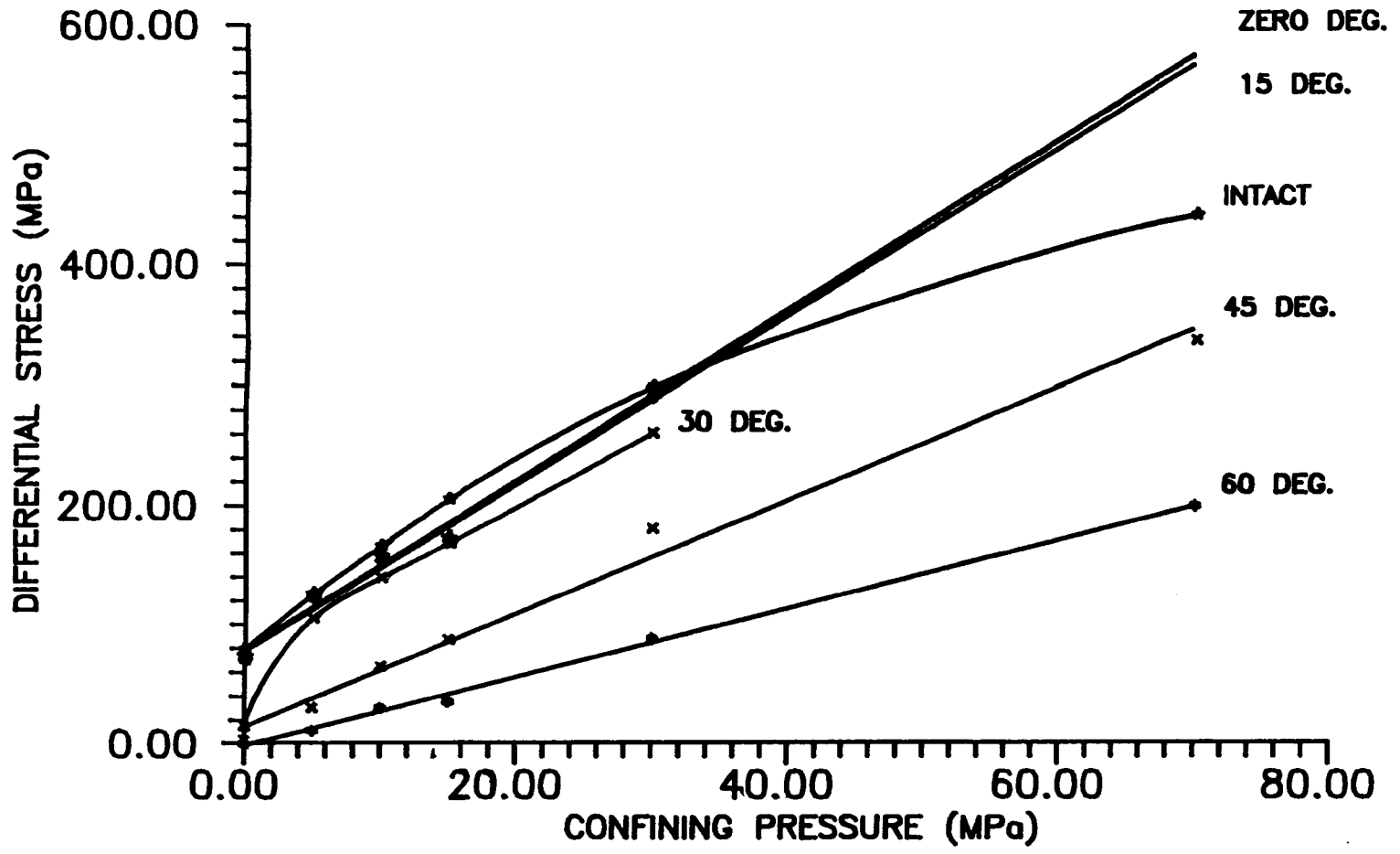

FIG 6. 80 DIFFERENTIAL STRESS VS CONFINING PRESSURE ENVELOPES FOR INTACT AND JOINTED (SPLIT BREAKAGE AND SAW CUT) STAINTON SANDSTONE

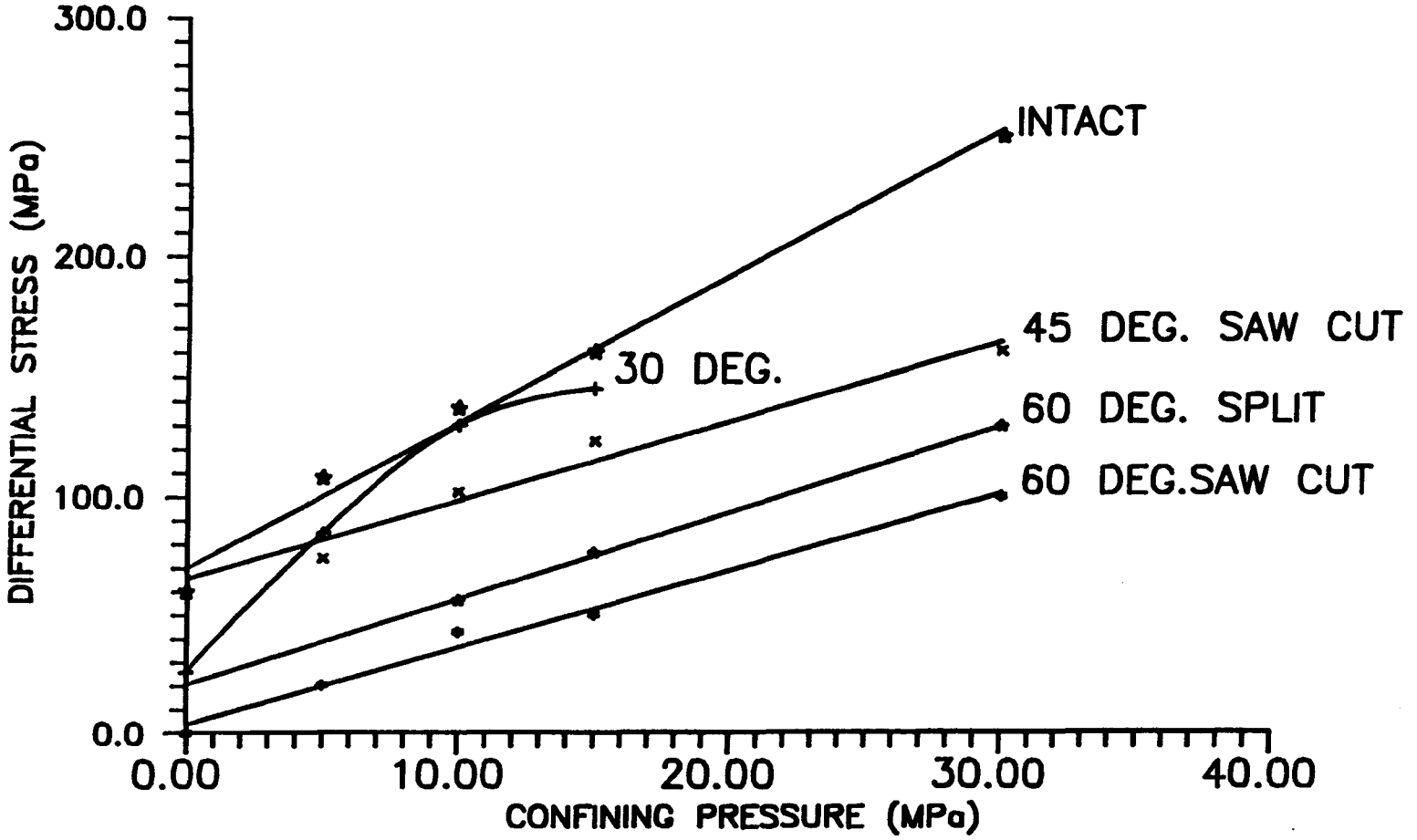

FIG 6.81 DIFFERENTIAL STRESS–CONFINING PRESSURE ENVELOPES FOR INTACT AND JOINTED (SAW CUT) DUMFRITH SANDSTONE

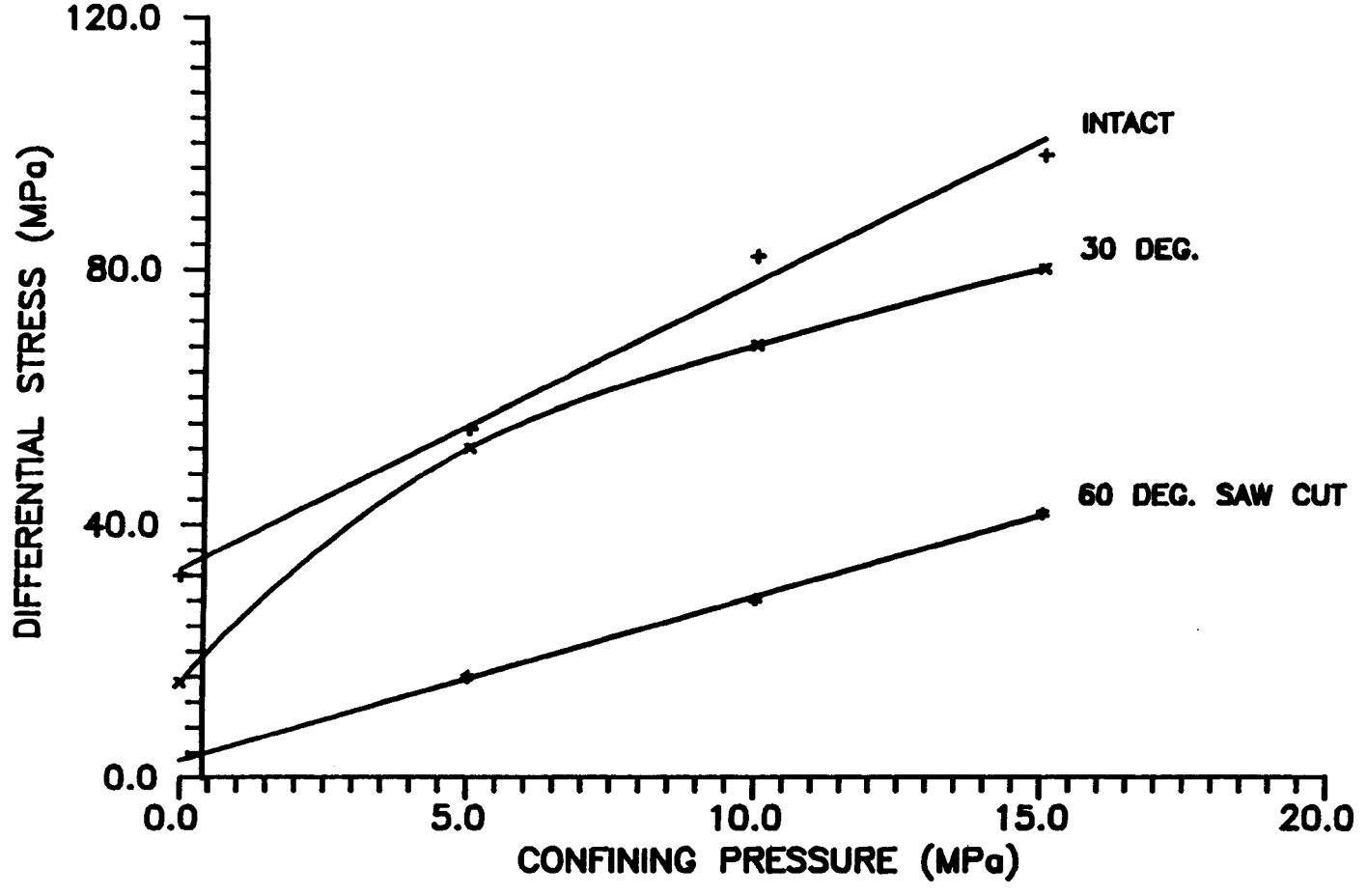

FIG 6.82 DIFFERENTIAL STRESS–CONFINING PRESSURE ENVELOPES FOR JOINTED (SPLIT BREAKAGE) PS SPECIMENS.

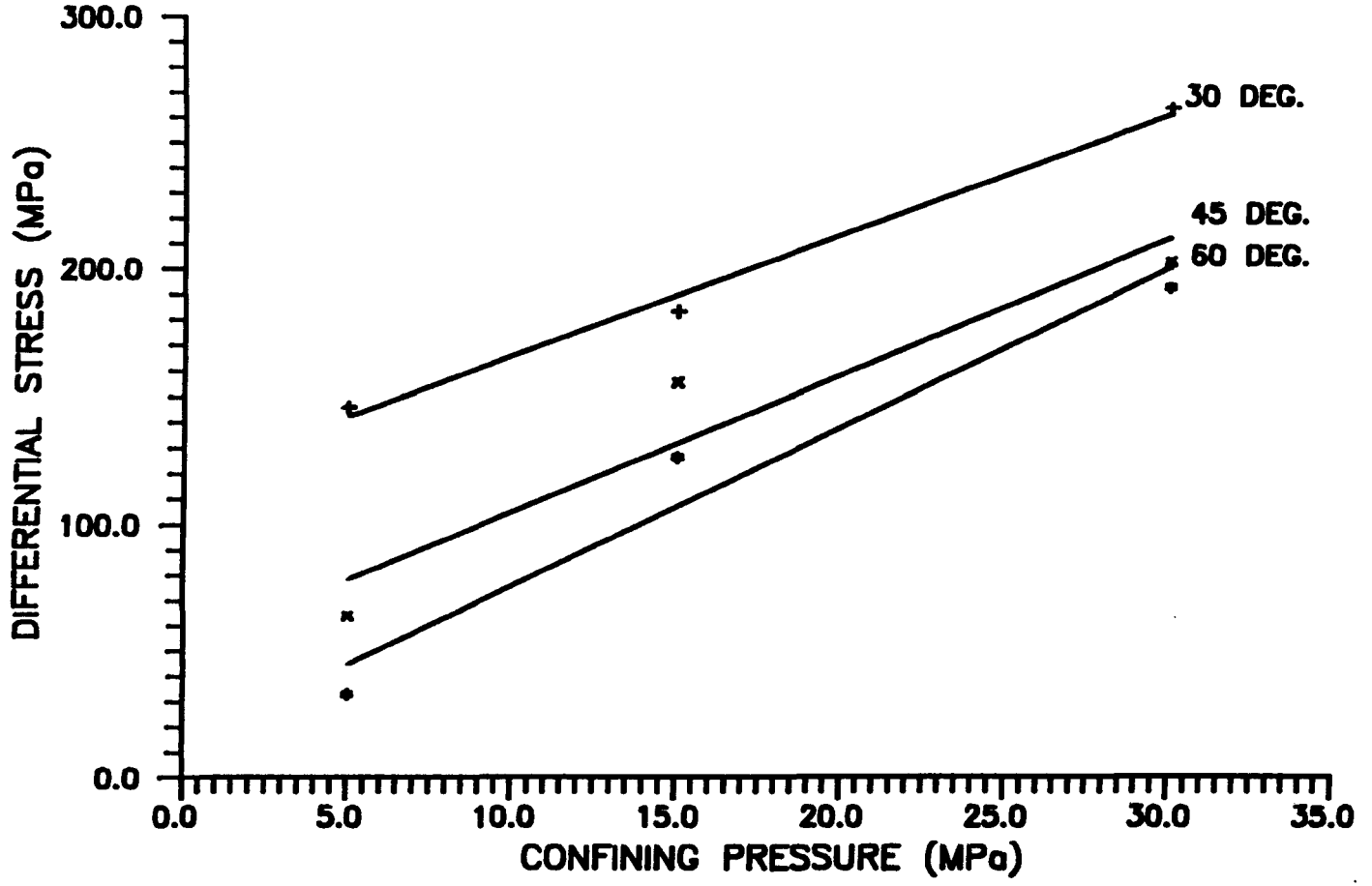

FIG 6.83 MOHR ENVELOPES FOR INTACT AND JOINTED (SAW CUT AND SPLIT) PS SPECIMENS

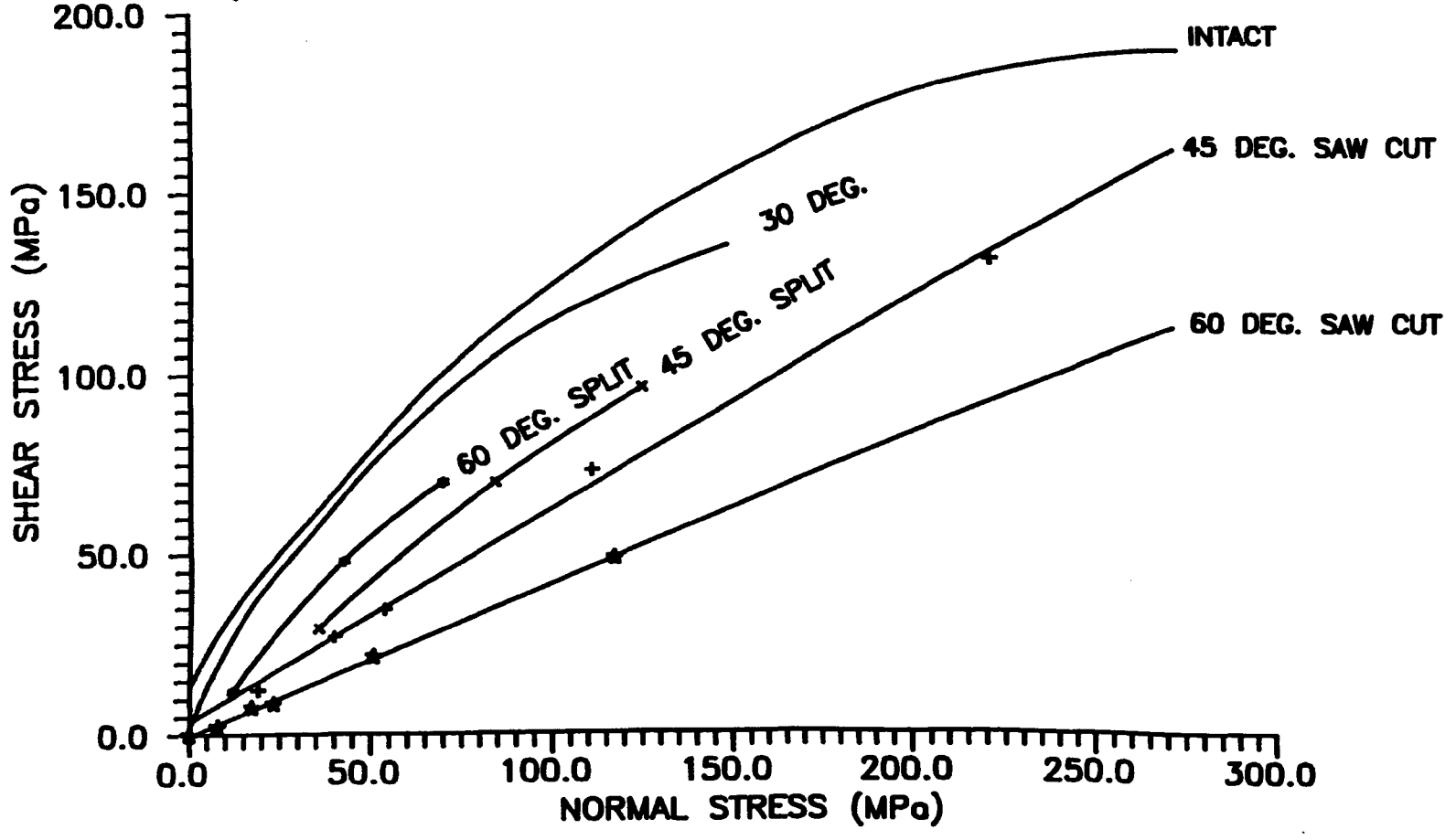

FIG 6.84 MOHR ENVELOPES FOR INTACT AND JOINTED (SAW CUT AND SPLIT) SS SPECIMENS

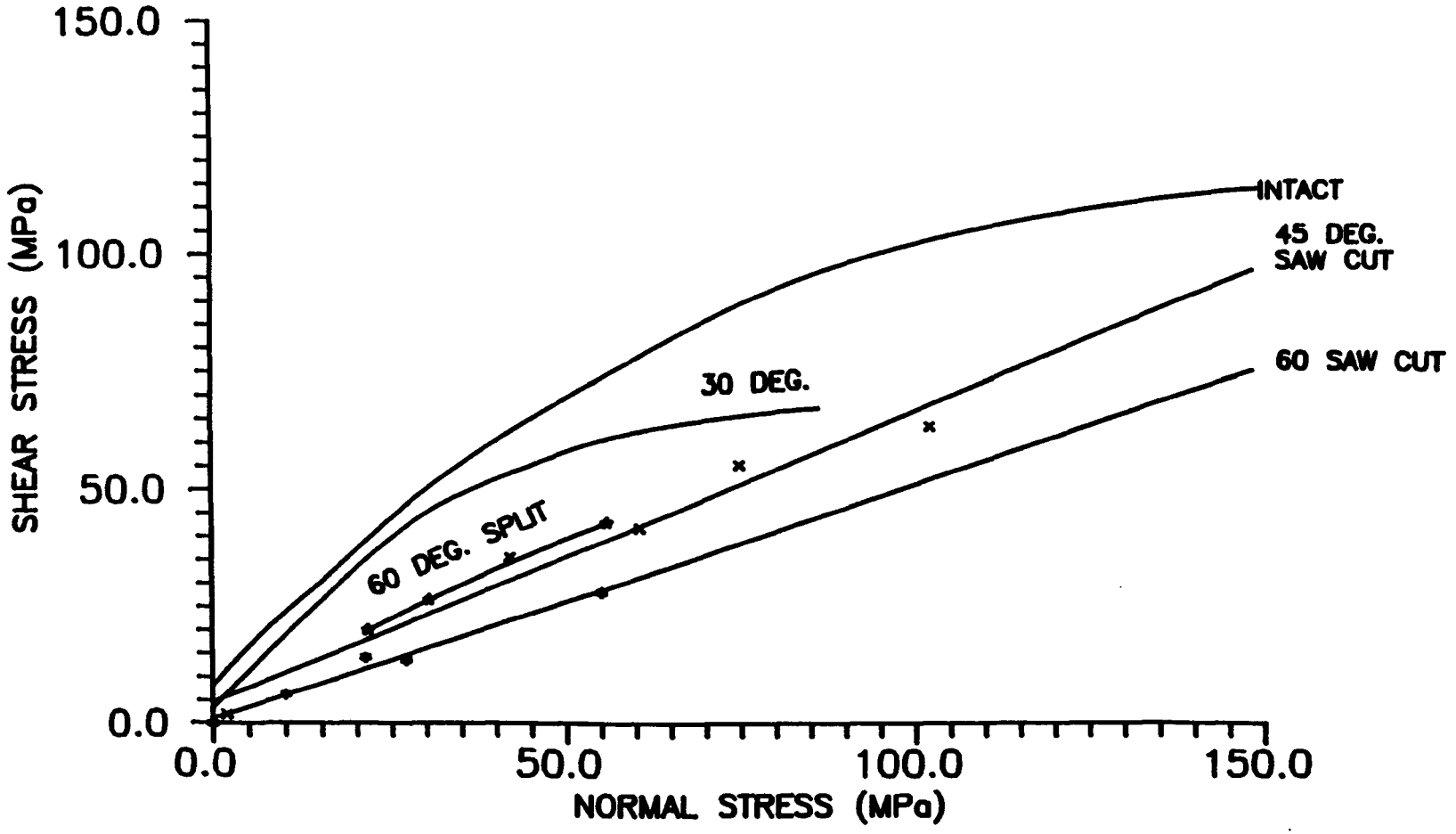

FIG 6.85 MOHR ENVELOPES FOR INTACT AND JOINTED (SAW CUT) DS SPECIMENS

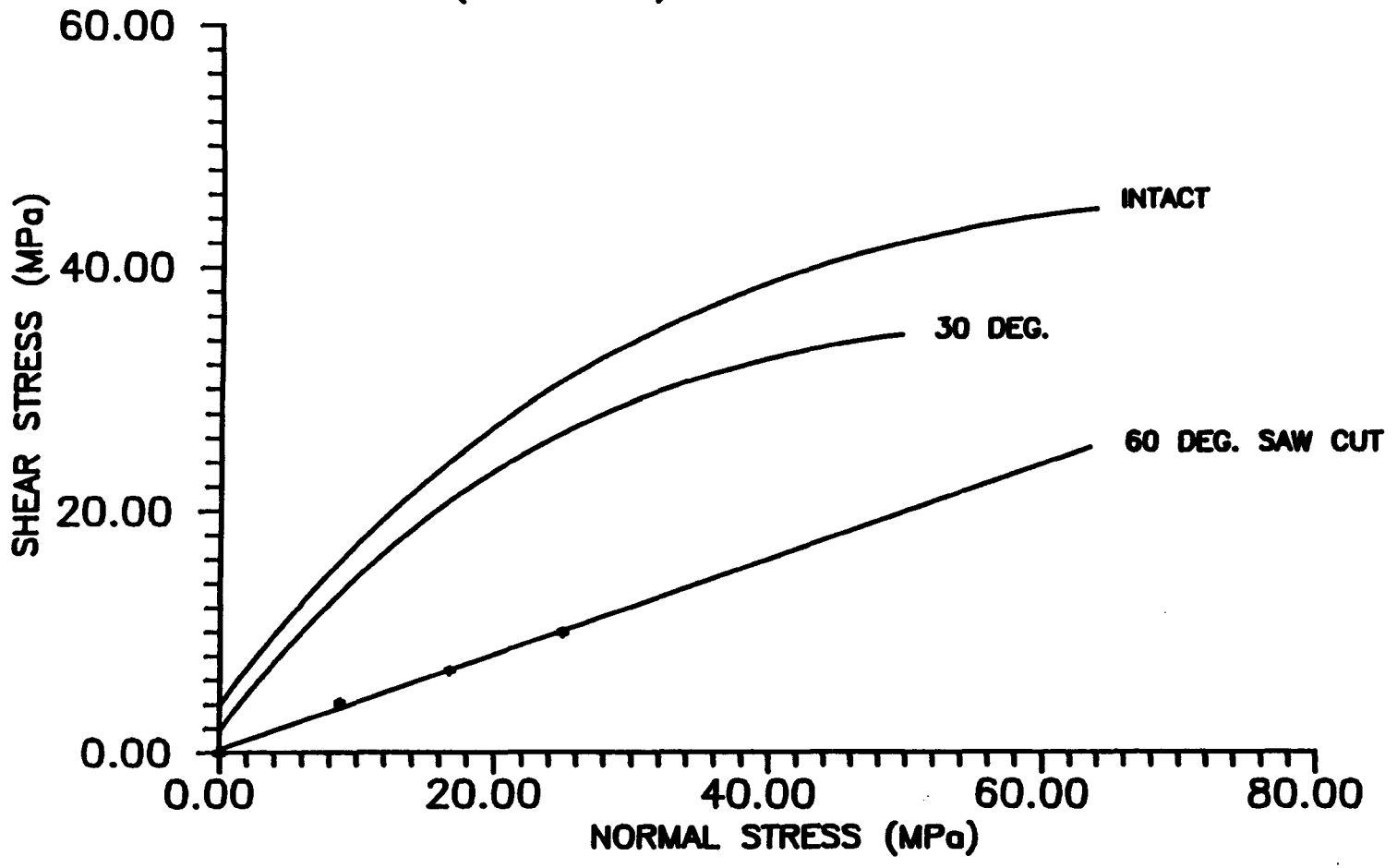

FIG. 6.36 TRIAXIAL SPECIMEN EQUILIBRIUM DURING SLIDING OVER THE JOINT PLANE.

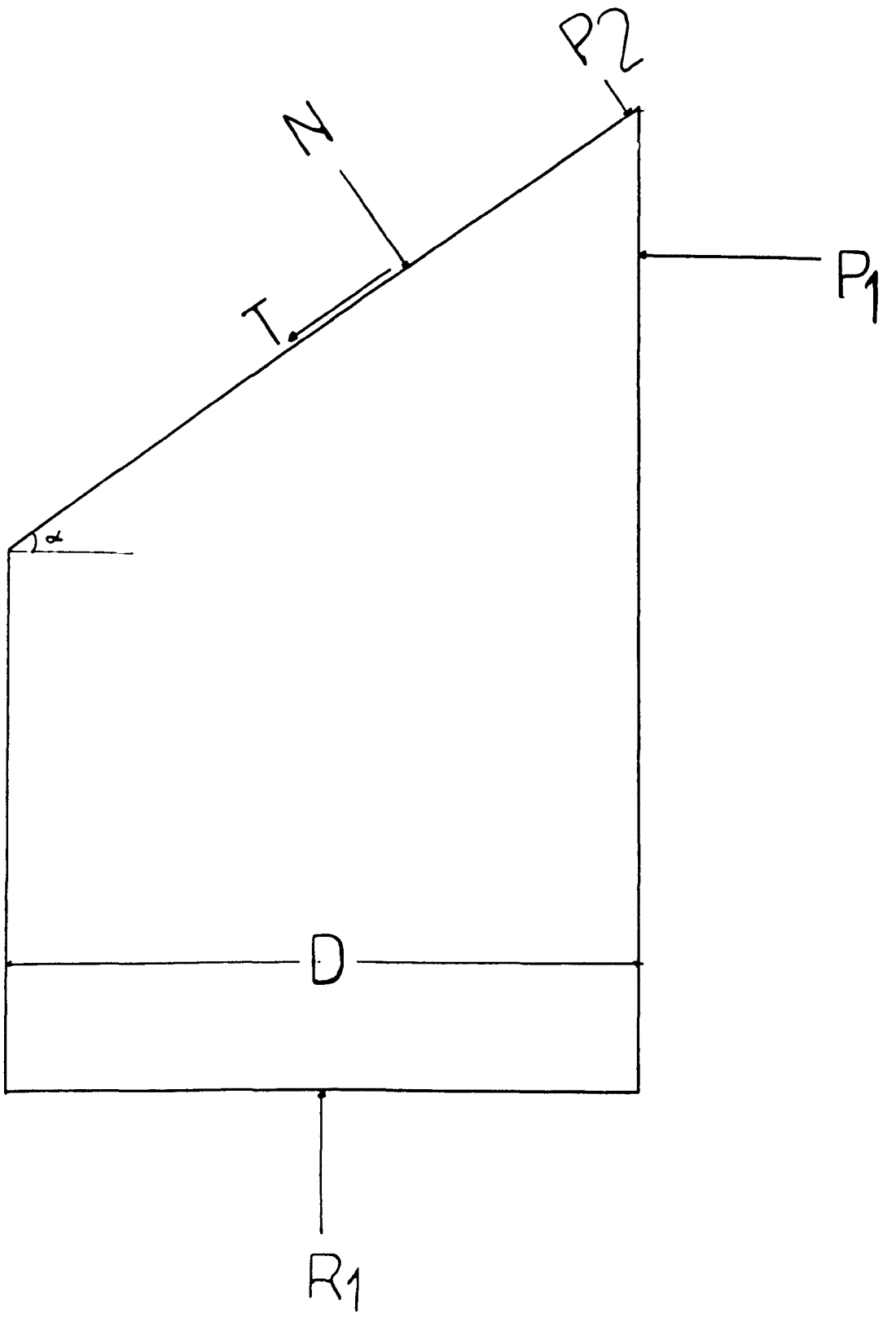

CHAPTER 7

TIME-DEPENDENT BEHAVIOUR OF JOINTED ROCK

7.1 INTRODUCTION

Time-dependent behaviour of discontinuities is important in many geotechnical applications: in rock slope stability for calculation and estimation of slope movements, study of earthquake mechanisms (time-dependent of stick-slips) and dynamic loading over short time periods (blast and seismic loads). Furthermore, it has been shown by Crawford and Curran (1982) that the rate effect is an important consideration in the design of engineering structures in jointed rock masses.

Strain rate effects on frictional behaviour of joints and faults have been of great interest to geophysicists and seismologists attempting to understand the mechanism and prediction of earthquakes. These studies have been mostly concentrated on the stick-slip characteristics and dependence of frictional sliding on the slip velocity. A detailed investigation is given in chapter 9.

There is a large number of research projects on the effect of strain or displacement rates on the axial stress-strain curves of intact specimens from laboratory compressive and tensile tests which have been mostly reviewed by Paterson (1978). Although the general agreement amongst workers is that the peak strength of rock specimens increases with increasing strain rates, there is not a uniform time-dependent characterization for different rock types in wide ranges of strain rates for different confining pressures.

The majority of the time-strain experiments have been carried out on intact specimens in uniaxial compression (Perkins et al, 1970; Houpert, 1979) and the general finding is

that uniaxial strength shows an increase of 5-10% over many orders of magnitude strain rate. Sangha and Dhir (1975) showed that for intact specimens increased confining pressure reduces the effects of straining and the relative strength-time relationship is independent of confining pressure.

Blanton (1981) showed that the apparent sudden increase in failure stress above a certain strain rate is due to machine inertia and does not reflect a real increase in material strength, and that the failure stresses of rocks tested were relatively insensitive to changes in strain rates in a certain range of strain rates. He summarized three types of observation with increasing rate of deformation:

(i) Either a constant strength or a constant rate of increase in strength;
(ii) A sudden increase in strength above a certain rate and
(iii) Apparent fluctuations in strength above a certain rate.

Recent investigations (Swan et al, 1989), however, in conjunction with mechanical properties of soft rocks such as shale, have shown rate effects of some significance upon shear resistance and strength as much as 40% for a 30-fold increase in strain rate.

The majority of the work on time-dependent frictional resistance in jointed rocks were conducted with high confinement (to study earthquake mechanisms) and only a few investigations have been undertaken at stress levels applicable to engineering structures (confining pressures or normal stresses up to 15 MPa). These experiments have been conducted mainly using the direct shear apparatus.

Schneider (1977) performed a direct shear test experiment on a weak clay rock (a shale with uniaxial strength of 3 MPa) to determine the time dependent behaviour of rock joints. The joints were established by a diamond saw cut parallel to the bedding. The

friction resistance was measured for each specimen at the same level of normal load, but in seven different shear displacement rates (1, 10, 100, 200, 1, 0.1 and 0.01 mm/min). He showed that in the tests with the same normal stress the frictional resistance is larger at higher shear rates. He concluded that the frictional resistance depends upon the normal stress and shear displacement rate.

Crawford and Curran (1981) conducted an investigation to determine the effects of the rate of shear displacement on the frictional resistance of rock discontinuities, using a direct shear test pertinent to this experiment. Four rock types were selected containing saw cut joints with various degrees of surface roughness under normal stresses up to 3 MPa.

They concluded that the frictional resistance of rock surfaces can be significantly influenced by the rate of shear displacement. The magnitude of the rate effect is dependent on the rock type and normal stress level.

At low normal stresses the soft material, dolomite, exhibited an increase in shear resistance up to a certain displacement rate after which it remained essentially constant. At higher normal stresses the resistance remained constant until it reaches the displacement rate at break point where upon it decreased.

For the granite specimen, of intermediate hardness, the frictional resistance was essentially independent of shear velocity, whereas for the hardest rocks, the syenite and sandstone specimens showed significant variations of shear resistance with rate of shear displacement.

7.2 EXPERIMENTAL PROGRAMME

An investigation was undertaken to determine the stress-strain behaviour of jointed rocks at various strain rates and at constant deformation in various stress conditions (stress relaxation). Three cases were considered:

(i) Gradually increasing compressive load at different constant strain rates;
(ii) Gradually increasing compressive load at changing strain rates;
(iii) Stress variations at a constant amount of displacement along the complete stress-strain curve for 5 minutes time duration (stress relaxation).

7.3 EXPERIMENTAL PROCEDURES

The equipment and techniques used in this study have been described in chapter 3. The tests were carried out triaxially on two types of sandstone (Penrith and Stainton sandstone) in the range of 0-30 MPa confining pressures. Both intact and jointed specimens with saw cut and split joints were tested. The jointed specimens contained joint in orientations of 30, 45 and 60^{o} to the minor principal stress.

7.4 GRADUALLY INCREASING COMPRESSIVE LOAD AT CONSTANT STRAIN RATES

7.4.1 STRESS AND DEFORMATION BEHAVIOUR

For the purpose of determining the effects of strain rate on the complete load-displacement curves of specimens containing a single joint, when subjected to gradually increasing compressive loading, a series of tests was conducted at constant strain rates

of 2.08 x 10^{-6} /s (slow rate), 4.17 x 10^{-5} /s (medium rate) and 8.33 x 10^{-4} /s (fast rate). The results are given in figures 7.1 to 7.8 for both Stainton and Penrith sandstone intact specimens.

It is observed from figure 7.1 that in zero confining pressure (uniaxial) a higher strain rate has resulted in a higher modulus of deformability (steeper positive slope before strength failure), and in a higher failure stress of the specimens. At 5, 10 and 15 MPa confinements (figures 7.2-7.4), however, one cannot observe the same trend as in unconfinement specimens (figure 7.1). Despite the increase of strain rate from slow to medium and then to fast rate, the modulus of deformability and failure stress have increased for 5 and 10 MPa confining pressures, but the differences in failure stresses at the medium and fast rates are not considerable, but are close. This is especially noticeable at 15 MPa confinement where peak stress is slightly higher at the medium rate than that of the fast rate. This behaviour may be attributed to:

(i) Effect of confining pressure which has decreased the strain rate effects and
(ii) The rate of change of strain rate.

Comparison of the three strain rates applied in this experiment shows that slow rate is 20 times slower than the medium rate, but 400 times slower than the fast rate, which is a very high range. Three points may be noted:

Firstly, a hundred order of magnitude changes in strain rate affects the mechanical characteristics of intact rocks being confined, rather than 10 order of magnitude.

Secondly, small changes in strain rate have no significant effects on the modulus of deformability and stress at failure of confined rocks.

Thirdly, Increased confining pressure decreases the strain rate effects.

Figures 7.5 to 7.8 illustrate the stress-strain plots of Stainton and Penrith sandstone specimens with saw cut joints and 30^{o} joint inclination under confining pressures of 0, 5, 10 and 15 MPa and applied strain rates of the slow and fast.

The effects of strain rate are much more pronounced than the intact Stainton sandstone specimens (figure 7.1 to 7.4), and there is a clear difference between two rocks at zero confinement. For Stainton sandstone specimens in zero confining pressure (figure 7.5 the lower plots) increase of strain rate from slow to fast has increased both the stress at failure and modulus of deformation; however, in figure 7.7 (lower plots) for Penrith sandstone specimens in zero confinement strain rate has been affected in a manner completely different from that of Stainton specimens for the same confining pressure. In Penrith sandstone specimens for both slow and fast rates (zero confining pressure) a considerable sliding movement has occurred along the joint plane, and also peak stress at the fast rate is less than that of the slow rate. In addition, the mechanism of deformation in Penrith sandstone specimens for both fast and slow rates is a combination of sliding over the joint plane and shear fracture through intact material, however, in Stainton sandstone specimens, particularly for fast rate, sliding over joint plane is not observed at all, but failure has occurred by shear fracture through intact rock. Information obtained from the petrological description of the thin section (appendix B) indicates that Penrith sandstone is a very hard and dense rock with a structure different from Stainton sandstone. It may therefore be concluded that type of rock plays a significant role in the strain rate effects in jointed rock particularly when the confining pressure is very low.

Change of strain rate seems to have the same effects on jointed Stainton and Penrith sandstone specimens with joint angle of 30^{o} in higher confining pressures, and the

effects on Penrith sandstone specimens are more pronounced than the Stainton sandstone specimens, particularly in 10 and 15 MPa confinements.

Increase in both peak stress and modules of deformation for both type of sandstone in 5 MPa confining pressure is significant when strain rate increases from slow to fast (figures 7.5 and 7.7 upper plots). In 10 and 15 MPa confining pressures, however, increase in both the stress at failure and modulus of deformability, because of change in strain rate (slow to fast), is not as much as 5 MPa for both sandstones, so that in Stainton sandstone specimens, it seems that strain rate effect has been diminished in these levels of confinements. It may be concluded that depending upon the type of jointed rock and increased confining pressure the effects of strain rate decrease significantly and become less important.

A most important observation in figures 7.5 to 7.8 is that the lower the strain rate (longer duration of loading), the flatter is the post peak region and this results in a further deformation at peak. This is a very significant finding as it indicates that the likelihood of violent failure of fractured jointed rock, if the strain rate increases- as may be found in yielding mine pillars left standing for a long period of time (Bieniawski, 1970)- will be less for the slower rate of straining.

The effects of strain rate on the stress-strain behaviour of jointed specimens in which mode of deformation is dominated by sliding through the joint plane are entirely different from the intact specimens, and of jointed specimens in which the mechanism of failure is similar to that of intact (for 30^{o} joint orientation, for instance).

Figures 7.9 and 7.10 illustrate the stress-strain curves of Stainton and Penrith sandstone specimens with saw cut joints inclined at 60^{o} in different confining pressures and strain rates. It is observed that change of strain rate (slow to fast) has resulted in a higher

stress at the onset of sliding for both rock types in confining pressures 5, 10 and 15 MPa. When sliding along the joint plane began, the behaviour seems to be different for change in confining pressure or rock type. In 5 MPa confinement in Stainton sandstone specimens (figure 7.9 lower plots) for slow strain rate, stress rose to a peak value, it then dropped to a residual level and after about 1% sliding along the joint plane, progressive sliding movement continued at a near constant stress level. The residual stress level is also higher than that of the fast strain rate curve.

In 15 MPa confining pressure, for the same rock (figure 7.9 upper plots), similar behaviour is observed for both fast and slow strain rates up to peak. However, as sliding movement progressed the stress level for slow rate continued in a level lower than the fast rate. Exactly the same behaviour is observed for slow and medium strain rates in Penrith sandstone specimens in 10 MPa confinement (figure 7.10 upper curves). In 5 MPa confinement, however, at slow and medium rates in Penrith sandstone specimens (figure 7.10 lower plots) sliding movement along the joint continued at nearly the same stress level for both rates.

As is observed from figures 7.9 and 7.10 the modulus of deformation was also affected significantly due to changes in the strain rate. For both rocks modulus of deformability has increased as strain rate increased (a steeper slope in faster rate plots) for different confining pressures applied in this experiment.

7.4.2 EFFECTS ON VOLUME CHANGE AND JOINT DEFORMATIONAL BEHAVIOUR

Effects of strain rate on sliding characteristics and deformational behaviour of jointed specimens in which sliding freely occurs along the joint surface are very pronounced. Figure 7.11 illustrates volumetric strain-axial strain curves for saw cut jointed Stainton

sandstone specimens at slow and fast rates and confining pressures 5 and 15 MPa. It is observed that increased strain rate has decreased the reduction in volume or increased strain rate has decreased the joint closure.A change of strain rate, for instance, from slow to fast for 5 MPa confinement has reduced the change in volume from average of 0.35% to 0.1% and for 15 MPa from 0.25% to 0.4%.

It may be concluded that a slower strain rate results in a further closure of the joint. This finding is important in the long-term behaviour of structures such as a dam constructed on a jointed rock mass in that whether it is built in a short or long period of time and also whether it is loaded at a fast or slow rate (such as a sudden flow of water to the dam because of high rainfall) this may lead to subsidence beneath the dam.

As is observed in figure 7.11 increased confining pressure has decreased the difference in volumetric strain between two slow and fast rates from the average of 0.25 (.35 - .1= .25) to 0.15 (.4 - .25= .15), namely about 40% ((0.25 - 0.15)/ .25X 100= 40%) reduction.

Comparison of the plots in figure 7.11 shows a distinct difference between the curves corresponding to the slow rate with those of the fast rate. A peak value is observed in the slow rate plots for both 5 and 15 MPa confinements which is related to a slight relative increase in volume, or in fact slight dilation of the joint at that point. In the plots corresponding to the fast rate, however, a relative expansion (increase in volume) is not observed at all, but there is a uniform reduction in volume throughout the test.

As noted in chapter 6 the fluctuations in asymptotic part of the curves such as those in figure 7.11 are due to errors in reading the oil level in the graded cylinder and not a relative expansion and contraction in the specimen volume.

Strain rate also affected the instantaneous Poisson's ratio significantly. As is observed in figure 7.12 the faster strain rate has resulted in a higher Poisson's ratio. Increased confining pressure has decreased the strain rate effect, so that instantaneous Poisson's ratio has decreased to a lower magnitude both at fast and slow rates due to increase in confining pressure from 5 to 15 MPa.

An interesting point in figure 7.12 is that the instantaneous Poisson's ratio for both 5 and 15 MPa confinements in slow strain rate plots dropped to a lower level, then it increased again and continued asymptotically. This discrepancy is better seen in figures 7.14 and 7.15 which show the axial stress-Poisson's ratio plots for both 5 and 15 MPa confining pressures. There is no similar observation, however, in the fast strain rate plots in any of the figures 7.12, 7.14 and 7.15.

This behaviour indicates that for slow rate at a certain interval of axial strain or axial stress which is at the onset of sliding over the joint surface, the rate of change of axial strain has become more than the rate of change of lateral strain (taking into account that instantaneous Poisson's ratio = $\varepsilon_2 / \varepsilon_1$). This is due to the fact that at the initiation of sliding a slight dilation occurred and caused the percentage increase in axial strain (because of normal displacement of the joint) to become more than the percentage increase in lateral strain. For fast strain rate, because of a lower degree of interlocking asperities, there is no dilation in the onset of sliding. For this reason a peak stress is not observed either in the stress-strain plots of the fast rate for both 5 and 15 MPa confinements (figures 7.9 plots of 5F and 15F).

Effects of strain rate are very pronounced as in figures 7.13 and 7.16. In figure 7.13 which indicates the axial strain-lateral strain of Stainton sandstone jointed specimens with 60^o inclination, it is observed that at a certain amount of axial strain (at 2%, for instance, on X axis) the corresponding lateral strain for fast rate is higher than the slow

rate for both 5 and 15 MPa confining pressures. Increased confinement has reduced this effect. In figure 7.16 (axial stress-lateral strain plots) which shows clearly the variation of the lateral strain from the beginning of loading, it is observed that the lateral strain has increased when strain rate has changed from slow to fast. The increase for lower confining pressure(5 MPa) is more than that of higher confinement (15MPa) at a certain level of stress (at 5 MPa axial stress, for instance, as in figure 7.16)

Influence of strain rate on the deformational behaviour and frictional resistance of rock joints may be ascribed to the fact that change of strain rate causes the real area of asperity contacts to change. Teufel and Logan (1978) showed that with a decrease in the displacement rate from 10^{-2} to 10^{-6} cm/s the real area of contact increased from about 5 to 14% of the apparent area. This behaviour affects both sliding resistance and deformational characteristics of rock joints. In fact, as the strain rate decreases, further interlocking asperities will results. It is for this reason that in figure 7.9 and 7.10 a change in the strain rate from slow to medium (figure 7.9) and from slow to fast (figure 7.10) sliding stress has decreased to a lower level in the beginning of sliding, and in fact because of reduction in interlocking asperities (due to decrease in real contact area) occurrence of peak stress has disappeared in both 5 and 15 MPa confining pressures in the plots corresponding to the fast rate (figure 7.9), and also in figures 7.11 to 7.13, for the same reason, the deformational characteristics of jointed specimens have been affected. It is clearly observed in figure 7.11, for instance, that when strain rate has changed to a fast rate, due to reduction in interlocking asperities (or reduction in real contact area over the joint surface) the damage in sliding surfaces has reduced. This means that the joint closure has decreased and therefore, reduction in the volumetric strain has become less than that of slow rate.

Because of a further asperity damage in continuation of sliding when a slow strain rate is applied the amount of gouge material over sliding surfaces increases considerably

more than that of the fast rate. This behaviour becomes more significant in higher confining pressures. The gouge material in this case acts as a layer of filling material which reduces the sliding resistance to a level lower than the fast rate as observed in the upper plots (15S and 15F) for 15 MPa confinement in figure 7.9. This behaviour is, of course, affected by other factors such as type of rock and the orders of magnitude increase or decrease in strain rate. For this reason the same trend for Penrith sandstone (figure 7.9 upper plots for 10 MPa confinement), which is much harder than the Stainton sandstone (figure 7.9) is not observed.

7.5 GRADUALLY INCREASING COMPRESSIVE LOAD AT CHANGING STRAIN RATES

To examine the response of jointed rock to a sudden change in strain rate, a series of tests was conducted on jointed specimens of Penrith sandstone and Stainton sandstone containing both a single saw cut and split breakage joints with inclinations of 30, 45 and 60°. Confining pressures 15 and 30 MPa were applied and three different strain rates (slow, medium and fast) as in section 7.4.1 were applied.

The significance of this investigation is evident in mining applications where the stoping operations may, in the case of pillars, cause redistribution of the load over the pillars such that these may be subjected to increasing or decreasing rates of strain (Bieniawski, 1970).

Loading the specimens started at a constant strain rate and continued at an arbitrarily chosen interval along the stress-strain curve; then the strain rate was changed to another magnitude and kept constant at another arbitrary interval. These events, using the three different strain rates, were repeated at various points throughout the stress-strain curves.

The complete stress-strain plots illustrating the results of this study are given in figures 7.17 to 7.22 from which the following observations are made:

Figures 7.17 and 7.18 show the stress-strain plots of Stainton and Penrith sandstone specimens containing split breakage (figure 7.17) and saw cut (figure 7.18) joints with 30° orientation (with respect to the minor principal stress). In this orientation mode of failure is dominated by shear fracture through intact material and is different from the 45 and 60° orientations which mechanism of deformation is dominated by sliding over the joint plane. Change of strain rate from slow to fast in the linear part of the curve before yield point (at point A in the lower graph in 7.17) has no significant effect on the stress and deformational behaviour of the specimen. However, a change of strain rate from fast to slow near to peak (point C) has reduced the peak stress to a lower level and the curve in this region has become flatter with respect to the middle curve (N15 in figure 7.17) in which a constant strain rate is used throughout the test. This implies that change of strain rate from fast to slow has decreased the stress at peak and resulted in a further deformation and flattening of the curve at the peak and therefore increased stability after strength failure. Furthermore, although in a part of the curve a fast strain rate has been applied (at point B) the peak stress is lower than that of the curve (the middle curve in figure 7.17) in which a constant strain rate has been applied throughout the test.

A similar behaviour is observed for 30 MPa confining pressure as in the upper plot in figure 7.17. Change of strain rate from fast to slow after yield point (at E) has resulted in changing the slope of the curve considerably, then changing from slow to fast (at point F) a higher stress has been resulted. It may be concluded that in jointed fractured rock containing joints with inclination 0 to 40° in which sliding is not the predominant mode of failure, because of change of strain rate, modulus of deformability changes, i.e. decrease of strain rate decreases modulus of deformation in the region after yield point.

In figure 7.18 the response is similar to the results shown in figure 7.17, i.e.: for the 15 MPa confining pressure (change of strain rate from slow to medium) and for 30 MPa (change of strain rate from medium to slow and subsequently from slow to medium) there has been no effect on the stress-strain behaviour of the specimens. However, for those exceed the yield point (195 MPa and 290 MPa in plots 15T and 30T respectively) change in strain rate (from medium to fast in plot 15T and from medium to slow in plot 30T) resulted in significant effect on the peak stress. It may be concluded that:

(i) Change of strain rate has no significant effect on the stress-strain characteristics of the specimens before yield point (for 30^{o} orientation). This finding is in agreement with the work of Peng and Podnieks (1972) on intact specimens where there is similarity in the mode of failure with the joint specimens with orientations of $0\text{-}40^{o}$.

(ii) Change of strain rate influences the stress and deformability of the specimens after yield point if the strain rate changes in a high order of magnitude (hundred orders of magnitude, i.e. slow to fast and not slow to medium).

(iii) Change of strain rate with any order of magnitude (slow to medium and or fast) in the peak region affects the peak stress and the corresponding strain (figure 7.18 points C and G) and the stability of rock increases after strength failure, because of the flattening of the curve at peak and decrease in the slope of the curve after peak, if the strain rate decreases suddenly .

Figure 7.19 illustrates stress-strain plots of Penrith sandstone specimens with a split breakage joint and 45^{o} inclination. The same confining pressure (15 MPa) has been applied for both tests, but one test (plot no. 15) was loaded at a constant strain rate (medium rate) throughout the test and the other (15T) was first loaded at the slow rate up to failure (from A to B), then strain rate was changed to the fast rate (at B). Comparison of two plots reveals that despite the fact that for the two tests the same

conditions were applied (the same joint orientation and confinement), because of change of strain rate, stress-strain characteristics were affected significantly. As is observed in figure 7.19 the slow strain rate (plot 15T from A to B) increased the first peak stress (with respect to the first peak in plot 15 in which a medium strain rate was applied throughout the test), and the fast strain rate (from C to B in plot 15T) has decreased the second peak stress (with respect to the second peak in plot 15). It may be concluded that decrease in the strain rate increases the sliding resistance of jointed rocks, or increase in the strain rate decreases the frictional sliding of jointed rocks.

This behaviour, as was discussed in the previous section, may be attributed to the fact that when the sliding velocity decreases the time for interlocking asperities increases. This results in a situation corresponding to an increase in the real contact area associated with an increase in interlocking of asperities leading to further frictional resistance. Inversely, when the strain rate increases to a faster rate, due to an increase in sliding velocity, interlocking of the asperities is reduced resulting in a decrease in frictional resistance.

Figure 7.20 illustrates stress-strain plots of Penrith sandstone specimens containing a split breakage joint with 45^{o} orientation. A change of strain rate from the fast to the slow rates at B has increased the stress path to an upper level, then with change in strain rate from the slow to the fast rates at C, stress has dropped to a lower level.

In figure 7.21 which illustrates the stress-strain plots of Penrith sandstone specimens with split joints inclined at 60^{o}, one of the test was performed at a constant medium strain rate (upper curve N30) throughout the test, and the second one at various strain rates in different points on the stress-strain curve. A confining pressure of 30 MPa was applied for both tests. Change of strain rate from medium to fast (at B) has no significant affect on the stress-strain behaviour of the specimen in this part (i.e. before

peak stress), however, in comparison with the upper curve (N30) the peak stress has dropped significantly. Figure 7.19 shows that decrease in strain rate has increased the peak stress. Inversely, in figure 7.21 increase in strain rate has resulted in a decrease in peak stress. Again, with a change in strain rate from fast to slow at C, the slope has increased considerably, i.e sliding resistance has increased in this part of the curve. However, change of strain rate at point E from fast to medium and then at F from medium to slow variation in stress level is not very significant. It is concluded that when sliding continues, because of further asperities damage and producing further gouge, the effect of strain rate becomes less important.

When the joint surface roughness is very low (saw cut joint) the effect of changing strain rate is also less significant, as in figure 7.22 in which saw cut joint specimens with 60^{o} orientations under 15 and 30 MPa confining pressures have been loaded at various strain rates and different points along the stress-strain curve. Change of strain rate in lower plot from slow to medium at B and then at C from medium to fast has no significant effect on the stress-strain characteristics. The same behaviour for 30 MPa confinement is also observed in the upper curve, however, at G because of change of strain rate from fast to slow and then at H from slow to fast rate, the change in slope of the curve at G and H is considerable. In fact, when the surface roughness is low a very high change in strain rate (i.e. hundred orders of magnitude) affects the stress-strain behaviour significantly.

7.6 STRESS VARIATIONS AT CONSTANT DISPLACEMENTS ALONG THE COMPLETE LOAD-DISPLACEMENT CURVE (STRESS RELAXATION)

Rate of reduction of the stress within a stressed body during a certain period of time has been termed "stress relaxation". During a relaxation test the displacement at a point is held constant, therefore, stress relaxation test may be interpreted as a particular case of

strain rate effect on the stress-strain characteristics of rock when the external strain rate is zero.

To study the phenomenon of relaxation the specimens of Penrith sandstone were held at constant deformation for 5 minutes at chosen arbitrary points along the complete stress-strain curves. The tests were performed on intact and jointed specimens for both saw cut and split joints with 30, 45 and 60^{o} orientations and confining pressures of 15 and 30 MPa. The stress-strain plots obtained are given in figures 7.23 to 7.25. As is observed in figure 7.23 there is almost no stress drop at the points selected below the elastic limit in both curves for intact specimens under both 15 and 30 MPa confinements. A small reduction may be attributed to the growth of microcracks in the specimens. Stress relaxation has started significantly at the points selected above the elastic limit (yield point) and increased after peak. For subsequent points in the post failure region the same behaviour is observed and in the residual region the stress relaxation seems to be constant at different points. It may be concluded that in intact rock, stress relaxation is initiated at the yield point and accelerated after peak because of development of cracks through the rock. Increased confining pressure seems to have decreased the amount of stress drop in comparison with the lower confinement.

In jointed specimens stress relaxation behaviour seems to depend upon different factors such as joint orientation, surface roughness and rock type. In figure 7.23 plot N15 corresponds to a jointed specimen with a split breakage joint in 30^{o} orientation. Although a considerable sliding movement over the joint plane for this joint orientation is not possible and failure occurs by shear fracture plane transcending the joint plane, the stress relaxation in the points selected below the elastic limit is considerable (in comparison with the upper plots for intact specimens).

Stress relaxation in other type of joints different in orientation and surface roughness behaved differently. Figures 7.24 and 7.25 illustrate the stress-strain curves of jointed specimens with 45 and 60° orientations for both saw cut and split joints. The most interesting aspects of these plots are:

(i) As the joint inclination increased the stress relaxation increased for both saw cut and split joints. That is, the magnitude of stress drops along the curve corresponding to 60° are greater than those of 45° at similar points.

(ii) Relaxation in the specimens containing saw cut joint is higher than that of split joint for both 45 and 60° orientations up to the peak stress. In fact, when the degree of interlocking asperities increases the stress drop decreases up to the peak stress (in split breakage joint).

(iii) Increased confining pressure has decreased the stress relaxation. This may be due to the fact that higher confinement gives rise to the further limitation in the growth of cracks both in intact and jointed specimens (through the asperities).

(iv) Comparing the saw cut and split joint plots reveals that in a saw cut joint, from the beginning of loading, stress relaxation at the selected points is observed and increases up to the peak and in the sliding region it remains nearly constant (figure 7.24 plots 15 and 30 and figure 7.25 plots 15r and 30r).

(v) In all cases, whether in intact or jointed specimens, the stress drop in each point of relaxation reaches a value that remain nearly constant after a certain relaxation time, and in fact the rock eventually attains stability under this new condition. By connecting the lowest point of stress drops of all the selected points along the curve, a plot is

obtained which represents the long-term stability of the jointed specimen. An example is given in figure 7.26.

Stress relaxation in intact rock has been attributed to the initiation of cracks which is started at a stress above the elastic limit and the magnitude of stress drop is proportional to the crack surface (Peng, 1972).

In jointed rock the behaviour of stress relaxation seems to be completely different from the intact rock. It may be ascribed to the deformational behaviour of joint asperities. As loading is initiated in a jointed specimen and stress rises, the asperities begin to interlock. When the displacement is held constant at a selected point along the stress-strain plot, due to the shear displacement of the joint at first the tips of asperities start to deform. Depend upon the stress level at which displacement is kept constant and the degree of surface roughness, the drop in stress varies. For this reason in saw cut joint (figure 7.25 plots 15R and 30R) in which interlocking asperities are low, even at low stress level, stress drop is higher than the split breakage joint (figure 7.25 plot N15). If the point for relaxation is selected at a higher stress level the asperities deform further and therefore, a further drop in stress is observed. This process is continued until a sliding movement along the joint surface is initiated. This leads to the failure of the asperities which is accompanied by a high drop in stress at the points selected in this region and the maximum drops in stress due to relaxation occur in this part.

A close distinction must be made between the stress relaxation in low surface asperity joints (such as saw cut) and that of high surface asperity joints (such as split breakage joints). In smooth surface joints the amount of stress drop, because of relaxation, in the different selected points along the complete stress-strain curves does not change greatly. As is observed in figure 7.25 for both 15 and 30 MPa confining pressures in the saw cut joint with 60^{o} orientation, the difference in stress drops for the various points selected

for relaxation are not too high, particularly after a little sliding over the joint the difference becomes less significant. However, in rough joints and also in intact specimens as much as stress is increased and reaches the maximum level and mainly after peak stress, the difference in stress drops in the selected points for relaxation is increased significantly. As is observed in figure 7.25 (plot N15) the stress drop at the point after peak is much higher than at the other points. The same trend for intact specimens is observed as in figure 7.23.

It may be concluded that in jointed rocks with a low level of surface roughness stress relaxation is less significant, and that in jointed rocks with a high level of surface roughness and also in intact rock, provided that the stress level has not reached its maximum, stress relaxation is less significant. In this case, if sliding is initiated in jointed rocks along the joint plane (at or after peak stress), stress relaxation has significant effects on the long-term behaviour of the jointed rock, and a significant effect on the stability of the structure being established in or on the jointed rock mass.

In addition, in a split joint (which has a rough surface) stress relaxation at the points after peak stress, i.e. when sliding continues over the joint, a drop in stress from one point to another point varies and it has a decreasing order of magnitude with continuation of sliding until the rough asperities are shear off completely. Thereafter, the stress drops remain nearly constant in the same manner as in smooth joints.

A limited number of research work at low stress levels have been performed on stress relaxation behaviour of intact rock in uniaxial testing condition by peng and Podnieks (1972) Peng (1973), Hudson (1971) and Bieniawski (1971), and their results are in agreement with this study with respect to intact specimens.

7.7 EFFECTS OF TIME AND LOADING CONDITIONS ON THE MODE OF DEFORMATION

Plates 7.1 to 7.13 illustrate the fractured intact and jointed specimens under various loading and straining conditions. It seems that strain rate has a significant effect on the modes of failure of both the intact and jointed specimens. At the faster strain rates (medium and fast) a shear fracture plane particularly in higher confining pressures (5 to 15 MPa) is clearly observed (plates 7.1, 7.3 and 7.6). As the strain rate decreased to the slow rate, despite the fact that a shear fracture plane is observed in the specimens, it seems that the shear plane is not as planar as fast and medium rates, and the number of secondary fractures is also considerably greater than that of the faster rates (plate 7.2 and 7.8).

In jointed specimens the effect of strain rate and loading conditions was found to be different from the intact specimens. For those specimens in which the mode of failure is dominated by sliding along the joint plane, strain rate has no effect on the mode of sliding especially for 60^{o} orientation (see chapter 4 plate 4.6 for modified system).

As the joint orientation was decreased to less than 40^{o}, namely when the mode of failure is not dominated purely by sliding over joint plane, but by a new shear fracture through intact material, the effect of the strain rate on the mode of failure is more pronounced. As plates 7.4, 7.5, 7.7 and 7.9 show at the fast strain rate a complete shear fracture plane, even at zero confinement (plate 7.4 the first specimen from left), is observed and the number of secondary fractures is very little, particularly at higher confining pressure (15 MPa). Inversely, at the slow strain rate in some cases, the shear plane is not clearly observed (plate 7.7 specimen no. 2 from left) and the number of secondary fractures is more than that of the fast rate.

The loading and straining conditions such as load cycling (increasing and decreasing load during a test at various points along the complete stress-strain plot), stress relaxation and variable strain rate at different points of the plot affect the mode of failure in both jointed and intact specimens significantly. These are observed in plates 7.9 to 7.13.

Difference in mode of failure at different strain rates in intact specimens has been attributed to the influence of lateral strain. At quicker rates of straining there is little time for the lateral strain to cause extensive damage of the rock material (Sangha and Dhir, 1972). It seems two factors have significant roles for the strain rate effects on mode of failure:

(i) At a quicker strain rate the time for dissipation of strain energy through the specimen is very low with respect to the slow rate and therefore, the rate of damage is reduced considerably. This behaviour is true in both jointed and intact specimens.

(ii) In jointed specimens in addition to (i), when sliding along the joint is not predominant the relative sliding movement over the joint at a slow strain rate is higher than that of a fast rate (compare the slow and fast rate plots in figure 7.5). This behaviour causes a further dislocation of the two halves of the specimens in a slow strain rate and therefore, a discrepancy in the modes of deformation.

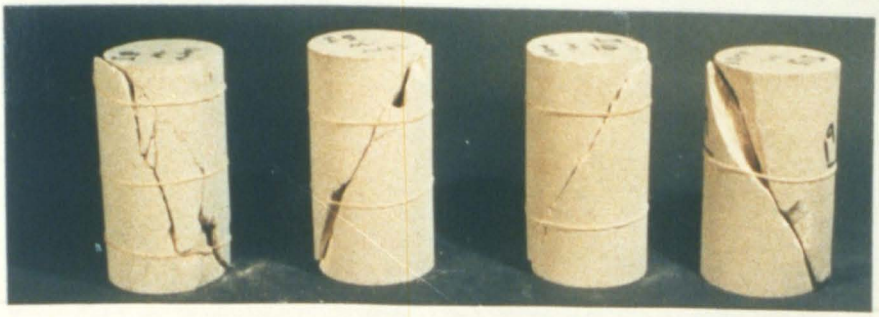

Plate 7.1 Fractured and deformed unjointed SS specimens, strain rate= 4.16×10^{-6}/s, confining pressure, left to right, 0, 5, 10, & 15 MPa.

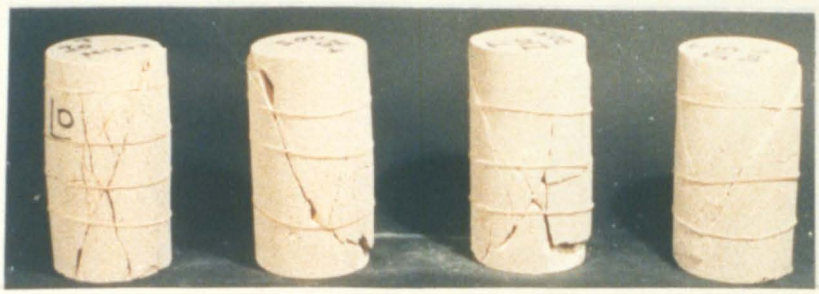

Plate 7.2 Fractured and deformed unjointed SS specimens, strain rate= 2.08×10^{-6}/s, confining pressure, left to right, 0, 5, 10 & 15 MPa.

Plate 7.3 Fractured and deformed unjointed SS specimens, strain rate= 8.33×10^{-4}/s, confining pressure, left to right, 0, 5, 10 & 15 MPa.

Plate 7.4 Fractured and deformed SS specimens, joint angle= 30°, strain rate= 8.33×10^{-4}/s, confining pressure, left to right, 0, 5, 10 & 15 MPa.

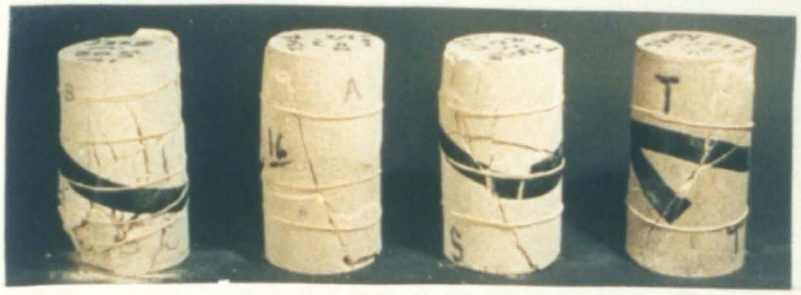

Plate 7.5 Fractured and deformed SS specimens, joint angle= 30°, strain rate= 2.08×10^{-6}/s, confining pressure, left to right, 0, 5, 10 & 15 MPa.

Plate 7.6 Fractured and deformed unjointed PS specimens, strain rate= 4.16×10^{-5}/s, confining pressre, left to right, 0, 5, 10 & 15 MPa.

Plate 7.7 Fractured and deformed jointed PS specimens, strain rate= 2.08×10^{-6}/s, confining pressure, left to right, 0, 5, 10 & 15 MPa. Joint angle = 30°

Plate 7.8 Fractured and deformed unjointed PS specimens, strain rate= 2.08×10^{-6}/s, confining pressure, left to right, 0, 5, 10 & 15 MPa.

Plate 7.9 Fractured and deformed PS specimens, joint angle= 30°, strain rate= 8.33 X 10^{-4} 1/s, confining pressure, left to right, 0, 5, 10 & 15 MPa.

Plate 7.10 Fractured and deformed PS specimens under different loading conditions, joint angle= 30°, type of loading: relaxation (no. 1) and cyclic loading (the rest), type of joint, left to right: saw cut (1 & 2 & 3) and natural (4 & 5), confining pressure, 15, 15, 30, 15 & 30 MPa.

Plate 7.11 Fractured and deformed PS specimens under different loading conditions, joint angle and type of joint, left to right: intact (1 & 2); 30°, saw cut (3 & 4); 30°, natural (5), type of loading: relaxation, confining pressure: 15, 30, 15, 30 & 30 MPa.

PLate 7.12 Fractured and deformed PS specimens under different loading and straining conditions, joint angle= 45°, type of joint, left to right: natural (1 & 2) and saw cut (3 & 4), type of loading and straining: relaxation, constant strain and loading rates, cyclic loading, different strain rates (slow to fast); confining pressure, 15, 30, 30, & 15 MPa.

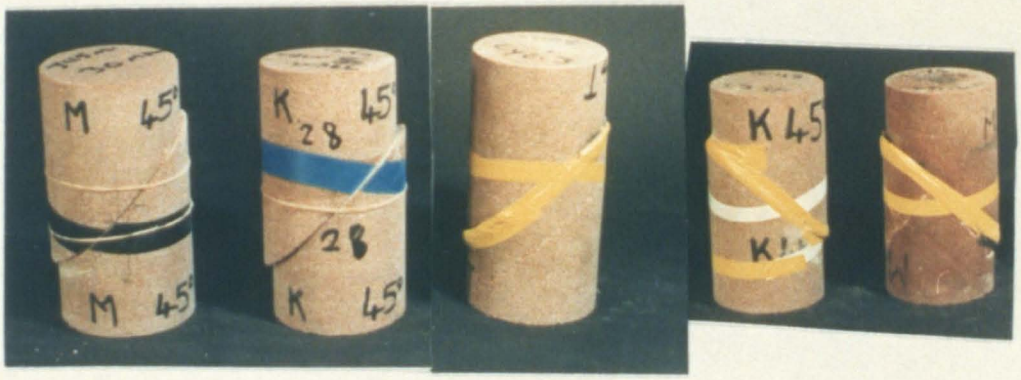

Plate 7.13 Sliding and deforming of PS specimens under different loading and straining conditions, joint angle= 45°, type of joint: left to right, saw cut (1 & 2) and natural (3 & 4 & 5); type of loading and straining: constant strain and loading rate, cyclic loading, different strain rates (fast to slow); confining pressure, 30, 30, 30, 15 & 30 MPa.

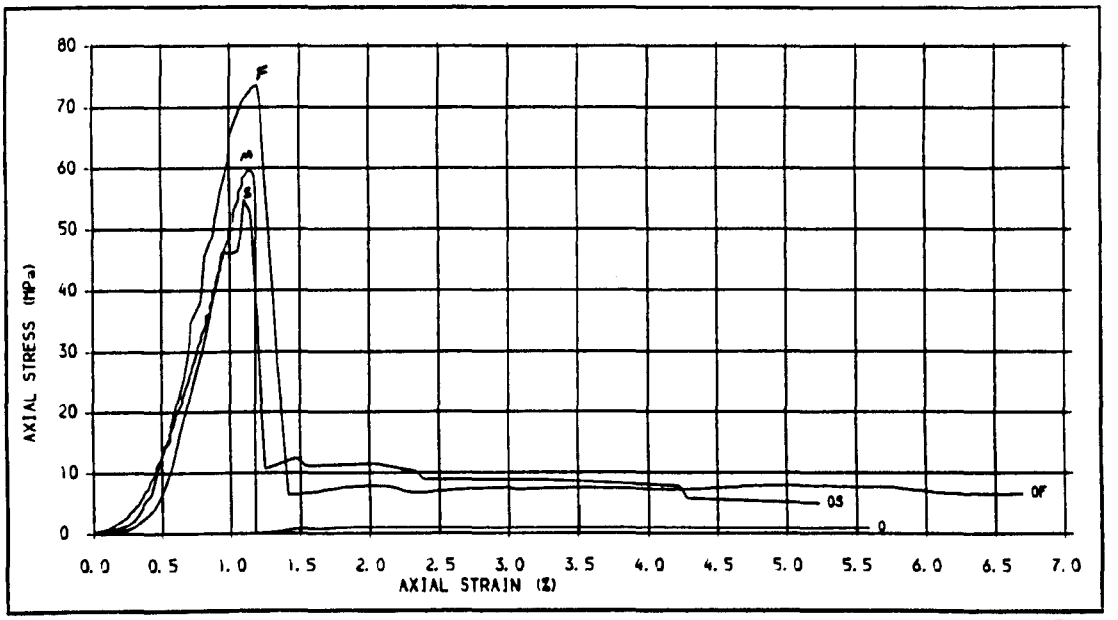

Fig. 71 . STRESS-STRAIN PLOTS FOR INTACT SS SPECIMENS, STRAIN RATES. SLOW (S), MEDIUM (M) AND FAST (F), CONFINING PRESSURE = 0

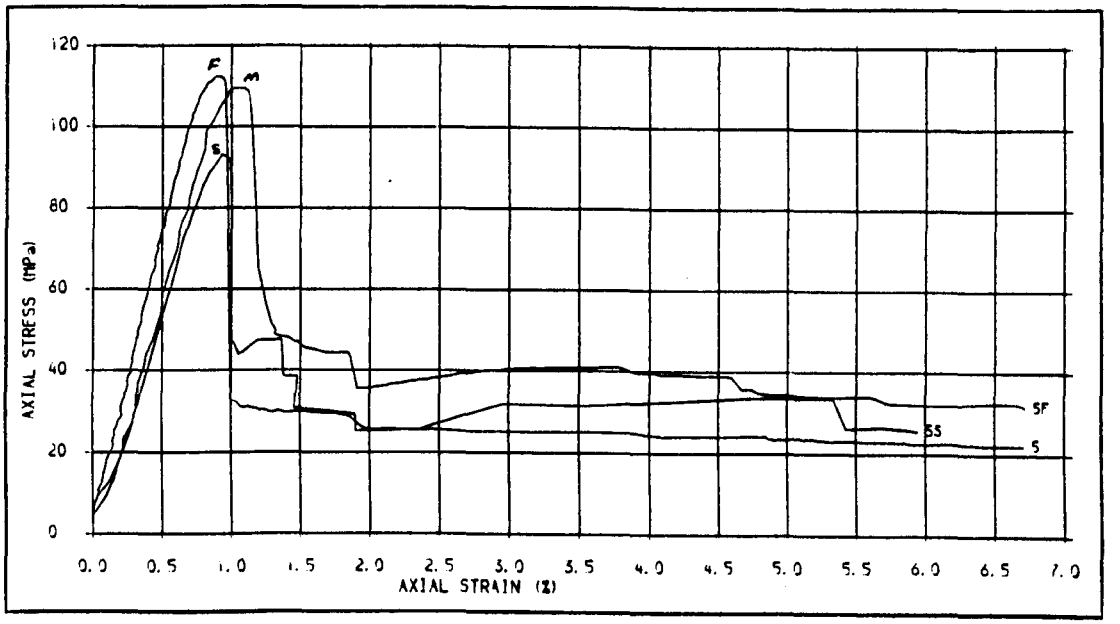

Fig. 72 . STRESS-STRAIN PLOTS FOR INTACT SS SPECIMENS, STRAIN RATES. SLOW, MEDIUM AND FAST CONFINING PRESSURE = 5 MPa

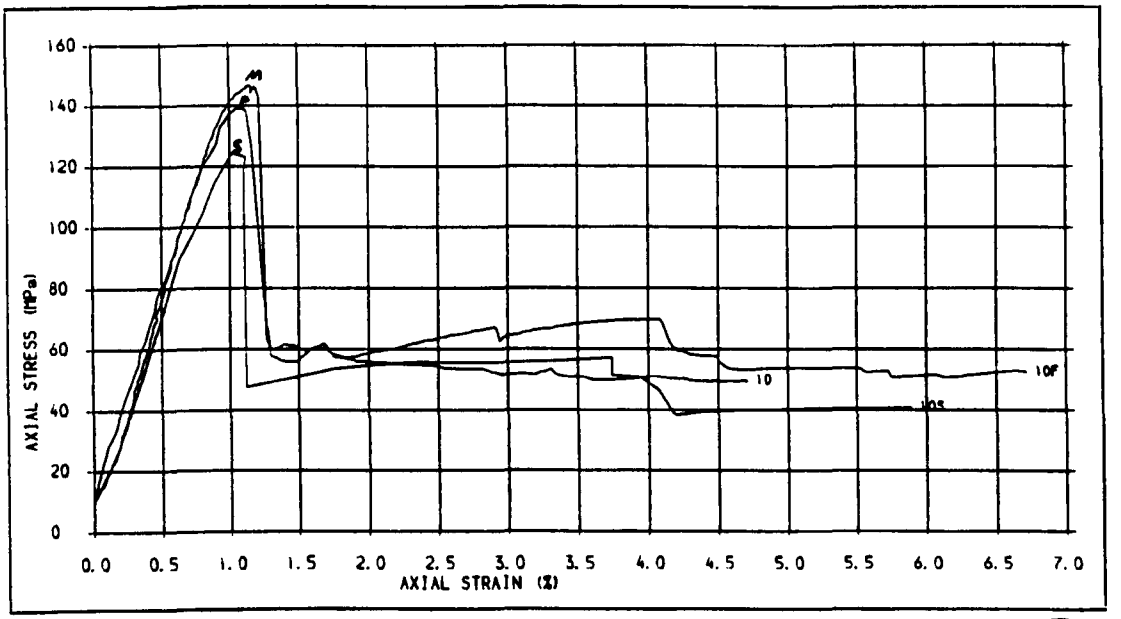

Fig. 23 . STRESS-STRAIN CURVES FOR INTACT SS SPECIMENS, STRAIN RATES. SLOW, MEDIUM AND FAST, CONFINING PRESSURE = 10 MPa

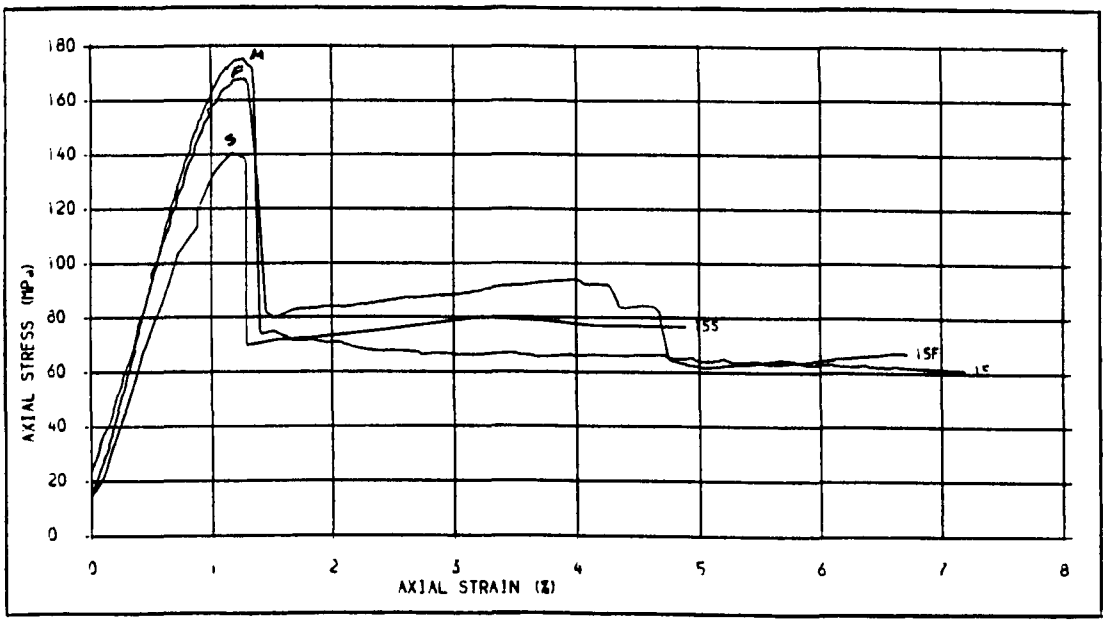

Fig. 24 . STRESS-STRAIN PLOTS FOR INTACT SS SPECIMENS, STRAIN RATES. SLOW, MEDIUM AND FAST CONFINING PRESSURE = 15 MPa

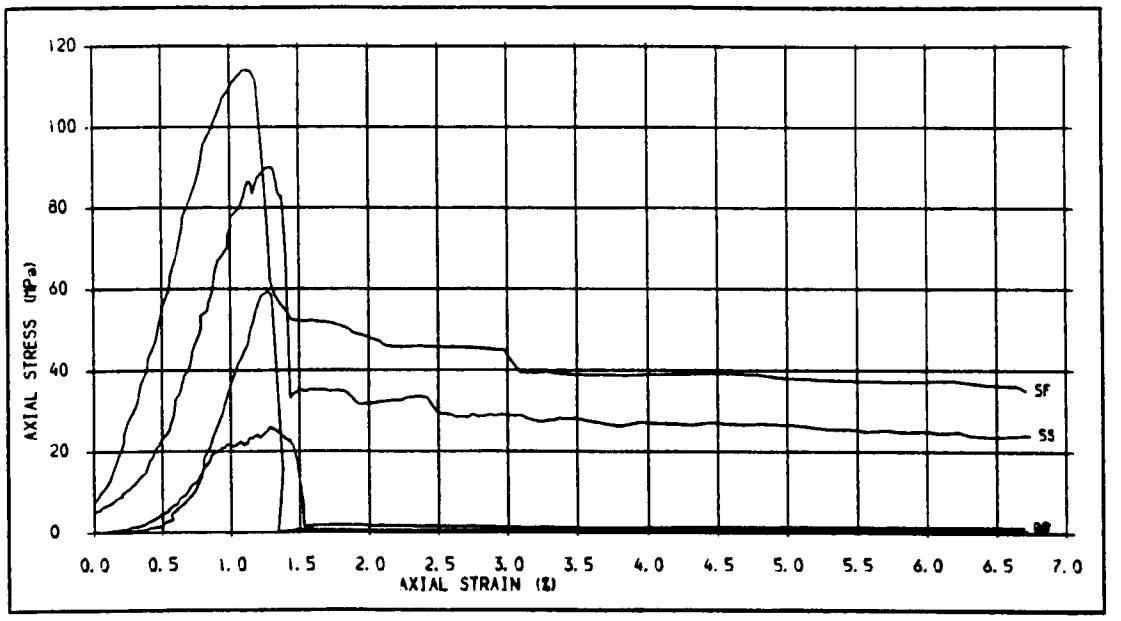

Fig. 25 . STRESS-STRAIN PLOTS FOR SS SPECIMENS, STRAIN RATES. SLOW AND FAST
JOINT ANGLE = 30 DEG., CONFINING PRESSURES = 0 AND 5 MPa.

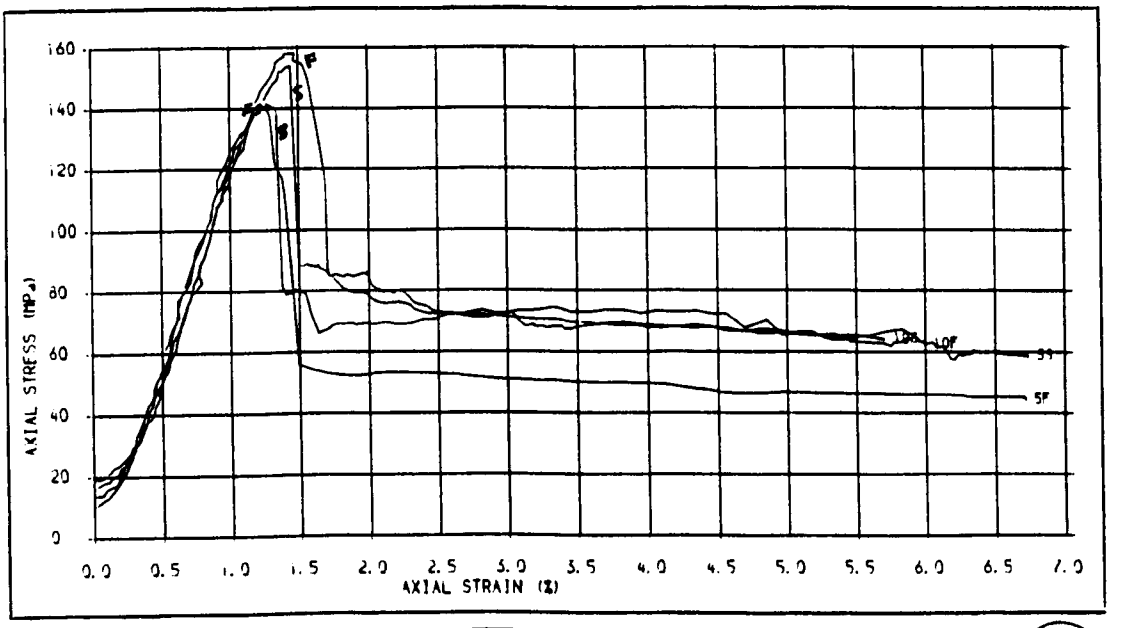

Fig. 26 . STRESS-STRAIN PLOTS FOR SS SPECIMENS. STRAIN RATES. SLOW AND FAST JOINT
ANGLE = 30 DEG. CONFINING PRESSURES = 10 AND 15 MPa.

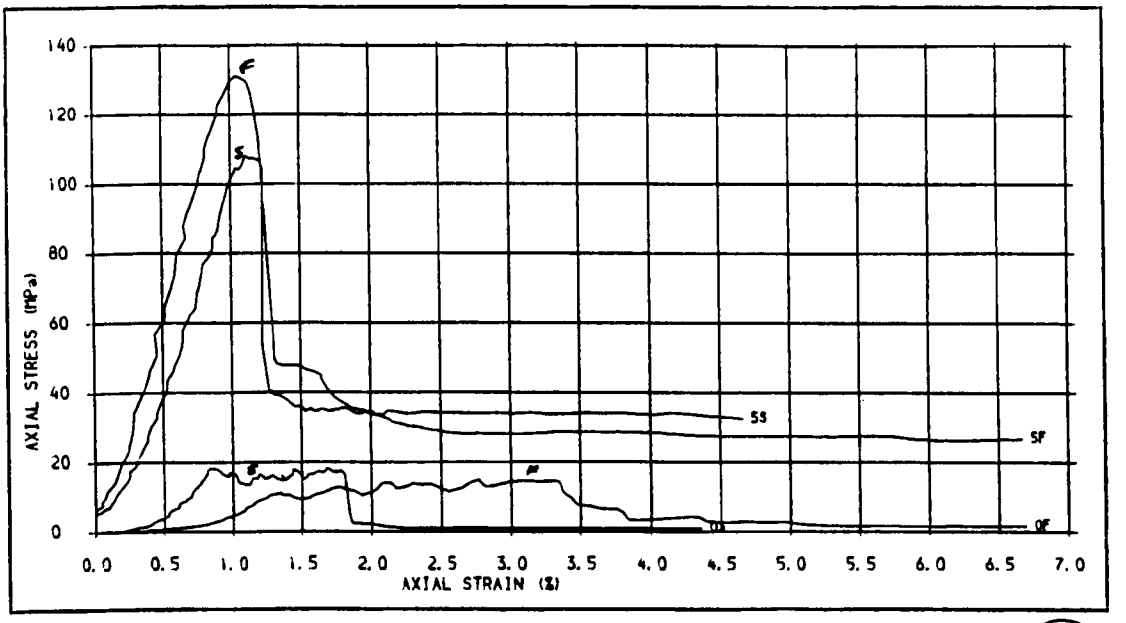

Fig. 27 . STRESS-STRAIN CURVES FOR PS SPECIMENS. STRAIN RATES. SLOW AND FAST JOINT ANGLE = 30 DEG., CONFININIG PRESSURES = 0 AND 5 MPa.

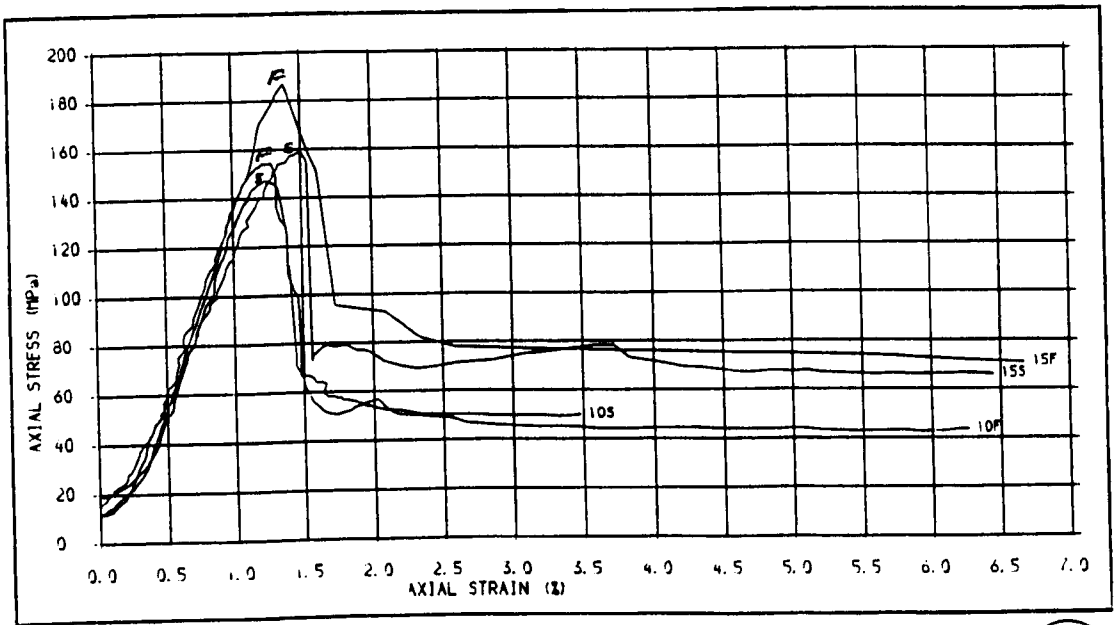

Fig. 28 . STRESS-STRAIN PLOTS FOR PS SPECIMENS. STRAIN RATES. SLOW AND FAST JOINT ANGLE = 30 DEG., CONFINIG PRESSURES = 10 AND 15 MPa.

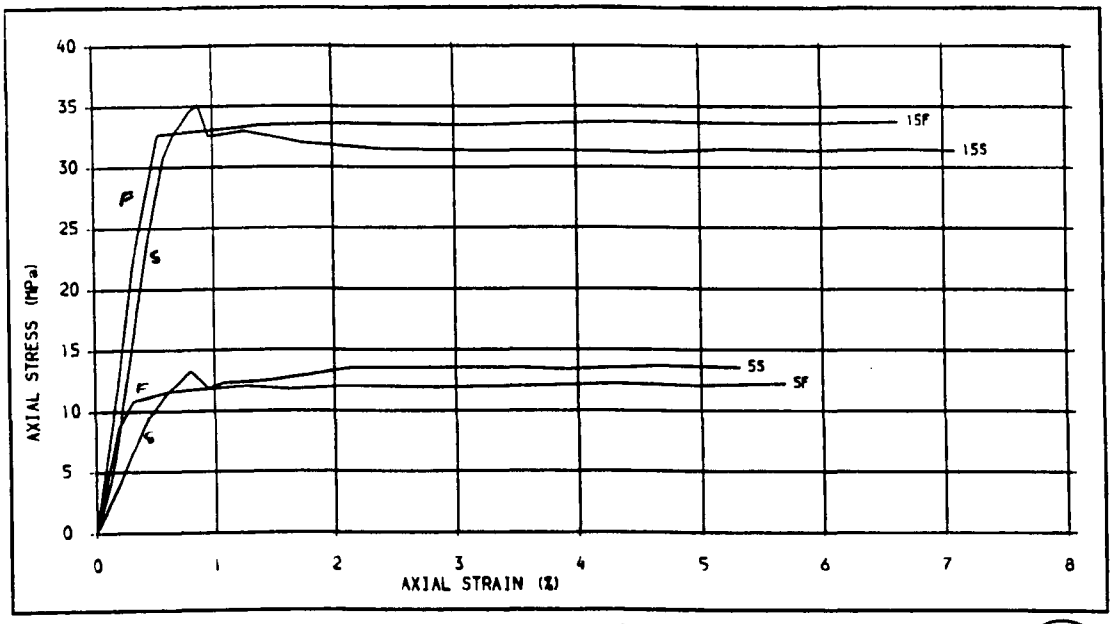

Fig. 7.9 . STRESS-STRAIN PLOTS FOR SS SPECIMENS. STRAIN RATES. SLOW AND FAST, JOINT ANGLE = 60 DEG., CONFINING PRESSURES = 0 AND 5 MPa.

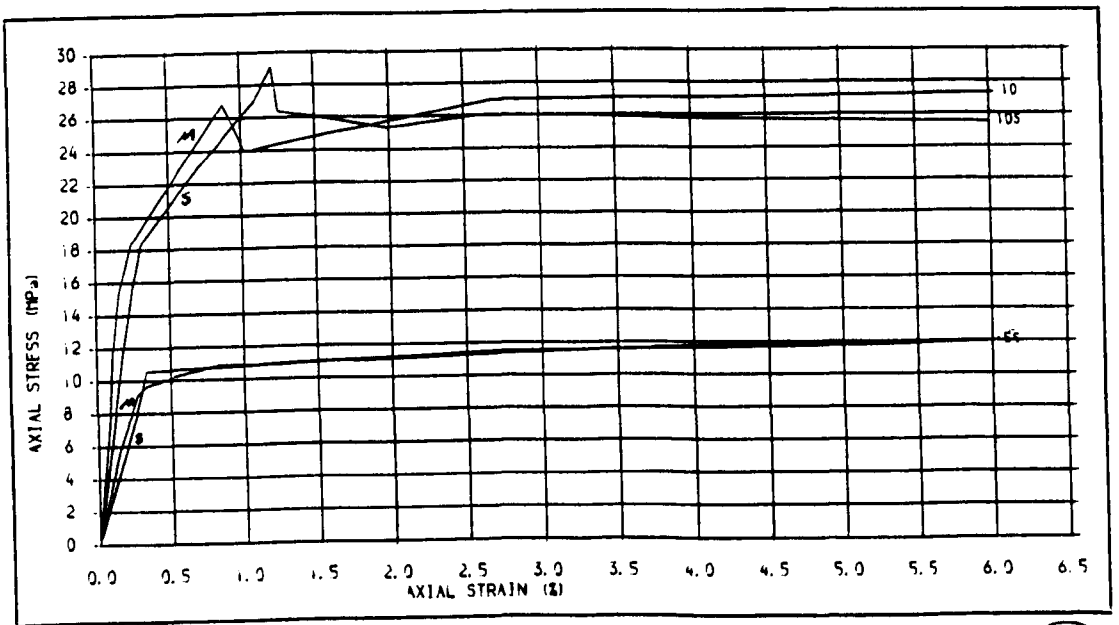

Fig. 7.10 . STRESS-STRAIN PLOTS FOR PS SPECIMENS. STRAIN RATES. SLOW AND FAST JOINT ANGLE = 60 DEC., CONFINING PRESSURES = 5 AND 10 MPa.

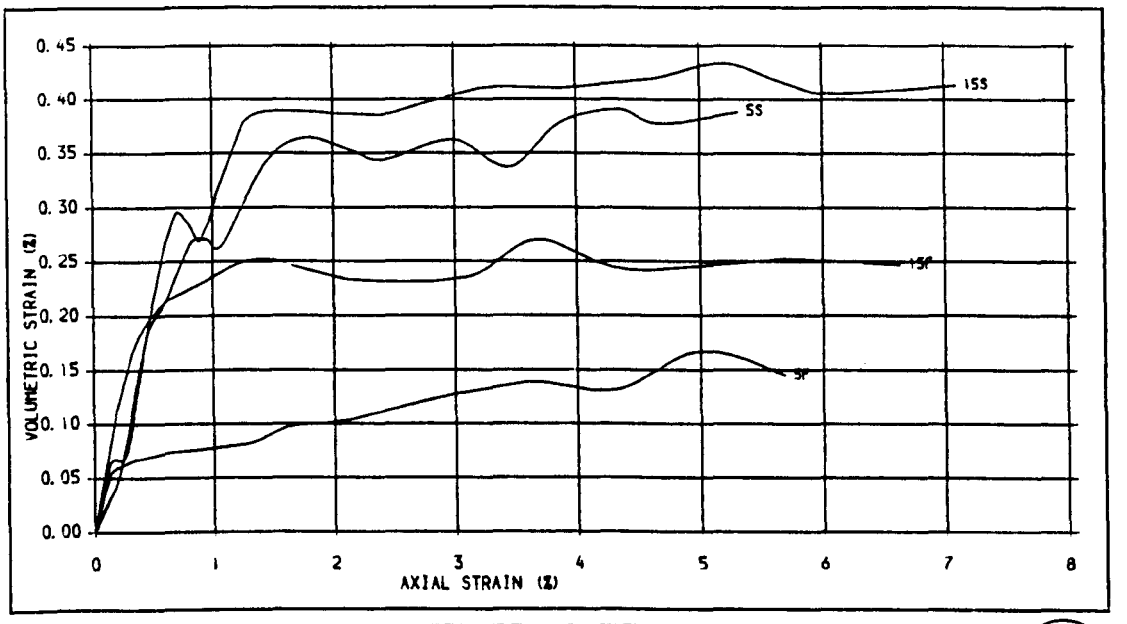

Fig. 7.11 : VOLUMETRIC STRAIN–AXIAL STRAIN PLOTS FOR SS SPECIMENS. STRAIN RATES. SLOW AND FAST, JOINT ANGLE = 60 DEG., CONFINING PRESSURES = 5 AND 15 MPa

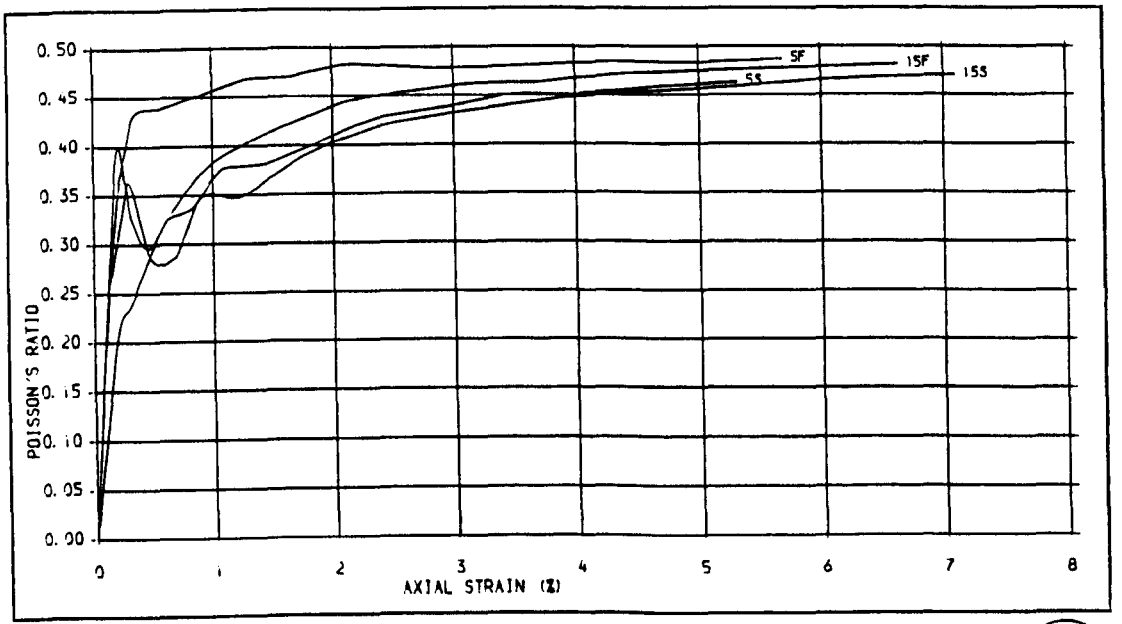

Fig. 7.12 : AXIAL STRAIN–INSTANTANEOUS POISSON'S RATIO PLOTS FOR SS SPECIMENS. STRAIN RATES. SLOW AND FAST, JOINT ANGLE = 60 DEG., CONFINING PRESSURES = 5 AND 15 MPa

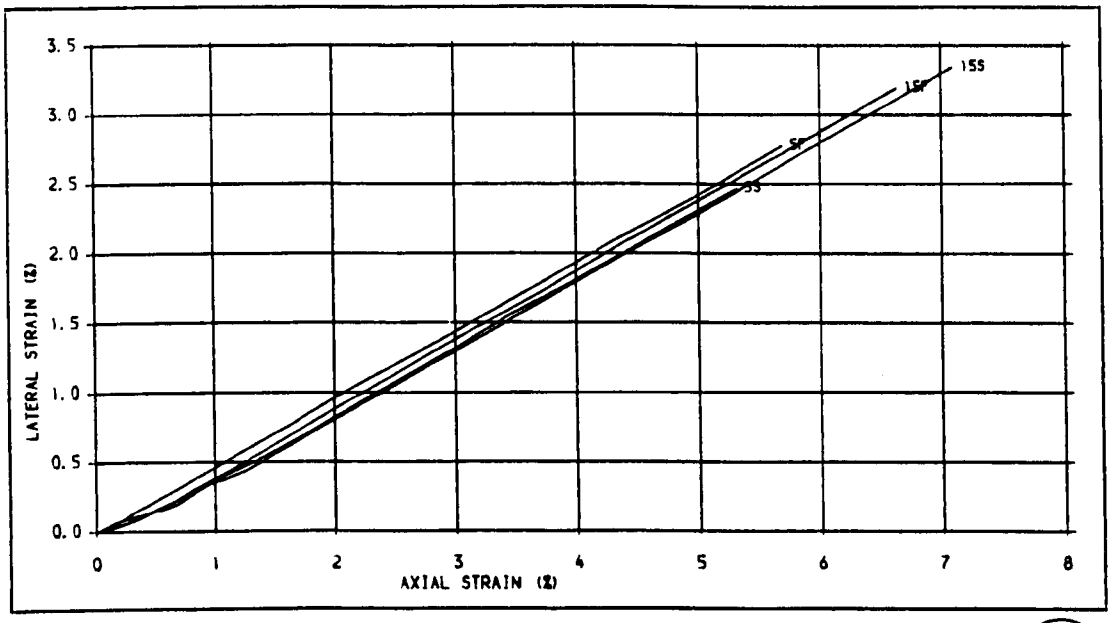

Fig. 7.13 : LATERAL STRAIN-AXIAL STRAIN PLOTS FOR SS SPECIMENS, STRAIN RATES, SLOW AND FAST, JOINT ANGLE = 60 DEG., CONFINING PRESSURES = 5 AND 15 MPa.

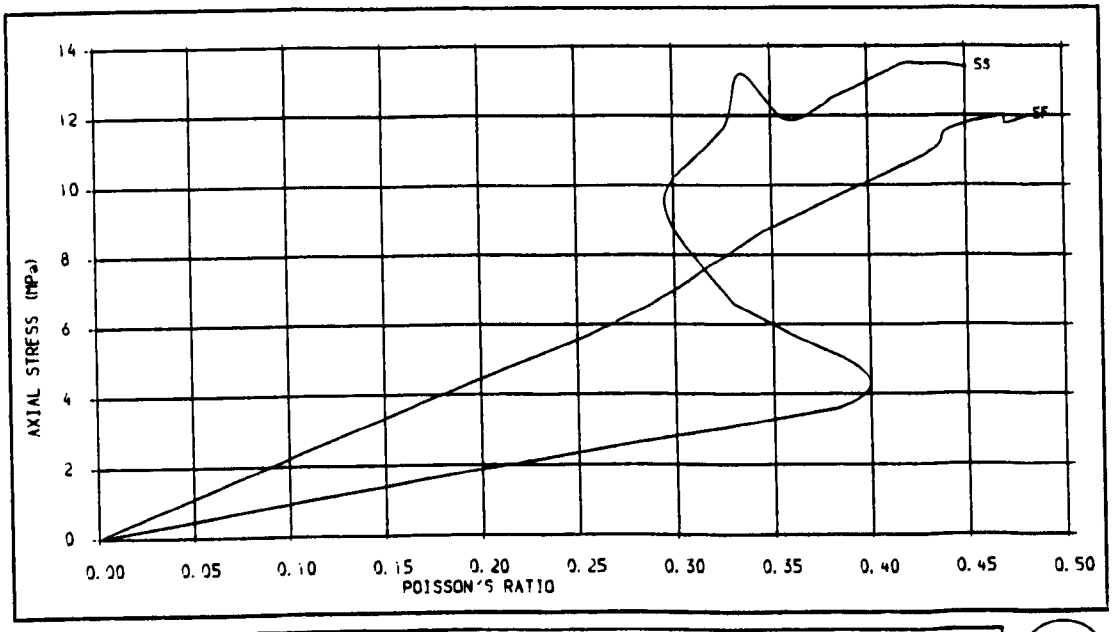

Fig. 7.14 : STRESS-INSTANTANEOUS POISSON'S RATIO PLOTS FOR SS SPECIMENS, STRAIN RATES, SLOW AND FAST, JOINT ANGLE = 60 DEG. (SAW CUT), CONFINING PRESSURE = 5 MPa

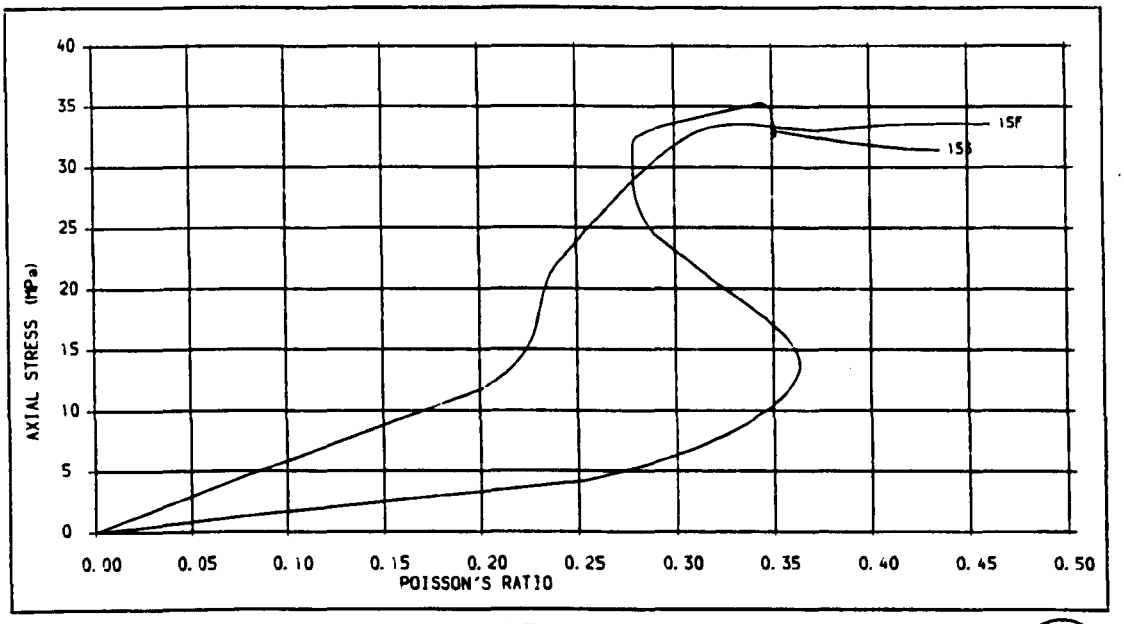

Fig. 7.15 . STRESS-INSTANTANEOUS POISSON'S RATIO PLOTS FOR SS SPECIMENS, STRAIN RATES. SLOW AND FAST, JOINT ANGLE = 60 DEG. (SAW CUT), CONFINING PRESSURE = 15 MPa.

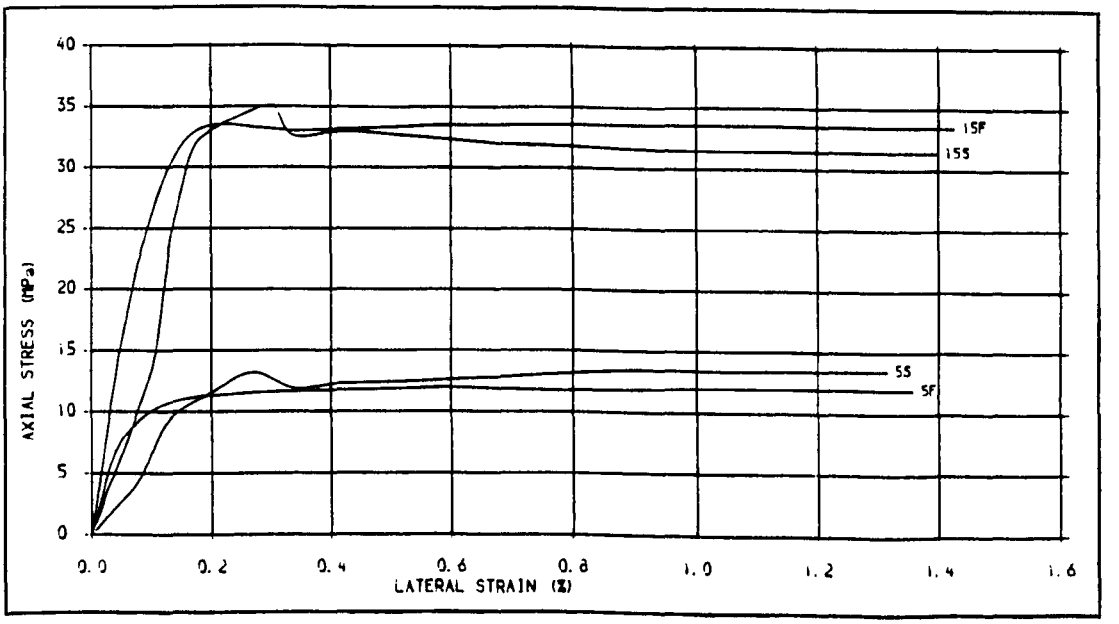

Fig. 7.16 . AXIAL STRESS-LATERAL STRAIN PLOTS FOR SS SPECIMENS, JOINT ANGLE = 60 DEG., STRAIN RATES. SLOW AND FAST, CONFINING PRESSURES = 5 AND 15 MPa

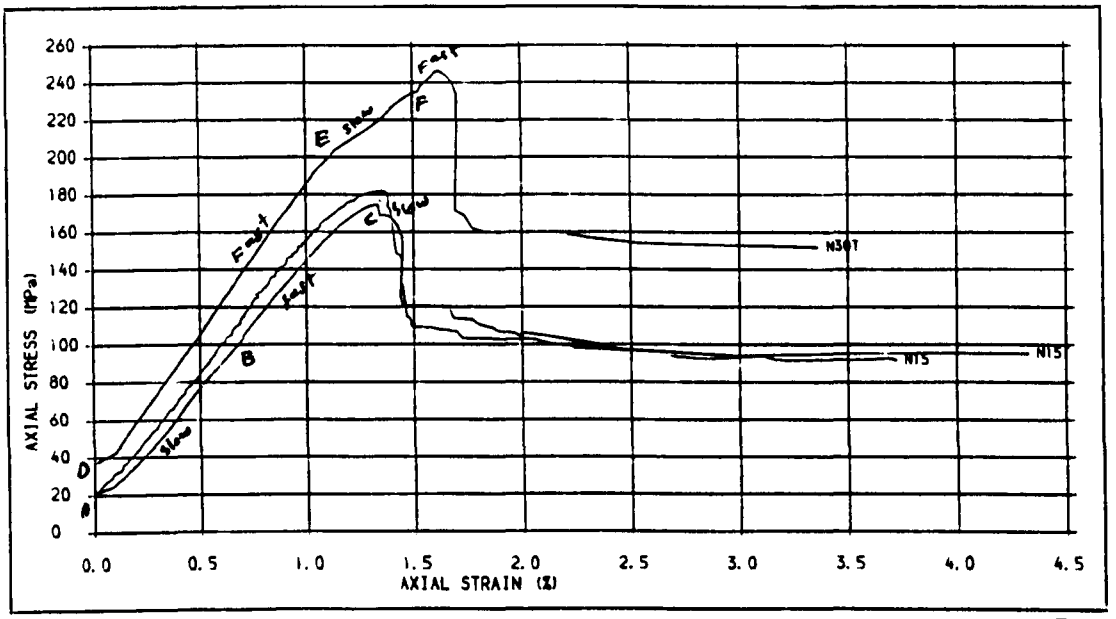

Fig. 7.17 . STRESS-STRAIN PLOTS FOR SS SPECIMENS AT CHANGING STRAIN RATES, JOINT ANGLE= 30 DEG. (NATURAL), CONFINING PRESSURES = 15 AND 30 MPa.

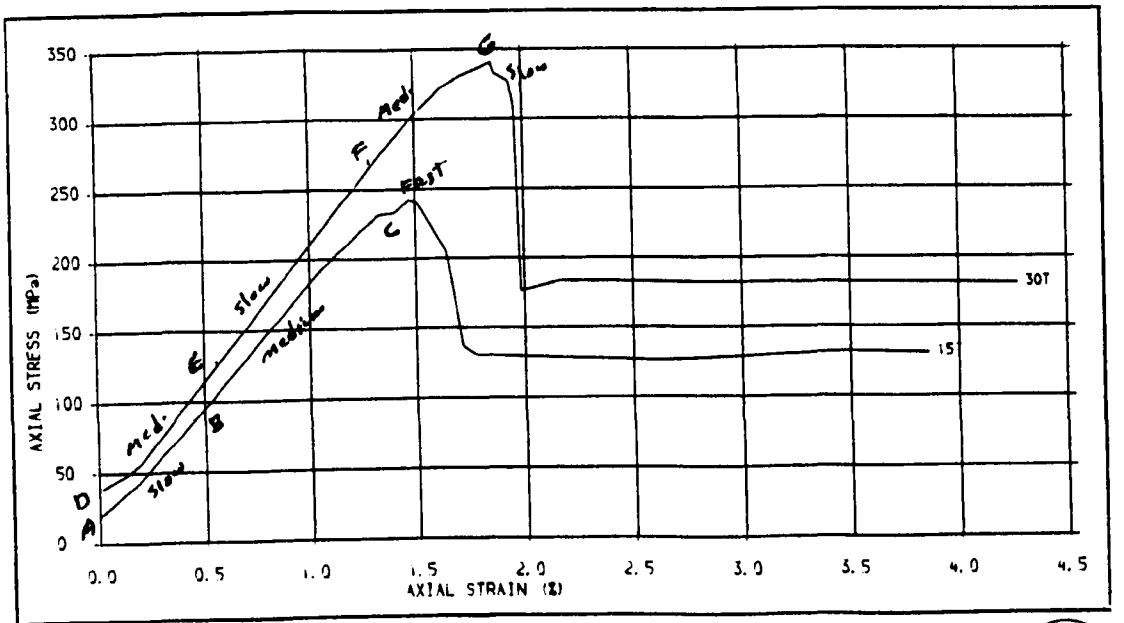

Fig. 7.18 . AXIAL STRESS-AXIAL STRAIN PLOTS FOR PS SPECIMENS AT CHANGING STRAIN RATES JOINT ANGLE = 30 DEG (SAW CUT), CONFINING PRESSURES = 15 AND 30 MPa.

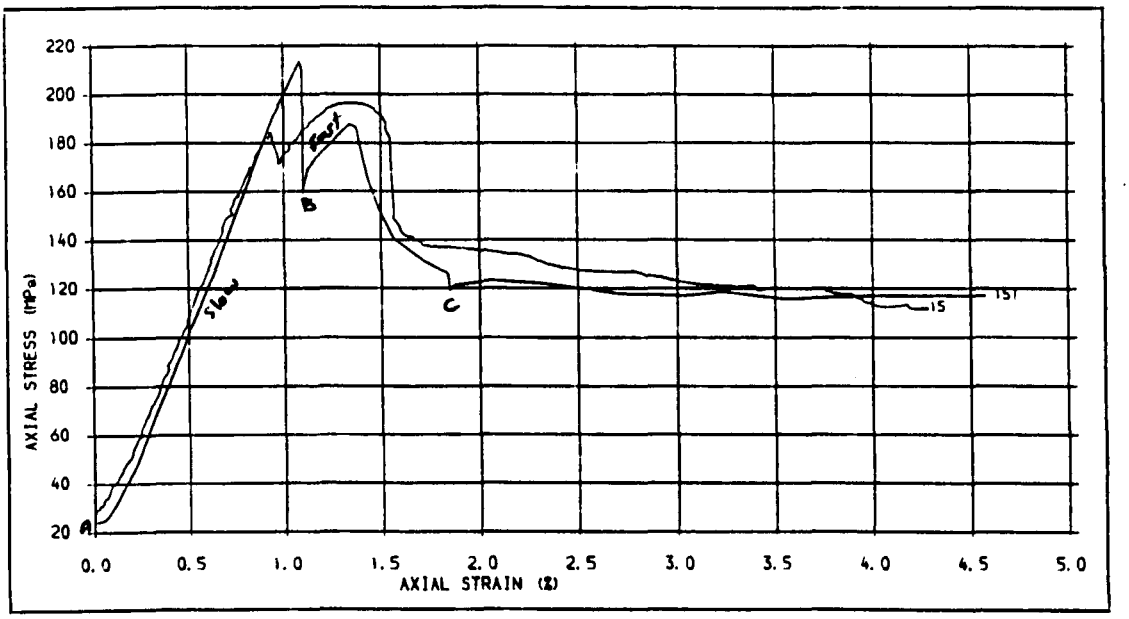

Fig. 7.19 : AXIAL STRESS-AXIAL STRAIN PLOTS FOR PS SPECIMENS AT CHANGING STRAIN RATES
JOINT ANGLE = 45 DEG. (NATURAL), CONFINING PRESSURE = 15 MPa

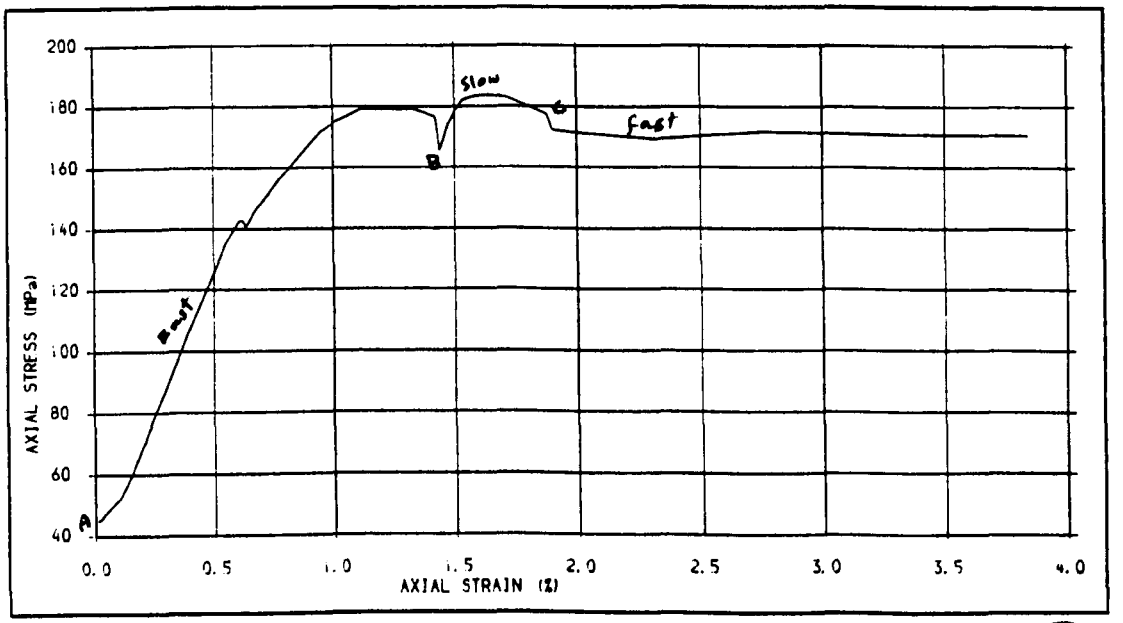

Fig. 7.20 : AXIAL STRESS-AXIAL STRAIN PLOT FOR A PS PECIMEN AT CHANGING STRAIN RATES (FAST AND SLOW), JOINT ANGLE = 45 DEG. (NATURAL), CONFINING PRESSURE = 30 MPa

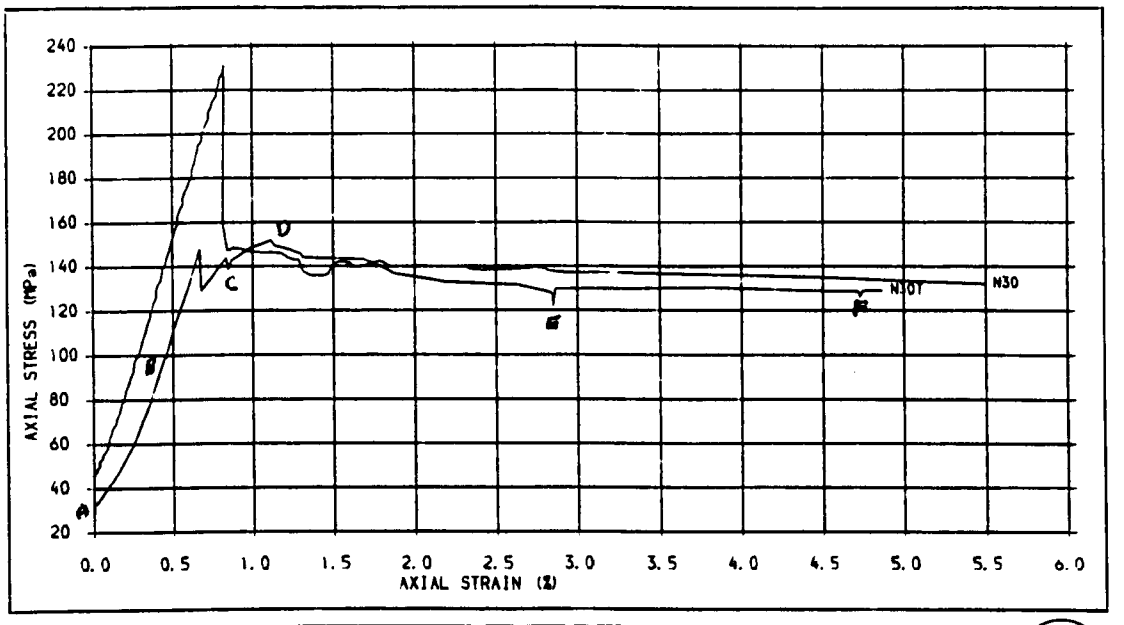

Fig. 421 . AXIAL STRESS-AXIAL STRAIN PLOTS FOR PS SPECIMENS AT CHANGING STRAIN RATES
JOINT ANGLE = 60 DEG. (NATURAL), CONFINING PRESSURE = 30 MPa.

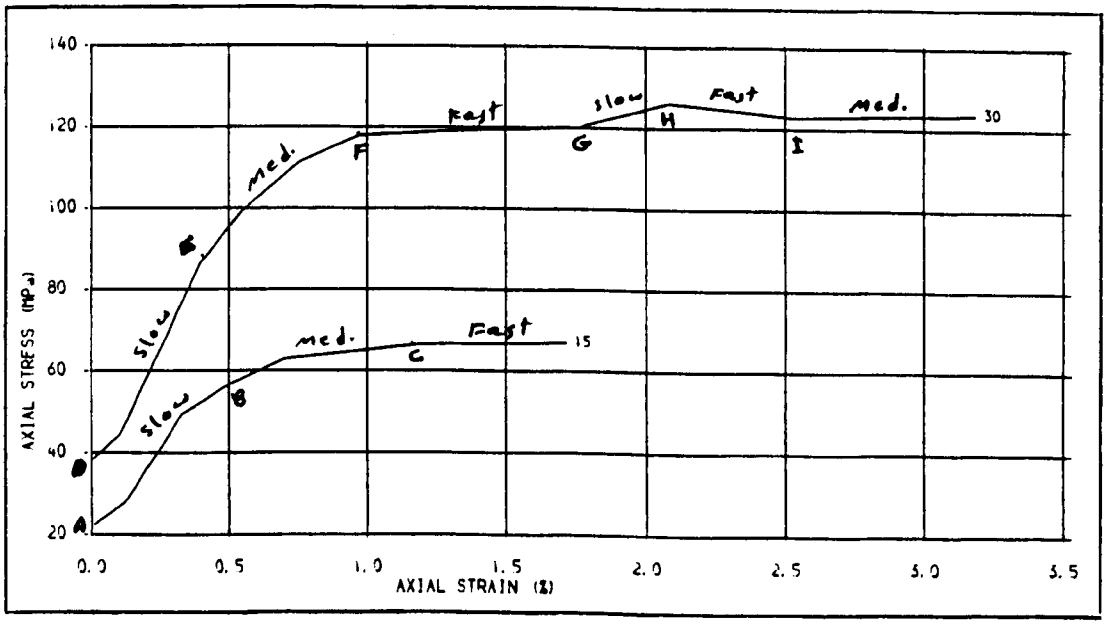

Fig. 422 . AXIAL STRESS-AXIAL STRAIN PLOTS FOR PS SPECIMENS AT CHANGING STRAIN RATES,
JOINT ANGLE = 60 DEG. (SAW CUT), CONFINING PRESSURES = 15 AND 30 MPa

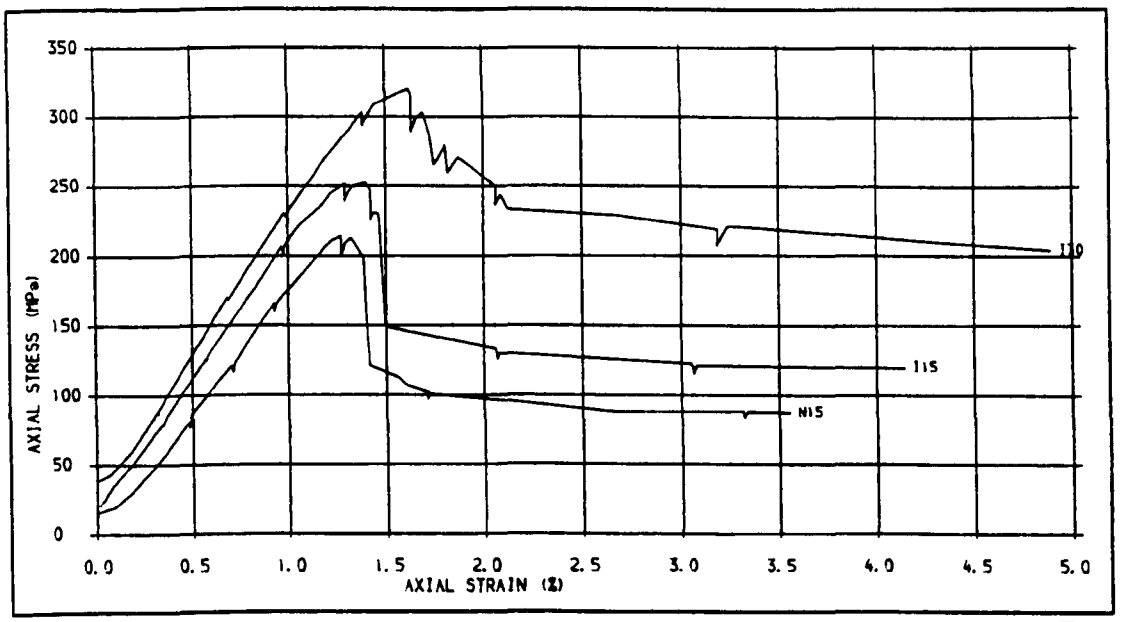

Fig. 723 . STRESS-STRAIN PLOTS FOR PS (INTACT AND JOINTED) SPECIMENS OBTAINED IN RELAXATION TESTS, JOINT ANGLE = 30 DEG., CONFINING PRESSURES = 15 AND 30 MPa.

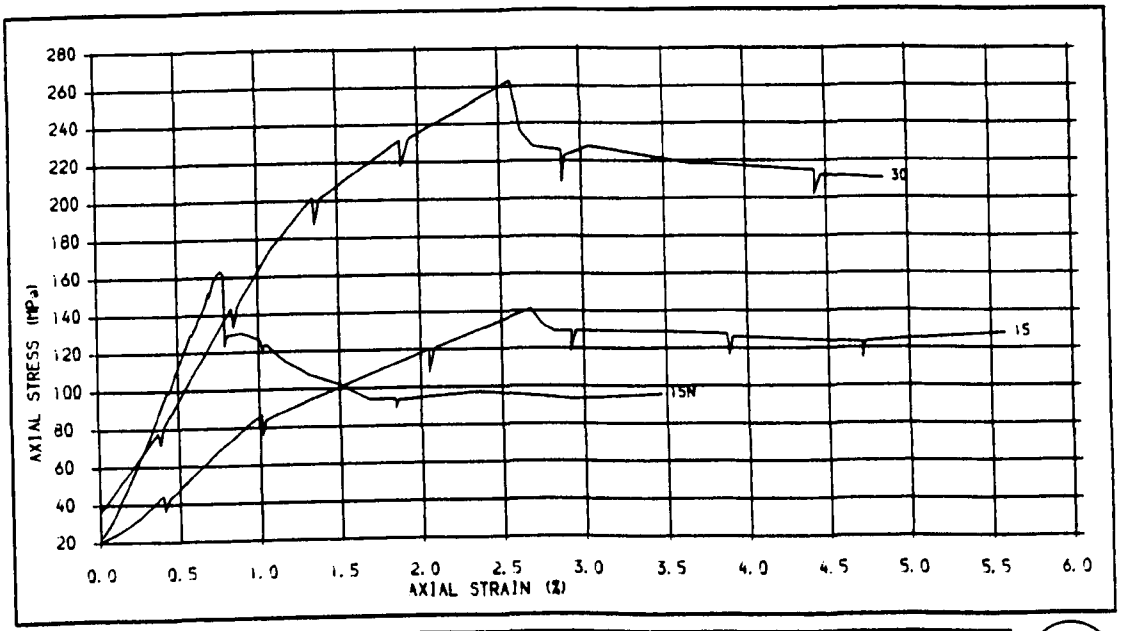

Fig. 724 . STRESS-STRAIN PLOTS FOR PS SPECIMENS OBTAINED IN RELAXATION TESTS ON SAW CUT AND NATURAL JOINTS, JOINT ANGLE= 45 DEG. CONFINING PRESSURES= 15 AND 30 MPa.

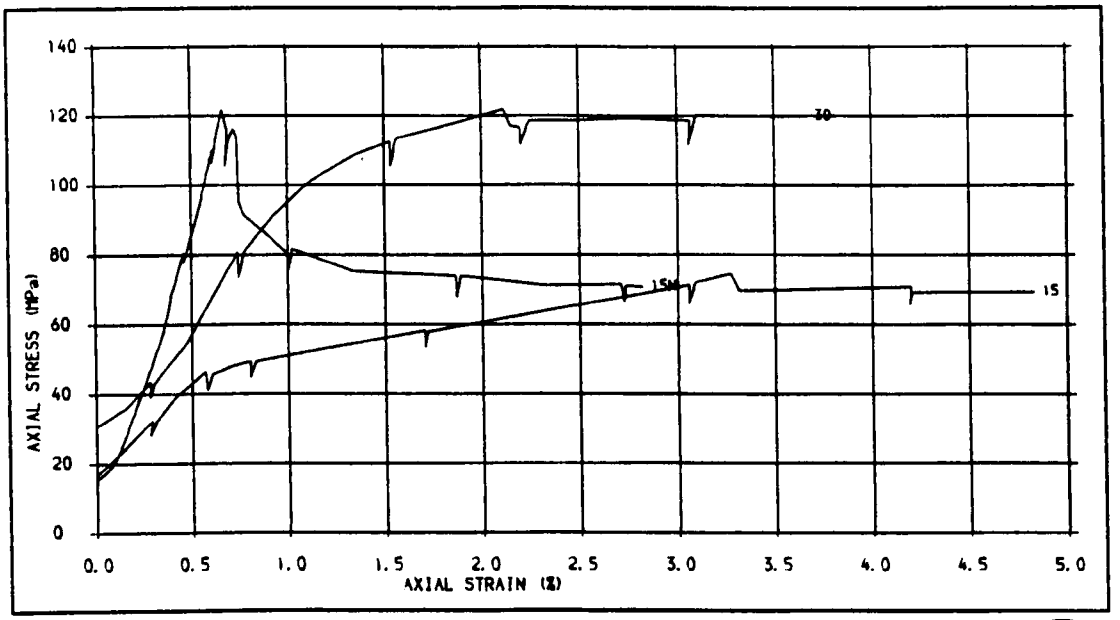

Fig. 725 .STRESS-STRAIN PLOTS FOR PS SPECIMENS OBTAINED IN RELAXATION TESTS WITH SAW CUT AND NATURAL JOINTS, JOINT ANGLE= 60 DEG., CONFINING PRESSURES= 15 AND 30 MPa.

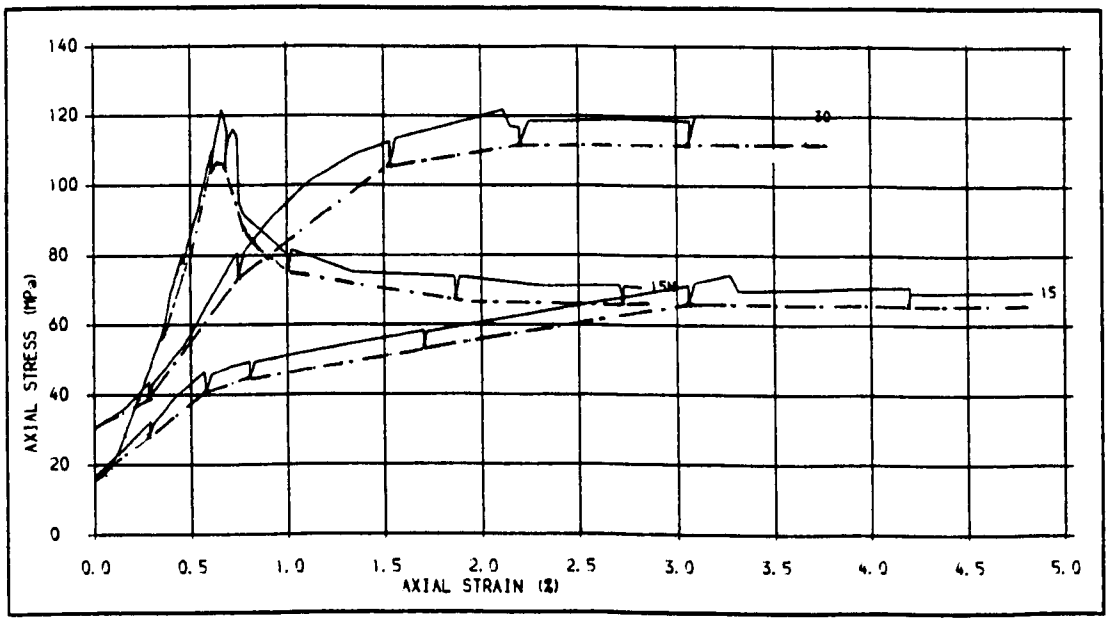

Fig. 726 .STRESS-STRAIN PLOTS FOR RELAXATION TESTS ON PS SPECIMENS (THE SAME AS FIG. 7.25) THE LOWER PLOTS OBTAINED BY CONNECTING THE POINTS AFTER RELAXATION.

CHAPTER 8

FAILURE CRITERIA FOR DISCONTINUOUS ROCK

8.1 INTRODUCTION

For the design of structures in rock, availability of a criterion capable of assessing the rock mass characteristics has always been a major task in rock mechanics, even when the rock mass has been predominantly a competent rock. The problem has been much more significant, however, when the rock mass contains planes of weakness, or is highly jointed or disintegrated. Consequently, various criteria have been proposed by different authors to evaluate the anisotropic and jointed rocks. Nearly all these criteria are based on a peak strength as the major parameter and insufficient attention has been paid to the magnitude of deformation and control of displacement throughout the rock. In order to achieve a clear view on the existing failure criteria for discontinuous rocks, some of the most important failure criteria for discontinuous rocks are reviewed.

8.2 WALSH AND BRACE FAILURE CRITERION

The Walsh-Brace (1964) theory is an extension of the McClintock and Walsh (1963) modification of Griffith's (1921) tensile failure theory. McClintock and Walsh assumed, as did Griffith, that the material is isotropic and the inherent flaws or Griffith's cracks are randomly oriented. For the case of non-randomly oriented cracks Walsh and Brace have derived a fracture criterion for discontinuous rocks. Non-randomly oriented Griffith's cracks may be assumed as joints, faults, bedding planes and other large scale features.

Strength according to this theory is determined by the elastic and surface characteristics of the material between the flaws, and by the length and sharpness of the flaws themselves. Walsh and Brace (1964) assume that the role of flaws is the dominant one

in determining brittle behaviour of anisotropic rocks. The long as well as the short cracks are such that the cracks close at relatively low values of stress applied, thereafter both normal and shear stresses are transmitted

According to this theory failure can originate from either the long or the small crack systems depending upon the orientation of the long crack to the applied stress (σ_1-σ_3). The differential stress required for fracture occurring at small, randomly oriented cracks is given for any confining pressure σ_3 by:

$$(\sigma_1-\sigma_3)_s = C_{os} + \frac{2\mu_s\sigma_3}{(1+\mu_s^2)^{1/2} - \mu_s} \qquad (8.1)$$

where C_{os} is the uniaxial compressive strength of the randomly oriented short crack material (in the present experiment uniaxial compressive strength of the intact rock), and μ_s is the coefficient of friction for the short crack (coefficient of internal friction for the intact rock in this experiment).

If fracture occurs through growth of the long crack which is oriented at angle β to σ_1, then the fracture stress at any confining pressure, σ_3, is given by:

$$(\sigma_1-\sigma_3)_L = \frac{C_{oL}\ [(1+\mu_L^2)^{1/2} - \mu_L\ ] + 2\mu_L\sigma_3}{2\ \sin\beta\ \cos\beta\ (1 - \mu_L \tan\beta\ )} \qquad (8.2)$$

where C_{oL} is the uniaxial compressive strength of the jointed rock for the most critical orientation of β, say 60^o, (to the minor principal stress), and μ_L is the coefficient of friction along the joint surface (coefficient of sliding friction).

The actual fracture stress for any given situation is found by evaluating (8.1) and (8.2) for any confining pressure and orientation of long crack (joint, fault,...). The smaller of

the two values $(\sigma_1 - \sigma_3)_s$ and $(\sigma_1 - \sigma_3)_L$ for any orientation must be the fracture stress of the material for that orientation.

8.3 HOEK'S CRITERION

Hoek's criterion is very similar to the Walsh and Brace (1964) theory. Hoek (1964) postulated that two distinct crack systems are present in an anisotropic material including a set of relatively large preferentially oriented cracks which lie along bedding planes, joints..., and a randomly oriented matrix of grain boundary cracks. He assumes that failure is tensile in nature, and on the basis of the modification to Griffith's theory by McClintock and Walsh (1963) when the normal stress across the crack surface is compressive, the stress required for fracture originating at small, randomly oriented cracks for any confining pressure σ_3,is given by :

$$\sigma_1 = \frac{-4\,\sigma_t}{(1-k)\,(1+\mu^2)^{1/2} - \mu\,(1+k)} \qquad (8.3)$$

where s_t is the uniaxial tensile strength of the randomly oriented short crack material and m is the coefficient of friction for short cracks, and k is the principal stress ratio σ_3/σ_1.

If, however, failure occurs as a result of the oriented preferential cracks (growth of the long crack systems as in the case of joints and faults) the fracture criterion for any confining pressure σ_3, is given by:

$$2\sigma_t = -1/2\{(\sigma_1-\sigma_3)\sin 2\beta - \mu[(\sigma_1+\sigma_3) - (\sigma_1-\sigma_3)\cos 2\beta]\} \qquad (8.4)$$

where σ_t is the uniaxial tensile strength for the most critical orientation of β (60^o in the present experiment) and m is the coefficient of friction for the long crack.

The criterion is only valid when the normal stress related to σ_1 and σ_3 is compressive, since this is the only condition in which crack closure can occur.

Since it is difficult to obtain reliable measurements of the uniaxial tensile strength of a brittle material, it is convenient to express the above equations in terms of the uniaxial compressive strength σ_c. The relation between the uniaxial tensile and compressive strength of a brittle material containing initially closed cracks can be approximated by substituting σ_3=0 in equation (8.3) (Bieniawski, 1967), giving:

$$\sigma_c = \frac{-4\,\sigma_t}{(1+\mu^2)^{1/2} - \mu} \qquad (8.5)$$

Substituting equation (8.5) into equation (8.3) yields :

$$\sigma_{1_e} = \sigma_3 [\ (1+\mu^2\ )^{1/2} + \mu_e / \ (1+\mu_e)^{1/2} - \mu_e\ ] + \sigma_c \qquad (8.6)$$

In the case of critical orientation of β (60^o in this experiment) the uniaxial tensile strength can be approximated by zero. Substituting $\sigma_t = 0$ into equation (4) yields:

$$\sigma_L = \sigma_3 \cdot \frac{\sin 2\beta + \mu_L \cos 2\beta + \mu_L}{\sin 2\beta + \mu_L \cos 2\beta - \mu_L} \qquad (8.7)$$

The theory may be evaluated by calculating the value of σ_{1s} and σ_{1L}, using equations (8.6) and (8.7), for a given confining pressure and orientation, then using the smaller of the two values as the fracture strength.

8.4 THEORY OF SINGLE PLANE OF WEAKNESS

The Walsh-Brace and Hoek theories assume that failure is due to tension, single plane of weakness theory, proposed by Jaeger (1960); however, is entirely different from those and assumes that the body fails in shear. The theory is the generalization of the Coulomb-Navier theory in which the behaviour of an isotropic material can be described in the ordinary way by a shear strength (or cohesion) and a coefficient of internal friction, but which is supposed to have a plane (or parallel planes) of weakness with different values of shear strength and coefficient of friction. The failure of the matrix material is described as:

$$\tau = S_o + \sigma \tan \phi \qquad (8.8)$$

where S_o is the cohesive strength of the material and $\tan \phi = \mu$ is the coefficient of internal friction. Failure along the plane of weakness is given by:

$$\tau = S' + \sigma \tan \phi' \qquad (8.9)$$

where S' and $\tan \phi' = \mu'$ are the cohesive strength and coefficient of friction across the plane of weakness.

Relating σ and τ to σ_1 and σ_3 (major and minor principal stresses) the failure criterion in a uniform medium is given by:

$$\tau_m = C_m \sin \phi + S_o \cos \phi \qquad (8.10)$$

where $\tau_m = (\sigma_1 - \sigma_3)/2$ is the maximum shear stress and $C_m = (\sigma_1 + \sigma_3)/2$ is the mean of the principal stresses. The final form of the equation (8.10) as a function of confining pressure and differential stress is derived as :

$$\sigma_1 - \sigma_3 = \frac{2\sin \phi}{1-\sin \phi} \sigma_3 + \frac{2S_o \cos \phi}{1-\sin \phi} \qquad (8.11)$$

which is a straight line on σ_1 - σ_3 coordinate axes.

For failure for a definite plane inclined at β to σ_1, using equation (8.9) is given by:

$$\tau_m \sin (2\beta + \phi') = C_m \sin \phi' + S' \cos \phi' \qquad (8.12)$$

The final form of equation (8.12) in terms of the maximum and minimum principal stresses σ_1 and σ_3 is given by :

$$\sigma_1 - \sigma_3 = \frac{2\sin \phi'}{\sin (2\beta+\phi') + \sin \phi'} \sigma_3 + \frac{2S' \cos \phi'}{\sin (2\beta + \phi') + \sin \phi'} \qquad (8.13)$$

This is also a straight line on σ_1 - σ_3 coordinate axes.

For any values of β and σ_3, fracture will take place either in the uniform part of the body or along the weakness plane (joint or fault). The lower of the two values (σ_1-σ_3) given by (8.11) and (8.13) is the fracture strength of the rock.

8.5 CONTINUOUSLY VARIABLE SHEAR STRENGTH

The variable shear strength theory was also proposed by Jaeger (1960) and is a second generalization of the Coulomb-Navier theory to describe the possible effect of the discontinuity on the strength of rock in which the internal friction, m, is a constant, but the cohesive strength, S_o, is continuously variable according to the relation

$$S_o = S_1 - S_2 \cos 2(\alpha - \beta) \qquad (8.14)$$

where S_1 and S_2 are constant and β is the inclination of plane of weakness to the direction of σ_1 and α is the orientation of β for which S_o is a minimum.

Assuming the Coulomb-Navier criterion $\tau = S_o + \mu\sigma$ for failure in any plane is held, Jaeger derived the following equation as the failure criterion :

$$(\tau_m + S_2 \sin 2\beta) \sin 2\alpha + (\mu\tau_m + S_2 \cos 2\beta) \cos 2\alpha = S_1 + \mu C_m \qquad (8.15)$$

where $\tau_m = (\sigma_1-\sigma_3)/2$ and $C_m = (\sigma_1+\sigma_3)/2$

Donath (1961) presented this criterion in terms of the σ_1 and σ_3 as:

$$\sigma_1 = \frac{\sigma_3 \cos \alpha \ (\sin \alpha + \mu \cos \alpha) - \beta \cos 2(\alpha - \beta) + S_1}{\sin \alpha \ (\cos \alpha - \mu \sin \alpha)} \qquad (8.16)$$

The criterion for failure is satisfied for positive values α (i.e $\alpha = 90 - \phi$) and there is only one plane of failure instead of two conjugate planes possible in the Coulomb-Navier case $S_2 = 0$.

8.6 MODIFIED VARIABLE COHESIVE STRENGTH THEORY

McLamore and Gray (1967) proposed that the variation of S_o can be described by the following relationship:

$$S_o = A_{1,2} - B_{1,2} \ [\cos 2(\alpha - \beta)]^n \qquad (8.17)$$

where A_1 and B_1 are constants that describe the variance over the range of $0^o < \alpha < \beta$ and A_2 and B_2 over the range of $\beta < \alpha < 90^o$. The factor n indicates the type of anisotropy and has the value of 1 or 3 for planar type of anisotropy (cleavage and possibly schistosity) and the value of 5 or 6 or greater for the linear type of anisotropy associated with bedding planes.

As noted Jaeger (1960) assumes that internal friction is constant for all orientations. This restriction was also modified by Donath (1972), and the final form of the criterion is expressed as follows:

$$\sigma_1 - \sigma_3 = \frac{2(S_o + \sigma_3 \tan \phi)}{\sec \phi - \tan \phi} \qquad (8.18)$$

$$S_o = a - b.\cos 2(\alpha - \beta) \qquad (8.19)$$

$$\tan \phi = c - d.\cos 2(\alpha - \beta) \qquad (8.20)$$

Thus, both S_o and tan ϕ can be made to vary systematically with β.

8.7 OTHER FAILURE CRITERIA

As opposed to the aforementioned theories which ignore the effect of intermediate principal stress, Ashour (1988) consider the effect of this stress (s_2) on failure in a multiaxial stress-state. The theory is based on Von Mises criterion for ductile metals and the subsequent modifications proposed by Mogi (1971) and Hsu et al (1984). The final form of the criterion for discontinuous rocks is

given by:

$$E \quad f(\sigma) \quad \text{(for failure)} \qquad (8.21)$$

where:

$$E = A\sigma_x^2 + B\sigma_y^2 + C\sigma_z^2 + D\sigma_x\sigma_y + E\sigma_x\sigma_z +$$

$$F\sigma_y\sigma_z + G\tau_{xy}^2 + H\tau_{xz}^2 + I\tau_{yz}^2 \qquad (8.22)$$

$$f(\sigma) = C_o + C_1\sigma + C_2\, e^{(a\sigma)} \qquad (8.23)$$

$$\sigma = \sigma_x + \sigma_y + \sigma_z \qquad (8.24)$$

The coefficients A, B, C, D, E, F, G, H, I, C_0, C_1, C_2 AND a are experimentally determined constants.

8.8 EMPIRICAL FAILURE CRITERIA TO ASSESS DISCONTINUOUS ROCK

A considerable number of empirical failure criteria have been proposed by different authors to evaluate broken and jointed rocks which are mostly based on Griffith's theory and its subsequent modifications, or on Coulomb and Mohr hypotheses.

Hobbs (1966) proposed a failure criterion to predict the relationship between the principal stresses at failure and between the normal and shear stresses at failure based on the cohesion theory of friction. The criterion was in agreement with the results obtained with broken specimens tested by Hobbs (1966 & 1970).

Bieniawski (1974) proposed relationships to estimate the triaxial strength of rock, irrespective of the magnitude of deformation, which are the normalized forms of the empirical failure criteria proposed by Murrell (1965) and Hoek (1968).

Bieniawski's criterion was modified by Brook (1979) in terms of the maximum shear stress and mean normal stress. Brook showed that estimation of triaxial strength by the modified form is very accurate and the only measurement required is the uniaxial compressive strength of the rock which can be easily obtained by a point load index test.

Yudhbir et al (1983) proposed an empirical failure criterion to estimate the strength of rock masses ranging from intact to disintegrated rocks. This criterion is a generalization of Bieniawski's criterion (1974).

Thiel and Zabuski (1987) proposed an empirical failure criterion for a jointed anisotropic rock mass, based on Coulomb's hypothesis and the shear failure criterion set out by Jaeger (1960).The criterion proposes relationships describing the variation of cohesion and uniaxial tensile strength with direction.

Hoek and Brown (1980 a,b) developed an empirical failure criterion to estimate the strength of rock where the rock mass quality ranges from intact to heavily jointed and disintegrated rock. They attempt to satisfy the following conditions:

a) The failure criterion should give good agreement with experimentally determined rock strength values.
b) The failure criterion should be expressed by mathematically simple equations, based to the maximum extent possible upon dimensionless parameters.
c) The failure criterion should offer the possibility of extension to deal with anisotropic failure and the failure of jointed rock masses.

The conceptual point has been provided by the original Griffith's theory and its modifications for tensile and compressive stress conditions (Hoek,1983). The process used by Hoek and Brown in deriving their empirical failure criterion was purely trial and error. The criterion is presented in terms of major and minor principal stresses at failure. The empirical equation is given by:

$$\sigma_1 = \sigma_3 + (m\sigma_c\sigma_3 + s\sigma_c^2)^{1/2} \qquad (8.25)$$

in which:

σ_1 = the major principal stress at failure;

σ_3 = the minor principal stress

σ_c = the uniaxial compressive strength of the intact material;

m and s = constant that depend on the properties of the rock and on the extent to which it had been broken before being subjected to the failure stresses σ_1 and σ_3

8.9 PROBLEMS ENCOUNTERED WITH THE EXISTING FAILURE CRITERIA FOR DISCONTINUOUS ROCKS

A considerable number of research work has been conducted by many workers to establish a versatile and comprehensive failure criterion. Although, they have succeeded in explaining many aspects of rock behaviour, they have failed to explain issues such as long term behaviour, stress relaxation effects, etc. Furthermore, such criteria cannot be extended beyond a limited range of stress conditions. In other words, practical design engineers are still searching for a failure criterion that fully meets all their requirements. Consequently, a large amount of research has yet to be done on rock failure criteria, possibly even more than what has been published to date (Waversick, 1968). Jaeger and Cook (1979) justifiably believe that failure criteria based on the actual mechanism of fracture, which are more sophisticated than the theories of Coulomb, Mohr and Griffith's, have yet to be developed.

None of the criteria reviewed in this chapter has direct reference to the magnitude of deformation as a major parameter in rock. Results of the tests performed in this work reveal that the amount of displacement along the joint surface is a fundamental parameter in jointed rock, and in fact, before obtaining any quantitative peak strength, this parameter would have to be considered and controlled.

On the other hand, neither theoretical nor empirical failure criteria reviewed have appreciated the effect of some very significant parameters such as time dependency, cyclic loading and stress relaxation associated with a structure where it is established on or in a rock mass.

The present experimental investigations indicates that the state of displacement is equally important to the state of stress. This significance is more understandable when such a criterion is used in designing of foundations of a dam or very large and heavy

equipment in nuclear power stations constructed on jointed rocks, where differential displacements are very significant.

There are several reasons indicating that the selection of peak stress as the only major parameter which is obtained by the evaluation of a failure criterion is not safe and reliable.

a) Figures 8.1 to 8.3 show the stress-strain plots for Penrith sandstone with saw cut joints in different confining pressures and orientation angles of 60, 45 and 30°. Comparison of the plots in each figure indicates that there is no similar relation between stress and strain at lower and higher confinements. At higher confining pressures (above 15 MPa) increase in strain is proportional to increase in strain; at lower confinements (below 15 MPa), however, such a relation is not observed. As is seen in figure 8.1 and 8.2 for 5 and 10 MPa confining pressures (figure 8.1) stress below 0.5% strain has reached its maximum; for 15 MPa , however, after more than 1% stress reached its peak. In figure 8.3 at 0 confinement a large amount of displacement has occurred and the deformational behaviour has become completely different from those of the higher confining pressures. In such cases, evaluation of the rock mass by the criteria in which stress at peak is the major parameter cannot be reliable. Furthermore, when the orientation angle changes to 45 and 60°, in some cases, there is no clear peak, and therefore, determination of an exact peak strength will be impossible. As a result, illustration of the differential stress (σ_1-σ_3) versus confining pressure (σ_3) on the basis of peak strength will be difficult.

b) In rough joints the magnitude of displacement along joint surface affects the strength of the rock significantly. Figure 8.4 illustrates the stress-strain plots for Penrith sandstone with split breakage joints and orientation angle of 30° for confining pressures of 5,15 and 30 MPa. The amount of peak strain differs in each curve, particularly the

dependency of strength to displacement around the peak is very high, so that with a little increase in displacement, the strength decreases about 28.5%, 59% and 44% for 5, 15 and 30 MPa confining pressure respectively. Increase of strain, for instance, at 5 MPa confining pressure from 0.8% to 0.9% the strength decreases more than 28% which is considerable. Therefore, use of a failure criterion on the basis of peak stress irrespective of displacement will result in a misleading design approach in such a situation.

c) There are cases in jointed rocks, especially when the surface roughness is relatively high, that more than one peak in the stress-strain curve at different percentages of strains is observed, so that. Figure 8.5 illustrates the stress-strain plot for a specimen containing a single joint with rough surface and orientation angle of 45°. of Two peaks at different amount of strains are clear observed and the second peak shows a higher magnitude in stress. Selecting any of the criteria reviewed as the appropriate failure criterion necessitates that the stress at the second peak be chosen as the strength because of its higher magnitude, however, the amount of strain is about 0.7% more than the first peak. Using a criterion for design of a structure in such a situation (the maximum accepted level), without determining the upper limit of the strain, the behaviour of the surrounding rock will not be controllable or predictable.

d) The present experimental investigation revealed that the effect of time on the stress-strain characteristics of jointed rock is very significant, and therefore, selecting a failure criterion on the basis of peak stress will not meet the necessary requirements. Figure 8.6 illustrates the stress-strain plots for the specimens containing planes of weakness with rough surfaces and orientation angle of 45°. The first plot shows the stress-strain curve for a specimen tested in the conventional way (applying constant strain rate throughout the test). The second plot shows the stress-strain curve for a specimen with the same joint orientation and under the same confining pressure, but with changing strain rates

at different points during the test. Comparison of the two plots reveals that the effect of strain rate on the magnitude of peak stress and also on the magnitude of strain is considerable. For instance, the peak stress in the first curve shows a magnitude more than 200 MPa with a strain about 1%, however, in the second curve the peak stress has decreased to less than 150 MPa with a strain of about 1.75%.

e) Increase or decrease in stress within a rock mass may affect the stress-strain characteristics of the rock. Figure 8.7 illustrates the stress-strain plots for the specimens containing rough surface joints with inclination angle of 45o and the same applied confining pressures. The first plot shows the stress-strain plot for the specimen in the conventional procedure, but the second one shows the stress-strain behaviour for the same specimen in which a cyclic loading (increase and decrease of stress at different points on the stress-strain curve), has been applied on the specimen. The stress and strain at peak for two cases differ significantly.

f) The experiments performed in this work show that the effect of stress relaxation on the stress-strain characteristics of rock is significant. Figure 8.8 illustrates the stress-strain plots for two jointed specimens with inclination of 45o for the same confining pressures. Plot one shows the stress-strain curve obtained in the conventional way, however, plot two shows the stress relaxation at different points on the stress-strain curve at a constant amount of strain for the relaxation time duration of 5 minutes. The resultant stress-strain curve obtained in this case is entirely different from plot 1 either in the magnitude of peak stress or strain in the two plots.

All of the cases referred to above prove, that selection of the peak stress as the basis of the failure criteria in discontinuous rocks is not adequate and reliable. Therefore, it is essential to develop a criterion on the basis of a parameter in addition to peak stress and capable of covering a wider area and adequately reliable for design purposes. Figures

8.9 to 8.11 illustrate the stress envelops for jointed specimens with orientation angles of 30 and 45° with smooth (saw cut) and rough (split breakage) joint surfaces. In each figure several curves are observed, each of which belongs to a certain magnitude of displacement ranging from 0.25% to 2%. The peak stress envelope has been also plotted in each figure. From the figures the significance of the strain magnitude or displacement through structure is clearly understandable. These figures reveal that for instance, when in a rock structure the differential strain is of paramount importance as in a foundation in rock, selecting a criterion in which the strain at peak is the major controlling parameter is unreliable. However, when the maximum allowable strain pertinent to the structure was determined, the related stress envelope is obtained.

8.10 PROPOSALS FOR A FAILURE CRITERION

The currently available criteria for discontinuous rocks employ the peak stress as the major controlling parameter while disregarding the influence of the associated displacement. A failure criterion on the basis of the experimental investigations carried out through this work is proposed to describe the behaviour of a jointed rock mass under various loading conditions and takes into consideration the major principal strain. This failure criterion is able:

- To support a sliding mode of failure.

It was shown (in chapter 6) that in jointed specimens in the range of the critical joint orientations, i. e. 45-65°, sliding movement along the joint is the predominant mode of failure. In this range of inclination the effect of the joint on both stress and strain is significant particularly when a great reduction in peak stress is observed and the stability of the jointed rock is controlled by the magnitude of displacement. For this reason in the proposed criterion the maximum axial strain at which sliding is initiated over the joint is taken as the major controlling parameter.

_ To take into account the applied loading conditions.

In chapter 7 it was shown that several parameters such as strain rate, stress relaxation and change of strain rate during loading period affect the stress-strain behaviour of rocks. In order to optimise all these effects the criterion has been based on the data obtained through different loading conditions investigated in this study.

Therefore, to start with, the failure criterion should be of the general form:

$$\sigma_1 - \sigma_3 = f(\varepsilon_1) \qquad (8.26)$$

For confining pressures ranging between 5-70 MPa the differential stress and its corresponding axial strain at which sliding commenced over the joint were calculated for the case of saw cut joints with 60° orientation which correspond to the most critical angle. A least square regression analysis was undertaken to fit the best curve on the values for Penrith sandstone giving an R value (coefficient of correlation) of 0.82 which combined with the trend of data.

The relationship obtained from the curve-fitting was of the form:

$$\sigma_1 - \sigma_3 = \frac{\varepsilon_1}{-0.0171\varepsilon_1 + 0.035} \qquad (8.27)$$

The fitted curve to the data is seen in figure 8.12 (plot 60S).

In order to achieve a comprehensive solution and to derive a criterion applicable to the jointed rock masses with wide range of joint orientation and joint surface roughness, similar curves were fitted to the data for 45 and 60° orientations for both smooth (saw

cut) and rough (split breakage) jointed specimens (figure 8.12 plots 45S, 45N and 60N). A curve for intact specimens of Penrith sandstone was also fitted to the data for the range of 0-70 MPa confining pressure (figure 8.12 plot INTACT). As is observed in figure 8.12 there is no common trend between the curves, since some are concave upward while other are downward. The curve for 60° orientation for saw cut joint (plot 60S) and the first part of the curve for 45° orientation with saw cut joint (plot 45S) are concave upward and the rest of the curves for both intact and jointed specimens are concave downward. This implies that:

(i) The stress-strain behaviour of jointed rocks is affected by the magnitude of confining pressure. For instance, plot 45S (figure 8.12) at low confinements (below 15 MPa) is concave upward, but at higher confining pressures (more than 15 MPa) the curvature has changed downward (see also table 8.1 for axial strain and differential stress at the initiation of sliding for various confining pressures).

(ii) The stress-strain behaviour for the joints with low and high degrees of surface roughness is different. The curve for saw cut joints (lower surface roughness) are concave upward; for the split joints (rough sliding surface), however, they are downward.

(iii) The stress-strain behaviour of jointed rocks differs with that of the intact rock significantly.

Therefore, the relation 8.27 cannot be representative of a jointed rock mass for different joint orientations and joint surface roughness. Furthermore, taking into consideration the differences in behaviour between lower and higher confinement, it seems that deriving a criterion for jointed masses should incorporate not only the differential stresses, but also the mean normal stress.

Table 8.1 Axial strain and differential stress at the initiation of sliding in various confining pressures for saw cut joint with 45° inclination.

confining pressure MPa	axial strain %	differential stress MPa
5	0.21	7.5
10	0.50	23
15	0.79	85
30	1.25	180
70	2.1	325

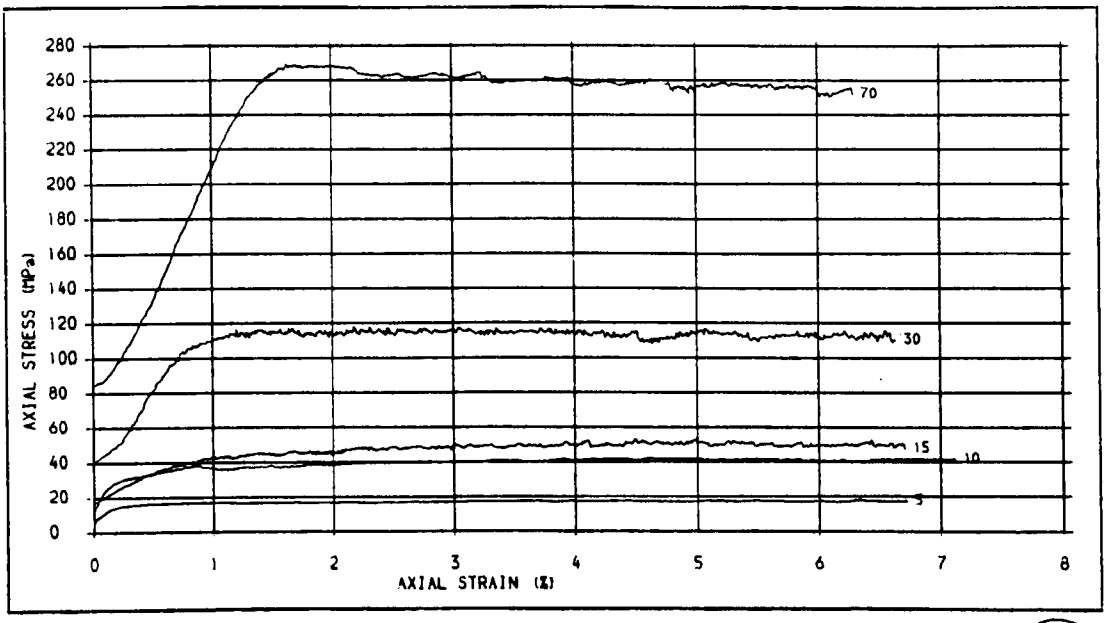

Fig. 81 . STRESS-STRAIN PLOTS FOR PS SPECIMENS WITH SAW CUT JOINTS, JOINT ANGLE = 60 DEG. CONFINING PRESSURES = 5, 10, 15, 30 AND 70 MPa.

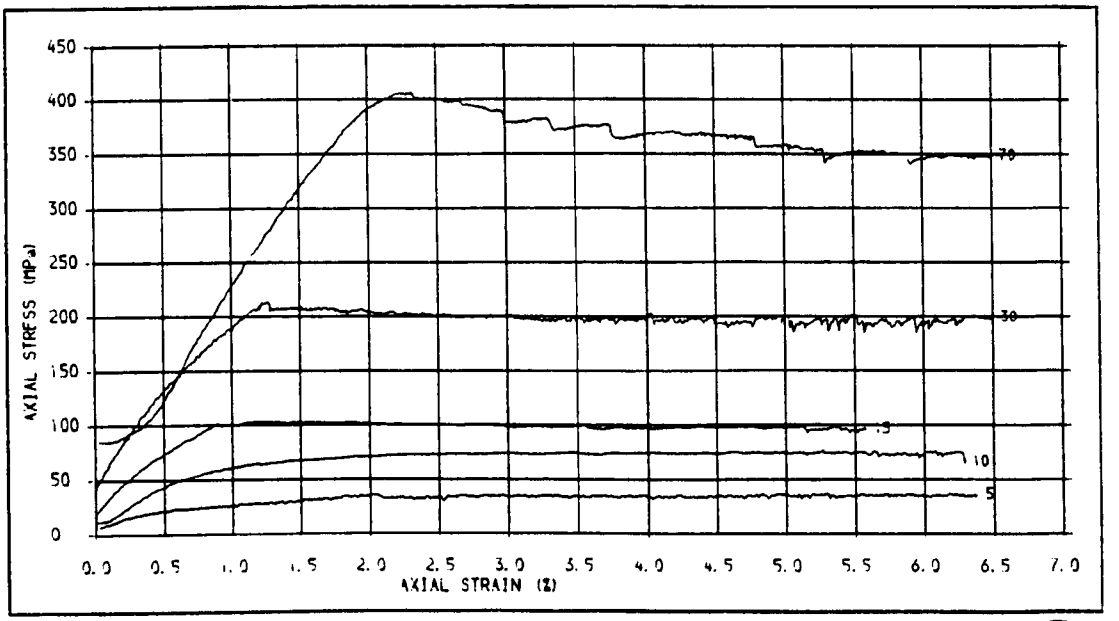

Fig. 82 . STRESS-STRAIN PLOTS FOR PS SPECIMENS WITH SAW CUT JOINTS, JOINT ANGLE = 45 DEG. CONFINING PRESSURES = 5, 10, 15, 30 AND 70 MPa

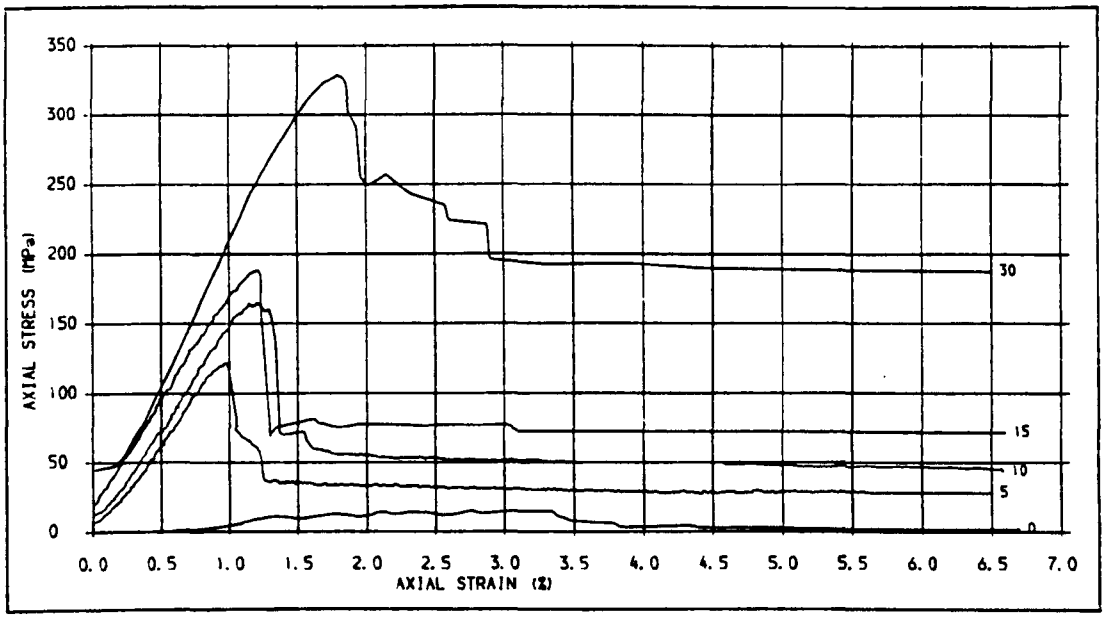

Fig. 83 . STRESS-STRAIN CURVES FOR PS SPECIMENS WITH SAW CUT JOINTS, JOINT ANGLE = 30 DEG. CONFINING PRESSURES = 0, 5, 10, 15 AND 30 MPa.

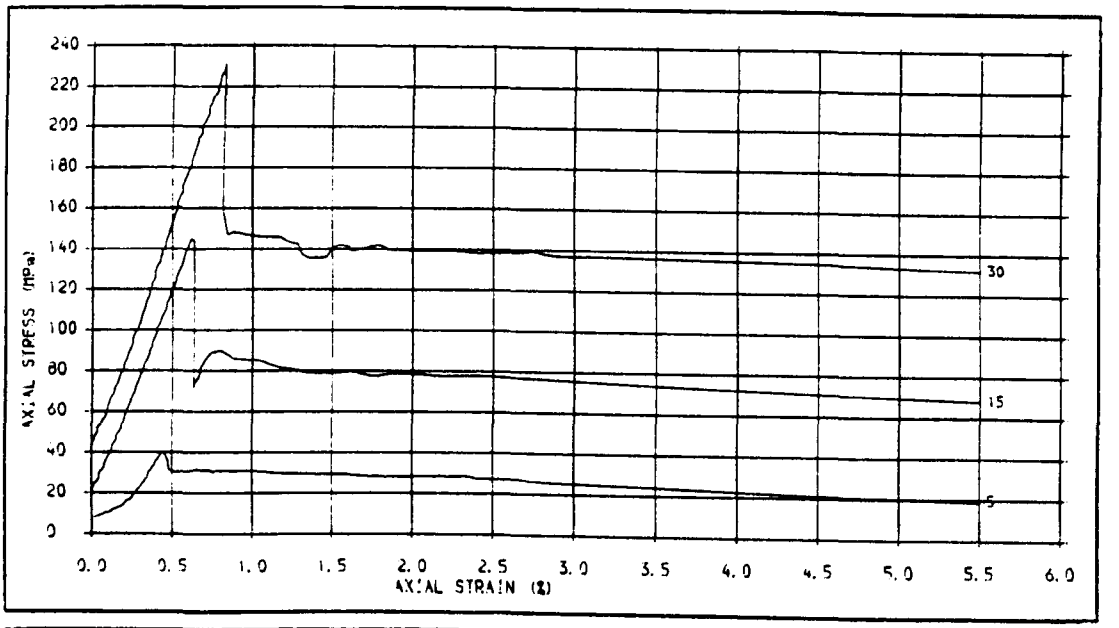

Fig. 84 STRESS-STRAIN CURVES FOR PS SPECIMENS WITH NATURAL JOINTS, JOINT ANGLE = 60 DEG. CONFINING PRESSURES = 5, 15 AND 30 MPa.

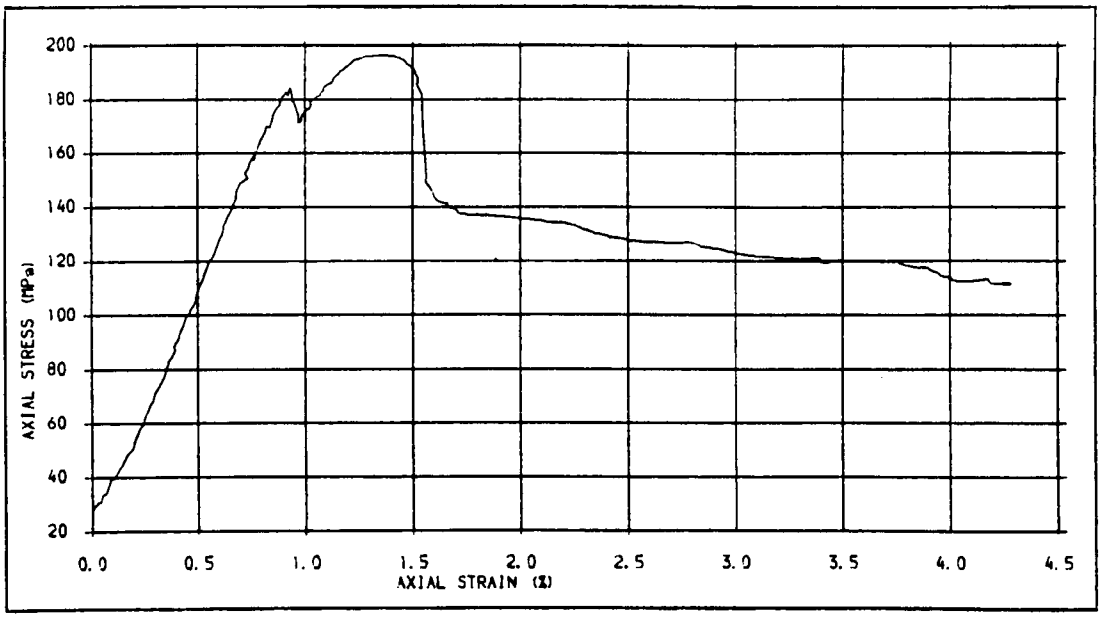

Fig. 85 . STRESS-STRAIN CURVE FOR A PS SPECIMEN WITH NATURAL JOINT, JOINT ANGLE = 45 DEG. CONFINING PRESSURE = 15 MPa.

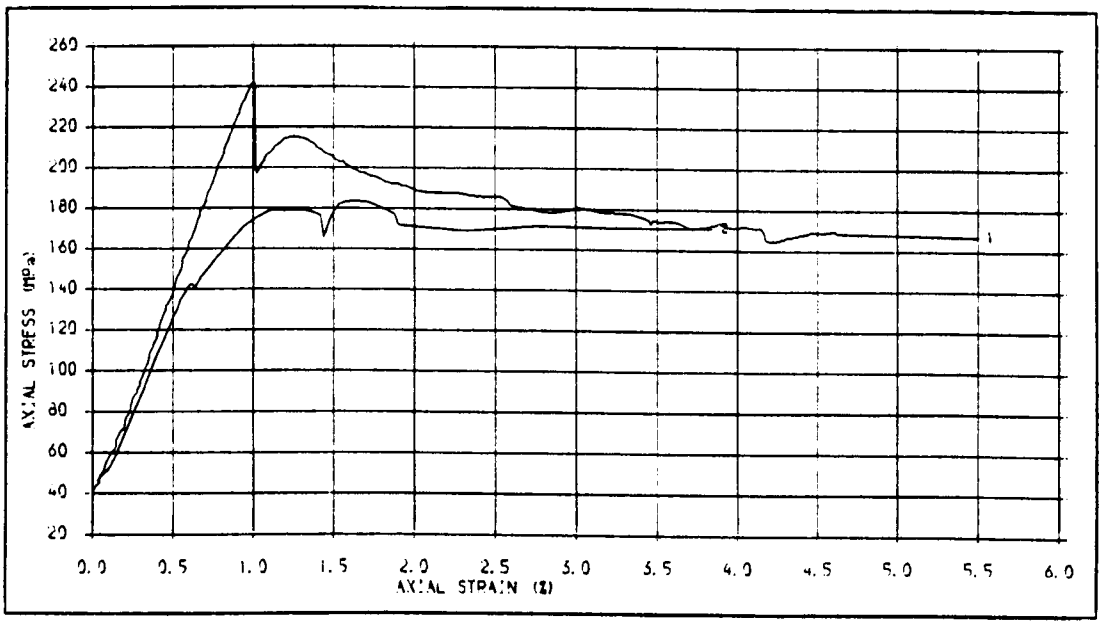

Fig. 86 . STRESS-STRAIN CURVES FOR PS SPECIMENS WITH NATURAL JOINTS, JOINT ANGLE = 45 DEG. PLOT 1. CONSTANT STRAIN RATE, PLOT 2. CHANGING STRAIN RATES, CONF. PRES. = 30 MPa

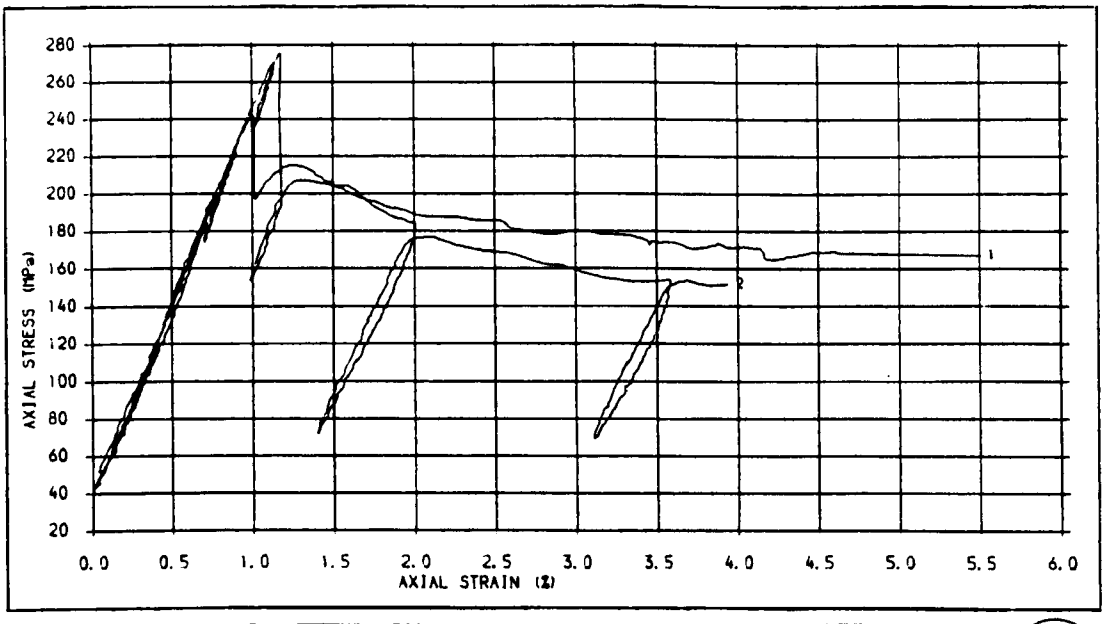

Fig. 87 . STRESS-STRAIN CURVES FOR PS SPECIMENS WITH NATURAL JOINTS, JOINT ANGLE = 45 DEG.
PLOT 1. CONSTANT STRAIN RATE, PLOT 2. CYCLIC LOADING, CONF. PRES. = 30 MPa

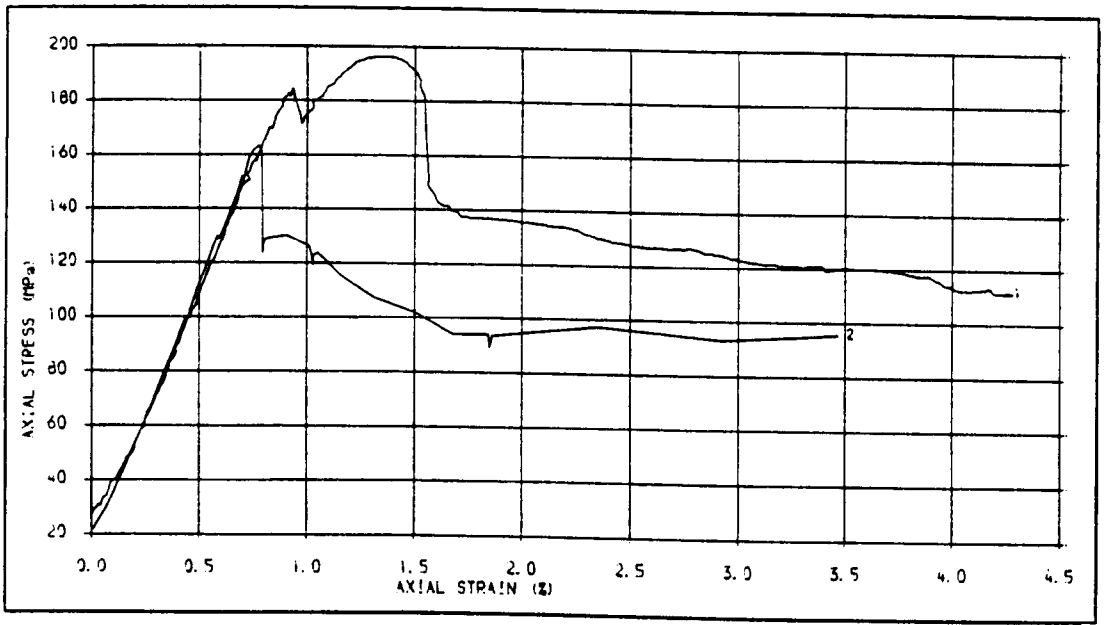

Fig. 88 . STRESS-STRAIN CURVE FOR PS SPECIMENS WITH NATURAL JOINT, JOINT ANGLE = 45 DEG.
PLOT 1. ORDINARY TEST, PLOT2. RELAXATION TEST, T, CONFINING PRESSURE = 15 MPa.

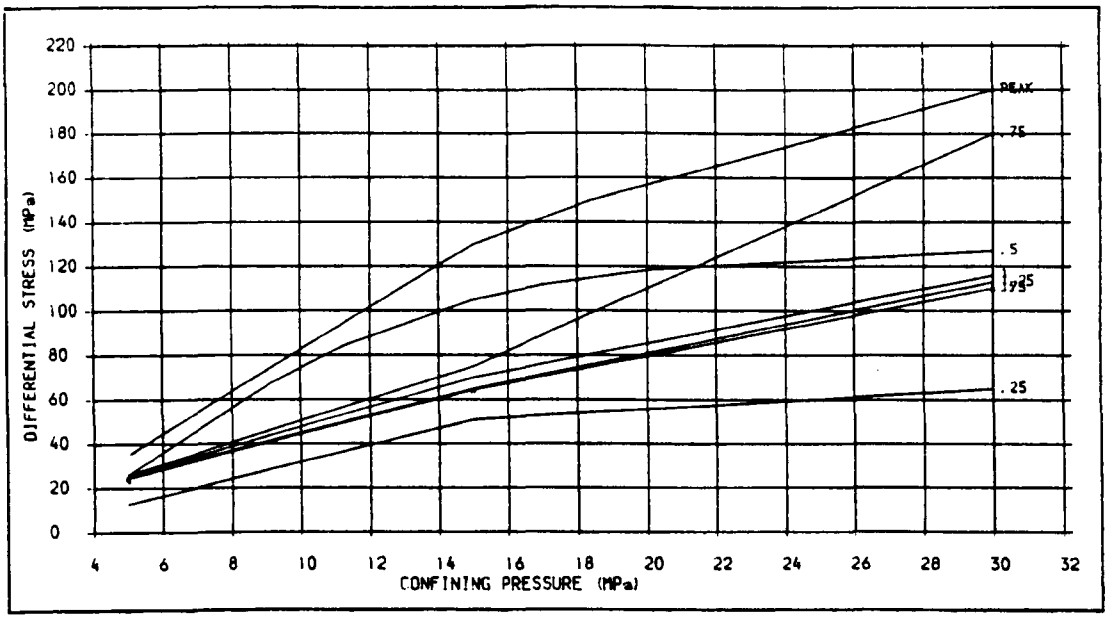

Fig. 89 . DIFFERENTIAL STRESS-CONFINING PRESSURE ENVELOPES AT DIFFERENT AXIAL STRAINS FOR PS SPECIMENS WITH NATURAL JOINTS, JOINT ANGLE = 60 DEG.

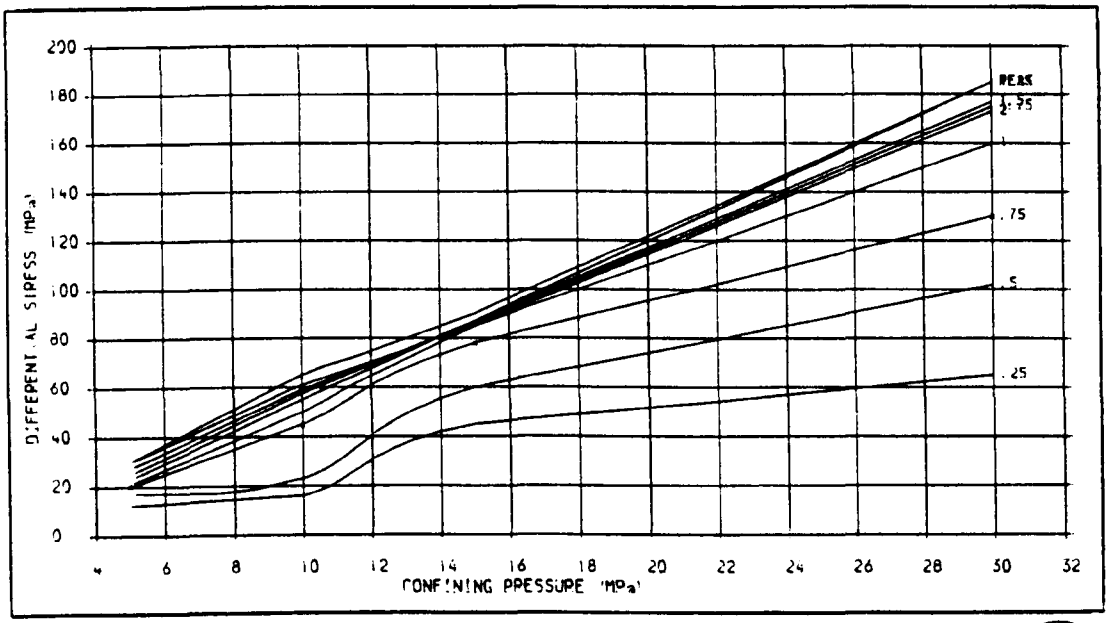

Fig. 810 .DIFFERENTIAL STRESS-CONFINING PRESSURE ENVELOPES AT DIFFERENT AXIAL STRAINS FOR PS SPECIMENS WITH SAW CUT JOINTS, JOINT ANGLE = 45 DEG.

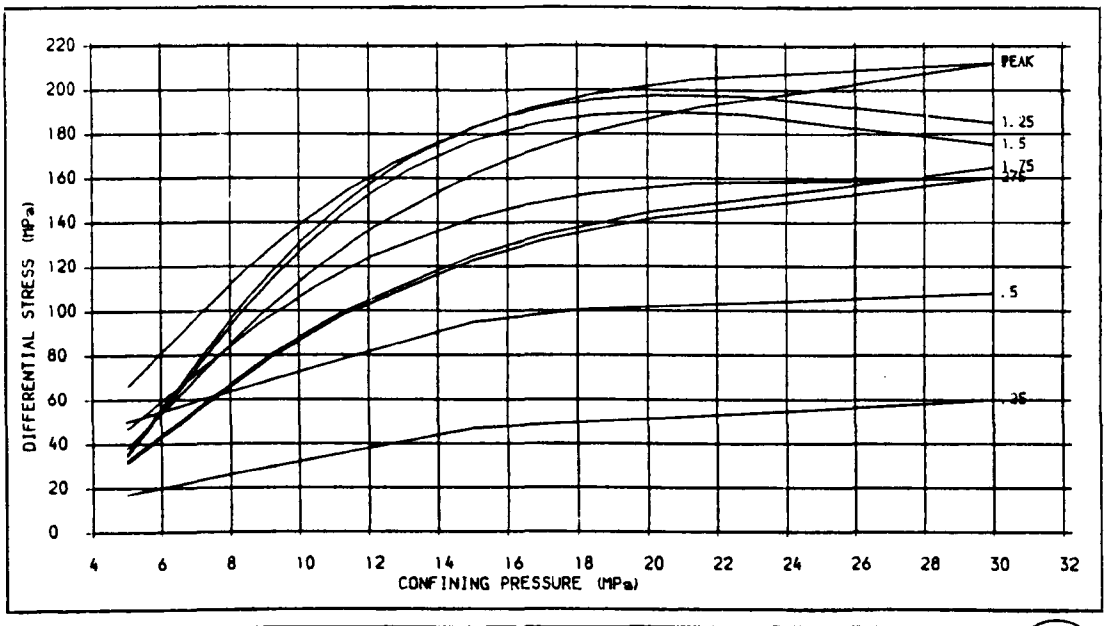

Fig. 3.1 .DIFFERENTIAL STRESS-CONFINING PRESSURE ENVELOPES AT DIFFERENT AXIAL STRAINS FOR PS SPECIMENS WITH NATURAL JOINTS, JOINT ANGLE=45 DEG.

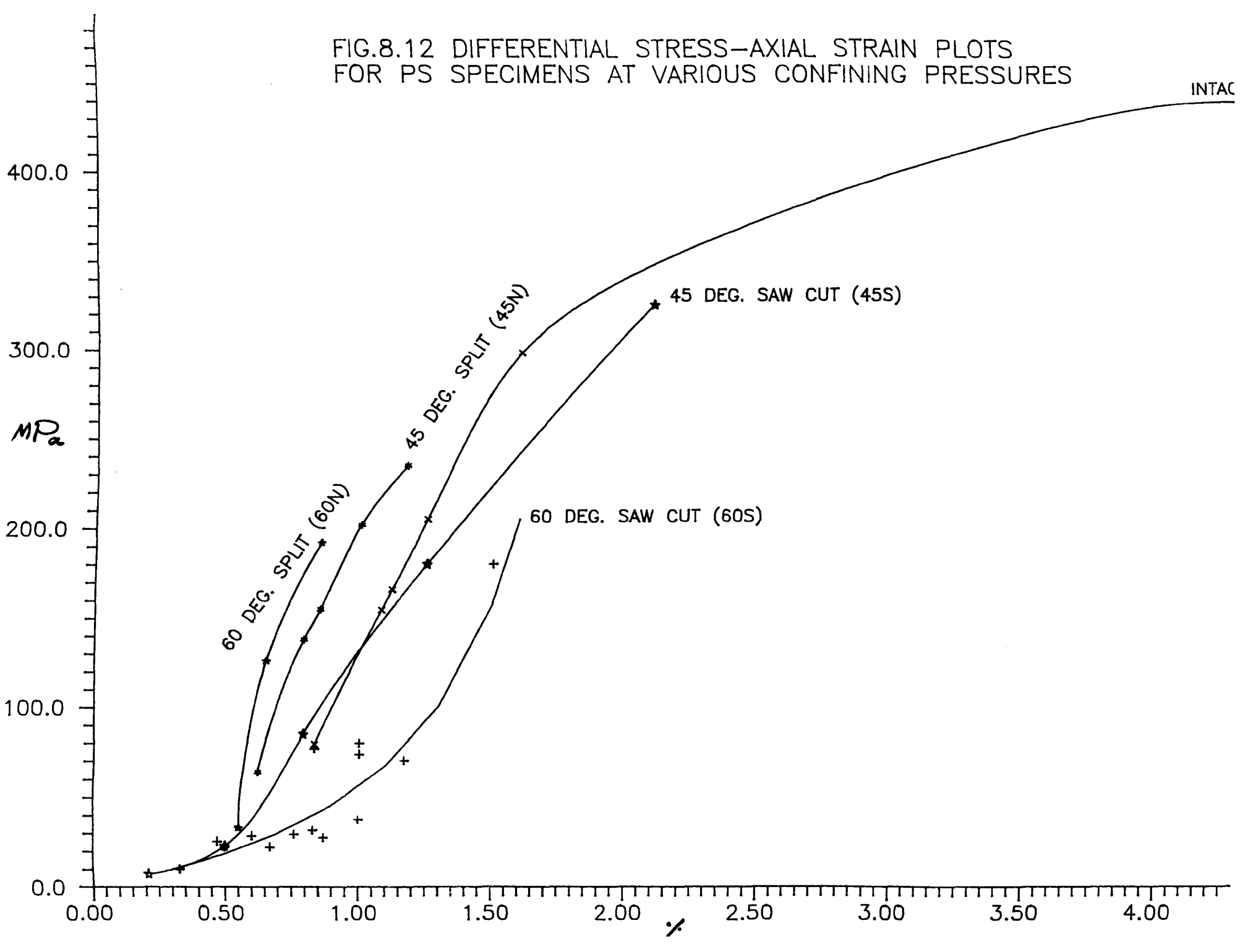
FIG.8.12 DIFFERENTIAL STRESS–AXIAL STRAIN PLOTS
FOR PS SPECIMENS AT VARIOUS CONFINING PRESSURES
INTAC
400.0
300.0
200.0
100.0
0.0
MPa
0.00
0.50
1.00
1.50
2.00
2.50
3.00
3.50
4.00
%
45 DEG. SAW CUT (45S)
45 DEG. SPLIT (45N)
60 DEG. SAW CUT (60S)
60 DEG. SPLIT (60N)

CHAPTER 9

STICK-SLIP CHARACTERISTICS OF JOINTED ROCK

9.1 INTRODUCTION

Stick-slip is a significant phenomenon in the study of metals especially where stick-slip at high velocity of slider movement is a troublesome phenomenon as in the machine-tool industry (Brockley, 1968). However, as this phenomenon has been observed by many workers in most studies of sliding friction in rocks, and as it is commonly believed to be one of the major approaches to the problem of understanding the earthquakes mechanism (Bridgman, 1936, Byerlee, 1970), considerable attention has been paid to it in rock mechanics.

Most of the laboratory experiments to study stick-slip phenomenon on rock surfaces have been made on small cylindrical specimens irrespective the end specimen conditions and stress system change during sliding.

Jaeger(1959) studied the stick-slip behaviour of rock on three different surfaces, namely, bare flat surfaces, surfaces of shear failure ,and plaster joints.The specimen diameter was 50.8 mm and the cylinder rests with its lower end on a spherical seat. In the bare flat surfaces there was a short initial period of sliding during which intimate contact was established over almost the whole surface. When this happened, subsequent movement was by a violent stick-slip process of large amplitude. In rock with surfaces of shear failure occasional small stick-slip occurred in the stress-strain curves. But in plaster joints after a large amount of displacement along surfaces and raising confining pressure to 100 MPa a series of small stick- slip occurred.

Brace and Byerlee(1966) have reported similar experiments on sawn surfaces and surfaces of shear fracture. The experiments were performed on dry Westerly granite for specimens 12.5 mm in diameter and 31.7 mm long. Stick-slip occurred under a wide range of conditions. Some of the specimens were saturated with water under a slight pore water pressure, whereas others were air dried. The normal stress on the sliding surfaces ranged from 1 MPa to 1.7 GPa. Some surfaces were smooth and slickensided, other were ground to a wide range of roughness, and still others were rough fracture surfaces which had been fitted back together. Stick-slip accompanied sliding on old or newly formed fractures under all of these conditions.

In other experiments Byerlee and Brace (1968) studied some important aspects of stick-slip for seven different rocks, on ground surfaces produced by saw cut, and joint shear surfaces produced by stressing the specimens to fracture. All specimens were 38 mm long and 15.8 mm in diameter. In these experiments the effect on stick-slip of strain rate, loading machine stiffness, and rock type have been considered. The rocks used in this study were divided into two types with respect to stick-slip. Type one rocks showed stable sliding on joint surfaces at low pressure, and stick-slip at intermediate and high pressures. Type two rocks showed stable sliding up to the highest pressures at which motion on a joint took place. They also showed that neither loading machine stiffness nor strain rate has much effect on the amplitude of the stress drop in stick-slip. The triaxial apparatus was that of Brace (1964) in which there was direct contact between piston and top platen. The interfaces between the specimen and steel end platens were not lubricated.

Byerlee(1967b), Byerlee and Brace(1969),Summers and Byerlee(1977) and Lockner et al(1982) made subsequent experiments in which the same triaxial apparatus as before was used. The specimens used were also very small (less than 30 mm in diameter) and no modification made on the specimen end platens.

Due to some disadvantages of the triaxial system, some workers have devised new apparatuses to investigate the sliding friction of rock surfaces. Most of them are based on the direct shear system.

Rae (1963) used a rotating system in which a slider was used on the curved surface of a rotating cylinder.

Hoskins et al(1968) used a symmetrical system in which one block with planar surface and parallel faces is forced between two others. A relatively large surface of sliding may be used in this apparatus. Stick-slip oscillations with increasing amplitudes were observed on very smooth surfaces, but not on rough ones.

Dieterich (1972 a,b) used a similar system to Hoskins et al (1968), but somewhat smaller. The blocks had dimensions of up to 60.0X60.0 mm and a thickness of 15 mm. Stick-slip oscillations have also been reported by this author on only smooth surfaces at all normal stresses between 2 to 85 MPa.

Drennon and Handy(1972) used a direct shear device to conduct the stick-slip tests. The shear apparatus consists of a large stationary rectangular specimen holder with a smaller movable holder placed on top, allowing about 25 mm travel. Normal load is transferred to the upper holder by a ball and socket. Stick-slip tests were carried out on a limestone under light loads ranging from 0.075 to 2 MPa. The initiation of stick-slip was found to depend upon the temperature increase. Below 100^{o} C there was no stick-slip movement.

All the testing machines referred to above, have serious design drawbacks which limit their use and introduce difficulties that make the results unreliable. In the direct shear

devices a block of rock is pushed to slide between two stationary blocks. The blocks are loaded normal to the sliding surfaces by a hydraulic ram. Consequently, two large moments are produced in the machine, resulting in high stress gradients over the sliding surfaces. Low normal stresses are produced across the sliding surfaces near the leading edge of the central block and high stresses near the trailing edge. An additional difficulty is that, two sliding surfaces are regulating the movement. It is generally of interest, however, to understand the behaviour of a single isolated surface (Scholz et al,1972). Chappell(1975) showed that when slip is induced in a system of blocks, there is always an associated moment or torque imposed on the surrounding blocks. Therefore, it is expected that the findings obtained on the basis of those procedures have been affected by the system's drawbacks.

Scholz et al(1972), in order to avoid these difficulties, developed an apparatus in a biaxial loading frame fitted with two 1 MN hydraulic rams and capable of operating at moderate normal loads, to study frictional sliding of granite. In subsequent studies by Johnson(1973,1975), Johnson and Scholz(1976), the same system was used to investigate stick-slip movements.

This system also has its own disadvantages, particularly it is not capable of high normal load. Furthermore, it seems that when a large amount of displacement takes place along the joint surface, misalignment through the specimen will occur.

9.2 OBJECTIVES

As pointed out, most of the experimental investigations performed on the stick-slip phenomenon have not been conducted employing favourable testing conditions. Specimen size, particularly undesirable testing systems have led to opposite, and perhaps misleading observations and conclusions. As a consequence, the following aspects were chosen for experimental investigation.

-To ascertain the overall effects of testing system constraints in relation to stick-slip phenomenon, and then, on the basis of the modified cell-specimen system to determine;

-the role of rock characteristics;

-the effect of surface roughness;

-the axial strain rate effects on stick-slip characteristics; and finally, assessment of this phenomenon

-in the presence of water (wet surfaces);

-in sliding of two different rocks on each other.

9.3 EXPERIMENTAL PROCEDURES

The experiment was carried out by the 5 MN servo-controlled testing system in the same way as described in chapter 3, the only difference being that, in this case, the joint inclination was only made 60^{o} relative to the direction of minor principal stress. Three type of surfaces were used: saw cut, ground and rough surfaces. Because of difficulties in making enough specimens, especially granite, some of the specimens were reused after regrinding or producing required roughness. Despite the fact that two flexible membranes were fitted over the specimens, some initial tests came to abrupt ends when confining pressure was applied. Examination of the ruptured membranes showed very small holes in the parts located at the sharp ends of the specimens. The problem was solved by fitting extra pieces of rubber over the sharp portions, before fitting the two flexible membranes.

9.4 SELECTION OF TYPE OF ROCKS

The main rocks during the experiments were three types of sandstones. However, when these were tested in the modified system, stick-slip was not observed. For this reason,

the decision was made to develop the investigations on some other rocks, and also to increase confining pressure up to 70 MPa, the highest limit of pressure applicable with the available facilities in the departmental laboratories. In order to achieve comprehensive and broad results, three other rocks were selected on the basis of their origins i.e igneous, sedimentary and metamorphic types. Therefore, a granite as an igneous, a limestone as a sedimentary and a slate as a metamorphic rocks were selected. The selected rocks with their petrological descriptions have been listed in appendix B. Selection of the granite was of particular interest, because considerable work on stick-slip phenomenon has been carried out on granite.

9.5 EVALUATION OF TESTING SYSTEMS IN RELATION WITH STICK-SLIP PHENOMENON

As described in chapter 4 the type and configuration of seat and platen in the cell-specimen system have significant effects on the sliding characteristics of the joint surface. In order to show this significance, a series of tests was performed, using three different combinations of seats and platens at the top and bottom of the specimens. In the first system a spherical seat was used at the top and a platen at the bottom; in the second system a steel disc was used at the top and another at the bottom, and in the third system, pairs of hardened steel discs were polished and lubricated with a molybdenum disulphide grease and used in the same way as in chapter 4 (modified cell-specimen system). Different confining pressures were applied, ranging from 5 to 70 MPa throughout the work. Stick-slip was observed very clearly during sliding in all of the rocks used in the experiment in the case of first and second configurations, namely when using one spherical seat or two flattened steel discs with no lubricant grease, as is often the case. In the third configuration, stable sliding occurred during movement for all of the rocks, except for granite in which very clear stick-slip took place for different confining pressures applied .

Figures 9.1 to 9.4 illustrate the typical plots obtained through three testing systems for various confining pressures. In systems one and two as sliding commenced along the joint surfaces a progressive change in the geometry of the cell-specimen system is started. As a result, two halves of the specimen are not in entire contact with each other during sliding, particularly for a large amount of shear displacement along the joint surfaces, the contact area between two parts reduces to only a limited portion. Consequently, an instability dominates the system and subsequently subsidiary fractures occur which appear in the form of stick-slip. Examination of the specimens tested by the first and second systems showed subsidiary fractures in the sharp ends of the specimens; however, such fractures did not occur in the specimens tested in the modified system (see chapter three plate 4.6). For this reason, as figure 9.1 shows, stick-slip in the specimens tested by systems one and two have occurred after a considerable shear displacement along the joint. However,in the third system, for example in granite, by starting sliding, stick-slip has also been started (figures 9.3 and 9.4). In fact, in the first and second systems, stick-slip sliding is not the property of the rocks , but the property of the systems. In other words, stick-slip in systems one and two is due to misalignment or in fact, an instability in the cell-specimen system. If such instability can be assumed to occur between two sides of a fault, systems one and two may be considered as appropriate models to simulate the phenomenon of stick-slip in any type of rock, and probably an appropriate model to evaluate shallow depth earthquakes. The third system is a very reliable model to assess the stick-slip characteristics in the frictional sliding of rocks in which this phenomenon occurs intrinsically such as granite.

The rest of the work is based on the experiments conducted by the modified system to study some important aspects of the stick-slip phenomenon in a correct and reliable way.

9.6 GENERAL OBSERVATIONS

In the series of tests performed in this experiment, especially on granite specimens, observations of interesting events either during the tests or on examination of the specimens after tests, are important in understanding the characteristics of stick-slip and the controlling mechanism of the phenomenon. Stick-slip was observed only in the granite specimens during sliding tested in the modified cell-specimen system. Plot one in figure 9.18 illustrates a cycle of stick-slip in a magnified scale. There is a similarity between this graph and the typical stress-strain plot in a very brittle rock. It seems that it might be possible to obtain the post peak portion of each cycle of stick-slip if the servo-controlled and stiff testing system possesses a very high sensitivity and stiffness.

A considerable increase in confining pressure was observed in each cycle of stick-slip when slip occurred. This is an indication of a volume change in the specimen or the joint dilation during a very short time of slip which is very similar to the change in the volume of an intact specimen in the uncontrollable post peak portion of the stress-strain curve in a brittle rock. Each cycle of stick-slip was also accompanied by an abrupt and violent slip which was very similar to the failure of a very hard and brittle rock.

A very interesting observation was the occurrence of successive violent slips on the sliding surfaces when the confining pressure was reduced to zero, thus stopping the test. This phenomenon might be an indication of a high interlocking of the asperities through the joint during sticks and then occurrence of violent fractures during slips.

On examining the specimens tested at different confining pressures, the following aspects were observed:

a) The sliding areas, the magnitude of the gouge produced and the depth of the grooves for different confining pressures and also in different rocks were not the same. In a lower confining pressure or in fact in a lower deviatoric stress, the damaged areas were considerably less than those of a higher pressure (plate 9.1). This was also different in different rocks. The damaged areas in a hard rock were less than those of a soft, when the same confining pressure was applied (compare plates 9.2 and 9.3). Proportional to the contact areas (damaged areas) the stress drops were different in different confining pressures. This observation indicates that a higher confining pressure results in an increase in axial stress, thus a further real contact area which leads to a higher stress drop in each cycle of stick-slip when slip occurs.

b) A margin of black ash was observable along the edge of each half of the specimens, particularly those tested in higher pressures (plate 9.2 and 9.3). Examination of the ash revealed that it was because of the intrusion of the rubber membranes into the joint during sliding under a high confining pressure. A smell of burned material after high pressure tests is an indication of the intrusion of the rubber into the joint.

Figure 9.5 illustrates a typical stress-strain plot for a jointed granite specimen in which stick-slip has occurred regularly. Five stages in the sliding mechanism can be isolated:

Region i

This region is indicated by an initial non-linearity of the axial stress-strain curve. It may be because of compaction and intrusion of the asperities in two halves of the specimen as loading is started.

Region ii

There is a part in this stage where it may be assumed that the asperities are deformed elastically.The upper limit of this region is the point at which sliding on the joint

surface is initiated. Region i and ii are similar to the mechanism of fracture in brittle rocks. Neither in region i nor ii stick-slip occurs.

Region iii

Sliding along the joint surface begins in this region and it is accompanied by a few irregular stick-slip with low and unequal amplitudes. In fact, instability through the sliding movement is started in this part.

Region iv

In this part of the curve a course of regular stick-slip with the same magnitude in stress drops is observed.

Region v

The stick-slip cycles, in this region, become irregular again, but with higher stress drop in each cycle.

The irregularity and regularity in stress drop in region iii to v may be attributed to the fact that, in the beginning of sliding the asperities have not been sheared off entirely, therefore, stick-slip in this part (region iii) are irregular with low amplitudes. However, when sliding continues considerably the irregularities over the sliding surfaces are diminished and gouge is produced. Thereafter, the sliding surface will be homogeneous. Consequently, regular stick-slip with nearly equal stress drops will be expected (region iv). When sliding continues during a long period of time the damaged areas through sliding surfaces develop and a layer of gouge unequal in thickness covers the sliding surfaces. In this condition irregular stick-slip unequal in stress drops are expected (region v). Eventually, continuation of sliding is expected to result in disappearing stick-slip and the beginning of stable sliding throughout.

It seems that after a large amount of displacement over sliding surfaces, a transition from stick-slip to stable sliding occurs. In order to simulate a large amount of displacement along a joint or fault, a number of tests were performed on the same specimen in a multi-stage test procedure. Figures 9.12, 9.13 and 9.14 illustrate the stress-strain plots of three runs on granite in which figure 9.12 shows the first run on a cleaned-used sliding surface. At 10 and 30 MPa confining pressures stick-slip was not observed at all. At 50 MPa confinement stick-slip was clearly observed; however, after seven stick-slip (figure 9.12), stable sliding occurred in a short interval of movement, then stick-slip continued with variable amplitudes. After increasing confining pressure to 70 MPa sliding resulted in regular stick-slip with higher amplitudes. In the second run (figure 9.13) at 50 MPa confining pressure stick-slip was not observed, however, increase of confining pressure to 70 MPa stick-slip occurred in a regular manner with, of course, a lower amplitude relative to the first run at the same confining pressure. In the third run (figure 9.14) stick-slip was diminished at different levels of confining pressures and stable sliding continued throughout. Comparison of the plots 9.12 to 9.14 shows that stress levels in the stable sliding portions are higher than in the stick-slip portions for the same confining pressures. On examination of the specimen after each run, a layer of gouge was observed over the sliding surfaces which in the third run was considerably thicker. In fact, because of production of a relatively thick layer of gouge over the sliding surfaces, a transition from stick-slip to stable sliding occurs. This is an important implication in predicting the behaviour of a fault in its long term movement, for example whether earthquakes will occur or not.

9.7 FACTORS INFLUENCING STICK-SLIP CHARACTERISTICS

There are many factors affecting the of stick-slip characteristics and behaviour, and most of them have been investigated before. On the basis of the modified cell-specimen system some of the significant factors are investigated.

9.7.1 EFFECT OF ROCK TYPE

Among the rocks studied in this experiment stick-slip was only observed in sliding surfaces of granite. Figure 9.19 illustrates stress-strain plots for granite specimens with saw cut joints tested at 10, 30 and 70 MPa confining pressures. Stick-slip was observed in all cases even at 10 MPa confining pressure. In ground sliding surfaces in granite, however, below 30 MPa confining pressure stick-slip disappeared (figure 9.4).

Figures 9.15, 9.16 and 9.17 illustrate stress-strain plots for two types of sandstones, slate and limestone respectively. Stick-slip was not observed during sliding in any of them, neither sedimentary nor metamorphic rocks in the range of confining pressures applied. Stick-slip in granite specimens was observed with the beginning of sliding, in the other rocks tested, even after 10 mm movement over joint surfaces, stick-slip did not occur at all. The microscopic thin section description of the rocks tested (appendix B) shows that in spite of similarity in some minerals of the rocks with those of granite such as quartz, stick-slip was not observed in sliding movements of the rocks tested other than granite. This implies that the type of mineral is not the only parameter to cause stick-slip to occur, but other factors such as hardness, crystalline structure, porosity and presence of soft minerals such as clay mineral may also have a fundamental role in the occurrence of stick-slip. Furthermore, it seems that stick-slip is an intrinsic property of some specific rock types in which stick-slip may occur under appropriate conditions (level of confining pressure, surface roughness, surface moisture contents, history of sliding surfaces and so on).

Stick-slip has been observed by some workers in the sliding movement of some rocks other than granite. Drennon and Handy (1972) observed stick-slip in limestone at and

above a normal load of 0.3 MPa (30 kg/cm), and Dieterich (1972) observed stick-slip on porous sandstone and some other rocks in a range of 2 to 85 MPa confining pressure.

9.7.2 EFFECT OF SURFACE ROUGHNESS

Three types of surfaces were used in this work: saw cut, ground and cleaned-used surfaces. Cleaned-used surfaces mean those specimens that have been used in the previous tests after cleaning the sliding surfaces from gouge. Stick-slip was observed in granite in all types of the surfaces used, but in different confining pressures for the three different surfaces. In the saw cut surfaces stick-slip was observed in the range of 10-70 MPa confining pressures (figure 9.19). However, on the ground and cleaned-used surfaces below 30 MPa confining pressures stick-slip disappeared (figures 9.4 and 9.12). This behaviour may be attributed to the fact that in a saw cut sliding surface, because of further irregularities with respect to a ground surface, contact between two surfaces is limited to only a portion of the sliding area (the tips of asperities are in contact), and therefore the applied confining pressures in the range of 10-30 MPa and the resulting deviatoric stress is high enough to interlock the asperities to the required level to cause stick-slip. In a ground sliding surface, however, because of a further real contact area between two surfaces (relative to the saw cut joint) the differential stress level at which stick-slip can possibly occur will increase. In reused sliding surfaces, although the sliding surfaces have been cleaned there is a considerable filling material (gouge) on the sliding surfaces which means a higher differential stress is required to interlock the asperities for the occurrence of stick-slip.

Figure 9.19 shows the stress-strain plots of saw cut granite in 10, 30, and 70 MPa confining pressure. In 10 MPa the stick-slip amplitudes was very small with very low stress drop in each cycle. Figure 9.4 shows that stick-slip in the ground surfaces has diminished below 30 MPa confining pressure, however, at this level of applied pressure,

after about 3% axial strain stick-slip has occurred with very low amplitudes which are very similar to the stick-slip on saw cut surfaces at 10 MPa confining pressure (figure 9.19 lower plot). By increasing confining pressure to 50 MPa (figure 9.4) and also to 70 MPa (figure 9.5), the occurrence of stick-slip is very clear with much higher amplitudes. When confining pressure decreased to 30 and then to 10 MPa (figure 9.4) stick-slip disappeared again and stable sliding continued. Presumably, this is due to the development of a layer of gouge over the sliding surfaces, which prevents entire contact and interlocking between asperities. In cleaned-used surfaces as in figure 9.12 the same behaviour as ground surfaces was observed. Up to 50 MPa confining pressure stick-slip has not occurred; in 50 and 70 MPa confining pressures, however, stick-slip is clearly present.

9.7.3 STRAIN RATE EFFECTS

A number of tests were carried out at strain rates of 2.08×10^{-6}/s (0.0125% /min), 4.17×10^{-5}/s (0.25% /min), 8.33×10^{-4}/s (% /min), and 4.17×10^{-3} /s (25% /min). Figure 9.19 illustrates the typical plots obtained. For 30 MPa confining pressure loading began at a strain rate of 4.17×10^{-5} /s (0.25%/min). After a number of stick-slip movement (figure 9.19 plot 30, the first portion) the strain rate was increased to 4.17×10^{-3} /s (second portion of the plot). For 70 MPa confining pressure (figure 9.19 first part of the top plot) loading began at a strain rate of 4.17×10^{-5}/s (0.25%/min). After 10 stick-slip movements, strain rate was reduced to 2.08×10^{-6}/s (second part of the top plot in figure 9.19). Finally after three stick-slip occurred the specimen was unloaded, and then immediately loaded at a fast strain rate of 8.33×10^{-4}/s (5%/min) as in figure 9.19 plot 70/3.

In general, two significant events are observed among these runs.

(i) As strain rate decreased to a slower rate, the differential stress increased to a higher value in each stick-slip amplitude.

(ii) Increase in strain rate resulted in decrease in stress drop in each cycle of stick-slip.

Analysis of shear and normal stresses over the sliding surfaces reveals that an increase in strain rate results in a decrease in the coefficient of static friction. The coefficient of static friction, u_s, is defined as t/s where t is the shear stress at which a stick-slip occurs.

Shear and normal stresses can be obtained as follows:

$$\sigma = (\sigma_1 + \sigma_3)/2 - (\sigma_1 - \sigma_3)/2 \cos 2\beta \qquad (9.1)$$

$$\tau = (\sigma_1 + \sigma_3)/2 \sin 2\beta \qquad (9.2)$$

In which, β is the joint orientation angle relative to specimen axis. In this experiment as $\beta = 60^o$, t may be given by:

$$\sigma = (\sigma_1 + \sigma_3)/2 - (\sigma_1 + \sigma_3)/4 \qquad (9.3)$$

$$\tau = (\sigma_1 - \sigma_3) \times 0.433 \qquad (9.4)$$

using $\mu_s = \tau/\sigma$ the following equation will be obtained.

$$\mu_s = 1.732(\sigma_1 - \sigma_3)/(\sigma_1 + 3\sigma_3) \qquad (9.5)$$

Equation (5) shows that m is proportional to the $(\sigma_1-\sigma_3)$, i.e. the deviatoric stress; it may be concluded that increase in strain rate leads to decrease in deviatoric stress or in fact reduction in the static coefficient of friction.

Figure 9.19 (plot 30 the second part of the curve from about 1.2% axial strain) illustrates the significance of a very fast strain rate. As can be seen, the level of stress has dropped significantly with respect to the first portion of the curve and the stick-slip amplitudes are very irregular. It implies that at a much faster strain rate, stick-slip may be disappear throughout sliding.

The dependency of the static coefficient of friction to time seems to be a logarithmic function, since an order of magnitude change in strain rate produces a few percent change in m_s . This dependency has shown in figure 9.20 for 70 MPa confining pressure and strain rates of 2.08 $x10^{-6}$/sec (0.0125%/min),4.17 $x10^{-5}$/sec (0.25%/min) , and 8.33 $x10^{-4}$ /sec.(5%/min). As is observed the relationship is not linear and if the curve is extrapolated from its two ends some interesting findings result. The lower end of the curve has intersected the X axis (strain rate). This implies that at a very fast strain rate m decreases dramatically and therefore stick-slip diminishes through sliding. On the other hand, the upper end of the curve continues asymptotically (parallel to the X axis) and it implies that at a very slow strain rate the static coefficient of friction tends to a constant value.

Time dependency in the stick-slip phenomenon has been reported by other workers. Byerlee and Brace (1968) in their experiment did not observed any significant effect, however, Deterich (1970), Scholz et al (1972) and Engelder et al (1975) showed that strain rate affects stick-slip characteristics.

9.8 FRICTIONAL SLIDING IN WET SURFACES

In order to assess the stick-slip characteristics in wet surfaces during sliding a series of tests were performed on granite with sliding surfaces of variable moisture content. The

amount of water added to moisten the sliding surfaces of the granite specimens for each series of test were: 0.615, 0.2171, 0.0362 mg/g respectively. In the first run, the surfaces of two halves of the specimen were left in contact with water for 15 minutes. As soon as the sliding surfaces became quite wet the test was performed immediately. In the second run, the same procedure was repeated but the amount of water was decreased to 0.2171 mg/g on the sliding surfaces. In the third run, moisture content was decreased significantly so that there was no observable water on the surfaces (0.0362 mg/g). Figures 9.10 and 9.11 illustrate the stress-strain plots in a multi-stage test procedure for the three runs. As figure 9.10 shows at all levels of confining pressures, stable sliding is observed with a low positive slop in each step. Plot one in figure 9.11 shows the curve for the second run. The same behaviour as the first run occurred in all stages.

Plot two (figure 9.11) illustrate the sliding behaviour on wet surfaces during the run three. As is observed stable sliding has continued in all stages up to 70 MPa confining pressure. At this level of stress irregular stick-slip has occurred which are quite different from those of dry sliding surfaces (for instance, figure 9.19). In each cycle of stick-slip in this case, a portion of stable sliding or an episodic sliding is observed. Episodic sliding is a type of sliding in which most of the sliding occurs in short spurts with little or no sliding in between (Scholz et al, 1972). On examination of the specimen after each run a little mixture of water with gouge was observed over sliding surfaces in the first and second run. In the third run the surfaces were apparently dry, but some near to yellow spectrums were observable throughout the sliding surfaces which were an indication of moisture on those parts. In fact presence of very little moisture over sliding surfaces makes the rock soft. This may be attributed to the fact that when water surrounds the crystals or grains interlocking of asperities decreases significantly. Consequently, stable sliding and disappearance of stick-slip is expected to occur.

The susceptibility of stick-slips to the presence of water has probably a significant role in the faulted areas in which stick-slip may occur. Depending upon the amount of moisture content through sliding surfaces it might be possible to predict the fault behaviour during sliding.

9.9 EVALUATION OF STICK-SLIP IN SLIDING OF TWO DIFFERENT ROCKS ON EACH OTHER

Frictional sliding of two different rocks is of paramount interest, particularly in the faulted areas, where the two sides of a fault are formed from different rocks. Three types of rocks were selected to combine with granite. Each specimen consisted of two halves from granite and another rock which separated by an orientation angle of 60° relative to the short axis of the specimen. The selected rocks include Stainton sandstone, Penrith Sandstone and slate. Two different sliding surfaces were also used: saw cut and ground surfaces.

Figures 9.6 to 9.9 illustrate the stress-strain plots obtained in this experiment. In figure 9.7 in which a saw cut sliding surface of Penrith sandstone was combined with granite and tested in a multi-stage procedure in steps of 10, 30, 50 and 70 MPa confining pressure, stable sliding was observed up to 30 MPa confining pressure. At this level of stress, stable sliding continued up to a certain amount of axial strain, then stick-slip was observed with very small amplitudes up to about 1.4% axial strain. Stick-slip then disappeared at this point after occurrence of a single stick-slip with a relatively high amplitude (figure 9.7 at about 1.4% axial strain). Stick-slip in this part of sliding was accompanied by violent movement exactly the same as other stick-slip in granitic sliding. With an increase in confining pressure to 50 MPa ,stable sliding continued throughout, however, in the beginning of this part, episodic sliding was observed after a short interval. After an increase in confining pressure to 70 MPa, sliding continued in

almost the same manner as 30 MPa in a greater scale, i.e in a limited portion of the sliding movement stick-slip occurred and eventually stable sliding dominated. This implies that occurrence of stick-slip in the faulted areas with combined rocks may be limited to a portion of the sliding movement of the faults.

Figure 9.6 illustrates the stress-strain plot of a test performed on a specimen of Penrith sandstone with ground sliding surface combined with granite under a confining pressure of 70 MPa. Stick-slip was observed after loading began with very low amplitudes, and gradually increased when sliding continued and eventually stable sliding dominated in an ascending order.

As is observed the static coefficient of friction is variable in this case (figure 9.6) and increases in each cycle of stick-slip even in the stable sliding part. This behaviour is different from that observed in granitic sliding, for instance figure 9.5 in which the static coefficient of friction is reasonably constant throughout. Comparison of figures 9.6 and 9.7 reveals that there is a similarity in behaviour between the two cases (the multi-stage and one-stage tests), at a certain level of differential stress (about 45 MPa in figure 9.6 and 170 MPa in figure 9.7) stick-slip has occurred and then stable sliding has dominated. The differential values after initiation of stable sliding in both cases are near to each other at the same magnitude of strain.

Figures 9.8 and 9.9 illustrate the stress-strain plots for Stainton sandstone and slate respectively in combination with granite. A stable sliding predominates throughout for both slate and Stainton sandstone, however, episodic sliding is observed in several parts of the plot in figure 9.8. This behaviour may be attributed to the similarity of the minerals in two types of sandstone especially in quartz, however, because of difference in the combination of the minerals the sliding behaviour of two sandstones in combination with granite is not the same.

The difference in behaviour of Penrith sandstone in combination with granite with the rest of the rock types tested may be attributed to the difference in the mineralogical structure of this rock in comparison with the other rocks. A thin section petrological description (appendix B) indicates that Penrith sandstone has mineralogical structure completely different from the rest of the rocks. This rock is a siliceous sandstone, well compacted by secondary quartz in the form of overgrowth on the detrital grains. The surfaces of the original grains are also picked out by a thin red-brown rim of iron oxide. On the other hand, no clay and mica minerals are present as the cement in this rock. Furthermore, it is very dense and non-porous, in specific, as the cementing materials are "secondary quartz" and "iron oxide" which have made it very hard.

9.10 DISCUSSION

Comparison of the stick-slip characteristics through the plots obtained from modified and non- modified cell-specimen systems reveals that the stick-slip characteristics and their controlling mechanism are different in the two systems. Figure 9.18 illustrates two plots in which plot one represents a typical cycle of stick-slip movements in the plots obtained in the modified system and plot two represents a typical cycle of stick-slip in the non-modified systems. In plot one brittle fracture is the controlling mechanism so that there is not a period of stable sliding at the peak, but a sudden drop in stress. However, in plot two a plastic instability is the controlling mechanism; there is an initial elastic increase in stress followed by a period of stable sliding, then a sudden drop in stress.

Several theories have been proposed to explain the mechanics of stick-slip phenomenon. Byerlee (1970) has reviewed these theories and pointed out the areas of uncertainty in applying the results of laboratory experiments related to stick-slip. He

also proposed a theory of friction based on brittle fracture (Byerlee ,1967a). According to this theory, in brittle rocks, the stick-slip movement during sliding are caused by sudden brittle failure of the interlocked irregularities on the surfaces. This theory may be accommodated to the results obtained through a modified system, but it is not always the case. In intact (fresh) surfaces of sliding such as saw cut and ground surfaces (figure 9.3 and 9.4) a mechanism of brittle fracture predominates. However, when the sliding surfaces are not fresh (intact) but other materials such as gouge or water (wet surfaces) are present a mechanism of plastic instability predominates. For instance, in sliding surfaces in which stick-slip occur after a large amount of movement (figures 9.12 and 9.14) or when the sliding surfaces are not entirely dry (wet surfaces) as in figure 9.11 (upper plot) stick-slip has occurred in occasional cycles after a period of stable sliding.

The theory of plastic instability was proposed by Rabinowicz (1959). In this theory there is an initial elastic increase in stress followed by a period of stable sliding, then a sudden drop in stress occurs. The subsequent cycles are repeated in the same way as cycle one. This theory may be applied to the results of the tests obtained through non-modified systems as in figures 9.1

Several parameters seem to affect the controlling mechanism of stick-slip. Among them effects of system constraints, filling materials and moisture content were shown on the controlling mechanism of stick-slip. Taking these factors into consideration this implies that it is impossible to apply a single theory to interpret the stick-slip behaviour.

It seems that strain rate also affects the mechanics of stick-slip phenomenon. Applying a very slow strain rate the mechanism of stick-slip transfers from brittle to plastic instability (figure 9.19 the last part of the highest plot) and at a fast strain rate there will be a transition from plastic to brittle instability. As pointed out decrease of strain rate results in an increase in the static coefficient of friction. Both increase in static

coefficient of friction and transition from brittle to plastic instability may be attributed to the fact that decrease of strain rate leads to the increase in the time of interlocking asperities, or reduction in velocity of sliding. As a result, due to the long term deformation of the irregularities a transition from brittle to plastic instability may be expected, and because of a longer time of contact between asperities a higher static coefficient of friction may be resulted.

Plate 9.1: Sliding surfaces of granite specimens with saw cut joint after test, confining pressure left to right: 10, 30 & 70 MPa.

Plate 9.2 Sliding surfaces of combined rock types, left to right, limestone-granite, granite-sandstone, sandstone-sandstone, granite-slate, confining pressure= 70 MPa.

Plate 9.3 Sliding surfaces of slate specimens with saw cut joints, confining pressure, left to right, 70 & 30 MPa.

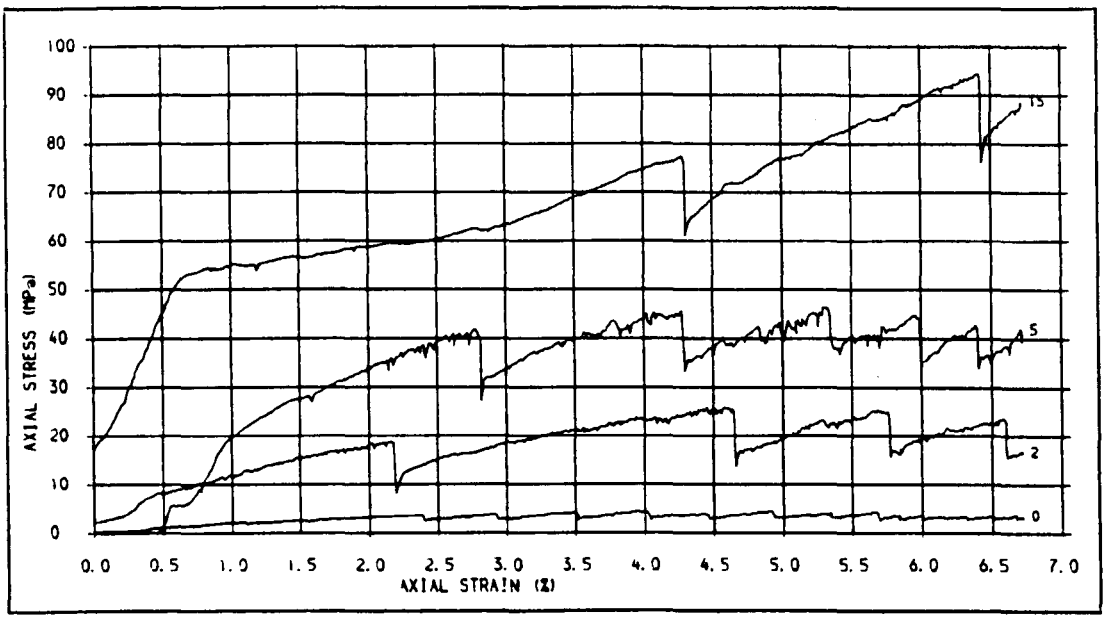

Fig. 9.1 . STRESS-STRAIN PLOTS FOR SS SPECIMENS TESTED IN THE NON-MODIFIED SYSTEM.
CONFINING PRESSURES = 0, 2, 5 AND 15 MPa.

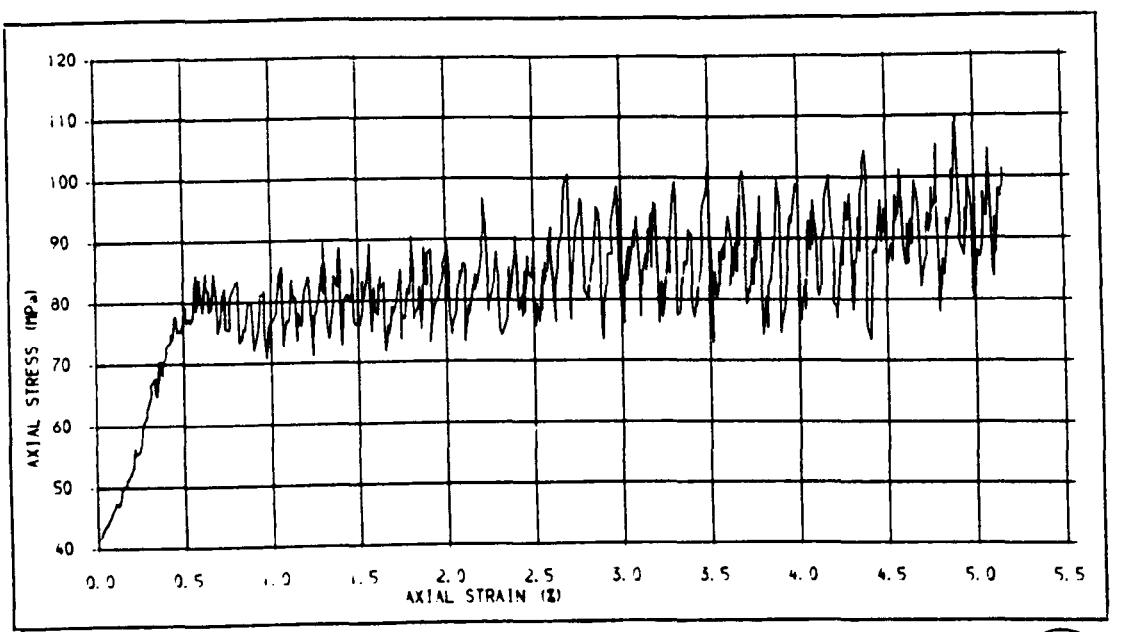

Fig. 9.2 . STRESS-STRAIN PLOT FOR A GRANITE SPECIMEN TESTED IN THE NON-MODIFIED SYSTEM.
CONFINING PRESSURE= 30 MPa

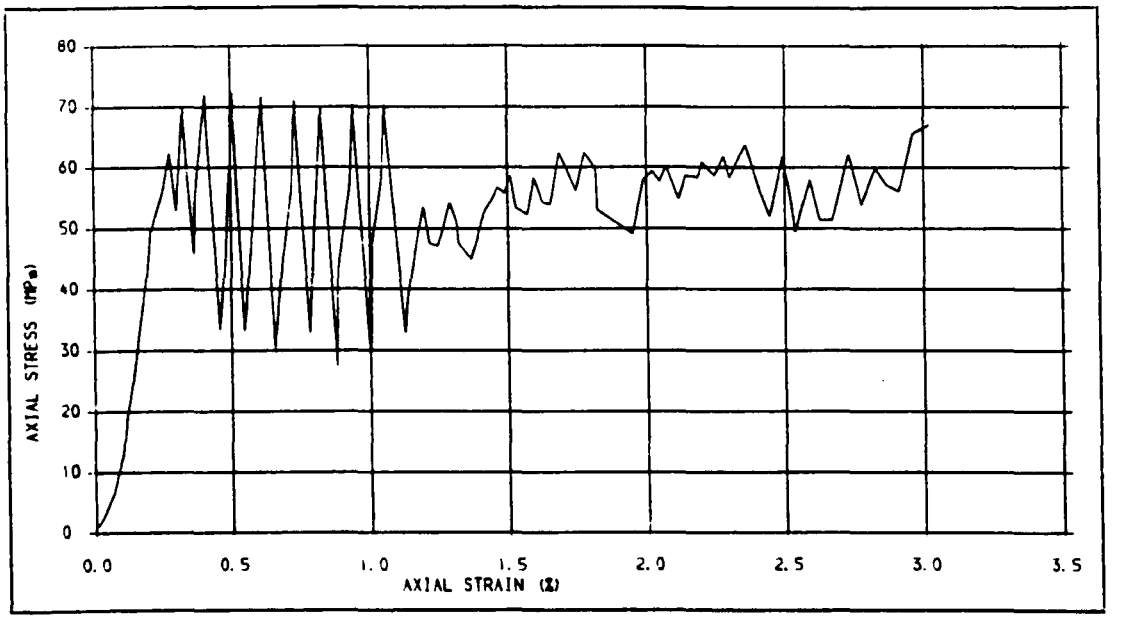

Fig. 9.3 . STRESS-STRAIN PLOT FOR A GRANITE SPECIMEN, STRAIN RATES: MEDIUM (0.25 % / min) AND VERY FAST RATE (SECOND PART OF THE PLOT, 25 % / min), CONF. PRESSURE= 30 MPa

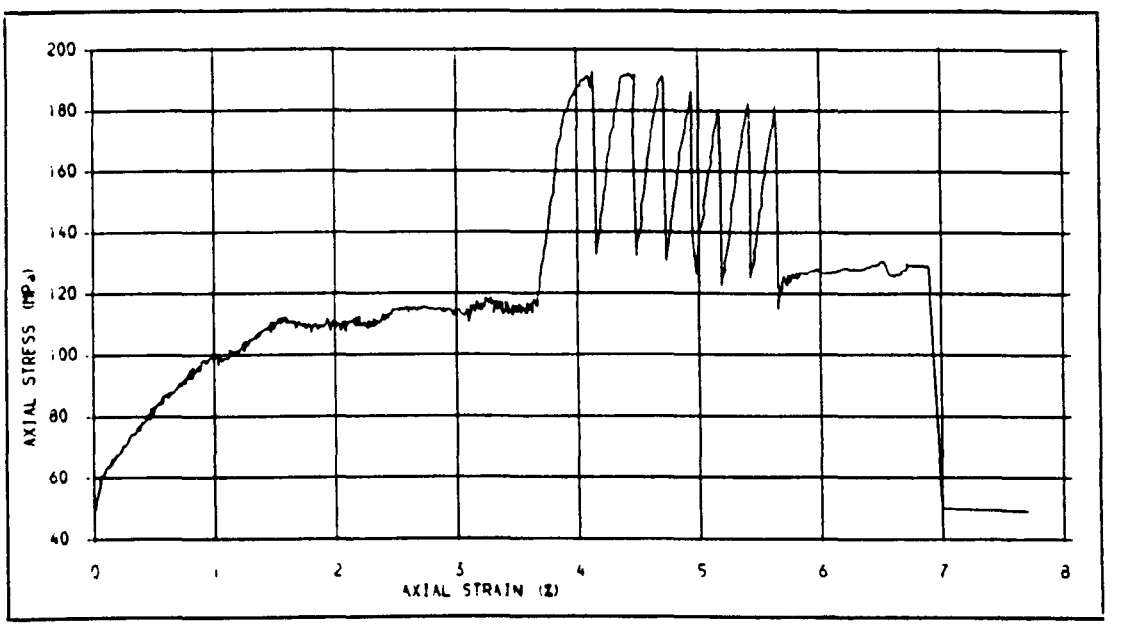

Fig. 9.4 . STRESS-STRAIN PLOT FOR A GRANITE SPECIMEN OBTAINED IN A MULTI-STAGE TEST IN STEPS OF 30, 70, THEN 30 AND 10 MPa CONFINING PRESSURES.

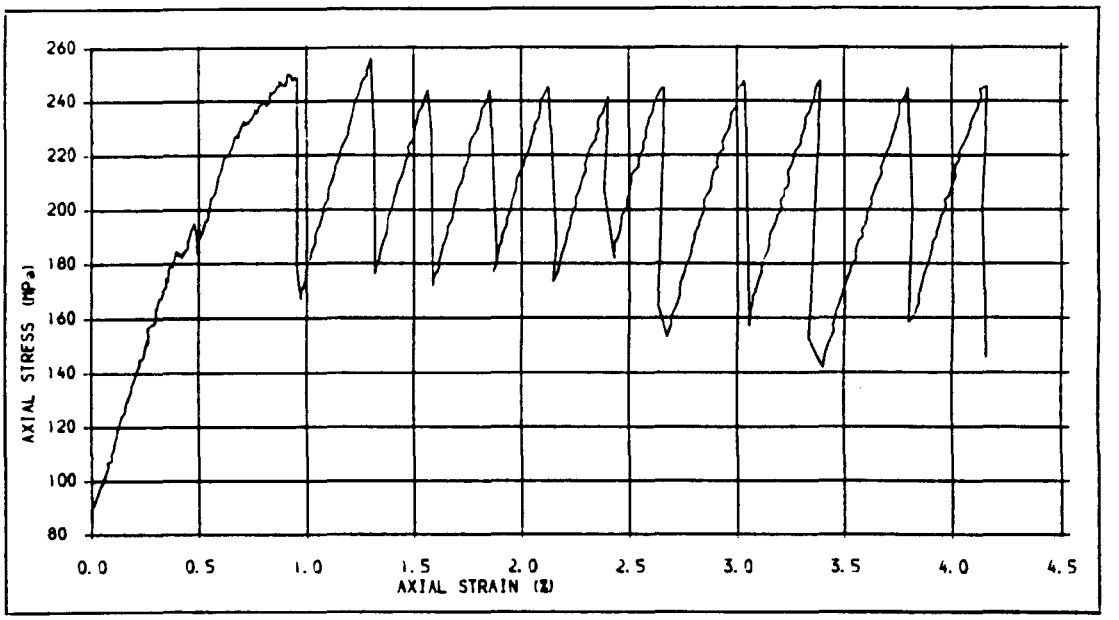

Fig. 95 . STRESS-STRAIN PLOT FOR A GRANITE SPECIMEN WITH SAW CUT SLIDING SURFACE
CONFINING PRESSURE= 70 MPa

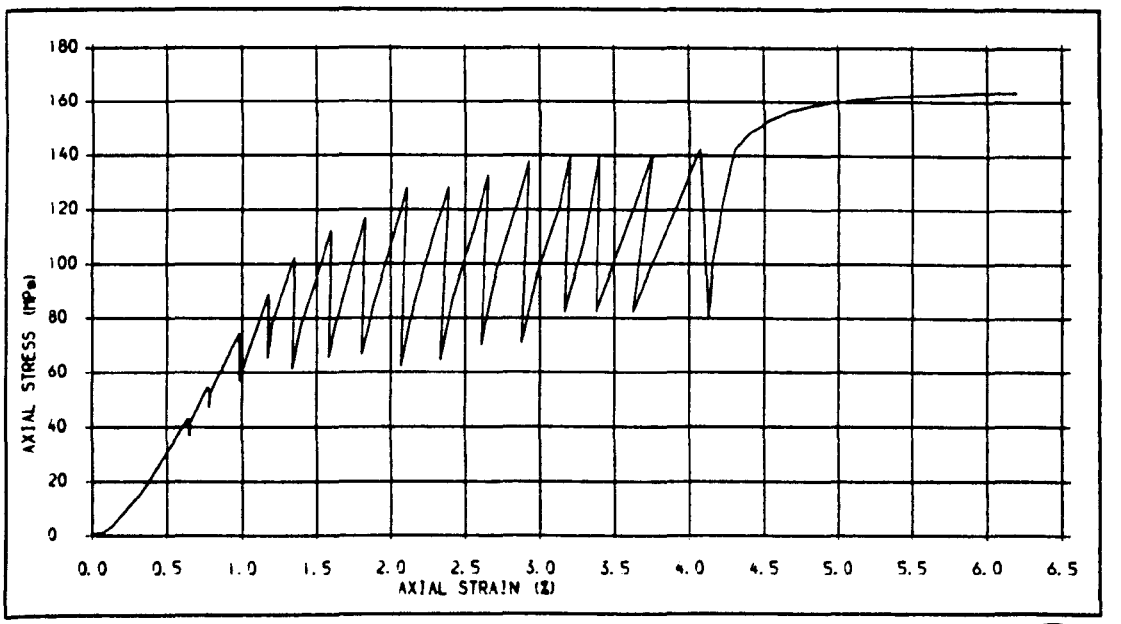

Fig. 96 . STRESS-STRAIN PLOT FOR COMBINATION OF PENRITH SANDSTONE AND GRANITE WITH GROUND
SLIDING SURFACES , CONFINING PRESSURE= 70MPa

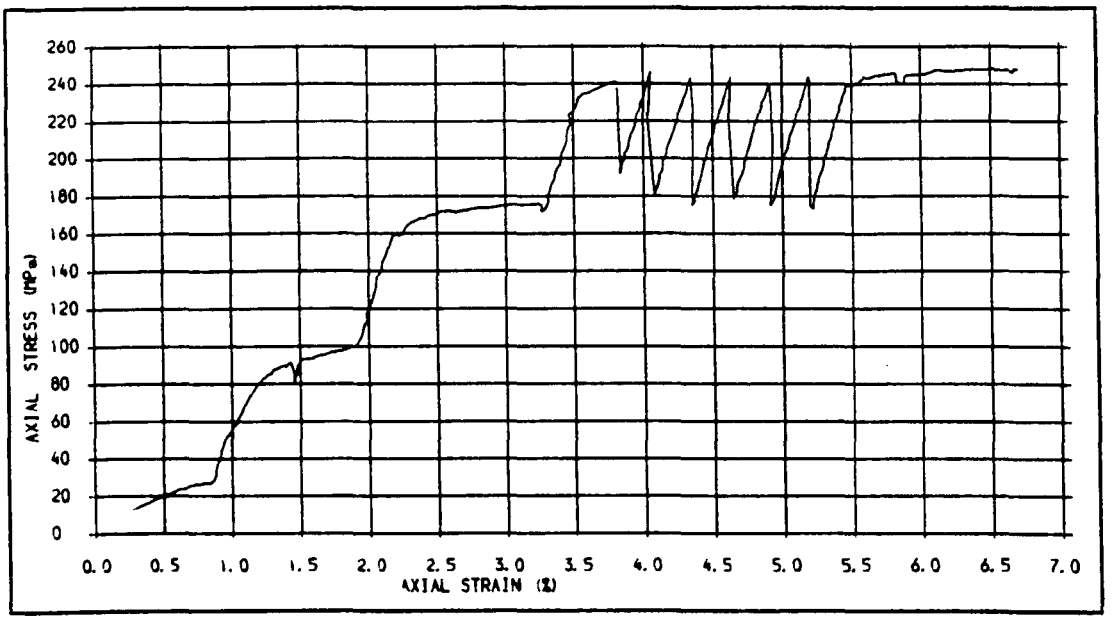

Fig. 97 . STRESS-STRAIN PLOT FOR COMBINATION OF PS & GRANITE WITH GROUND SLIDING SURFACES IN A MULTI-STAGE TEST. CONFINING PRESSURES IN STEPS OF 10, 30, 50 AND 70 MPa.

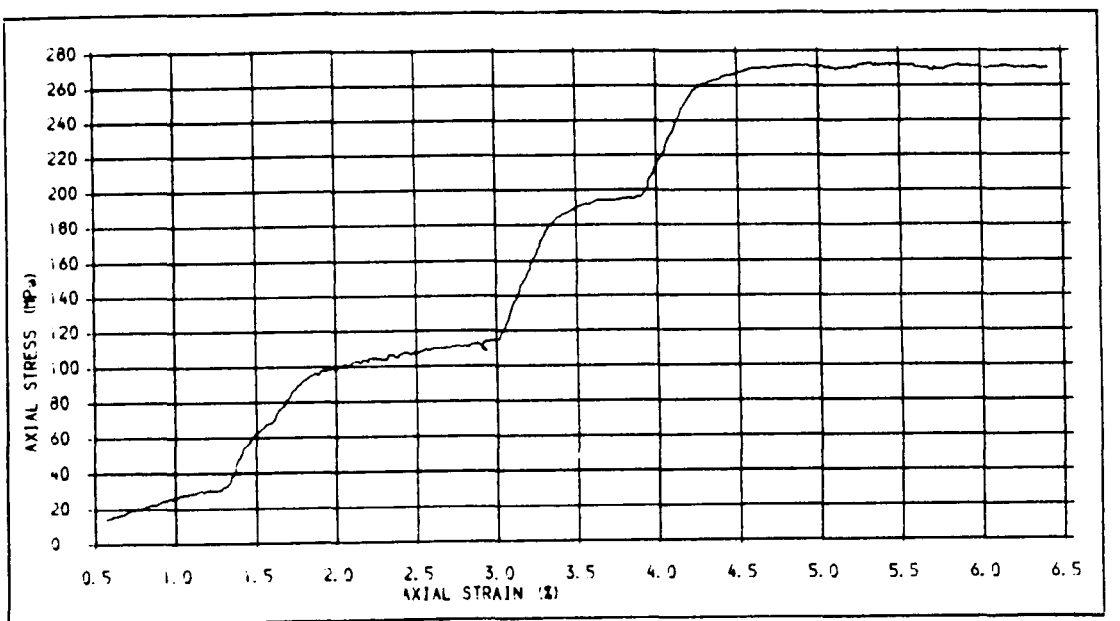

Fig. 98 . STRESS-STRAIN CURVE FOR COMBINATION OF STAINTON SANDSTONE AND GRANITE IN A MULTI-STAGE TEST, CONFINING PRESSURES IN STEPS OF 10, 30, 50 AND 70 MPa.

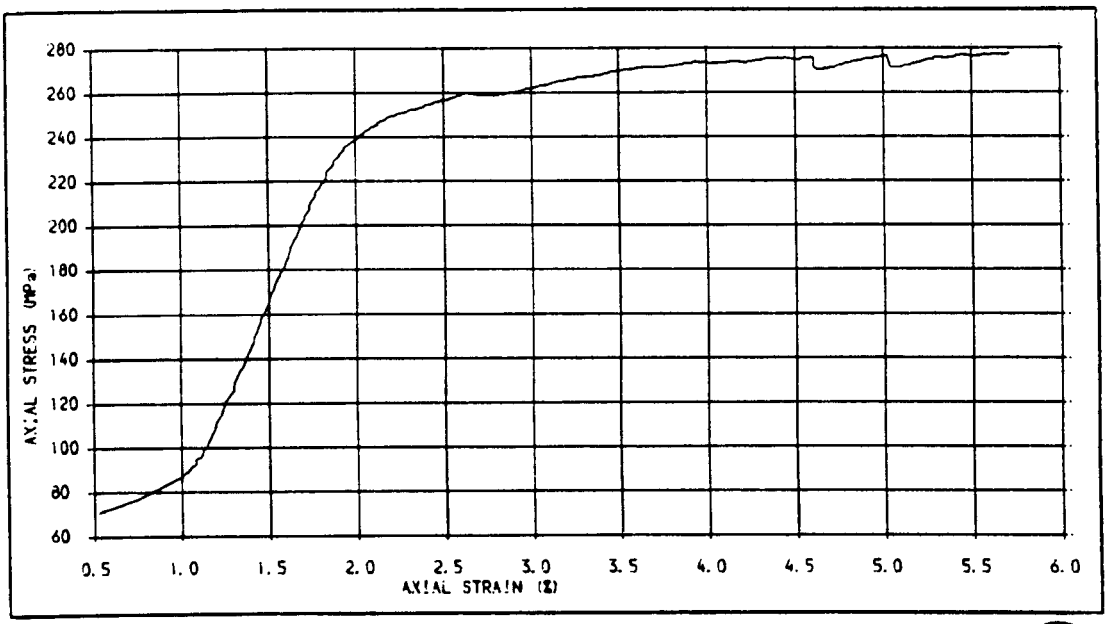

Fig. 99 . STRESS-STRAIN CURVE FOR COMBINATION OF SLATE AND GRANITE.
CONFINING PRESSURE = 70 MPa.

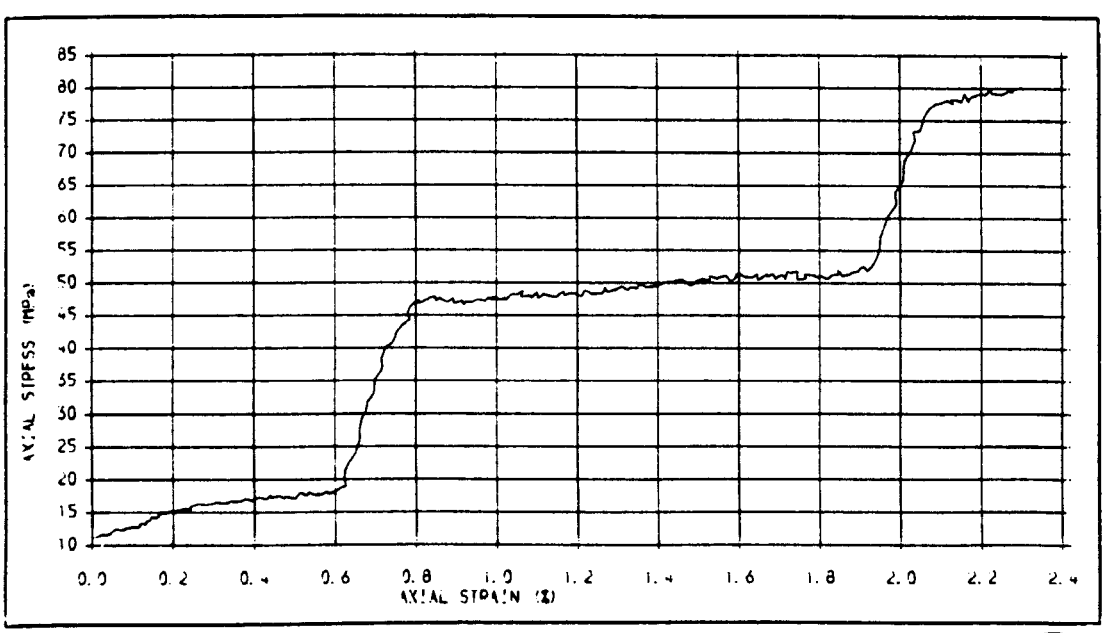

Fig. 910 . STRESS-STRAIN PLOT FOR A GRANITE SPECIMEN WITH WET SLIDING SURFACE (.615 mg
PER UNIT WEIGHT). MULTI-STAGE TEST IN STEPS OF 10, 50 AND 50 MPa

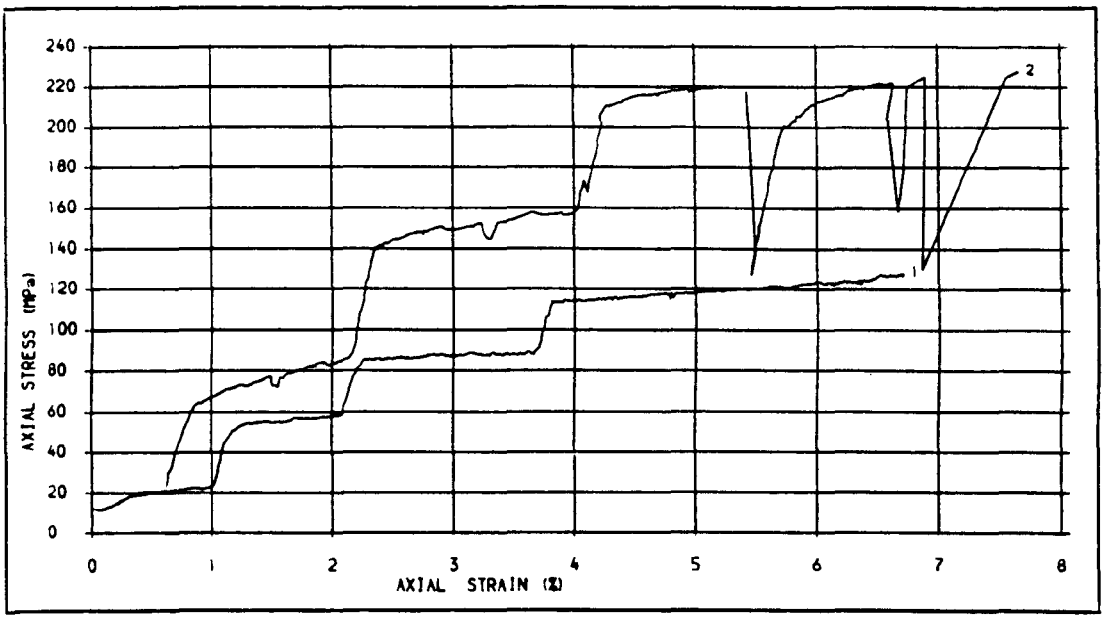

Fig. 9.11 .STRESS-STRAIN CURVES FOR GRANITE SPECIMENS WITH WET SLIDING SURFACES, LOWER PLOT .2171, UPPER PLOT .0362 mg WATER. CONFINING PRESSURES. 10, 30, 50 AND 70 MPa

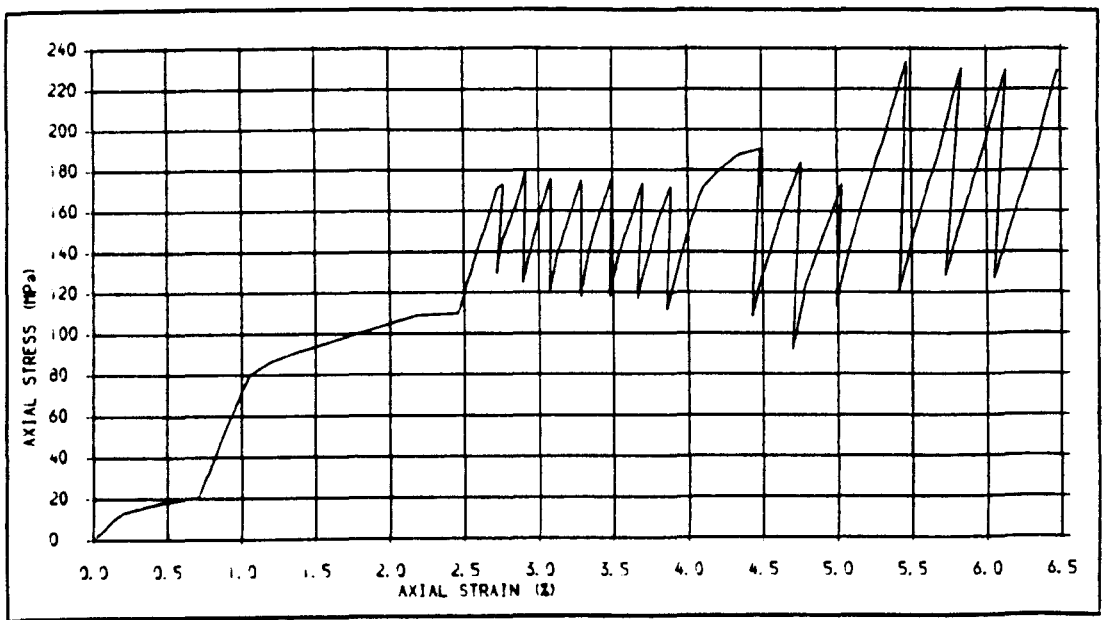

Fig. 9.12 .STRESS-STRAIN PLOT FOR A GRANITE SPECIMEN. TEST REPEATED ON THE SAME SLIDING SURFACE, RUN ONE, CONFINING PRESSURES IN STEPS OF 10, 30, 50 AND 70 MPa

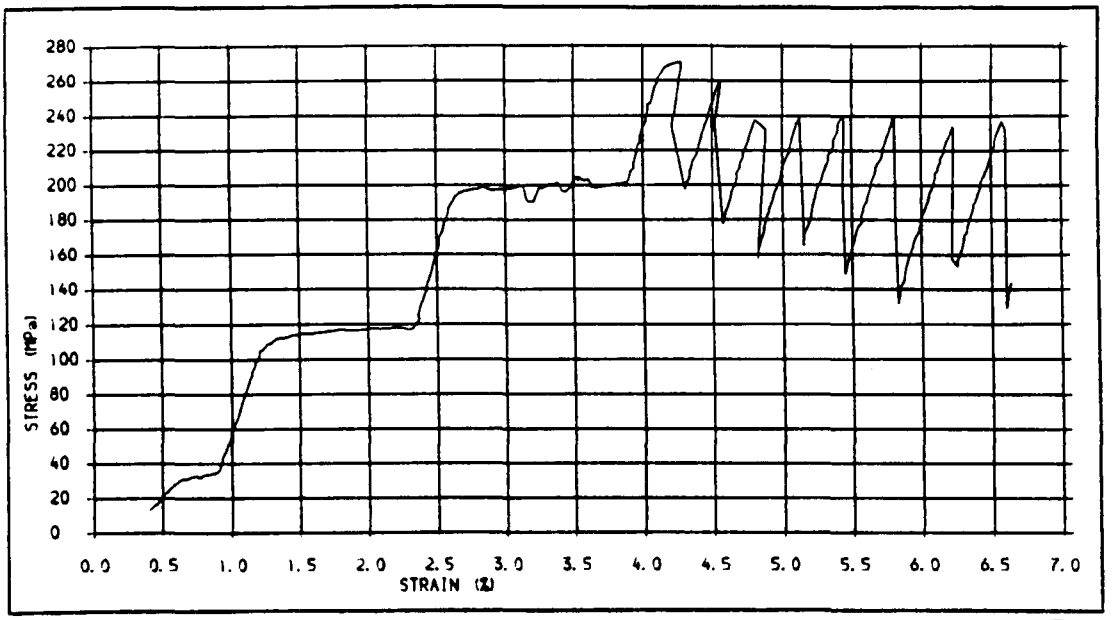

Fig. 9.13 . STRESS-STRAIN PLOT FOR A GRANITE SPECIMEN. TEST REPEATED ON THE SAME SLIDING SURFACE, RUN 2, CONFINING PRESSURES. 10, 30, 50 AND 70 MPa

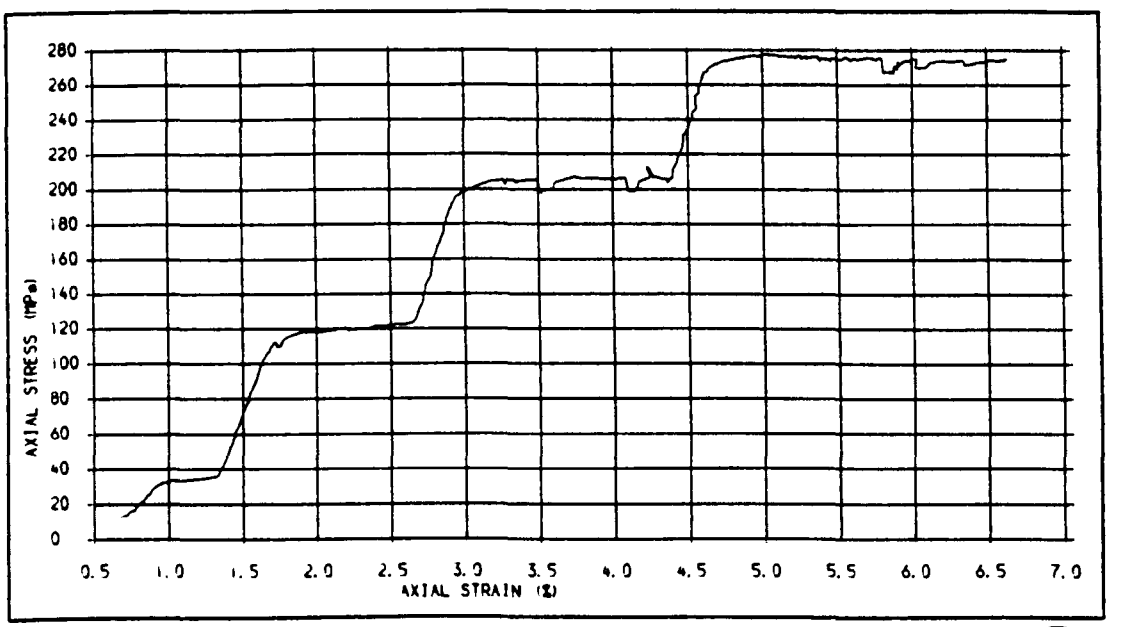

Fig. 9.14 . STRESS-STRAIN CURVE FOR A GRANITE SPECIMEN. TEST REPEATED ON THE SAME SLIDING SURFACE, RUN 3, CONFINING PRESSURES IN STEPS OF 10, 30, 50 AND 70 MPa.

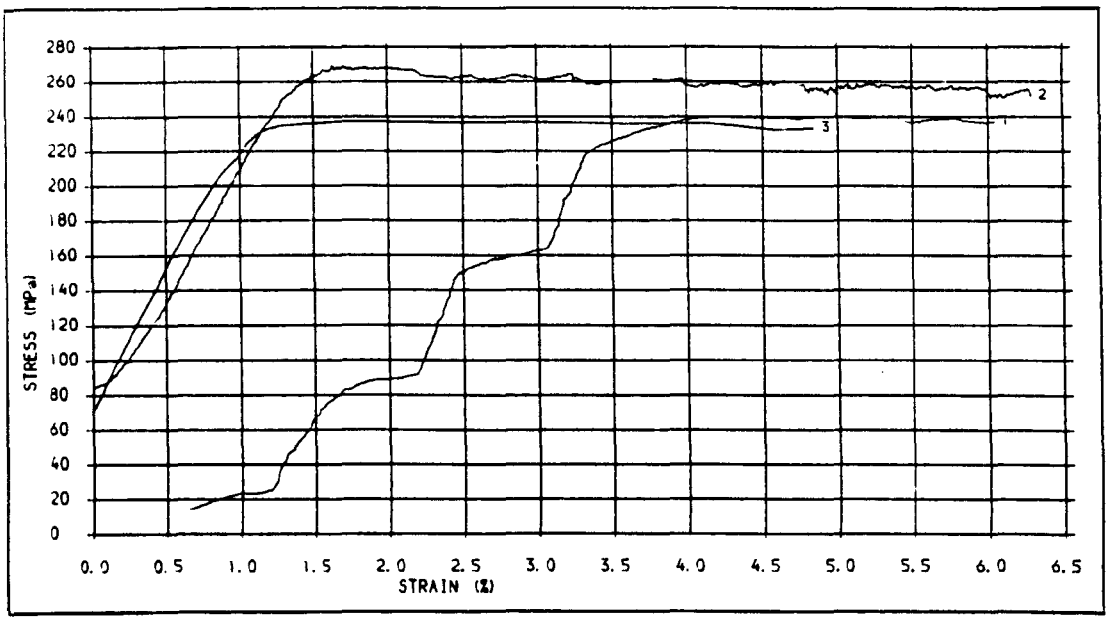

Fig. 9.15 . STRESS-STRAIN CURVES FOR PS SPECIMENS WITH SAW CUT (PLOT 1) AND GROUND SLIDING SURFACE (PLOT 2) AND A SS SPECIMEN. CONFINING PRE. . 70 AND 10, 30, 50 AND 70 MPa

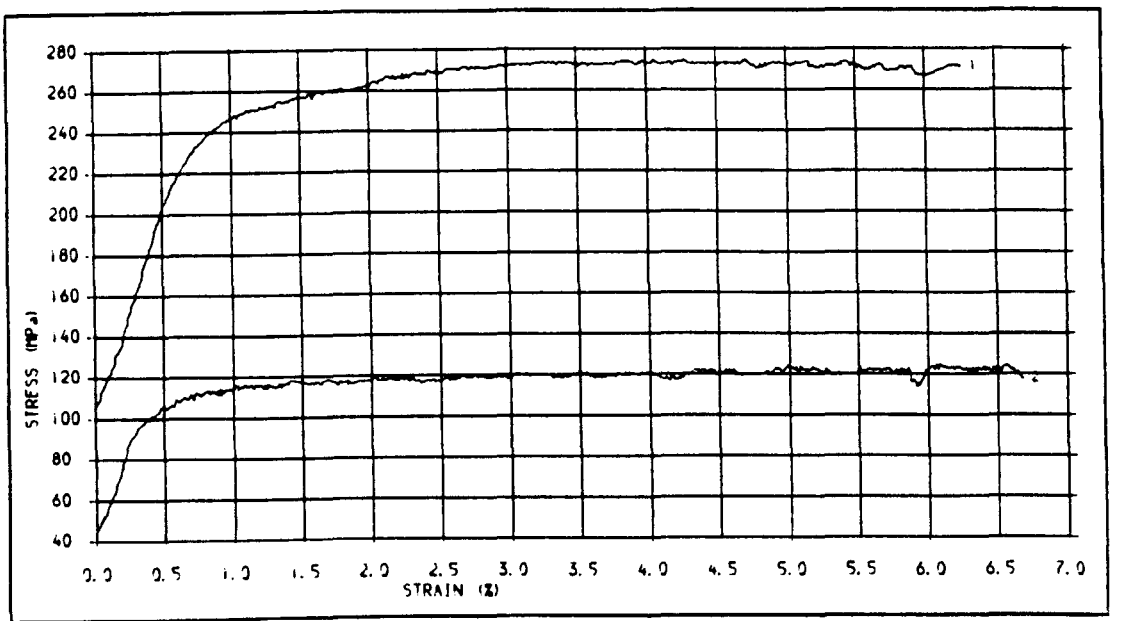

Fig. 9.16 . STRESS-STRAIN CURVES FOR SLATE SPECIMENS WITH SAW CUT JOINTS. CONFINING PRESSURE 30 AND 70 MPa.

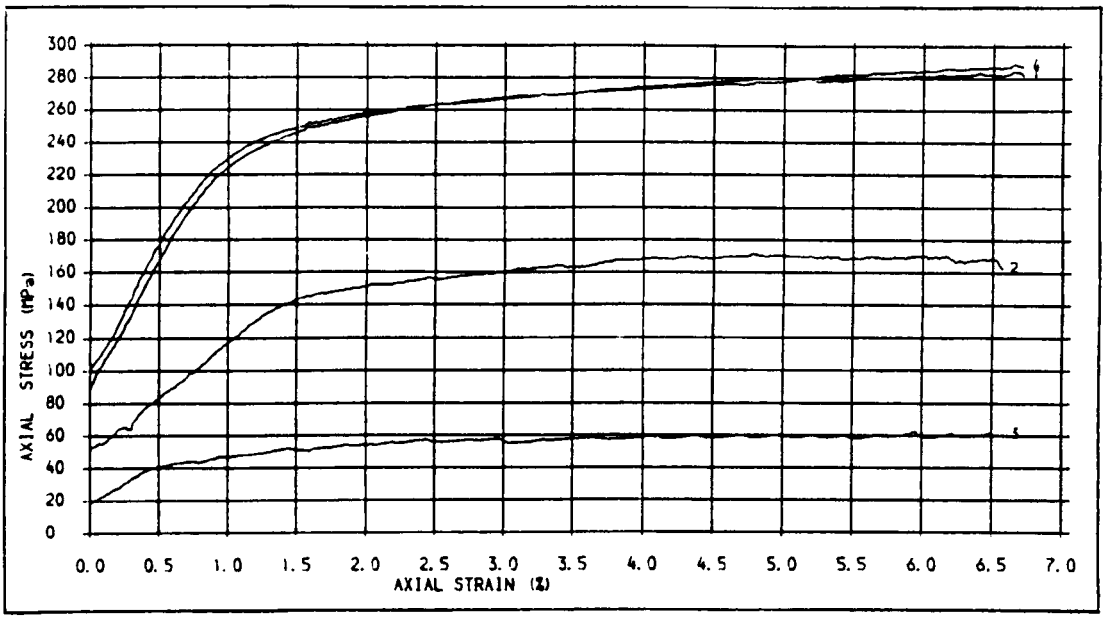

Fig. 9.17 . STRESS-STRAIN CURVES FOR LIMESTONE SPECIMENS WITH SAW CUT (PLOT 1, 2 AND 3) AND GROUND (PLOT 4) SLIDING SURFACES. CONFINING PRESSURES. 10, 30, 70 AND 70 MPa

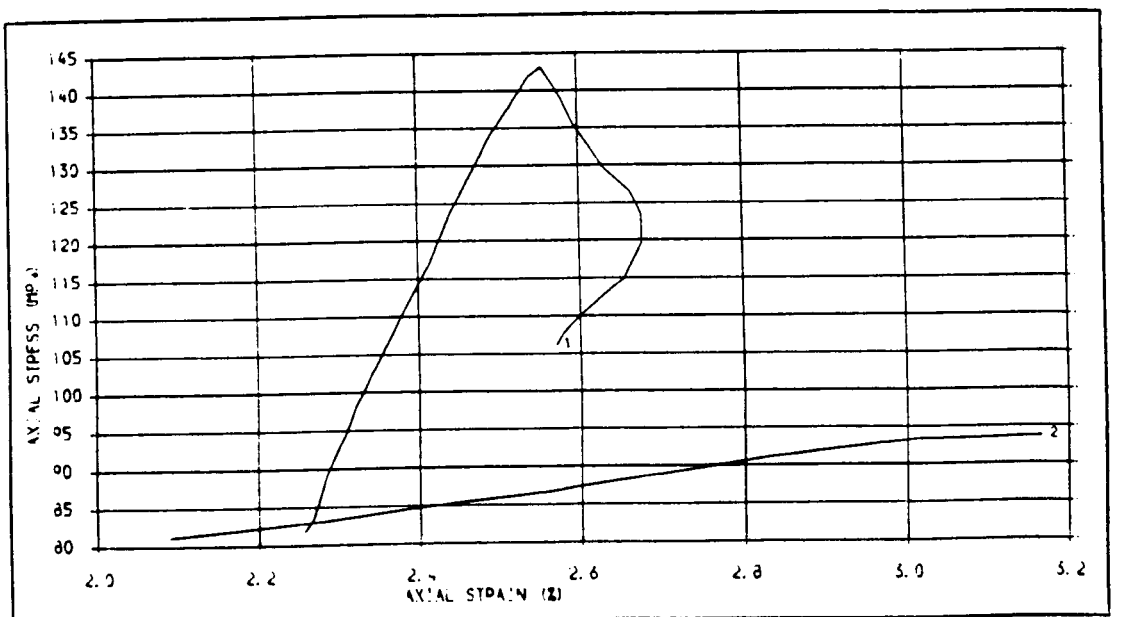

Fig. 9.18 . STRESS-STRAIN PLOTS FOR TYPICAL CYCLES OF STICK SLIPS IN MODIFIED (PLOT 1) AND NON-MODIFIED (PLOT 2) CELL SPECIMEN SYSTEMS.

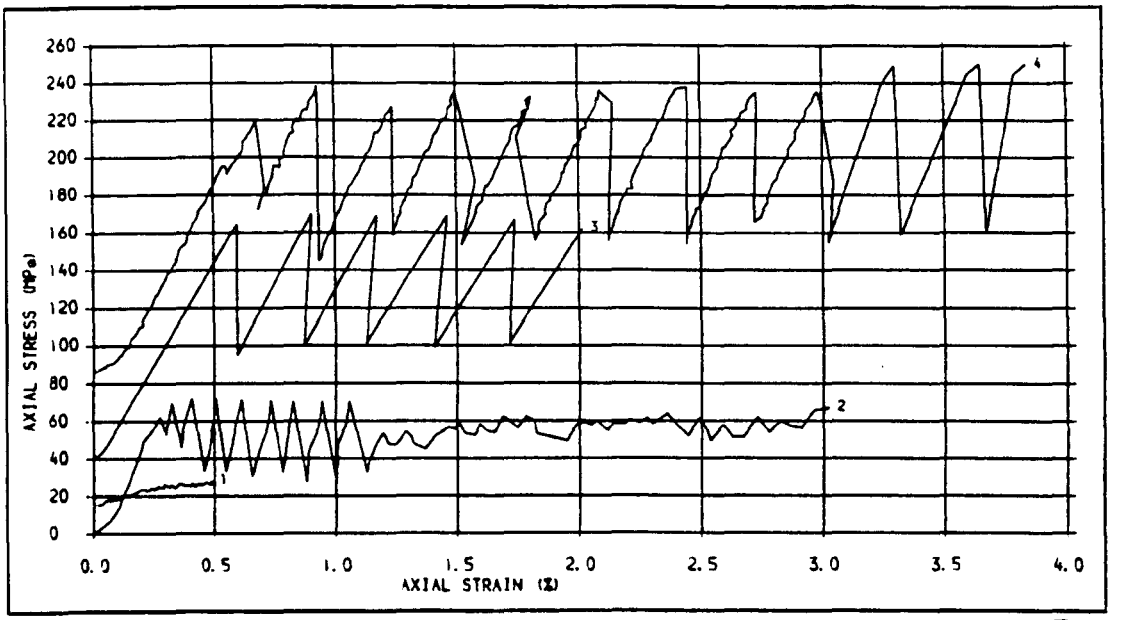

Fig. 9.9 . STRESS-STRAIN PLOTS FOR GRANITE SPECIMENS AT DIFFERENT STRAIN RATES. CONFINING PRESSURES. 10, 30, 70 AND 70 MPa.

FIG. 9.20: STATIC COEFFICIENT OF FRICTION VS LOG STRAIN RATE.

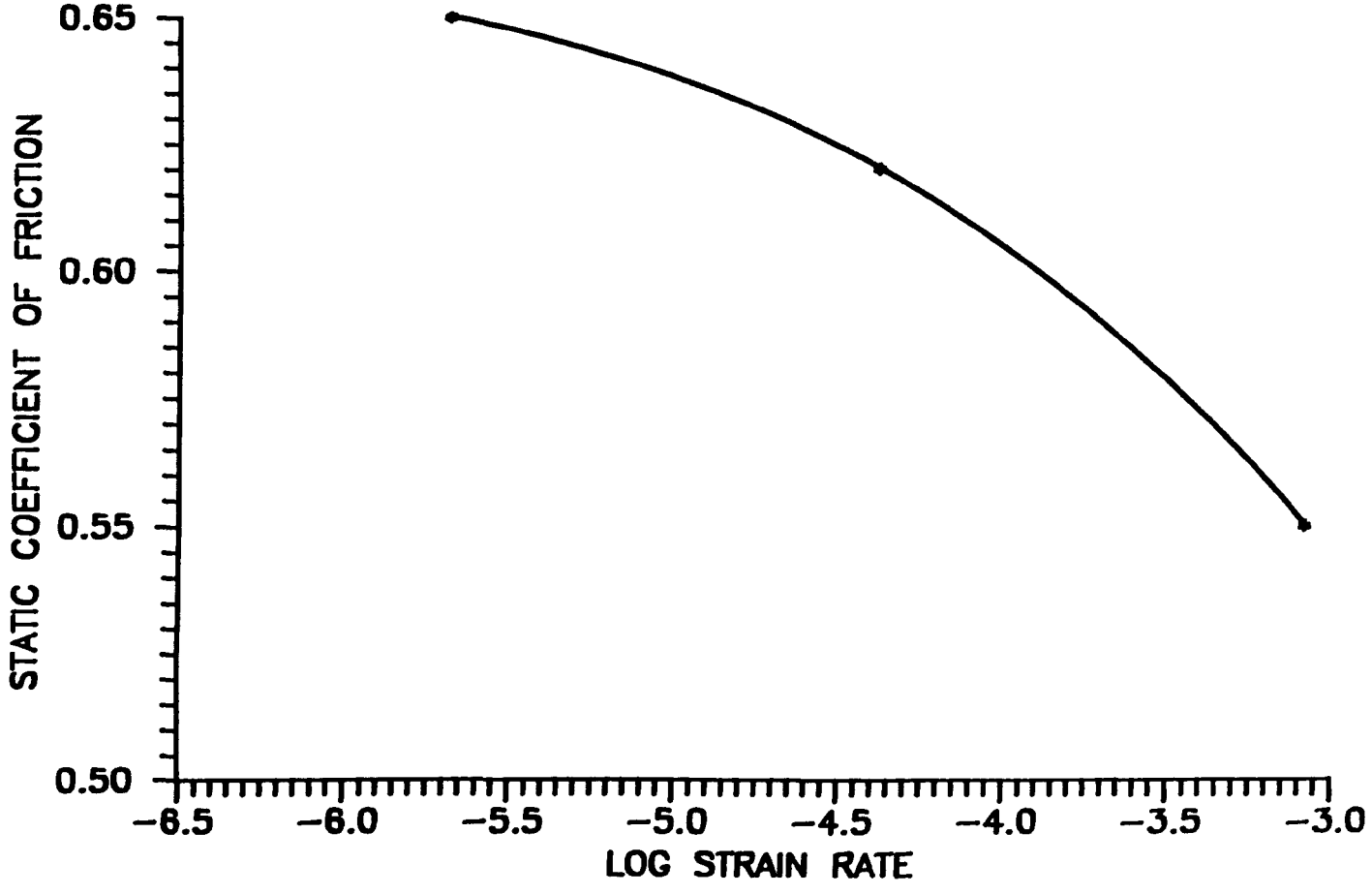

CHAPTER 10

CONCLUSIONS AND RECOMMENDATIONS

10.1 INTRODUCTION

The aim of this research project was to explore the behavioural characteristics of rocks containing a single joint under triaxial loading conditions and to investigate the influence of joint inclination, joint type, confining pressure and time on the mechanical and sliding behaviour of jointed rock. A 5 MN servo-controlled stiff testing system was employed to conduct the tests triaxially. A measuring system was used in connection with the servo-system that could monitor continuously the axial stress and strain and logged data for subsequent analysis. The volumetric changes in the laboratory specimens were measured when the specimens were compressed triaxially and the procedure for calculation of volumetric strain was improved.

The first objective was to examine the significance of changes in the geometry of the cell-specimen system during sliding over the joint surface and the effects of the end-specimen conditions on the sliding behaviour. Thereafter, the work was extended to study the mechanical characteristics of jointed rocks containing a single plane of weakness under a satisfactory end-specimen condition.

10.2 EFFECTS OF SYSTEM CONSTRAINTS ON THE EXPERIMENTAL RESULTS

An experimental investigation was conducted to evaluate the significance of cell-specimen configuration in triaxial testing of jointed specimens. The results indicate that inserting hardened steel discs between the platens and either end of the specimens, and lubricating between the discs and platens with molybdenum desulphide grease is the

most satisfactory arrangement to prevent the change in the geometry of the cell-specimen system during sliding (modified system). Other configurations such as using a spherical seat at the top or bottom of the specimen, and a pair of steel discs with no lubricant grease affect the results both in quality and quantity. The most important system influences can be listed as follows:

1. Peak strength and its corresponding strain in jointed specimens were greatly affected, where the system did not maintain a full contact of sliding surfaces. The difference for a confining pressure of 5 MPa and 60^{o} orientation tested in the two modified and non-modified cell-specimen systems obtained 80.4% in peak stress and 64.7% in the corresponding strain.

2. Sliding characteristics of jointed surfaces were different in the two testing systems. In the modified system continuous sliding was observed along the joint plane with no stress drop, however, in the non-modified system sliding was accompanied by violent stick-slip.

3. The post-failure and residual regions of the stress-strain curve in jointed and intact specimens differed significantly in the two systems. The effects appeared in the form of fluctuations in stress and stick-slip events where the non-modified system was used.

4. The mode of sliding and failure of the specimens were different in the two systems. There was a considerable number of subsidiary fractures extra to the major shear failure plane, or around the sliding joint surfaces, where the specimens were tested in the non-modified system.

10.3 STRENGTH AND DEFORMABILITY OF JOINTED ROCKS

Three rock types were tested triaxially and their volumetric changes were measured. The rock types tested were: Stainton sandstone, Penrith sandstone and Dumfrith sandstone. Three types of joints were established through the specimens: saw cut, split breakage and shear-surface joints. The joints were formed in different orientations of 0, 15, 30, 45 and 60°. Both intact and jointed specimens were tested and confining pressures 0-70 Mpa were applied.

Confining pressure had a pronounced effect upon the stress-strain properties of the rocks tested whether intact or jointed specimens with any orientation. The effect of increased confining pressure on the jointed specimens with 45 and 60° orientations in which failure dominated by sliding along the joint plane was remarkable. To evaluate this effect a ratio was defined as the "strength descending coefficient" which is the ratio of the strength of jointed specimen to that of the intact specimen. For 45° orientation (Penrith sandstone specimens with saw cut joints), for instance, increase in confining pressure from 15 to 30 then to 70 Mpa resulted in an increase in the strength coefficient from 0.424 (15 Mpa) to 0.604 (30 Mpa) then to 0.761 (70 Mpa). That is, as confining pressure increases, the strength of jointed specimen becomes nearer to the intact strength.

The sliding characteristics of jointed specimens with saw cut joints were different in low and high confinements. In low confining pressures (below 15 Mpa) sliding continued asymptotically with a slight increase in the stress value or at a nearly constant stress level. In higher confining pressures (30-70 Mpa), however sliding continued with a gradually decrease in stress value. Sliding behaviour in split breakage joints was the same in both low and high confinements; after dropping the stress to a residual value

sliding continued with a gradual decrease in stress value at all levels of confining pressures.

Joint inclination had a significant effect on both failure stress and strain. The failure strength decreased when joint inclination increased. The highest decrease in strength was observed at about 60° inclinations. The three rocks tested held linear relationships between differential stress and confining pressure for 45 and 60° inclinations whether saw cut or split breakage joints. This shows that the linear Coulomb-Navier criterion holds well for the critical joint orientations (45-65°) under the confining pressures 0-70 Mpa.

Differential stress versus confining pressure envelope for 60° orientation in split breakage joints possessed a higher slope with respect to 45°. This behaviour revealed the significance of surface roughness in the most critical joint orientation (60°). Mohr envelope for 60° inclination in split breakage joints was also above that of 45° in both saw cut and split breakage joints, i.e. a higher coefficient of sliding friction or a higher shear strength across the joint for this orientation.

The effect of joint inclination on the deformational behaviour of the rocks tested even for the inclination of 0 and 15° was unavoidable. When joint inclination increased the strain at peak increased. This behaviour in saw cut joints was much more pronounced.

It was found that the apparent modulus of deformability of jointed specimens, or in fact for a jointed rock mass, is displacement dependent. To be specific, in the assessment and determination of the modulus of deformation in a jointed rock mass the upper limit of the maximum allowable displacement through the joint must be introduced. Thereafter, the appropriate modulus of deformability may be determined.

Shear strength and the coefficient of friction of the rocks tested were highly affected by the joint and its inclination. Reduction in both shear strength and coefficient of sliding friction for 45 and 60° inclinations in saw cut joints was very dramatic. The sliding friction angle in 60° orientation (saw cut) was decreased to about 22° which is less than the half the intact Penrith sandstone. The Mohr envelope for saw cut joints in 45 and 60° orientations held linear for the three rocks tested. For the split joints with the same inclinations, however, the Mohr envelopes were non-linear; therefore, the Coulomb-Navier theory is an appropriate criterion to evaluate the shear strength across the joint with low surface roughness (saw cut) but not for rough surfaces (split breakage joints).

The volumetric strain versus axial strain curves showed a systematic change with confining pressure both in jointed and intact specimens. A large reduction in the volumetric expansion occurred for an increase in confining pressure at low confinements and expansion diminished as confining pressure increased. When confining pressure increased to above a certain threshold value, dependent upon the rock type, no volumetric expansion occurred.

In jointed specimens volumetric changes did not show a unique behaviour, but depended upon the amount of the joint orientation, joint type and the mechanism of deformation. For the orientations in which the mechanism of deformation was characterized by sliding along the joint plane volumetric deformation was completely different from that of the intact specimens, no volumetric expansion occurred either at low or at high confining pressures, but relative expansion and then contraction occurred when sliding began. This was more remarkable in the joints with high degree of surface roughness (split breakage joints) which was a measure of joint dilation (displacement perpendicular to the joint plane).

Instantaneous Poisson's ratio decreased as confining pressure was increased both in the intact and jointed specimens and reached a near constant value which for both jointed and intact specimens was 0.5 corresponding to zero volume change in the specimen with deformation.

Lateral strain decreased with increased confining pressure in both jointed and intact specimens. In intact specimens the maximum rate of change of straining occurred in the neibourhood of the peak stress and then reduced to a near constant value. In jointed specimens the rate of change of lateral straining depended upon the joint inclination and the degree of surface roughness. For the orientations in which sliding movement occurred freely over the joint, as much as the joint was rougher a higher rate of lateral straining occurred at the initiation of sliding which was an indication of the joint dilation at that position.

Three modes of deformation were recognized:

(i) continuous sliding along the joint which was observed through the specimens containing joint with 45-65^{o} orientations.
(ii) New shear failure within the intact material which was observed through the specimens containing joints with 30^{o} orientations and less
(iii) Composite mode of deformation involving the rock material and the joint. It was observed in the specimens containing saw cut joints with 45^{o} orientations (Stainton sandstone).

10.4 TIME-DEPENDENT BEHAVIOUR OF JOINTED ROCKS

Time-dependent effects on the behavioural characteristics of jointed specimens were investigated in three cases:

(i) Gradually increasing compressive load at constant strain rates;

(ii) Gradually increasing load at changing strain rates;

(iii) Stress variations at constant displacements along the complete stress-strain curve for 5 minutes time duration (stress relaxation).

Three different strain rates were applied: 2.08 X 10^{-6}/s (slow rate), 4.17 X 10^{-5}/s (medium rate) and 8.33 X 10^{-4}/s (fast rate). The significant results may be listed as follows:

(i) For intact specimens in zero confining pressure (uniaxial test) a higher strain rate resulted in a higher modulus of elasticity (steeper positive slope before strength failure) and in a higher failure stress of the specimens. Increased confining pressure reduced the strain rate effects. Small changes in strain rates had no significant effect on the modulus of deformability and stress at failure of the confined intact rocks.

(ii) Strain rate had no similar effects on Penrith and Stainton sandstone specimens with 30^{o} orientations under the uniaxial condition. In Stainton sandstone specimens increased strain rate for zero confinement increased the stress at peak and the mode of failure was predominant by shear fractures through the intact material. In Penrith sandstone specimens under the same conditions, however, increased strain rate decreased the stress at peak and the mode of failure was a combination of sliding and shear fracture. That is to say, strain rates had no similar effect on the jointed specimens of different rocks under uniaxial condition.

(iii) Effects of strain rates on the stress-strain behaviour of the jointed specimens in which mode of failure was dominated by sliding over the joint ($45\text{-}60^{o}$) was found to be completely different from the intact specimens. Change of strain rate from slow to fast

resulted in a higher stress value at the initiation of sliding for both rock types under different confining pressures. The behaviour became different in different rocks when sliding continued. Modulus of deformability also increased when strain rate increased in various confining pressures.

(iv) Increased strain rates decreased the reduction in volume of the specimens, or a slower strain rate resulted in a further closure of the joints. Increased confining pressure reduced this effect.

(v) Strain rate affected the instantaneous Poisson's ratio significantly. The faster strain rate resulted in a higher Poisson's ratio. Increased confining pressure decreased this effect. At slow strain rate at the initiation of sliding the rate of change of axial straining became higher than the rate of change of lateral straining which was an indication of joint dilation at that position.

(vi) Increased strain rate increased the lateral strain in the jointed specimen. Increased confining pressure decreased this effect.

(vii) Change of strain rate had no significant effect on the stress-strain characteristics of the specimens before yield point (for 30^{o} orientation). This finding was in agreement with the behaviour of the intact specimens in which there is similarity in the mode of failure with the joint specimens with orientations of 0-40^{o}.

(viii) Change of strain rate influenced the stress and deformability of the specimens after yield point if the strain rate changed in a high order of magnitude (hundred orders of magnitude,i.e. slow to fast and not slow to medium).

(ix) Change of strain rate with any order of magnitude (slow to medium and or fast) in the peak region affected the peak stress and the corresponding strain, and the stability of rock increased after strength failure because of the flattening of the curve at peak and decrease in the slope of the curve after peak, when the strain rate decreased suddenly.

(x) Decrease in strain rate increased the sliding resistance of jointed specimens, or increase in strain rate decreased the frictional sliding of the joints.

(xi) When sliding continued because of a further asperities damage and therefore a further gouge over the sliding surfaces the effects of strain rates became less important.

(xii) The effect of changing strain rates on the sliding behaviour of joints was less significant for low surface roughness (saw cut joints) and a very high change in strain rate (i.e. change of strain rate from slow to fast and not slow to medium) affected the sliding characteristics (in low roughness joints).

(xiii) In intact specimens stress relaxation was initiated at the yield point and accelerated after peak because of the cracks development through the rock. Increased confining pressure seemed to decrease the amount of stress drops.

(xiv) As the joint inclination increased the stress relaxation increased in both saw cut and split breakage joints. Namely, the magnitude of stress drops along the curve corresponding to 60^{o} were greater than those of 45^{o} at similar points.

(xv) Relaxation in the specimens containing saw cut joints was higher than that of split joints for both 45 and 60^{o} orientations up to peak stress. In fact, as the degree of interlocking asperities increased, the stress drop decreased in pre-peak region (in split joints).

(xvi) Increased confining pressure decreased the stress relaxation. This may be due to the fact that higher confinement gives rise to further limitation in the growth of cracks both in intact and jointed specimens (through the asperities).

(xvi) Comparing the saw cut and split breakage joint plots revealed that in saw cut joints, from the beginning of loading, stress relaxation at the selected points was observed and increased up to the peak and in the sliding region it remained nearly constant.

(xvii) In all cases whether in intact or jointed specimens, the stress drop in each point of relaxation reached a certain value then remained nearly constant after a certain relaxation time, and in fact the rock eventually attained stability under the new condition. Connecting the lowest point of stress drops for all the selected points along the curve a plot was obtained which represents the long-term stability of the jointed specimen.

(xviii) In jointed rocks with low level of surface roughness (saw cut) stress relaxation was found to be less significant, and in jointed rocks with a high level of surface roughness and also in intact rock, as long as the stress level had not reached its maximum, stress relaxation was less significant. In this case, in jointed rocks if sliding was initiated along joint plane (at or after peak stress) stress relaxation had significant effects on the long-term behaviour of the jointed rock, or in fact a significant effect on the stability of the structure being established in or on the jointed rock mass.

(xix) Strain rate had a significant effect on the modes of failure for both the intact and jointed specimens. At the faster strain rates (medium and fast) a shear fracture plane, particularly in higher confining pressures (5 to 15 MPa), was clearly observed. As the

strain rate was decreased to the slow rate, despite the fact that a shear fracture plane was observed in the specimens, it seems that the shear plane was not as planar as fast and medium rates, and the number of secondary fractures were also considerably more than that of the faster rates.

(xx) It seemed two factors had significant roles in the strain rate effects on mode of failure:

a) At a faster strain rate the time for dissipation of strain energy through the specimen is very low with respect to the slow rate and therefore, the rate of damage reduces considerably. This behaviour is true in both jointed and intact specimens.

b) In jointed specimens in addition to (a), when sliding along the joint is not predominant the relative sliding movement over the joint at a slow strain rate is higher than that of a fast rate (figure 7.5 compare the slow and fast rate plots). This behaviour causes a further dislocation of the two halves of specimens in a slow strain rate and therefore, a discrepancy in the modes of deformation.

10.5 EVALUATION OF FAILURE CRITERIA FOR DISCONTINUOUS ROCKS

Documentary evidence based on the experimental investigations conducted through this work shows that the failure criteria in which the maximum stress at failure is the major controlling factor is not adequate and reliable for design purposes. The most significant and controlling parameter seems to be the allowable and pre-determined magnitude of displacement (or percentage of strain) throughout the rock surrounding the structure. Consideration of the strain at failure (maximum allowable strain) results in obtaining the associated stress envelope under the real conditions of the rock structure. Then on

the basis of the maximum allowable displacement introduced through the rock mass the design parameters may be determined.

10.6 FRICTIONAL SLIDING WITH RESPECT TO STICK-SLIP PHENOMENON

For assessment of the testing system constraints on the stick-slip characteristics and to explore the most important aspects of the stick-slip phenomenon under satisfactory testing conditions, a series of triaxial tests were conducted on six rock types: granite, slate, limestone and three types of sandstone applying confining pressures 0-70 MPa and employing the modified and non-modified cell-specimen systems.The most important conclusions are:

1. Whether or not the system of the cell-specimen provided a full contact between sliding surfaces, there were two types of stick-slip in which either brittle or plastic instability were the controlling mechanism.

2. Stick-slip was not an intrinsic sliding property of all the rocks tested; however, sliding movement in any rock under a particular instability condition such as incomplete contacts between two halves of a specimen or two sides of a fault, may lead to stick-slip.

3. Stick-slip may occur through sliding of surfaces with different degrees of roughness, but not at the same level of confining pressures or deviatoric stresses.

4. Production of a layer of gouge over the sliding surfaces, due to a large amount of sliding movement, led to a transition from stick-slip to stable sliding.

5. Strain rate variation influenced stick-slip characteristics. Increase in strain rate resulted in decrease in both the stress drops and static coefficient of friction.

6. The occurrence of stick-slip was very susceptible to the presence of water. Presence of a very little moisture over the sliding surfaces caused stick-slip to disappear or occasional stick-slip to occur.

7. Stick-slip occurred through sliding of two different rocks on each other (Penrith sandstone and granite) in a limited period of sliding on.

10.7 RECOMMENDATIONS

Certain suggestions are presented in this section which aim in extending the research into the mechanical properties of jointed rocks specifically on the time-dependent effects and stick-slip phenomenon in order to clarify further the previous works and obtain wider generalization on stick-slip phenomenon and other aspects of jointed rocks

.

(i) The displaced oil from the triaxial cell during straining of the specimens is measured in a graded cylinder up to a maximum accuracy of 0.5 cc which is not high enough to achieve precise volumetric strain obtained by calculation for the jointed specimens in which sliding over the joint plane is predominant. This problem led to occasional fluctuations in volumetric strain-axial strain plots in the sliding portions. The servo-controlled intensifier apparatus (made available after the completion of the tests) which is able to measure the displaced oil automatically seems to overcome this problem. A series of tests should be conducted by using this device and comparing the results with those of obtained through this work.

(ii) A comprehensive evaluation of the strain rate effects on frictional resistance and other aspects of jointed rocks and withdrawal of a postulated mechanism for the phenomena observed, required further investigations with consideration of other factors such as mineralogy, ploughing, water and temperature which might be expected to influence the static and dynamic characteristics of rock joints. The effects of rock type, joint surface roughness and confining pressure were only investigated in this study.

(iii) As noted before in most of the previous work especially where the triaxial system has been employed, very small specimens have been used. Although in the present work, the specimens used were larger, further work is still needed to test specimens with large dimensions to assess any scale effect.

(iv) The highest applied confining pressure in this experiment was 70 MPa corresponding to a depth of the order of 3 km. For extension of the findings to a broader area and deeper formations higher confining pressures must be used. Under very high pressures soft rocks are expected to become ductile and it is important to verify whether under these conditions stick-slip motion will take place. On the other hand, investigation on stick-slip characteristics for hard rocks under very high confining pressure and comparison with those in low and intermediate pressures may prove to be significant.

(v) In order to conduct the required tests for achieving the aims outlined in (iii) and (iv) a triaxial cell capable of very high confining pressure and very large specimens (specimen diameter bigger than 75mm) must be designed with consideration of the end-specimen conditions pertinent to jointed specimens similar to the modified cell-specimen system in this work.

(vi) Despite the fact that in the present study, investigation on stick-slip phenomenon has been conducted on six different rocks, a further number of rock materials should still be tested from several categories of rocks especially those rocks on which the same experiments have been performed in the past by other workers to clarify the findings on stick-slip and to explore further generalized and realistic results on this phenomenon.

(vii) A strong shock or vibratory motion is imposed to the 5 MN loading frame (as a part of the servo-controlled system) in each cycle of stick-slip which affects the results. In order to reduce or eliminate this effect it seems a stiffer frame is required particularly for higher confining pressures. On the other hand, the number and types of spacers which are used to fill the interval between the plunger and the top plate of the loading frame affect the post-peak characteristics of rock and also the mode of slip in each cycle of stick-slip. Therefore, close attention must be paid to decrease this distance for the sake of reducing the number of spacers and hence, to increase the stiffness of the system.

(viii) Derivation of a criterion for the jointed media applicable in various conditions, it is required to investigate further in laboratory (performing triaxial experiments on specimens containing several joint patterns and not only on the specimens with a single joint) and then to conduct theoretical analysis.

REFERENCES

Ashour H.A. (1988)
A compressive strength criterion for anisotropic rock materials
Can. Geotech. J., vol. 25, no.2, 233-237

Atkinson J. H. and P. L. Bransby (1978)
The mechanics of soils, an introduction to critical state soil mechanics,
McGrow-Hill, London.

Barton N. R. and V. Choubey (1977)
The shear strength of rock joint in theory and practice,
Rock Mechanics, 10, 1-54.

Barton N. R. (1986)
Deformational phenomena in jointed rock,
Geotechnique, 36, no 2, 147-167

Bieniawski Z.T.(1967)
Mechanism of brittle fracture of rock
National Mechanical Engineering Research Institute, Council for science and industrial research, Pretoria, South Africa, CSIR Report MEG 580.

Bieniawski Z. T. (1969)
Deformational behaviour of fractured rock under multiaxial compression,
Proc. Int. Conf. Structure, Solid Mechanics and Eng. Design,
John Wiley & son, London, 55/1-55/10.

Bieniawski Z. T. (1970)
Time-dependent behaviour of fractured rock
Rock Mechanics, 2, 123-137.

Bieniawski Z.T.(1974)
Estimating the strength of rock materials
J. S. Afr. Inst. Min. Metall., 74, 312-320.

Blanton T. L. (1981)
Effects of strain rates from 10^{-2} to 10 /s in triaxial compression tests on three rocks,
Int. J. Rock Mech. Min. Sci., 18, 47-62.

Brace W. F. (1964)
Brittle fracture of rocks
In State of stress in the Earth's Crust, edited by W. R. Judd, 110-178, American Elsevier, New York.

Brace W. F.and J.D. Byerlee (1966)
Stick-slip as a mechanism for earthquakes
Science 156, 990-992

Bridgman P. W. (1936)
Shearing phenomena at high pressure of possible importance to geology
J. Geol., 44, 653-669

Bridgman P. W. (1949)
Volume changes in the plastic stages simple compression,
J. Sci., 15, 287-96.

Brockley C. A.and H.R. Davis (1968)
The time dependence of static friction
Trans. Am. Soc. Mech. Engrs. ser. F, 90, 35-41

Brook N. (1979)
Estimating the triaxial strength of rocks
Technical note, Int. J. Rock Mech. Min. Sci., 16, 261-264.

Brown E. T. (1970)
Strength of models of rock with intermittent joints,
J. Soil Mech. Found. Div., ASCE, 96, SM 6, 1935-49.

Brown E. T. and D. H. Trollope (1970)
Strength of a model of jointed rocks
J. Soil Mech. Found. Div., ASCE, 96, SM 2, 685-704.

Brown E.T. (1986)
Rock characterization testing and monitoring, ISRM suggested methods, Pergamon Press.

Buzdar S. A. R. K. (1968)
A laboratory investigation into the mechanical properties of some sedimentary rocks with special reference to potash,
Ph.D. Thesis, University of Newcastle upon Tyne.

Byerlee J. D. (1967a)
Theory of friction based on brittle fracture
J. Appl. Phys. 38, 2928-2934.

Byerlee J. D. (1967b)
Frictional characteristics of granite under high confining pressures
J. Geophys. Res., 72, 3639-48

Byerlee J. D. (1968)
Brittle-ductile transition in rocks,
J. Geophys. Res., 73, 4741-50.

Byerlee J. D.and W.F. Brace (1968)
High-pressure mechanical instability in rocks
Science 164, 713-715

Byerlee J. D. (1970)
The mechanics of stick slip
Tectonophysics 9, 475-486.

Byerlee J. D. (1975)
The fracture strength and frictional strength of Veber sandstone,
Int. J. Rock Mech. Min. Sci., 12, 1-4.

Carman V. Th. (1911)
Fetigskeitsversuche unter allseitigem druch, zeits verein ductsch,
Ing., 55, 1749-57.

Chappell B. A. (1975)
The effect of constraints on the deformational response of slip along planar joint
Int. J. Rock Mech. Min. Vol. 12, 265-270

Crawford A. M. and J. H. Curran (1982)
The influence of rate-and displacement-dependent shear resistance on the response of rock slopes to seismic loads,
Int. J. Rock Mech. Min. Sci., 19, 1-8.

Crawford A. M and J H. Curran (1981)
The influence of shear velocity on the frictional resistance of rock discontinuities,
Int. J. Rock Mech. Min. Sci., 18, 505-518.

Crouch S. L. (1970a)
Experimental determination of volumetric strains in failed rock,
Int. J. Rock Mech. Min. Sci., 7, 589-3.

Crouch S. L. (1970b)
The influence of failed rock on the mechanical behaviour of underground excavations,
Ph.D. Thesis, University of Minnesota.

Crouch S. L. (1972a)
A note on post failure stress-strain path dependence in norite,
Int. J. Rock Mech. Min. Sci., 9, 197-4.

Crouch S. L. (1972b)
The post-failure behaviour of norite in triaxial compression,
Eng. Geol., 6, 19-30.

Deklotz E. J., J. W. Brown and O. A. Stemler (1966)
Anisotropy of schistose gneiss,
Proc. of the first Cong. of the ISRM, 1, 465-70, Lisbon.

Dieterich J. D. (1970)
Time dependence of stick-slip (abstract)
EOS Trans. AGU, 51, 423

Dieterich J. H. (1972b)
Time-dependent friction as a possible mechanism for after shocks
J Geophys. Res. 77, 3771-3781

Donath F.A. (1961)
experimental study of shear failure in anisotropic rocks
Bull. Geol. Soc. Am., 72, 985-90

Donath F. A. (1962)
Role of layering in geological deformation,
Trans. N. Y. Acad. Sci., 24, 236-49.

Donath F. A. (1964)
Strength variation and deformational behaviour of in anisotropic rock,
In state of stress in the Earth's crust, W. R. Judd (Ed.), New York, Elsevier, 281-297.

Donath F.A. (1972)
Effects of cohesion and granularity on deformational behaviour of anisotropic rock
In:Studies in mineralogy and precamberian geology, B.R.Doe and D.K. Smith(eds),
Geol. Soc. Am., Memoir 135, 95-128

Drennon C. B. and R. L. Handy (1972)
Stick-slip of lightly loaded limestone,
Int. J. Rock Mech. Min. Sci., 9, 603-615.

Edmond J. M. and M. S. Paterson (1972)
Volume changes during the deformation of rocks at high pressures,
Int. J. Rock Mech. Min. Sci., 9, 161-82.

Einstein H. H., R. A. Nelson, R. W. Bruhn and R. C. Hirschfeld (1969)
Model studies of jointed rock behaviour,
In Rock Mechanics in Theory and Practice, Proc. 11th Sym. on Rock Mechanics, Held at the University of California, Berkeley, W. H. Sonerton (Ed.).

Engelder J. T.,J.M. Logan, and J.Handin (1975)
The sliding characteristics of sandstone on quartz fault-gouge
Pure and Appl. Geophys. 113, 69-86

Farmer I. W. (1983)
Engineering behaviour of rocks,
2nd edition, Chapman Hall.

Goodman R. E. (1976)
Methods of geological engineering in discontinuous rocks,
St.Paul: West.

Griffith A.A.(1921)
The phenomena of rupture and flow in solids
Phil. Trans. Roy. Soc. A221, 163-97

Handin J. and D. W. Stearns (1964)
Sliding friction of rock,
Trans. Am. Geophys. Un., 45, 103.

Hawkes I. and M. Meller (1970)
Uniaxial testing in rock mechanics laboratories.
Eng. Geol., 4, 177-285.

Hoek E.(1964)
Fracture of anisotropic rock
J. South Afr. Inst. Min. and Met. vol.1, no 10, 510-518

Hoek E.(1968)
Brittle fracture of rock
In: Rock mechanics in engineering practice, eds. Stagg and Zienkiewicz, London, John Wiley & sons, 93-124.

Hoek E.(1983)
Strength of jointed rock masses
Twenty third Rankine lecture, Geotechnique, vol.33,no 3, 187-223.

Hoek E. and E.T. Brown (1980a)
Underground excavation in rock, 527 pp. London: The Inst.of Mining and Metall.

Hoek E. and E.T. Brown (1980b)
Empirical failure criterion for rock masses,
J. Geotech. Eng. Div. ASCE, 106, GT9, 1013-1035.

Hobbs D.W. (1966)
A study of the behaviour of a broken rock under triaxial compression, and its applications to mine roadways
Int. J. Rock Mech. Min. Sci., 3, 11-43

Hobbs D.W. (1970)
The behaviour of broken rock under triaxial compression
Int. J. Rock Mech. Min. Sci., 7, 125-148

Horino F. G and M. L. Ellikson (1970)
A method of estimating the strength of rock containing plane of weakness,
U. S. Bureau of Mines, report investigation 7449, U. S. Bureau of Mines.

Houpert R. (1979)
The fracture behaviour of rocks,
4th Int. Cong. ISRM, 3, 107-114.

Hsu T.R., G. Pizey and H.A. Ashour (1984)
On an analytical method for in-situ fracture of oil sand formation
Proceedings, 35th Annual Technical Meeting of the petroleum Society of the Canadian Institute of Mining and Metallurgy, Calgary.

Hudson J. A. (1971)
Effect of time on the behaviour of failed rock,
Nature, 232, 185-186.

Jaeger J. C. (1959)
The frictional properties of joints in rock
Geofis. pura appl. 43, 148-158

Jaeger J.C. (1960)
Shear failure of anisotropic rocks
Geologic. Magazine, vol.97, 65-72

Jaeger J. C. and N. G. W. Cook (1969)
Friction in granular material,
Proc. of the Civil Eng. Materials Conf., Southampton, in Solid Mechanics and Eng. Design, part1, A. M. Te'eni (Ed.), 257-66. London, Wiley.

Jaeger J. C. (1970)
The behaviour of closely jointed rock,
Proc. 11th Sym. on Rock Mech. Berkley, published by AIME, New York, 57-68.

Jaeger J. C. (1972)
Rock mechanics and engineering,
Caimbridge University Press.

Jaeger J.C. and N.G.W. Cook (1979)
Fundamentals of rock mechanics
3rd edn. London: Chapman and Hall.

Johnson T. (1973)
Source parameters for stick-slip and for earthquakes
Science 179, 278-280

Johnson T. L. (1975)
A comparison of frictional sliding on granite and dunite surfaces
J. Geophys. Res. 80, 2600-2605

Johnson T. L.and C.H. Scholz (1976)
Dynamic properties of stick slip friction of rock
J. Geophys. Res. 81, 881-888

Kovari K. and A. Tisa (1975)
Multiple failure state and strain controlled triaxial tests,
Rock Mechanics, 7, 17-33.

Lajtai E. Z. (1976)
The influence of interlocking rock discontinuities on compressive strength (model experiments)
Rock Mechanics and Engineering geology, 5-6, 217-228.

Lane K. S. and W. J. Heck (1964)
Triaxial testing for strength of rock joints,
Proc. 6 Sym. Rock Mech. Rolla, Mo, 98-108.

Locker D. A.,R. Summer, D.Moore and J.D. Byerlee (1982)
Laboratory measurements of reservoir rock from the Geysers Geothermal Field, California
Int. J. Rock Mech. Min. Sci. 19, 65-80

McClintock F.A. and J.B. Walsh (1963)
Friction on Griffith cracks in rocks under pressure
Proceedings, Fourth U.S. Nat Cong. App. Mech., 1015-1021

McLamore R. and K.E. Gray (1967)
The mechanical behaviour of anisotropic sedimentary rocks
J. Engng. for industry, Trans. Am. Soc. Mech. Engrs. Ser. B, 89, 62-73.

Mogi K. (1966)
Some precise measurements of fracture strength of rocks under uniform compressive stress,
Rock Mech. Eng. Geol., 4, 41-55.

Mogi K. (1971)
Fracture and flow of rocks under high triaxial compression
J. Geophy. Res., 76, 1255-1269.

muller L. (1964)
Application of rock mechanics in the design of rock slopes,
In: State of stress in the earth's crust, W.r. Judd (Ed.), 575-605, Elsevier, New York.

Murrel S.A.F. (1965)
The effects of triaxial stress systems on the strength of rock at atmospheric temperatures
Geophys. J. Roy. Astr. Soc., vol.10, 231-281.

Obert L. and W. I. Duvall (1967)
Rock mechanics and the design of structures in rock,
Wiley, New York.

Paterson M. S. (1978)
Experimental rock deformation- the brittle field,
Springer-Verlag, printed in Germany.

Patton F. D. (1966)
Multiple modes of shear failure in rock,
Proc. 1st Cong. ISRM, 1, 509-13, Lisbon.

Peng S. and E. R. Podnieks (1972)
Relaxation and the behaviour of failed rock,
Int. J. Rock Mech. Min. Sci. 9, 699-712.

Peng S. S. (1973)
Time-dependent aspects of rock behaviour as measured by a servo-controlled hydraulic testing machine,
Int. J. Rock Mech. Min. Sci., 10, 235-246.

Perkins R. D., S. J. Green and M. Friedman (1970)
Uniaxial stress behaviour of porphyritic Tonalite at strain rates to 10^3 /s,
Int. J. Rock Mech. Min. Sci. 7, 527-35.

Pomeroy C. D., D. W. Hobbs and A. Mahmoud (1971),
The effect of weakness plane orientation on the fracture of Bransley Hards by triaxial compression,
Int. J. Rock Mech. Min. Sci., 8, 227-238.

Price A. M. (1979)
The effect of confining pressure on the post-yield deformation characteristics of rocks,
Ph.D Thesis, University of Newcastle upon Tyne.

Rabinowicz E. (1959)
A study of the stick-slip process
in: Friction and wear R. Davies (Editor), Elsevier, London, 149- 161.

Rea D. (1963)
The measurement of the coefficient of friction of some rocks during continuous rubbing
J. Scient. Instrum. 40, 438-440

Rosengren K. J. and J. C. Jaeger (1968)
The mechanical properties of an interlocked low-porosity aggregate,
Geotechnique, 18, 317-26.

Rosengren K. J. (1968)
Rock mechanics of the Black Star Open Cuts, Mount Isa,
Ph. D. Thesis, Australian National University.

Sangha C. M. and R. K. Dhir (1972)
Influence of time on the strength, deformation and fracture properties of a lower devonian sandstone,
Int. J. Rock Mech. Sci., 9, 343-354.

Sangha C. M. and R. K. Dhir (1975)
Strength and deformation of rock subjected to multiaxial compressive stresses,
Int. J. Rock Mech. Min. Sci., 12, 277-282.

Schneider H. J. (1977)
The time dependence of friction of rock joints,
Bull. IAEG 16, 235-239.

Scholz C. H. (1968a)
Microfracturing and the inelastic deformation of rock in compression,
J. Geophys. Res., 73, 1417-32.

Scholz C. H. Molnar and T. Johnson (1972)
Detailed studies of frictional sliding of granite and implications for the earthquake mechanism
J. geophy. Res. 77, 6392-6406

Serafim J. L. (1966)
Geological exploration for a dam site,
Proc. 1st. Cong. ISRM, 2, 667-74, Lisbon.

Summers R. and J.D. Byerlee (1977)
A note on the effect of fault gouge composition on the stability of frictional sliding
Int. J. Rock Mech. Min. Sci. 14, 155-160.

Swan G., J. Cook, S. Bruce and R. Meehan (1989)
Strain rate effects in Kimmeridge Bay shale,
Int. J. Rock Mech. Min. Sci., 26, 135-149.

Tuefel L. W and J. M. Logan (1978)
Effect of displacement rate on the real area of contact and temperature generated during frictional sliding of Tennessee sandstone
Pure Appl. Geophys., 116, 841-865.

Thiel K. and L. Zabuski (1987)
Empirical failure criterion for a jointed anisotropic rock mass
6th Int. Conf. on Rock Mech., Montreal, Rotterdam: A.A. Ball, 563-568.

Bureau of reclamation (1954)
Bond strength between concrete and rock from Monticello dam site project,
California, concrete laboratory report, no. c-761.

Walsh J.B. and W.F. Brace (1964)
A fracture criterion for brittle anisotropic rock
J. Geophys. Res., vol.69, 3449-56.

Walsh J. B. and W. F. Brace (1966)
Cracks and pores in rocks,
Proc. 1st Cong. ISRM, 1, 643-6, Lisbon.

Wawersik W.R. (1968)
Detailed analysis of rock failure in laboratory compression tests
Ph.D Thesis, University of Minnesota, Minneapolis.

Wawersik W. R. (1975)
Technique and apparatus for strain measurements on rock in constant confining pressure experiments,
Rock Mechanics, 7, 231-41.

Youash Y. Y. (1966)
Experimental deformation of layered rocks,
Proc. the first Cong. of the ISRM, 1, 787-95, Lisbon.

Yudhbir, W. Lemanza and F. Prinzl (1983)
An empirical failure criterion for rock masses
Proceedings of the 5th Int. Cong. Rock Mech., ISRM, vol.1, B1-B8.

APPENDIX A

LIST OF COMPUTER PROGRAMS FOR USE IN DATA MONITORING SYSTEM

1. PROGRAM: DATA LOGGING

```
program COLLECT;          (*SIRIUS VERSION*)


TYPE
ptr = ^integer;


var
ch    : integer;
ORB   : absolute [$E808:00] byte ;
          (* Memory Layout Of  *)
ORA   : absolute [$E808:01] byte ;
          (* 6522 Register Set *)
DDRB  : absolute [$E808:02] byte ;
DDRA  : absolute [$E808:03] byte ;
PCR   : absolute [$E808:12] byte ;
F : text;
FN : string ;
READ1,READ0 :integer;
EXTERNAL FUNCTION @IBMDOS ( FUNC:integer; parm:ptr):integer;
procedure DELAY (PAR : integer);
             (* General Purpose Delay Procedure *)
 var
  I : integer ;
 begin                          (*begin of DELAY *)
 for I := 1 to PAR do
 begin
 end
 end ;                           (*end of DELAY *)

  procedure GETFILE;
  begin                          (* begin of GETFILE *)
  writeln('filename for data logging (format:abcdefg.jkl):');
  read(FN);
  end;
  procedure LOG;        (* Reads Data From The A/D Card *)
  var                   (* Number Of Reads Done is The  *)
  READ1,READ0:integer ;
  HIGHBYTE,LOWBYTE : byte ;    (* Is Returned In Result*)
  pm:ptr;
  begin
```

```
                        (* begin of COLLECT *)
REPEAT
ch:=@IBMDOS (S0B,pm);
writeln (ch) ;

DDRB :=$FF;
DDRA :=$1;
PCR  :=$AA;

ORB :=$20;
DELAY (50);
ORB := $1 ;                              (* Start Reading *)
DELAY (50) ;
HIGHBYTE := ORA ;                       (* Read High Byte *)
LOWBYTE := ORA ;                        (* Read Low Byte *)

READ1 :=shl (HIGHBYTE,4) ! shr (LOWBYTE,4) ;
                           (* Generate Reading *)
                           (*(HIGHBYTE*16)    *)
                           (*   +(LOWBYTE/16  *)
DDRB :=$FF;
DDRA :=$00;
PCR  :=$AA;

ORB :=$00;
DELAY (50);
ORB :=$00;
DELAY (50);
HIGHBYTE :=ORA;
LOWBYTE :=ORA;

READ0 :=shl (HIGHBYTE,4) ! shr(LOWBYTE,4);

writeln(F,read1:10, read0:10 );
write (chr(27),'Y',chr(31+12),chr(31+25));
write (read1 :5,read0:5);


 UNTIL ch =$FF;
 end;                              (* end of LOG     *)

 begin  (* This is the main program *)
 GETFILE;
 assign(F,FN);
 rewrite(F);
 LOG;
 close(F,read1);
 close(F,read0)

 end.
```

2. PROGRAM: DATA CORRECTION

```
program AVERAGE ;

var
F1,f2 :text;
FN1,FN2 :string;
X,Y :real;
Xs,Ys :real;

procedure FILENAME;

 begin
writeln('input filename :');
read (FN1);
writeln('output filename:');
read (FN2)
end;

procedure MEAN;

var
INDEX :integer;
X,Y,Xs,Ys :real;
begin
while not eof(F1) do
begin (*begin of main loop*)
index :=0;
Xs :=0;
Ys :=0;
REPEAT
index :=index + 1;
readln (F1,X,Y);
Xs :=Xs+X;
Ys :=Ys+Y
UNTIL ((index =5) OR (eof(F1)));
Xs :=Xs/index;
Ys :=Ys/index;
writeln (F2,Xs:10:4,Ys:10:4)
end
end;
begin (*this is the main program*)
FILENAME;
assign (F1,FN1);
assign (F2,FN2);
reset (F1);
rewrite (F2);
MEAN;
close (F1,X);
close (F1,Y);
close (F2,Xs);
close (F2,Ys)
end.
```

3. PROGRAM: STRESS (MPa) AND STRAIN (%) CALCULATION

```
program STRESS_STRAIN;

var
F1,F2 :text;
FN1,FN2 :string;
X,Y,STRESS,STRAIN,DIAM,HEIGHT,PI :real;

procedure FILENAME;
begin
writeln ('input filename:');
read (FN1);
writeln ('output filename:');
read (FN2);

end;

procedure CONVERSION;
begin

pi :=4*arctan(1.0);
writeln ('Height of the specimen (mm):');
read (height);
writeln ('Diameter of the specimen (mm):');
read (diam);

while not eof(F1) do
begin
readln (F1,X,Y);
strain :=X*100/404.82/height;
stress :=Y/(5193.7*pi*sqr(diam/1000/2));
writeln (F2,strain:10:4,stress:10:4);

end;
end;

begin (*This is the main program*)

FILENAME;
assign (F1,FN1);
assign (F2,FN2);
reset (F1);
rewrite (F2);
CONVERSION;
close (F1,X);
close (F1,Y);
close (F2,strain);
close (F2,stress)

end.
```

APPENDIX B

THIN SECTION PETROLOGICAL DESCRIPTION

A thin section was performed with the aim of identifying types of mineral, cementing materials, homogeneity and other microscopic features of the rocks tested. A brief description is given as follows:

1. Dumfrith Sandstone

The colour is pale reddish brown with : quartz, crystals of feldspar, clay minerals and mica. Clay minerals and mica are present as the cementing materials. Suture contact between grains and some parts of the thin section indicates pressure solution in this rock. Most of the grains are subangular, rounded and medium sorting. Small crystals of muscovite squashed among the quartz grains and opaque minerals also scattered among them.

2. Stainton Sandstone

It is pinkish grey with: quartz (90-95%), muscovite (less than 1%), opaque minerals (4-5%). The grains are subangular and rounded in diameter of 100-300 u with sutur contacts. Contacts between grains have been provided by calcite cement in some parts, and by interlocking the grains in other parts. The thin section shows pressure solution.

3. Penrith Sandstone

The colour is pale reddish brown and it is a siliceous sandstone with rounded quartz grains (60-800 u in diameter) up to 98%, well compacted by secondary (authigenic)

quartz in the form of overgrowth on the detrital grains. The surfaces of original grains are picked out by a thin red-brown rim of iron oxide. Some of the grains as a result of pressure have broken.

Where overgrowth well developed, the shape of the grains changed from rounded to subhedral. This rock is hard and does not have any prosity and permibility.

4. Matlock Limestone

The colour is very light grey with minerals: calcite (as a calcite cement and skeleton of fossils) and micrite. Calcite crystals are clear and some skeletal of fossils are also present.It has undergone compaction, and cement as a sparry calcite and overgroth cement around the echinoderm are present.

5. Dalbeatie Granite

It is pinkish grey in colour with minerals: quartz (60-65%), feldspar (30-35%), mica (3-5%). Most of the crystals of feldspar (orthose) have undergone kaolinization. Very small crystal of muscovite scattered throughout the feldspar crystals.

6. Dinorwic Slate

It is dark grey and a cryptocrystaline rock (may be clay minerals), with fine crystals of muscovite scattered, and dark opaque minerals in some parts. The cryptocrystaline material compacted well and it seems that have undergone very low metamorphism. More than 50% of the rock is opaque minerals, and very fine crystals of quartz are present.

APPENDIX C

THE STEP BY STEP PROCEDURE OF PRODUCING CYLINDRICAL SPECIMENS CONTAINING SPLIT BREAKAGE JOINTS

1. Cut a 200 mm cube side.
2. Cut groove for breakage.
3. Mark off the center line for the cores at the required angle from the groove.
4. Mark off the two parallel faces at 90 degrees to the core center-line.
5. Cut the two parallel faces.
6. Mark off the two center holes for the core locking studs.
7. Mark off the oversize core positions for lineage up core barrel.
8. Drill the 'core locking stud' holes.
9. Break the sample in the testing machine by applying a small load slowly, using two of round steel bars.
10. Clamp the two sample halves together and fit the core locking studs.
11. Clamp to the table and cut the cores.
12. Remove the core and take out the center locking stud after first making a reference mark across the breakage point.
13. Insert steel center pin to hold the core together.
14. Cut the core to length.
15. Grind core parallel and to required length, then remove center pin.

APPENDIX D

PROGRAM TO CALCULATE VOLUMETRIC STRAIN, LATERAL STRAIN,

AND INSTANTANEOUS POISSON'S RATIO FOR SIMPLIFIED METHOD

```
program SIMPEL;
(*simplified method to calculate volumetric strain*)

var
F1,F2,F3,F4,F5,F6 :text;
FN1,FN2,FN3,FN4,FN5,FN6 :string;
Vo,Fo,Hs,Ds,As,Vs,E,V,DELTA,PI,EBS1,EBS2,POISSON,
SIGMA1,SIGMA3:real;
Dvr,Ar,Rr,Vr,dV,N,L,Vt,dl,F,X,Y,Cf,Xo,Yo,Cx,Cy,LOAD:real;

procedure FILENAME;

begin
writeln ('Enter input filename :');
read (FN1);
writeln ('Enter ebs1 vs poisson filename :');
read (FN2);
writeln ('Enter ebs1 vs delta filename :');
read (FN3);
writeln ('Enter ebs1 vs ebs2 filename :');
read (FN4);
writeln ('Enter ebs1 vs sigma1 filename:');
read (FN5);
writeln ('Enter delta vs sigma1 filename:');
read (FN6);
end;

procedure CALCULATION;

begin
PI :=4*arctan(1.0);
Hs :=150;
Ds :=75;
Rr :=3.9;        (*radius of the ram*)
E :=270000;
writeln ('Enter oil compressibility factor :');
read (Fo);
```

```
writeln ('Enter confining pressure (MPa):');
read (sigma3);
writeln ('Enter origin coordinate (Xo) in digit :');
read (Xo);
writeln ('Enter origin coordinate(Yo) in digit:');
read (Yo);
writeln ('conversion fact (Cx) X on .1 Cx=.786(N),1(O),
X on 50 Cx= 1.572 :');
read (Cx);
writeln ('con fac (Cy) Y on 0.5 Cy =1501.26(N),1930(O),
Y on 0.2 Cy= 558.06 :');
read (Cy);
As:=(pi*sqr(Ds/1000/2));
       (*cross sectional area of specimen(m2)*)
V=As*Hs*1000;              (*specimen volume(cm3)*)
N :=0.25;
Ar:=sqr(Rr)*pi;
while not eof(F1) do
begin
readln (F1,X,Y,Vo);
(*axial displacement ,axial load,displaced oil*)
sigma1 :=(Y-Yo)/(Cy*As);
ebs1 :=((X-Xo)/(Cx*Hs))*(1-(sigma1-(2*N*sigma3))/E);
dl :=(ebs1*Hs)/100;
Dvr :=Ar*dl*((1-2*n)*(sigma1+2*sigma3))/(10*E);
Vr :=Ar*dl/10-Dvr;
Vt :=Vo*Fo;
dV :=Vr-Vt ;       (*dV is the specimen volume change*)
delta :=dV*100/V;   (*delta is the volumetric strain*)
ebs2 :=(ebs1-delta)/2;
poisson :=ebs2/ebs1;
writeln (F2,ebs1:10:4, poisson:10:4);
writeln (F3,ebs1 :10:4,delta :10:4);
writeln (F4,ebs1:10:4,ebs2:10:4);
writeln (F5,ebs1:10:4,sigma1:10:4);
writeln (F6,delta:10:4,sigma1:10:4);
end;
end;

begin                    (*this is the main program*)

FILENAME;
assign (F1,FN1);
assign (F2,FN2);
assign (F3,FN3);
assign (F4,FN4);
assign (F5,FN5);
```

```
assign (F6,FN6);
reset (F1);
rewrite (F2);
rewrite (F3);
rewrite (F4);
rewrite (F5);
rewrite (F6);
CALCULATION;
close (F1,X);
close (F1,Y);
close (F1,Vo);
close (F2,ebs1);
close (F2,poisson);
close (F3,ebs1);
close (F3,delta);
close (F4,ebs1);
close (F4,ebs2);
close (F5,ebs1);
close (F5,sigma1);
close (F6,delta);
close (F6,sigma1);

end.
```